frontiers | Research Topics

# Metabolomics perspectives for clinical medicine, volume II

**Edited by**
Danuta Dudzik, Víctor González-Ruiz, Hector Gallart-Ayala and Julia Kuligowski

**Published in**
Frontiers in Molecular Biosciences

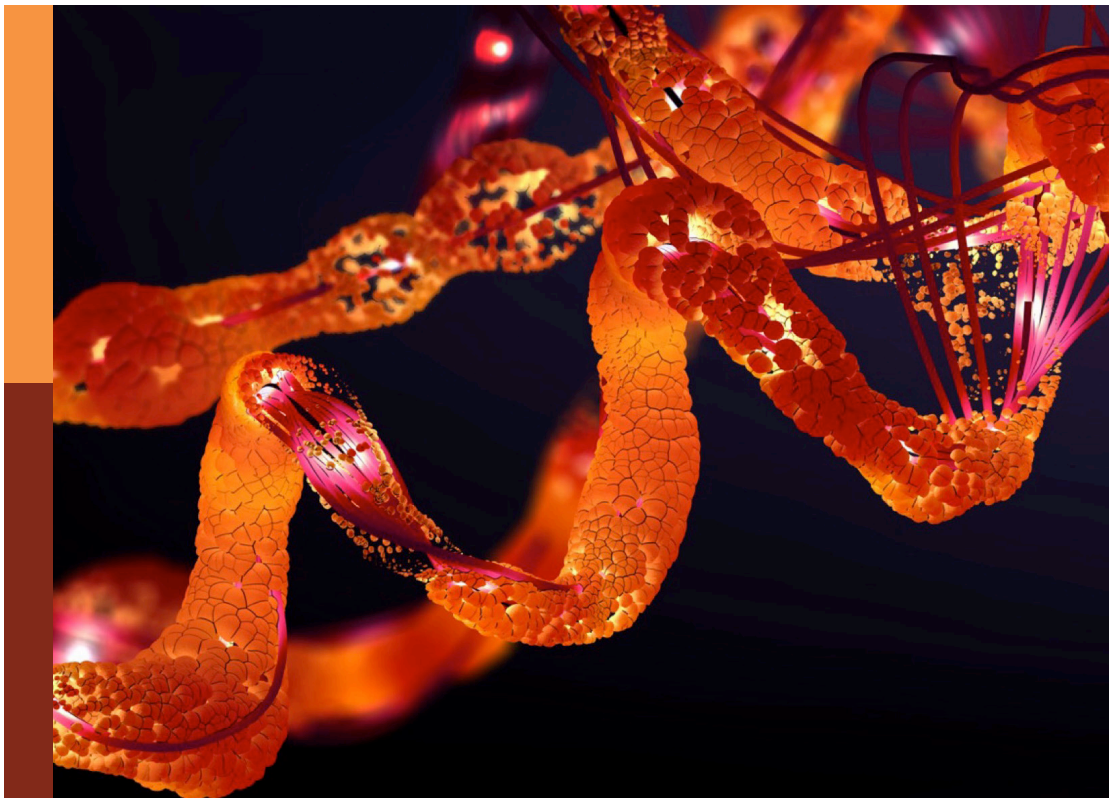

ISSN 1664-8714
ISBN 978-2-8325-6172-0
DOI 10.3389/978-2-8325-6172-0

## About Frontiers

Frontiers is more than just an open access publisher of scholarly articles: it is a pioneering approach to the world of academia, radically improving the way scholarly research is managed. The grand vision of Frontiers is a world where all people have an equal opportunity to seek, share and generate knowledge. Frontiers provides immediate and permanent online open access to all its publications, but this alone is not enough to realize our grand goals.

## Frontiers journal series

The Frontiers journal series is a multi-tier and interdisciplinary set of open-access, online journals, promising a paradigm shift from the current review, selection and dissemination processes in academic publishing. All Frontiers journals are driven by researchers for researchers; therefore, they constitute a service to the scholarly community. At the same time, the *Frontiers journal series* operates on a revolutionary invention, the tiered publishing system, initially addressing specific communities of scholars, and gradually climbing up to broader public understanding, thus serving the interests of the lay society, too.

## Dedication to quality

Each Frontiers article is a landmark of the highest quality, thanks to genuinely collaborative interactions between authors and review editors, who include some of the world's best academicians. Research must be certified by peers before entering a stream of knowledge that may eventually reach the public - and shape society; therefore, Frontiers only applies the most rigorous and unbiased reviews. Frontiers revolutionizes research publishing by freely delivering the most outstanding research, evaluated with no bias from both the academic and social point of view. By applying the most advanced information technologies, Frontiers is catapulting scholarly publishing into a new generation.

## What are Frontiers Research Topics?

Frontiers Research Topics are very popular trademarks of the *Frontiers journals series*: they are collections of at least ten articles, all centered on a particular subject. With their unique mix of varied contributions from Original Research to Review Articles, Frontiers Research Topics unify the most influential researchers, the latest key findings and historical advances in a hot research area.

Find out more on how to host your own Frontiers Research Topic or contribute to one as an author by contacting the Frontiers editorial office: frontiersin.org/about/contact

# Metabolomics perspectives for clinical medicine, volume II

**Topic editors**

Danuta Dudzik — Medical University of Gdańsk, Poland
Víctor González-Ruiz — University of Geneva, Switzerland
Hector Gallart-Ayala — Université de Lausanne, Switzerland
Julia Kuligowski — La Fe Health Research Institute, Spain

**Citation**

Dudzik, D., González-Ruiz, V., Gallart-Ayala, H., Kuligowski, J., eds. (2025). *Metabolomics perspectives for clinical medicine, volume II*. Lausanne: Frontiers Media SA. doi: 10.3389/978-2-8325-6172-0

# Table of contents

frontiers | Frontiers in Molecular Biosciences

TYPE Editorial
PUBLISHED 13 March 2025
DOI 10.3389/fmolb.2025.1577050



OPEN ACCESS

EDITED AND REVIEWED BY
Michal Ciborowski,
Medical University of Bialystok, Poland

*CORRESPONDENCE
Danuta Dudzik,
danuta.dudzik@gumed.edu.pl

RECEIVED 14 February 2025
ACCEPTED 03 March 2025
PUBLISHED 13 March 2025

CITATION
Dudzik D, Kuligowski J, González-Ruiz V and Gallart-Ayala H (2025) Editorial: Metabolomics perspectives for clinical medicine, volume II. *Front. Mol. Biosci.* 12:1577050. doi: 10.3389/fmolb.2025.1577050



# Editorial: Metabolomics perspectives for clinical medicine, volume II

Danuta Dudzik[1]*, Julia Kuligowski[2], Víctor González-Ruiz[3] and Hector Gallart-Ayala[4]

[1]Department of Biopharmaceutics and Pharmacodynamics, Faculty of Pharmacy, Medical University of Gdańsk, Gdańsk, Poland, [2]Neonatal Research Group, Health Research Institute Hospital La Fe (IIS La Fe), Valencia, Spain, [3]Centro de Metabolómica y Bioanálisis (CEMBIO), Facultad de Farmacia, Universidad San Pablo-CEU, CEU Universities, Madrid, Spain, [4]Metabolomics and Lipidomics Facility, Faculty of Biology and Medicine, University of Lausanne, Lausanne, Switzerland

KEYWORDS

**clinical metabolomics, biomarker discovery, chronic diseases, personalised medicine, translational medicine**

Editorial on the Research Topic
Metabolomics perspectives for clinical medicine, volume II

Metabolomics, including lipidomics, is a rapidly evolving field that profoundly impacts clinical medicine. It facilitates precise disease diagnosis, personalized treatment strategies, and the identification of novel biomarkers and mechanisms of pathogenesis. Advancements in mass spectrometry and computational approaches have enabled the detection and identification of metabolites and lipids in complex biological samples, providing a comprehensive biochemical profile of an individual's health status. Unlike genomics, which reveals genetic predisposition, metabolomics captures the actual dynamic interplay of biochemical pathways, environmental influences, and disease progression, making it a powerful tool for clinical applications (Mohr et al., 2024; Singh et al., 2023; Misra, 2020; Marques et al., 2024). This Research Topic, "*Metabolomics Perspectives for Clinical Medicine: Volume II*," brings together seven original research articles, one opinion, and one review, offering diverse insights into the evolving role of metabolomics in clinical research.

The primary objective of the published original reports was to improve diagnostic accuracy and patient stratification by integrating metabolomic data with traditional clinical approaches. The study by Chamoso-Sánchez et al. focuses on identifying metabolic subtypes (or metabotypes) in childhood obesity using a multiplatform metabolomics approach. The study recognizes that childhood obesity is a complex condition influenced by genetic and environmental factors. Therefore, the objective was to improve patient classification beyond traditional clinical and genetic assessments. The application of factor analysis and hierarchical clustering resulted in the identification of three distinct metabolic subtypes, despite traditional genetic and clinical markers failing to classify these patients effectively. The findings suggest that metabolomics can improve patient stratification and support personalized treatment strategies, offering a more precise approach to predicting disease risks and treatment responses. In the articles by Godzien et al. and Sieminska et al., the role of lipids in non-small cell lung cancer (NSCLC) is explored, focusing on their potential as biomarkers for differentiating between adenocarcinoma (ADC) and squamous cell carcinoma (SCC) subtypes, and investigating the role of oxidized phosphatidylcholines

(oxPCs) in NSCLC patients. In the study by Godzien et al., the authors observe that long-chain oxPCs (LCh-oxPCs) were the predominant form in plasma, whereas short-chain oxPCs (SCh-oxPCs) constitute the main fraction in tissue in NSCLC patients. The study highlights that oxidized lipids play a dual role in lung cancer, acting as both protective and harmful agents depending on their structure and concentration. LCh-oxPCs have been associated with protective functions in lung endothelium, whereas SCh-oxPCs contribute to cellular damage and inflammation, potentially driving tumor progression. The authors conclude that the SCh-oxPCs accumulated in the cancer tissue of NSCLC patients, due to their high toxicity, could be considered a potential therapeutic target. Sieminska et al. reveal differences in the profile of oxPCs and monoacylglycerol phosphatidic acids (LPAs) between ADC and SCC subtypes. The study by Lokhov et al. aimed to explore the application of a clinical blood metabogram (CBM) in early-stage Parkinson's disease (PD) diagnosis. The primary objective was to assess the CBM's ability to detect metabolic alterations in the blood characteristic of PD, providing a non-invasive diagnostic tool that could improve early detection and disease monitoring. The study employed direct-infusion mass spectrometry and principal component analysis together with metabolite set enrichment analysis to analyze blood samples. The findings indicate that CBM can effectively distinguish PD patients from healthy controls, with a diagnostic accuracy of 77%, a specificity of 71%, and a sensitivity of 82%. The authors conclude that CBM could be integrated into clinical practice for PD diagnosis, disease progression monitoring, and treatment evaluation, offering a promising avenue for personalized medicine. The novelty in the study by Dudzik et al. lies in the application of metabolomics to distinguish between early-onset and late-onset gestational diabetes mellitus (GDM) using both targeted and untargeted approaches. The study's findings indicate that specific lipid and carbohydrate metabolism alterations are strongly associated with GDM, with distinct metabolic signatures differentiating early-onset and late-onset cases. These findings suggest that metabolomics can enhance GDM diagnostics by providing deeper insights beyond traditional glucose measurements and clinical markers, paving the way for more personalized treatment strategies. The research by Warmuzińska et al. investigates lipidomic alterations in kidney grafts during warm ischemia and preservation, utilizing solid-phase microextraction combined with liquid chromatography-high-resolution mass spectrometry. The primary objective was to evaluate how different preservation methods, including normothermic and hypothermic perfusion, affect lipid metabolism in kidney grafts. By employing a minimally invasive chemical biopsy technique, the study enabled repeated sampling of the same tissue, allowing real-time monitoring of metabolic alterations during the transplantation process. The study's findings indicate that normothermic *ex vivo* kidney perfusion has a beneficial effect on graft function and the chemical biopsy technique allows tracking alterations in the graft throughout the entire transplantation procedure. Pietrowska et al., using targeted metabolomics based on the AbsoluteIDQ ®p180 kit, investigate differences in concentrations of various metabolites in aqueous humor collected from both eyes of the same patients. The authors conclude that with a few exceptions, a single eye was representative of the fellow eye in terms of the concentration of most of the analyzed metabolites. The review by Ye et al. focuses on the role of glutamine metabolic reprogramming in hepatocellular carcinoma (HCC), a highly lethal liver cancer. The study highlights how altered glutamine metabolism supports tumor growth, immune evasion, and therapy resistance. The authors discuss how cancer cells rewire glutamine metabolism to fuel biosynthetic pathways, maintain redox balance, and activate key signalling pathways like mTORC1, which promotes tumor progression. Additionally, the review explores glutamine-related metabolites as potential biomarkers for early HCC detection and treatment response monitoring. The authors evaluate metabolic targeting therapies, such as glutaminase inhibitors, which aim to disrupt tumor-specific glutamine dependencies, offering new therapeutic opportunities. Finally, the opinion paper by Yang et al. discusses recent advancements in mass spectrometry imaging (MSI) for metabolomics and its potential impact on biomedical research and clinical applications. This powerful analytical technique enables the spatial localization of metabolites within biological tissues, providing valuable insights into disease mechanisms and metabolic alterations at the cellular level. Therefore, the authors highlight how MSI overcomes the limitations of traditional metabolomics by preserving spatial context, which is crucial for understanding tissue-specific metabolic variations in diseases like cancer and neurodegenerative disorders. Additionally, the paper explores the integration of MSI with other omics approaches, to achieve a more comprehensive molecular profile.

All studies highlight the potential of metabolomics and lipidomics in advancing personalized medicine by improving disease classification, early diagnosis, and targeted treatment strategies. However, all the authors recognize the challenges that remain in translating these findings into clinical practice, including the need for standardized methodologies, addressing environmental and lifestyle influences on metabolic phenotypes, and the need to improve data interpretation. Consequently, future studies should prioritize the validation of metabolic biomarkers, the optimization of analytical workflows, and the identification of patient subgroups that would most benefit from metabolic-based interventions. This, in turn, should pave the way for more effective and individualized healthcare solutions.

## Author contributions

DD: Writing–original draft, Writing–review and editing. JK: Writing–original draft, Writing–review and editing. VG-R: Writing–original draft, Writing–review and editing. HG-A: Writing–original draft, Writing–review and editing.

## Funding

The author(s) declare that no financial support was received for the research, authorship, and/or publication of this article.

## Conflict of interest

The authors declare that the research was conducted in the absence of any commercial or financial relationships that could be construed as a potential conflict of interest.

The author(s) declared that they were an editorial board member of Frontiers, at the time of submission. This had no impact on the peer review process and the final decision.

## Generative AI statement

The author(s) declare that no Generative AI was used in the creation of this manuscript.

## Publisher's note



## References

Marques, L., Costa, B., Pereira, M., Silva, A., Santos, J., Saldanha, L., et al. (2024). Advancing precision medicine: a review of innovative *in silico* approaches for drug development, clinical pharmacology and personalized healthcare. *Pharm.* 16 (3), 332. doi:10.3390/PHARMACEUTICS16030332

Misra, B. (2020). Individualized metabolomics: opportunities and challenges. *Clin. Chem. Lab. Med.* 58, 939–947. doi:10.1515/cclm-2019-0130

Mohr, A. E., Ortega-Santos, C. P., Whisner, C. M., Klein-Seetharaman, J., Jasbi, P., Sa, J. K., et al. (2024). Navigating challenges and opportunities in multi-omics integration for personalized healthcare. *Biomed*. 12 (7), 1496. doi:10.3390/BIOMEDICINES12071496

Singh, S., Sarma, D. K., Verma, V., Nagpal, R., and Kumar, M. (2023). Unveiling the future of metabolic medicine: omics technologies driving personalized solutions for precision treatment of metabolic disorders. *Biochem. Biophys. Res. Commun.* 682, 1–20. doi:10.1016/J.BBRC.2023.09.064

frontiers | Frontiers in Molecular Biosciences

TYPE Original Research
PUBLISHED 29 March 2023
DOI 10.3389/fmolb.2023.1166182



OPEN ACCESS

EDITED BY
Julia Kuligowski,
La Fe Health Research Institute, Spain

REVIEWED BY
Guillermo Quintas,
Leitat Technological Center, Spain
Juan Sanchez Naves,
Opthalmedic and I.P.O., Balearic Island, Spain

*CORRESPONDENCE
Diana Anna Dmuchowska,
diana.dmuchowska@umb.edu.pl
Michal Ciborowski,
michal.ciborowski@umb.edu.pl

†These authors have contributed equally to this work

SPECIALTY SECTION
This article was submitted to Metabolomics, a section of the journal Frontiers in Molecular Biosciences

RECEIVED 14 February 2023
ACCEPTED 17 March 2023
PUBLISHED 29 March 2023

CITATION
Pietrowska K, Dmuchowska DA, Godlewski A, Grochowski ET, Wojnar M, Gosk W, Konopinska J, Kretowski A and Ciborowski M (2023), Extent of interocular (a)symmetry based on the metabolomic profile of human aqueous humor.
*Front. Mol. Biosci.* 10:1166182.
doi: 10.3389/fmolb.2023.1166182



# Extent of interocular (a)symmetry based on the metabolomic profile of human aqueous humor

Karolina Pietrowska[1†], Diana Anna Dmuchowska[2*†], Adrian Godlewski[1], Emil Tomasz Grochowski[2], Malgorzata Wojnar[2], Wioleta Gosk[1], Joanna Konopinska[2], Adam Kretowski[1,3] and Michal Ciborowski[1*]

[1]Clinical Research Center, Medical University of Bialystok, Bialystok, Poland, [2]Department of Ophthalmology, Medical University of Bialystok, Bialystok, Poland, [3]Department of Endocrinology, Diabetology and Internal Medicine, Medical University of Bialystok, Bialystok, Poland

**Aims:** Interocular comparison of the metabolomic signature of aqueous humor (AH) was performed. The aim of the study was to quantitatively evaluate the symmetry in concentrations of various metabolites belonging to different categories.

**Methods:** The study included AH samples from 23 patients, 74.17 ± 11.52 years old, undergoing simultaneous bilateral cataract surgery at the Ophthalmology Department of the Medical University of Bialystok, Poland. Liquid chromatography coupled with tandem mass spectrometry (LC-MS/MS)-based targeted metabolomics and lipidomics analyses of AH samples were performed using the AbsoluteIDQ® p180 kit. Out of 188 metabolites available in the kit, 67 were measured in the majority (>70%) of the samples: 21/21 amino acids, 10/22 biogenic amines, 9/40 acylcarnitines, 0/14 lysophosphatidylcholines, 21/76 phosphatidylcholines, 5/15 sphingolipids, and 1/1sum of hexoses.

**Results:** The comparison of both eyes revealed that the concentrations of metabolites did not differ significantly ($p < 0.05$) except for taurine ($p = 0.037$). There was moderate-to-strong positive interocular correlation ($r > 0.5$) between most metabolites regarding concentration. This was confirmed by the high intraclass correlation coefficient (ICC) values of different levels, which varied for the different metabolites. However, there were exceptions. Correlations were not significant for 2 acylcarnitines (tiglylcarnitine and decadienylcarnitine) and 3 glycerophospholipids (PC aa C32:3, PC aa C40:2, and PC aa C40:5).

**Conclusion:** With a few exceptions, a single eye was found to be representative of the fellow eye in terms of the concentration of most of the analyzed metabolites. The degree of intraindividual variability in the AH of fellow eyes differs for particular metabolites/metabolite categories.

KEYWORDS

**ophthalmology (MeSH), symmetry, aqueous humor (AH), mass spectrometry, LC-MS/MS, metabolomics (OMICS)**

# 1 Introduction

Although eyes are paired organs, numerous anatomic asymmetries have been described, even in ophthalmically healthy patients (Cameron et al., 2017). Asymmetry has been demonstrated, e.g., for intraocular pressure, axial length, corneal, optic nerve head, and retinal parameters (Li et al., 2013; Hwang et al., 2014; Jacobsen et al., 2015; Linderman et al., 2018; Baniasadi et al., 2020; Jiang et al., 2021; Albarrán-Diego et al., 2022; Song and Hwang, 2022).

Aqueous humor (AH) is produced by the ciliary body, a part of the uveal tract. Although no studies evaluating the interocular symmetry of the ciliary body are available, another constituent of the uveal tract, choroid, has been investigated extensively. Choroidal differences exist between normal fellow eyes in adults, i.e., in the absence of obvious pathology (Yang et al., 2016; Kim et al., 2021; Lu et al., 2022). Consequently, one may expect that the metabolomic profile of AH may differ between fellow eyes.

Metabolomics is the complex assessment of metabolites, small molecules, lipids, and carbohydrates, among others (Pietrowska et al., 2017; Pietrowska et al., 2018a). It facilitates knowledge about physiology and pathophysiology as well as biomarkers of occurrence, type and stage of disease, and response to treatment. It thus allows the identification of disturbed metabolic pathways. One of the advantages of metabolomics is its close relation with phenotype (Kell et al., 2005). The identification of sources of bias is of the utmost importance for proper research planning and the interpretation of results. Biological variability due to exogenic and endogenic factors is one such source of bias (Crews et al., 2009; Kim et al., 2014). It is therefore important to know whether clinically relevant differences between both eyes can be expected. Previous reports on the biological variability of other fluids, e.g., serum, plasma, urine, and cerebrospinal fluid are available (Crews et al., 2009; Kim et al., 2014). However, they are not transferable to AH due to differences in their composition. To date, there have been no reports on the within-subject variability of AH collected at the same time. Our study aims to address this gap.

Metabolomics is a young and dynamic discipline that is attracting growing attention in ophthalmic research. The AH metabolomic profiles are altered in ophthalmic and systemic diseases, e.g., glaucoma, pseudoexfoliation syndrome, diabetic eye disease, and myopia, among others (Pietrowska et al., 2018b; Buisset et al., 2019; Myer et al., 2020a; Myer et al., 2020b; Dmuchowska et al., 2020; Grochowski et al., 2020; Dmuchowska et al., 2021a). However, there are still ambiguities, including the issue of biological variability. Some studies have included one eye of an individual, selected randomly or according to disease severity. However, the laterality of the included eyes may have affected the results. Consequently, the question arises whether one eye is representative for the other eye of the same patient in terms of AH metabolomics signatures. The detection of asymmetry may support proper study planning and interpretation. Furthermore, it might facilitate personalized medicine and indicate the need for further assessment of potential local factors (e.g., blood supply) that may play a significant role and would need to be taken into account in future studies.

The aim of the study is to quantitatively evaluate the symmetry of concentrations of various metabolites belonging to different categories. This targeted metabolomics and lipidomics study compares the AH composition between fellow eyes of the same patients. To the best of our knowledge, the current investigation presents the first report on interocular comparison of the metabolomic signature of AH.

# 2 Materials and methods

## 2.1 Study participants and sample collection

The study included AH samples from 23 patients undergoing simultaneous bilateral cataract surgery (SBCS) at the Ophthalmology Department of the Medical University of Bialystok, Poland, from 21 January 2021 to 02 December 2021 (Dmuchowska et al., 2021b). The systemic comorbidities and medications used are presented in Supplementary Table S1. The following were criteria for exclusion from the study: the presence of concomitant ocular disorders except for cataract, history of surgery or trauma, and/or diabetes mellitus.

All patients underwent a standard preoperative procedure. At 20 min before the surgery, they simultaneously and bilaterally received topical application of the following: proxymetacaine hydrochloride, tropicamide, phenylephrine, levofloxacin, diclofenac, and timolol. One hour before the surgery, the patients received oral hydroxyzine for mild sedation. Standard disinfection with 5% ophthalmic povidone iodine was implemented 2 min before beginning the procedure. Before cataract extraction, the anterior chamber of the eye was punctured using a 30 G needle; approximately 50–100 µL of AH was aspirated, transferred to Eppendorf tubes (Eppendorf, Hamburg, Germany), frozen, and stored at −80°C until the analysis. The surgeries were performed in the morning from 8 a.m. to 12 p.m., with a timespan of within 15–20 min between fellow eyes of the same patients.

## 2.2 Metabolomics analysis

The targeted metabolomics analysis of AH samples was performed using liquid chromatography coupled with tandem mass spectrometry (6470 LC–MS/MS, Agilent Technologies, Santa Clara, California, United States), applying the methodology and reagents included in the AbsoluteIDQ® p180 kit (Biocrates Life Sciences AG, Innsbruck, Austria). This commercially available kit allows the quantitative measurement of 188 metabolites: 21 amino acids, 22 biogenic amines, 40 acylcarnitines, 14 lysophosphatidylcholines, 76 phosphatidylcholines, 15 sphingolipids, and the sum of hexoses. The sample preparation was performed according to the Kit User Manual, which has already been described in the literature (Sawicka-Smiarowska et al., 2021), with minor modifications. The sample volume used for the analysis was optimized (unpublished data, 2022), and 30 µL of AH sample was used, instead of 10 µL recommended by the manufacturer for plasma/serum.

Spectral data processing and quantification were conducted using MetIDQ software (version Oxygen DB110-3005-290, Biocrates, Life Science AG, Innsbruck, Austria). The performance of the analytical assay was evaluated by analyzing quality control

**TABLE 1 Baseline patient characteristics.**

| Characteristics | Value |
|---|---|
| Number of patients | 23 |
| Age, years, mean ± SD (years) | 74.17 ± 11.52 |
| Sex, female, n (%) | 13 (56.5) |
| BMI, mean ± SD | 27.99 ± 5.45 |
| AXL, right eye, mm, median (Q1; Q3) | 23.07 (22.56; 23.88) |
| AXL, left eye, mm, median (Q1; Q3) | 23.01 (22.49; 23.82) |

BMI, body mass index; AXL, axial length.

(QC) samples at three concentration levels, where the middle level (QC2) was injected three times. After normalizing the data based on the QC samples, metabolites with a coefficient of variation (CV) higher than 30% in the QC samples were excluded. Primarily, the data below the limit of detection (LOD) were treated as missing. Additional filtering was performed to retain metabolites detected in at least 70% of the samples. Subsequently, missing values were replaced with concentrations obtained based on the calibration curves but located below the lowest concentration point on the calibration curve. All obtained concentrations were divided by three to take into account higher sample volume used. Finally, a data matrix consisting of concentrations of 67 metabolites was forwarded for statistical analysis.

## 2.3 Statistical analysis

Statistical analysis was carried out using R software, version 4.0.5. For each metabolite, calculations of Spearman's correlation coefficient and for paired Wilcoxon test between concentrations for both eyes were conducted. Chan YH has provided the following suggestion for interpreting Spearman's correlation coefficient (r rho): >0.5 or ≤ 0.5, moderate to strong; −0.3 to 0.3, poor; in between, fair correlation (Chan, 2003). For the Wilcoxon test, both non-adjusted and adjusted *p*-values are presented (based on the Benjamini–Hochberg correction for multiple comparisons). The interclass correlation coefficient (ICC) was calculated for each metabolite between two eyes, assuming a two-way model and absolute agreement. Koo and Li have provided the following suggestion for interpreting ICC: < 0.50, poor; 0.50–0.75, moderate; 0.75–0.90, good; and >0.90, excellent (Koo and Li, 2016). In addition, the relative mean difference was calculated as left eye minus right eye divided by the average concentration in two eyes. Linear regression analysis was used to verify the relationship between certain metabolites and clinical parameters (age, sex, body mass index (BMI), and axial length (AXL)). All calculations were based on a significance level of 0.05.

SIMCA−P + 13.0.3.0 (Umetrics, Umeå, Sweden) was used for multivariate statistical analysis. It was not possible to build appropriate quality orthogonal partial least squares-discriminant analysis (OPLS-DA) models discriminating left eye from right one based on their metabolic profiles.

# 3 Results

The demographic and clinical data are presented in Table 1. As the metabolomic signatures of both eyes were analyzed from the same patients, the demographic and systemic factors remained the same. There was no statistical difference in axial length ($p = 0.818$) between fellow eyes.

Overall, 67 of 188 metabolites fulfilled the criteria for inclusion based on the cutoff levels of CV and LOD: 21/21 amino acids, 10/22 biogenic amines, 9/40 acylcarnitines, 0/14 lysophosphatidylcholines, 21/76 phosphatidylcholines, 5/15 sphingolipids, and 1/1 sum of hexoses.

Table 2 presents the mean concentration values and relative mean difference between both eyes.

After the application of Benjamini–Hochberg correction, the comparison of both eyes with Wilcoxon tests revealed that the concentrations of metabolites, except for taurine, did not differ significantly (Table 3). In general, there was a moderate-to-strong positive interocular correlation (r > 0.5) for most of the metabolites. This was confirmed with ICC values of different levels, which were variable throughout different metabolites. However, there were exceptions: correlations were not significant for 2 acylcarnitines (C5:1 and C10:2) and 3 glycerophospholipids (PC aa C32:3, PC aa C40:2, and PC aa C40:5).

We investigated the following clinical factors for association with these five metabolites: age, sex, body mass index (BMI), and axial length (AXL) (Table 4). Only BMI was found to be associated with C5:1 ($p = 0.008$).

Although the taurine concentration differed significantly between fellow eyes and was found lower in the left eye of only four patients (Figures 1, 2), there was a linear relation (as visualized in Figure 2) with a good ICC (0.861 $CI_{95}$ [0.478–0.952]) and strong correlation (r = 0.89, $p < 0.001$).

# 4 Discussion

The partial anatomical asymmetry of both eyes has been described in the literature (Li et al., 2013; Hwang et al., 2014; Jacobsen et al., 2015; Yang et al., 2016; Cameron et al., 2017; Linderman et al., 2018; Baniasadi et al., 2020; Jiang et al., 2021; Kim et al., 2021; Albarrán-Diego et al., 2022; Lu et al., 2022; Song and Hwang, 2022). We investigated whether this extrapolates to the AH metabolomic composition. The aim of the study was to determine whether concentrations of various metabolites in one eye are representative of the fellow eye of the same patient.

In general, there were minimal interocular differences and substantial interocular correlation in most of the studied metabolites. However, we found some differences between both eyes. We demonstrated interocular asymmetry, though with high correlation, for concentrations of taurine. Taurine is an aminosulfonic acid that plays a role in several intracellular biological processes, including osmoregulation, antioxidation, and retinal development (Ripps and Shen, 2012). The retina is the most taurine-rich organ in the body, containing more taurine than any other amino acid (Castelli et al., 2021). People following vegetarian

**TABLE 2 Metabolite concentration values in fellow eyes.**

| Metabolite category | Metabolite name[a] | Eyes with metabolite concentration above LOD (%) | Mean concentration±SD in right eye [μM] | Mean concentration±SD in left eye [μM] | Relative mean difference (%) between fellow eyes | Coefficient of variation for QC2 |
|---|---|---|---|---|---|---|
| Acylcarnitines | C0 | 100.0 | 17.009 ± 5.352 | 17.149 ± 5.226 | 0.8 | 7.3 |
| | C2 | 100.0 | 4.208 ± 1.266 | 4.174 ± 1.193 | −0.8 | 9.8 |
| | C3 | 100.0 | 0.432 ± 0.246 | 0.448 ± 0.240 | 3.6 | 6.03 |
| | C3-DC (C4-OH) | 84.8 | 0.021 ± 0.007 | 0.021 ± 0.007 | 0.8 | 7.9 |
| | C4 | 100.0 | 0.129 ± 0.041 | 0.136 ± 0.044 | 5.9 | 7.9 |
| | C5 | 100.0 | 0.143 ± 0.048 | 0.150 ± 0.051 | 4.7 | 7.7 |
| | C5-OH (C3-DC-M) | 97.8 | 0.031 ± 0.007 | 0.032 ± 0.010 | 4.5 | 9.9 |
| | C5:1 | 89.1 | 0.015 ± 0.010 | 0.015 ± 0.009 | −3.0 | 13.4 |
| | C10:2 | 89.1 | 0.031 ± 0.009 | 0.029 ± 0.006 | −6.3 | 27.0 |
| Aminoacids | Ala | 100.0 | 405.507 ± 117.704 | 425.304 ± 124.295 | 4.8 | 4.4 |
| | Arg | 100.0 | 108.304 ± 27.027 | 111.536 ± 26.590 | 2.9 | 10.2 |
| | Asn | 100.0 | 36.275 ± 6.141 | 37.268 ± 6.595 | 2.7 | 3.5 |
| | Asp | 100.0 | 3.153 ± 1.461 | 3.806 ± 2.040 | 18.8 | 2.2 |
| | Cit | 100.0 | 4.942 ± 1.723 | 4.996 ± 1.803 | 1.1 | 4.3 |
| | Gln | 100.0 | 830.638 ± 106.162 | 848.333 ± 124.914 | 2.1 | 7.5 |
| | Glu | 100.0 | 10.390 ± 4.624 | 11.655 ± 5.516 | 11.5 | 6.02 |
| | Gly | 100.0 | 35.270 ± 18.793 | 37.725 ± 20.386 | 6.7 | 8.2 |
| | His | 100.0 | 76.246 ± 13.773 | 78.449 ± 12.471 | 2.9 | 9.7 |
| | Ile | 100.0 | 70.725 ± 22.952 | 73.319 ± 23.170 | 3.6 | 9.3 |
| | Leu | 100.0 | 161.957 ± 38.741 | 167.768 ± 36.503 | 3.5 | 8.9 |
| | Lys | 100.0 | 177.449 ± 26.257 | 186.232 ± 21.099 | 4.8 | 9.9 |
| | Met | 100.0 | 35.342 ± 5.680 | 36.412 ± 5.666 | 3.0 | 8.9 |
| | Orn | 100.0 | 27.881 ± 8.664 | 28.735 ± 8.760 | 3.0 | 10.3 |
| | Phe | 100.0 | 108.609 ± 19.193 | 112.507 ± 16.839 | 3.5 | 8.4 |
| | Pro | 100.0 | 50.878 ± 23.456 | 53.620 ± 26.263 | 5.3 | 7.2 |
| | Ser | 100.0 | 201.681 ± 46.241 | 204.536 ± 38.421 | 1.4 | 8.4 |
| | Thr | 100.0 | 125.116 ± 27.449 | 127.826 ± 28.299 | 2.1 | 5.0 |
| | Trp | 100.0 | 30.839 ± 4.088 | 31.946 ± 5.184 | 3.5 | 9.1 |
| | Tyr | 100.0 | 96.000 ± 12.242 | 99.913 ± 14.891 | 4.0 | 9.4 |
| | Val | 100.0 | 275.348 ± 59.049 | 285.710 ± 52.170 | 3.7 | 10.0 |
| Biogenic Amines | ADMA | 100.0 | 0.539 ± 0.114 | 0.548 ± 0.113 | 1.6 | 5.6 |
| | alpha-AAA | 100.0 | 1.814 ± 0.579 | 1.705 ± 0.542 | −6.2 | 12.2 |
| | Carnosine | 100.0 | 0.026 ± 0.033 | 0.027 ± 0.030 | 4.3 | 10.5 |
| | Creatinine | 100.0 | 53.261 ± 18.331 | 53.604 ± 19.004 | 0.6 | 3.8 |
| | Kynurenine | 100.0 | 0.948 ± 0.198 | 0.973 ± 0.241 | 2.6 | 8.9 |

(Continued on following page)

**TABLE 2 (*Continued*) Metabolite concentration values in fellow eyes.**

| Metabolite category | Metabolite name[a] | Eyes with metabolite concentration above LOD (%) | Mean concentration±SD in right eye [μM] | Mean concentration±SD in left eye [μM] | Relative mean difference (%) between fellow eyes | Coefficient of variation for QC2 |
|---|---|---|---|---|---|---|
| | Met-SO | 100.0 | 0.533 ± 0.164 | 0.535 ± 0.176 | 0.3 | 11.02 |
| | Putrescine | 100.0 | 0.155 ± 0.051 | 0.160 ± 0.047 | 3.5 | 5.6 |
| | SDMA | 100.0 | 0.501 ± 0.158 | 0.507 ± 0.171 | 1.3 | 6.5 |
| | t4-OH-Pro | 100.0 | 5.038 ± 3.050 | 5.207 ± 2.820 | 3.3 | 8.1 |
| | Taurine | 100.0 | 65.652 ± 25.612 | 75.319 ± 29.669 | 13.7 | 5.9 |
| Glycerophospholipids | PC aa C32:0 | 97.8 | 0.036 ± 0.028 | 0.038 ± 0.044 | 6.7 | 6.4 |
| | PC aa C32:1 | 80.4 | 0.021 ± 0.016 | 0.021 ± 0.021 | 1.5 | 8.5 |
| | PC aa C32:3 | 71.7 | 0.001 ± 0.001 | 0.001 ± 0.001 | 13.1 | 18.2 |
| | PC aa C34:1 | 100.0 | 0.264 ± 0.209 | 0.258 ± 0.302 | −2.2 | 7.03 |
| | PC aa C34:2 | 87.0 | 0.135 ± 0.118 | 0.124 ± 0.158 | −8.7 | 8.03 |
| | PC aa C36:1 | 100.0 | 0.068 ± 0.054 | 0.067 ± 0.078 | −1.2 | 9.8 |
| | PC aa C36:3 | 76.1 | 0.058 ± 0.053 | 0.054 ± 0.076 | −6.9 | 8.02 |
| | PC aa C36:4 | 95.7 | 0.086 ± 0.080 | 0.089 ± 0.126 | 2.6 | 9.1 |
| | PC aa C38:3 | 89.1 | 0.032 ± 0.033 | 0.030 ± 0.041 | −5.4 | 7.0 |
| | PC aa C38:4 | 73.9 | 0.077 ± 0.079 | 0.075 ± 0.102 | −3.7 | 8.7 |
| | PC aa C38:5 | 73.9 | 0.030 ± 0.029 | 0.028 ± 0.042 | −6.4 | 8.5 |
| | PC aa C38:6 | 73.9 | 0.036 ± 0.037 | 0.036 ± 0.051 | −1.4 | 7.3 |
| | PC aa C40:2 | 76.1 | 0.001 ± 0.001 | 0.001 ± 0.001 | 23.1 | 5.7 |
| | PC aa C40:5 | 76.1 | 0.007 ± 0.007 | 0.007 ± 0.009 | 3.6 | 10.03 |
| | PC aa C40:6 | 82.6 | 0.032 ± 0.022 | 0.032 ± 0.035 | 0.1 | 8.0 |
| | PC ae C34:1 | 97.8 | 0.013 ± 0.014 | 0.013 ± 0.018 | 0.1 | 8.2 |
| | PC ae C36:3 | 89.1 | 0.005 ± 0.006 | 0.006 ± 0.010 | 3.4 | 7.9 |
| | PC ae C36:4 | 73.9 | 0.021 ± 0.018 | 0.019 ± 0.022 | −11.1 | 6.4 |
| | PC ae C36:5 | 71.7 | 0.010 ± 0.011 | 0.010 ± 0.018 | 2.1 | 9.7 |
| | PC ae C38:4 | 76.1 | 0.012 ± 0.014 | 0.010 ± 0.020 | −13.2 | 8.3 |
| | PC ae C40:5 | 91.3 | 0.003 ± 0.003 | 0.003 ± 0.004 | 23.2 | 7.0 |
| Sphingolipids | SM C16:0 | 73.9 | 0.146 ± 0.148 | 0.143 ± 0.214 | −2.4 | 9.9 |
| | SM C16:1 | 97.8 | 0.025 ± 0.019 | 0.024 ± 0.026 | −1.8 | 10.2 |
| | SM C18:0 | 71.7 | 0.053 ± 0.051 | 0.055 ± 0.079 | 4.5 | 10.6 |
| | SM C18:1 | 95.7 | 0.032 ± 0.032 | 0.030 ± 0.034 | −8.5 | 9.9 |
| | SM C24:1 | 71.7 | 0.076 ± 0.088 | 0.078 ± 0.130 | 2.5 | 12.6 |
| Sugars | H1 | 100.0 | 4,045.594 ± 2,514.684 | 3,940.290 ± 2,260.815 | −2.6 | 9.8 |

[a]The full list of individual metabolites is available at https://biocrates.com/wp-content/uploads/2022/02/biocrates-p180-list-of-metabolites-v2-2021.pdf (accessed 30 October 2022).
LOD, limit of detection; QC, quality control.

or vegan diets have been shown to have lower levels of taurine in their plasma (Laidlaw et al., 1988). However, this would not explain the interocular difference.

On the other hand, correlations were not significant but the concentrations were comparable for two acylcarnitines (C5: 1 and C10: 2) and three glycerophospholipids (PC aa C32: 3, PC aa C40: 2,

**TABLE 3 Comparison of metabolite concentrations between fellow eyes.**

| Metabolite category | Metabolite name[a] | Eyes with metabolite concentration above LOD (%) | ICC between both eyes | | Correlation between both eyes | | *p*-value of WILCOXON test | |
|---|---|---|---|---|---|---|---|---|
| | | | ICC | 95% CI | r | p[b] | Without correction for multiple comparisons | With BENJAMINI–HOCHBERG correction for multiple comparisons |
| Acylkarnitines | C0 | 100.0 | 0.928 | 0.838–0.969 | 0.93 | **<0.001** | 0.6 | 0.7 |
| | C2 | 100.0 | 0.927 | 0.837–0.969 | 0.87 | **<0.001** | 0.8 | 0.9 |
| | C3 | 100.0 | 0.974 | 0.941–0.989 | 0.95 | **<0.001** | 0.2 | 0.6 |
| | C3-DC (C4-OH) | 84.8 | 0.650 | 0.328–0.836 | 0.59 | **0.003** | 0.7 | 0.8 |
| | C4 | 100.0 | 0.904 | 0.772–0.960 | 0.94 | **<0.001** | 0.02 | 0.3 |
| | C5 | 100.0 | 0.867 | 0.715–0.941 | 0.83 | **<0.001** | 0.3 | 0.6 |
| | C5-OH (C3-DC-M) | 97.8 | 0.653 | 0.344–0.836 | 0.58 | **0.004** | 0.3 | 0.6 |
| | C5:1 | 89.1 | 0.085 | 0.259–0.344 | −0.10 | 0.639 | 0.9 | 0.9 |
| | C10:2 | 89.1 | 0.350 | −0.057-0.659 | 0.36 | 0.095 | 0.3 | 0.6 |
| Aminoacids | Ala | 100.0 | 0.941 | 0.840–0.976 | 0.88 | **<0.001** | 0.04 | 0.5 |
| | Arg | 100.0 | 0.855 | 0.692–0.935 | 0.81 | **<0.001** | 0.4 | 0.6 |
| | Asn | 100.0 | 0.870 | 0.719–0.943 | 0.87 | **<0.001** | 0.2 | 0.6 |
| | Asp | 100.0 | 0.750 | 0.432–0.893 | 0.77 | **<0.001** | 0.01 | 0.2 |
| | Cit | 100.0 | 0.958 | 0.905–0.982 | 0.96 | **<0.001** | 0.8 | 0.9 |
| | Gln | 100.0 | 0.709 | 0.432–0.865 | 0.60 | **0.003** | 0.3 | 0.6 |
| | Glu | 100.0 | 0.896 | 0.694–0.960 | 0.95 | **<0.001** | 0.006 | 0.2 |
| | Gly | 100.0 | 0.928 | 0.836–0.969 | 0.89 | **<0.001** | 0.1 | 0.6 |
| | His | 100.0 | 0.784 | 0.562–0.902 | 0.68 | **<0.001** | 0.3 | 0.6 |
| | Ile | 100.0 | 0.910 | 0.803–0.961 | 0.88 | **<0.001** | 0.3 | 0.6 |
| | Leu | 100.0 | 0.806 | 0.600–0.912 | 0.78 | **<0.001** | 0.3 | 0.6 |
| | Lys | 100.0 | 0.475 | 0.108–0.733 | 0.45 | **0.03** | 0.1 | 0.6 |
| | Met | 100.0 | 0.653 | 0.344–0.835 | 0.56 | **0.006** | 0.5 | 0.6 |
| | Orn | 100.0 | 0.901 | 0.785–0.957 | 0.93 | **<0.001** | 0.4 | 0.6 |
| | Phe | 100.0 | 0.648 | 0.339–0.832 | 0.42 | **0.05** | 0.5 | 0.6 |
| | Pro | 100.0 | 0.953 | 0.889–0.980 | 0.89 | **<0.001** | 0.1 | 0.6 |
| | Ser | 100.0 | 0.812 | 0.607–0.916 | 0.87 | **<0.001** | 0.5 | 0.7 |
| | Thr | 100.0 | 0.926 | 0.836–0.968 | 0.93 | **<0.001** | 0.4 | 0.6 |
| | Trp | 100.0 | 0.548 | 0.195–0.778 | 0.57 | **0.004** | 0.6 | 0.7 |
| | Tyr | 100.0 | 0.519 | 0.159–0.760 | 0.62 | **0.002** | 0.3 | 0.6 |
| | Val | 100.0 | 0.790 | 0.571–0.905 | 0.73 | **<0.001** | 0.4 | 0.6 |
| Biogenic Amines | ADMA | 100.0 | 0.921 | 0.824–0.965 | 0.87 | **<0.001** | 0.6 | 0.7 |
| | alpha-AAA | 100.0 | 0.688 | 0.400–0.853 | 0.60 | **0.003** | 0.2 | 0.6 |
| | Carnosine | 100.0 | 0.976 | 0.944–0.990 | 0.92 | **<0.001** | 0.4 | 0.6 |

(Continued on following page)

**TABLE 3 (*Continued*) Comparison of metabolite concentrations between fellow eyes.**

| Metabolite category | Metabolite name[a] | Eyes with metabolite concentration above LOD (%) | ICC between both eyes | | Correlation between both eyes | | *p*-value of WILCOXON test | |
|---|---|---|---|---|---|---|---|---|
| | | | ICC | 95% CI | r | p[b] | Without correction for multiple comparisons | With BENJAMINI–HOCHBERG correction for multiple comparisons |
| | Creatinine | 100.0 | 0.987 | 0.970–0.994 | 0.97 | **<0.001** | 0.7 | 0.8 |
| | Kynurenine | 100.0 | 0.744 | 0.487–0.882 | 0.80 | **<0.001** | 0.3 | 0.6 |
| | Met-SO | 100.0 | 0.651 | 0.329–0.836 | 0.78 | **<0.001** | 0.4 | 0.6 |
| | Putrescine | 100.0 | 0.895 | 0.772–0.954 | 0.88 | **<0.001** | 0.3 | 0.6 |
| | SDMA | 100.0 | 0.964 | 0.917–0.984 | 0.97 | **<0.001** | 1.0 | 1.0 |
| | t4-OH-Pro | 100.0 | 0.972 | 0.937–0.988 | 0.93 | **<0.001** | 0.2 | 0.6 |
| | Taurine | 100.0 | 0.861 | 0.478–0.952 | 0.89 | **<0.001** | 0.001 | 0.04 |
| Glycerophospholipids | PC aa C32:0 | 97.8 | 0.770 | 0.531–0.896 | 0.77 | **<0.001** | 0.99 | 1.0 |
| | PC aa C32:1 | 80.4 | 0.763 | 0.515–0.892 | 0.77 | **<0.001** | 0.97 | 1.0 |
| | PC aa C32:3 | 71.7 | 0.154 | 0.126–0.280 | −0.11 | 0.6 | 0.7 | 0.8 |
| | PC aa C34:1 | 100.0 | 0.778 | 0.542–0.900 | 0.75 | **<0.001** | 0.2 | 0.6 |
| | PC aa C34:2 | 87.0 | 0.576 | 0.218–0.796 | 0.54 | **0.007** | 0.09 | 0.6 |
| | PC aa C36:1 | 100.0 | 0.828 | 0.634–0.923 | 0.75 | **<0.001** | 0.4 | 0.6 |
| | PC aa C36:3 | 76.1 | 0.623 | 0.287–0.821 | 0.60 | **0.003** | 0.05 | 0.5 |
| | PC aa C36:4 | 95.7 | 0.342 | −0.087-0.660 | 0.52 | **0.01** | 0.2 | 0.6 |
| | PC aa C38:3 | 89.1 | 0.602 | 0.256–0.810 | 0.52 | **0.010** | 0.5 | 0.6 |
| | PC aa C38:4 | 73.9 | 0.631 | 0.298–0.826 | 0.61 | **0.002** | 0.4 | 0.6 |
| | PC aa C38:5 | 73.9 | 0.510 | 0.124–0.760 | 0.65 | **0.001** | 0.1 | 0.6 |
| | PC aa C38:6 | 73.9 | 0.466 | 0.065–0.735 | 0.63 | **0.001** | 0.06 | 0.5 |
| | PC aa C40:2 | 76.1 | 0.053 | −0.359-0.448 | −0.001 | >0.9 | 0.6 | 0.7 |
| | PC aa C40:5 | 76.1 | 0.680 | 0.376–0.851 | 0.36 | 0.09 | 0.7 | 0.9 |
| | PC aa C40:6 | 82.6 | 0.669 | 0.357–0.846 | 0.70 | **<0.001** | 0.3 | 0.6 |
| | PC ae C34:1 | 97.8 | 0.853 | 0.683–0.935 | 0.50 | **0.02** | 0.8 | 0.9 |
| | PC ae C36:3 | 89.1 | 0.640 | 0.312–0.831 | 0.43 | **0.04** | 0.8 | 0.9 |
| | PC ae C36:4 | 73.9 | 0.820 | 0.626–0.919 | 0.44 | **0.04** | 0.2 | 0.6 |
| | PC ae C36:5 | 71.7 | 0.773 | 0.534–0.897 | 0.55 | **0.006** | 0.3 | 0.6 |
| | PC ae C38:4 | 76.1 | 0.759 | 0.513–0.890 | 0.59 | **0.003** | 0.08 | 0.6 |
| | PC ae C40:5 | 91.3 | 0.681 | 0.389–0.850 | 0.48 | **0.02** | 0.4 | 0.6 |
| Sphingolipids | SM C16:0 | 73.9 | 0.804 | 0.590–0.912 | 0.68 | **0.001** | 0.07 | 0.6 |
| | SM C16:1 | 97.8 | 0.780 | 0.545–0.900 | 0.57 | **0.004** | 0.4 | 0.6 |
| | SM C18:0 | 71.7 | 0.760 | 0.511–0.891 | 0.63 | **0.001** | 0.3 | 0.6 |

(Continued on following page)

**TABLE 3 (*Continued*) Comparison of metabolite concentrations between fellow eyes.**

| Metabolite category | Metabolite name[a] | Eyes with metabolite concentration above LOD (%) | ICC between both eyes | | Correlation between both eyes | | *p*-value of WILCOXON test | |
|---|---|---|---|---|---|---|---|---|
| | | | ICC | 95% CI | r | p[b] | Without correction for multiple comparisons | With BENJAMINI–HOCHBERG correction for multiple comparisons |
| | SM C18:1 | 95.7 | 0.852 | 0.686–0.934 | 0.66 | **0.001** | 0.3 | 0.6 |
| | SM C24:1 | 71.7 | 0.814 | 0.608–0.917 | 0.75 | **<0.001** | 0.2 | 0.6 |
| Sugars | H1 | 100.0 | 0.971 | 0.934–0.988 | 0.89 | **<0.001** | 0.6 | 0.7 |

[a]The full list of individual metabolites is available at https://biocrates.com/wp-content/uploads/2022/02/biocrates-p180-list-of-metabolites-v2-2021.pdf (accessed 30 October 2022).
[b]$p < 0.05$ in bold.
LOD, limit of detection; ICC, interclass correlation coefficient; CI, confidence interval; r rho Spearman correlation coefficient.

**TABLE 4 Effect of age, sex, BMI, and AXL on interocular differences (right eye–left eye) on selected metabolites.**

| Characteristics | C5: 1[a] | | C10: 2 | | PC aa C32: 3 | | PC aa C40: 2 | | PC aa C40: 5 | |
|---|---|---|---|---|---|---|---|---|---|---|
| | β (SE) | p[b] | β (SE) | p | β (SE) | p | β (SE) | p | β (SE) | p |
| Age, years | 0.0003 (0.0004) | 0.5 | −0.0003 (0.0003) | 0.2 | −0.0001 (0.0001) | 0.2 | 0.00001 (0.00004) | 0.9 | 0.0001 (0.0003) | 0.9 |
| Sex, female | 0.002 (0.006) | 0.7 | −0.0003 (0.004) | 0.9 | 0.001 (0.001) | 0.3 | −0.001 (0.001) | 0.3 | −0.002 (0.003) | 0.6 |
| BMI | **−0.001 (0.001)** | **0.008**[b] | −0.0003 (0.0003) | 0.4 | 0.0001 (0.0001) | 0.2 | −0.00001 (0.0001) | 0.9 | −0.0001 (0.0003) | 0.7 |
| AXL, right eye, mm | −0.003 (0.003) | 0.3 | −0.002 (0.002) | 0.3 | −0.0002 (0.0004) | 0.6 | −0.00002 (0.0003) | 0.9 | 0.001 (0.002) | 0.5 |
| AXL, left eye, mm | −0.001 (0.003) | 0.6 | −0.0009 (0.002) | 0.6 | 0.00001 (0.0003) | 1.0 | −0.0001 (0.0002) | 0.6 | 0.001 (0.001) | 0.4 |

Linear regression analysis. β beta coefficient, SE, standard error; BMI, body mass index; AXL, axial length.
[a]The full list of individual metabolites is available at https://biocrates.com/wp-content/uploads/2022/02/biocrates-p180-list-of-metabolites-v2-2021.pdf (accessed 30 October 2022).
[b]$p < 0.05$ in bold.

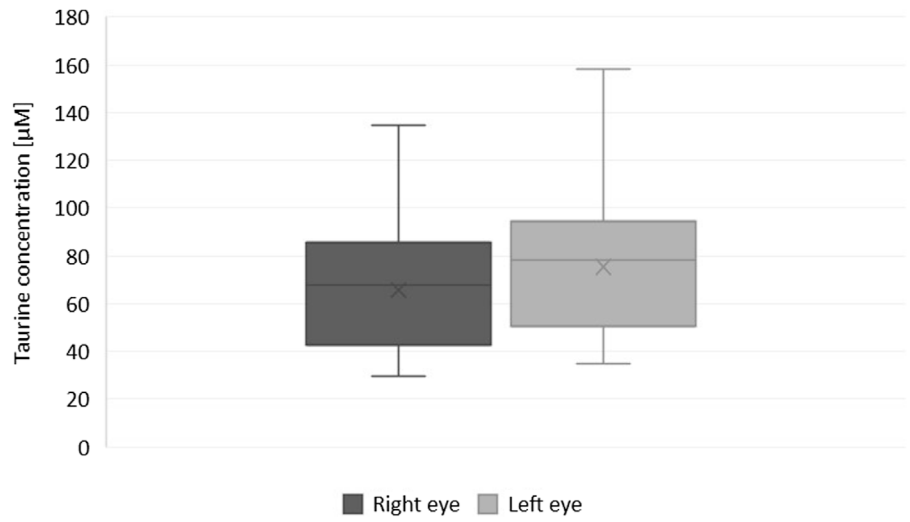


FIGURE 1
Box and whisker plot showing differences in the concentration of taurine in fellow eyes (Wilcoxon test with Benjamini–Hochberg correction for multiple comparisons, $p = 0.037$).

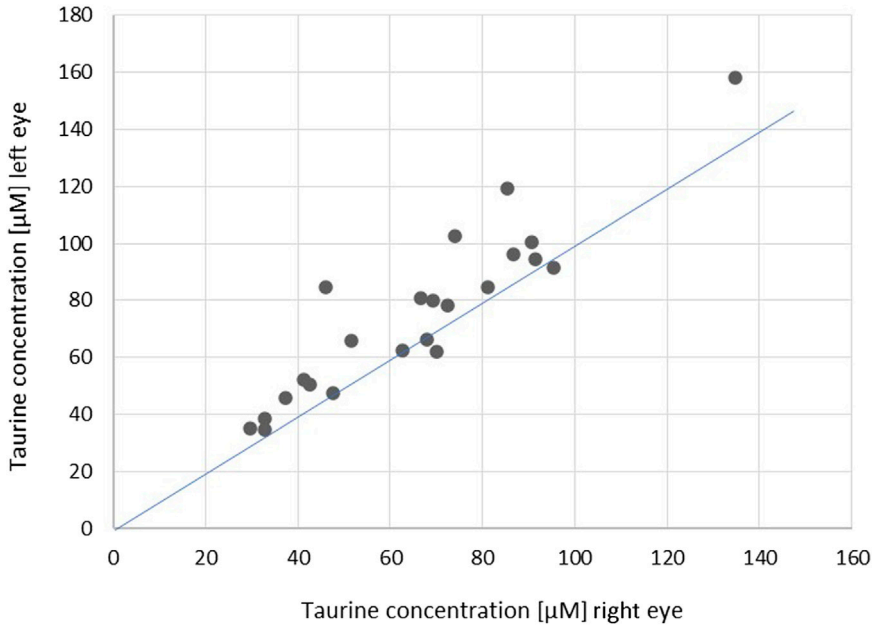


FIGURE 2
Scatterplot showing correlations of the concentration of taurine in fellow eyes (r = 0.89, $p < 0.001$; ICC = 0.861 [0.478–0.952]). The blue line indicates the theoretical perfect interocular agreement of concentrations.

and PC aa C40: 5). Using regression analysis, we tested their association with clinical factors (age, sex, BMI, and AXL). Except for the association of C5: 1 with BMI, no other relations were confirmed.

The general role of acylcarnitines is to transport acyl groups (organic acids and fatty acids) from the cytoplasm into the mitochondria so they can be broken down to produce energy. This process is known as beta-oxidation. C5: 1 is a member of the most abundant group of carnitines in the body, comprising more than 50% of all acylcarnitines quantified in tissues and biofluids (Makarova et al., 2019). Glycerophospholipids (including phosphatidylcholine) are the main component of biological membranes.

We speculate that the asymmetry of these six metabolites could be due to different rates of either production or metabolism. In contrast to this locally based hypothesis, the asymmetry in the anatomy is worth noting. Lu et al., who assessed the asymmetry of choroidal thickness, suspected that it can be attributed to asymmetrical choroidal blood flow. This may result from an anatomical asymmetry of the aortic arch and common carotid arteries, as well as from the variable anatomy of ciliary arteries and choroidal venous drainage (Lu et al., 2022). In case of two acylcarnitines and two PCs coefficient of variation calculated for the QC2 samples was higher than observed between-eyes variability (Table 2), therefore, observed variations can partly be affected by the analytical variability.

According to Cameron et al., researchers should avoid the potential pitfall of forcing an expectation of symmetry on paired structures, and clinicians should be aware of both the benefits and limitations in extrapolating single-eye data to the fellow eye in diagnosis and prognosis (Cameron et al., 2017). Based on our results, we confirm that the assumption of metabolomic symmetry of AH composition in fellow eyes should be approached with caution, as there may be asymmetry in the case of certain metabolites/metabolite categories. It is worth mentioning, that we did not observe the relationship between inter-individual variability in metabolites' concentrations and between-eyes differences in the concentrations (data not shown). Our findings may have clinical significance when planning studies and interpreting results.

The main limitation of the study is the relatively low number of participants, which were all from a single center. The use of a single ethnicity minimizes the confounding effects of ethnicity but impacts the generalizability of the results. Furthermore, only selected groups of metabolites were analyzed in the study. Due to the cross-sectional design, patients with ocular disease at a very early stage or those who will later develop ocular diseases may have been included. However, as opposed to the relatively easy collection of, e.g., blood or urine, AH can only be obtained surgically in low amounts of about 0.1 mL. Therefore, longitudinal studies are rather infeasible. Additionally, applied methodology allows measurement of only 188 specific metabolites. Untargeted metabolomics may reveal intraocular differences in other metabolites, not included in the kit used. Another limitation is the lack of information on the Lens Opacities Classification System (LOCS) grading. It would be helpful for the interpretation of our results, e.g., taurine levels. There is only the information regarding the opacified layer of the lens but with interindividual variability (cortical/nuclear/subcapsular, Supplementary Table S1. Baseline characteristics of patients). However, on the slit lamp examination the cataracts were symmetrical within the same individuals.

On the other hand applied technology allows quantification of metabolites, which would not be possible using untargeted approach. Another strength of the study is the simultaneous

analysis of a relatively high number of metabolites from different groups. Furthermore, the simultaneous collection of AH from fellow eyes is a rather unique situation. Samples obtained in such a way would make it possible to minimize the between-group impacts of genetic, dietary, lifestyle, systemic, or environmental factors, as their influence is presumably comparable on both eyes (e.g., age, BMI, sex, smoking, diet, circadian rhythms, time of year, concomitant systemic diseases, and medication) (Crews et al., 2009).

Our results may serve as a basis for future studies. An interesting direction of future research would be the analysis of intraindividual biological variability of AH in time. As the acquisition of AH is surgical, patients with bilateral delayed (not simultaneous) cataract surgery could be included. The knowledge of results from the current study would be helpful to properly interpret such findings. Our results require validation in a different cohort and for different groups of metabolites. Variable analytical methodology using a multiplatform approach would be valuable for this purpose. In addition, the correlation of metabolite concentrations in serum and AH might help in identifying metabolites whose concentrations are more locally dependent. The intraindividual variability in the metabolome between eyes of different axial lengths would be informative as well as relation to the LOCS grading.

## 5 Conclusion

On the basis of our findings, we conclude that one eye is representative of the fellow eye in terms of the concentration of most of the analyzed metabolites, with only a few exceptions.

The degree of intraindividual variability in the AH of fellow eyes differs within particular metabolites/metabolite categories.

## Data availability statement

The raw data supporting the conclusion of this article will be made available by the authors, without undue reservation.

## Ethics statement

The studies involving human participants were reviewed and approved by the Medical Ethics Committee of the Medical University of Bialystok (decisions no. R-I-002/154/2014 and R-I-002/140/2018) and conformed with the provisions of the Declaration of Helsinki. The patients/participants provided their written informed consent to participate in this study.

## Author contributions

Conceptualization: KP, DD, and MC; methodology and software: KP, DD, AG, EG, and WG; formal analysis: KP, DD, and MC; investigation: KP, DD, and AG; resources: DD, JK, AK, and MC; data curation: KP, AG, EG, and WG; writing—original draft preparation: KP, AG, and DD; writing—review and editing: JK, AK, and MC; visualization: KP, DD, MW; supervision: DD, MC. All authors have read and approved the final manuscript.

## Funding

This work was supported by the National Science Centre, Poland (grant no. 2021/05/X/NZ5/00723).

## Conflict of interest

The authors declare that the research was conducted in the absence of any commercial or financial relationships that could be construed as a potential conflict of interest.

## Publisher's note

All claims expressed in this article are solely those of the authors and do not necessarily represent those of their affiliated organizations, or those of the publisher, the editors and the reviewers. Any product that may be evaluated in this article, or claim that may be made by its manufacturer, is not guaranteed or endorsed by the publisher.

## Supplementary material

The Supplementary Material for this article can be found online at: https://www.frontiersin.org/articles/10.3389/fmolb.2023.1166182/full#supplementary-material

## References

Albarrán-Diego, C., Poyales, F., López-Artero, E., Garzón, N., and García-Montero, M. (2022). Interocular biometric parameters comparison measured with swept-source technology. *Int. Ophthalmol.* 42 (1), 239–251. doi:10.1007/s10792-021-02020-8

Baniasadi, N., Rauscher, F. G., Li, D., Wang, M., Choi, E. Y., Wang, H., et al. (2020). Norms of interocular circumpapillary retinal nerve fiber layer thickness differences at 768 retinal locations. *Transl. Vis. Sci. Technol.* 9 (9), 23. doi:10.1167/tvst.9.9.23

Buisset, A., Gohier, P., Leruez, S., Muller, J., Amati-Bonneau, P., Lenaers, G., et al. (2019). Metabolomic profiling of aqueous humor in glaucoma points to taurine and spermine deficiency: Findings from the eye-D study. *J. Proteome Res.* 18 (3), 1307–1315. doi:10.1021/acs.jproteome.8b00915

Cameron, J. R., Megaw, R. D., Tatham, A. J., McGrory, S., MacGillivray, T. J., Doubal, F. N., et al. (2017). Lateral thinking - interocular symmetry and asymmetry in neurovascular patterning, in health and disease. *Prog. Retin Eye Res.* 59, 131–157. doi:10.1016/j.preteyeres.2017.04.003

Castelli, V., Paladini, A., d'Angelo, M., Allegretti, M., Mantelli, F., Brandolini, L., et al. (2021). Taurine and oxidative stress in retinal health and disease. *CNS Neurosci. Ther.* 27 (4), 403–412. doi:10.1111/cns.13610

Chan, Y. H. (2003). Biostatistics 104: Correlational analysis. *Singap. Med. J.*44 (12), 614–619.

Crews, B., Wikoff, W. R., Patti, G. J., Woo, H. K., Kalisiak, E., Heideker, J., et al. (2009). Variability analysis of human plasma and cerebral spinal fluid reveals statistical significance of changes in mass spectrometry-based metabolomics data. *Anal. Chem.* 81 (20), 8538–8544. doi:10.1021/ac9014947

Dmuchowska, D. A., Pietrowska, K., Krasnicki, P., Grochowski, E. T., Mariak, Z., Kretowski, A., et al. (2020). *Letter to the editor:* Metabolomics of aqueous humor in diabetes mellitus. *J. Ocul. Pharmacol. Ther.* 36 (8), 580–581. doi:10.1089/jop.2020.0076

Dmuchowska, D. A., Pietrowska, K., Krasnicki, P., Kowalczyk, T., Misiura, M., Grochowski, E. T., et al. (2021a). Metabolomics reveals differences in aqueous humor composition in patients with and without pseudoexfoliation syndrome. *Front. Mol. Biosci.* 8, 682600. doi:10.3389/fmolb.2021.682600

Dmuchowska, D. A., Pieklarz, B., Konopinska, J., Mariak, Z., and Obuchowska, I. (2021b). Impact of three waves of the COVID-19 pandemic on the rate of elective cataract surgeries at a tertiary referral center: A polish perspective. *Int. J. Environ. Res. Public Health* 18 (16), 8608. doi:10.3390/ijerph18168608

Grochowski, E. T., Pietrowska, K., Kowalczyk, T., Mariak, Z., Kretowski, A., Ciborowski, M., et al. (2020). Omics in myopia. *J. Clin. Med.* 9 (11), 3464. doi:10.3390/jcm9113464

Hwang, Y. H., Song, M., Kim, Y. Y., Yeom, D. J., and Lee, J. H. (2014). Interocular symmetry of retinal nerve fibre layer thickness in healthy eyes: A spectral-domain optical coherence tomographic study. *Clin. Exp. Optom.* 97 (6), 550–554. doi:10.1111/cxo.12218

Jacobsen, A. G., Bendtsen, M. D., Vorum, H., Bøgsted, M., and Hargitai, J. (2015). Normal value ranges for central retinal thickness asymmetry in healthy caucasian adults measured by SPECTRALIS SD-OCT posterior Pole asymmetry analysis. *Invest. Ophthalmol. Vis. Sci.* 56 (6), 3875–3882. doi:10.1167/iovs.14-15663

Jiang, J. H., Pan, X. F., Lin, Z., Moonasar, N., Ye, C., Zhang, S. D., et al. (2021). Interocular asymmetry of visual field loss, intraocular pressure, and corneal parameters in primary open-angle glaucoma. *Ophthalmic Res.* 64 (5), 857–862. doi:10.1159/000510716

Kell, D. B., Brown, M., Davey, H. M., Dunn, W. B., Spasic, I., and Oliver, S. G. (2005). Metabolic footprinting and systems biology: The medium is the message. *Nat. Rev. Microbiol.* 3 (7), 557–565. doi:10.1038/nrmicro1177

Kim, K., Mall, C., Taylor, S. L., Hitchcock, S., Zhang, C., Wettersten, H. I., et al. (2014). Mealtime, temporal, and daily variability of the human urinary and plasma metabolomes in a tightly controlled environment. *PLoS One* 9 (1), e86223. doi:10.1371/journal.pone.0086223

Kim, M. S., Lim, H. B., Lee, W. H., Kim, K. M., Nam, K. Y., and Kim, J. Y. (2021). Wide-field swept-source optical coherence tomography analysis of interocular symmetry of choroidal thickness in healthy young individuals. *Invest. Ophthalmol. Vis. Sci.* 62 (3), 5. doi:10.1167/iovs.62.3.5

Koo, T. K., and Li, M. Y. (2016). A guideline of selecting and reporting intraclass correlation coefficients for reliability research. *J. Chiropr. Med.* 15 (2), 155–163. doi:10.1016/j.jcm.2016.02.012

Laidlaw, S. A., Shultz, T. D., Cecchino, J. T., and Kopple, J. D. (1988). Plasma and urine taurine levels in vegans. *Am. J. Clin. Nutr.* 47 (4), 660–663. doi:10.1093/ajcn/47.4.660

Li, H., Healey, P. R., Tariq, Y. M., Teber, E., and Mitchell, P. (2013). Symmetry of optic nerve head parameters measured by the heidelberg retina tomograph 3 in healthy eyes: The blue mountains eye study. *Am. J. Ophthalmol.* 155 (3), 518–523.e1. doi:10.1016/j.ajo.2012.09.019

Linderman, R. E., Muthiah, M. N., Omoba, S. B., Litts, K., Tarima, S., Visotcky, A., et al. (2018). Variability of foveal avascular zone metrics derived from optical coherence tomography angiography images. *Transl. Vis. Sci. Technol.* 7 (5), 20. doi:10.1167/tvst.7.5.20

Lu, J., Zhou, H., Shi, Y., Choe, J., Shen, M., Wang, L., et al. (2022). Interocular asymmetry of choroidal thickness and vascularity index measurements in normal eyes assessed by swept-source optical coherence tomography. *Quant. Imaging Med. Surg.* 12 (1), 781–795. doi:10.21037/qims-21-813

Makarova, E., Makrecka-Kuka, M., Vilks, K., Volska, K., Sevostjanovs, E., Grinberga, S., et al. (2019). Decreases in circulating concentrations of long-chain acylcarnitines and free fatty acids during the glucose tolerance test represent tissue-specific insulin sensitivity. *Front. Endocrinol. (Lausanne)* 10, 870. doi:10.3389/fendo.2019.00870

Myer, C., Abdelrahman, L., Banerjee, S., Khattri, R. B., Merritt, M. E., Junk, A. K., et al. (2020a). Aqueous humor metabolite profile of pseudoexfoliation glaucoma is distinctive. *Mol. Omics.* 16, 425–435. doi:10.1039/c9mo00192a

Myer, C., Perez, J., Abdelrahman, L., Mendez, R., Khattri, R. B., Junk, A. K., et al. (2020b). Differentiation of soluble aqueous humor metabolites in primary open angle glaucoma and controls. *Exp. Eye Res.* 194, 108024. doi:10.1016/j.exer.2020.108024

Pietrowska, K., Dmuchowska, D. A., Samczuk, P., Kowalczyk, T., Krasnicki, P., Wojnar, M., et al. (2017). LC-MS-Based metabolic fingerprinting of aqueous humor. *J. Anal. Methods Chem.* 2017, 6745932. doi:10.1155/2017/6745932

Pietrowska, K., Dmuchowska, D. A., Krasnicki, P., Mariak, Z., Kretowski, A., and Ciborowski, M. (2018a). Analysis of pharmaceuticals and small molecules in aqueous humor. *J. Pharm. Biomed. Anal.* 159, 23–36. doi:10.1016/j.jpba.2018.06.049

Pietrowska, K., Dmuchowska, D. A., Krasnicki, P., Bujalska, A., Samczuk, P., Parfieniuk, E., et al. (2018b). An exploratory LC-MS-based metabolomics study reveals differences in aqueous humor composition between diabetic and non-diabetic patients with cataract. *Electrophoresis* 39, 1233–1240. doi:10.1002/elps.201700411

Ripps, H., and Shen, W. (2012). Review: Taurine: A "very essential" amino acid. *Mol. Vis.* 18, 2673–2686.

Sawicka-Smiarowska, E., Bondarczuk, K., Bauer, W., Niemira, M., Szalkowska, A., Raczkowska, J., et al. (2021). Gut microbiome in chronic coronary syndrome patients. *J. Clin. Med.* 10 (21), 5074. doi:10.3390/jcm10215074

Song, M. Y., and Hwang, Y. H. (2022). Interocular symmetry of optical coherence tomography parameters in healthy children and adolescents. *Sci. Rep.* 12 (1), 653. doi:10.1038/s41598-021-04563-3

Yang, M., Wang, W., Xu, Q., Tan, S., and Wei, S. (2016). Interocular symmetry of the peripapillary choroidal thickness and retinal nerve fibre layer thickness in healthy adults with isometropia. *BMC Ophthalmol.* 16 (1), 182. doi:10.1186/s12886-016-0361-7

frontiers | Frontiers in Molecular Biosciences

TYPE Opinion
PUBLISHED 21 April 2023
DOI 10.3389/fmolb.2023.1169449



OPEN ACCESS

EDITED BY
Hector Gallart-Ayala,
Université de Lausanne, Switzerland

REVIEWED BY
Wei He,
Lawrence Livermore National Security,
United States

*CORRESPONDENCE
Shi Qiu,
qiushihnyx@163.com
Aihua Zhang,
aihuatcm@163.com

†Aihua Zhang, https://orcid.org/0000-0002-3784-4472

RECEIVED 19 February 2023
ACCEPTED 13 April 2023
PUBLISHED 21 April 2023

CITATION
Yang Q, Cai Y, Guo S, Wang Z, Qiu S and Zhang A (2023), Localization analysis of metabolites from complex biological samples-recent analytical technique of mass spectrometry imaging.
*Front. Mol. Biosci.* 10:1169449.
doi: 10.3389/fmolb.2023.1169449



# Localization analysis of metabolites from complex biological samples-recent analytical technique of mass spectrometry imaging

Qiang Yang[1], Ying Cai[1], Sifan Guo[1], Zhibo Wang[1], Shi Qiu[2]* and Aihua Zhang [1,2]*

[1]GAP Center and Graduate School, Heilongjiang University of Chinese Medicine, Harbin, China, [2]International Advanced Functional Omics Platform, Scientific Experiment Center, Hainan Medical University, Haikou, China

KEYWORDS

**mass spectrometry imaging, target, metabolomics, diagnosis, metabolite**

Recently, some studies based on analytical methods and the application of mass spectroscopic imaging technology have been published in some academic journals. These studies have shown that mass spectrometry imaging (MSI) is the dominant technology applied in spatial localization, through scanning slices of biological samples and generating charged ions, obtaining the spatial distribution characteristics of various molecules via ion detectors, and performing data dimensionality reduction, statistical calculation, and visual analysis. These articles promote the development of MSI technology, which helps to efficiently and accurately mine MSI data to identify important molecular signatures, promote the application of MSI in clinical diagnosis, drug research and other fields, and lay the foundation for screening biomarkers of related diseases and elucidating the pharmacodynamic mechanism of drugs in organ microregions.

Spatial metabolomics uses MSI technology to analyze the species, content and spatial distribution of metabolites in different tissues and organs, can overcome the bottleneck of spatial information loss in traditional metabolomics research (Qiu et al., 2023). Spatial metabolomics technology mainly relies on MSI and metabolomics technology. The specific process should include sample preparation, matrix selection and coverage, data acquisition and analysis, *etc.* (Figure 1). Luo et al. (2023) had identified a novel metabolic subtype of type 2b mitotic muscle fibers by cross-analyzing metabolomics analysis with MSI data. Fingerprint metabolites enriched include acylcarnitines, cyclic ADP-ribose, and thiamine pyrophosphate, *etc.*, which have anti-fatigue metabolic properties. Visualizing muscle fibers by using MSI may improve our understanding of muscle fiber remodeling under physiological and pathological conditions.

Linear dimensionality reduction methods, such as principal component analysis (PCA) and non-negative matrix factorization (NNMF), are widely used in MSI data analysis. In recent years, the non-linear dimensionality reduction method T-distributed random neighbor embedding has been widely used in omics data analysis. By means of dimensionality reduction, redundant information and noise information in high-dimensional space can be effectively removed, and the accuracy of image recognition can be improved. PCA, as one of the commonly used linear dimension reduction methods, uses the projection method to compress the high dimensional space to the low dimension, and maintains the characteristics that contribute the most to the variance of the data set. Non-linear dimensionality reduction is widely used in image data recognition

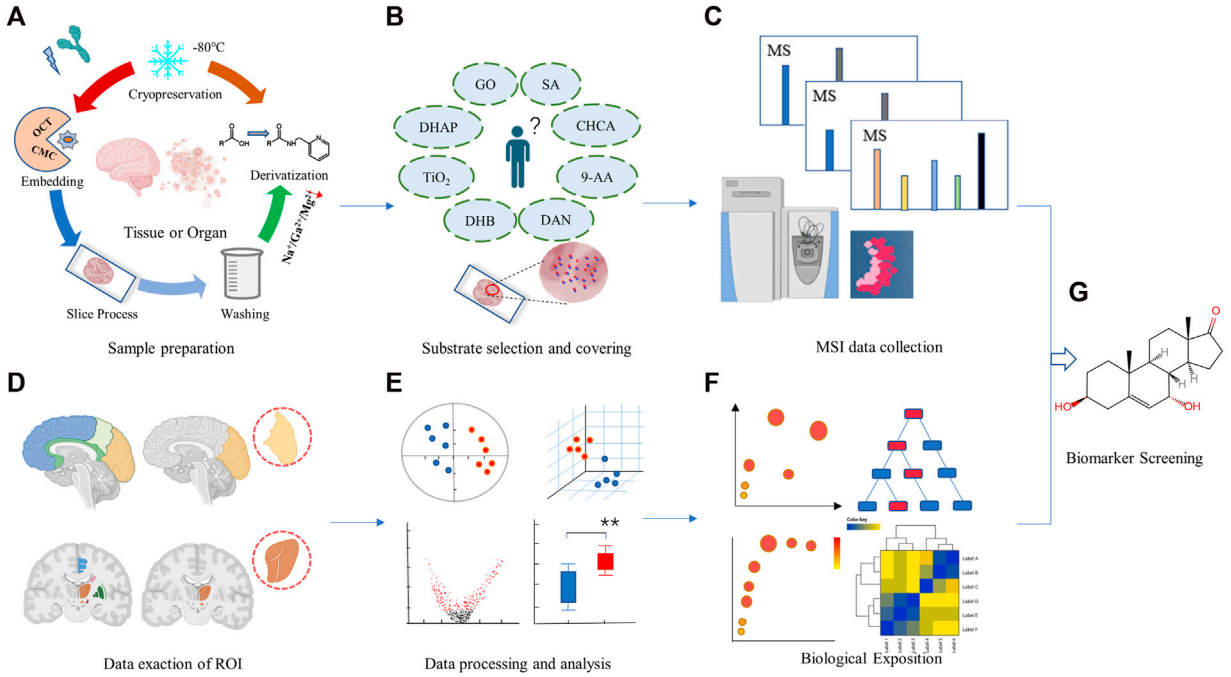


FIGURE 1
Analysis workflow for a typical spatial metabolomics. It mainly covers two parts: mass spectrometry imaging **(A–C)** and metabolomics studies **(D–F)**. Sample collection and pretreatment for mass spectrometry imaging **(A)**, selection and embedding of matrix **(B)**, data collection and analysis for mass spectrometry imaging **(C)**, Data exaction of ROI **(D)**, data processing and analysis **(E)**, and biological function description **(F)**. Biomarker screening and discovery **(G)**. The figure is created by BioRender and MetaboAnalyst.

problems to obtain better recognition results. As an unsupervised learning algorithm, NNMF is mainly used to extract useful features in multi-dimensional data, and has gradually become a widely accepted method for data processing in research fields such as biomedicine and image recognition. Recently, Abdelmoula et al. (2021) had developed a peak processing and data analysis method based on neural networks. This method is a molecular model used to predict atomic data by associating encoded features with primary data by minimizing the error between original and real data. This method is suitable for analyzing MSI low capacity data without preprocessing and peak extraction, and is generally applicable to different acquisition devices. Optimizing the data processing process and establishing a data clustering analysis scheme are crucial in MSI's data analysis.

The brain is the central target of central nervous system diseases, and most central nervous system (CNS) drugs will produce pharmacological effects by acting on the brain. Therefore, mining the spatial information of drugs and related endogenous metabolites in the brain is of great significance for evaluating the drug efficacy and elaborating the relevant mechanism of action. Brain imaging techniques are used for the analysis of brain tissue structure, which cannot be comprehensively analyzed at the molecular level, and the types of substances that can be monitored are also limited. To be precise, a single metabolomics method can only reflect the average level of metabolites in a sample and lacks spatial distribution information. Liu D et al. (2022) studied the effects of olanzapine (OLZ) drugs on brain tissue and found that olanzapine exerted therapeutic effects or caused adverse reactions by regulating the metabolism of aspartate, glutamate and glycerophospholipid. Jin B et al. (2022) also investigated the spatiotemporal and dynamic distribution characteristics of endogenous metabolites in mouse brain microregions under YZG-331 intervention, and found the functional metabolite GABA related to the drug effect of YZG-331, and located the metabolic pathways "GABAergic synapse" and "histidine metabolism". This study is helpful to interpret the mechanism of drug action of new drug candidates for the central nervous system and to find potential multi-targets, and to provide a visual analysis method for drug development.

MSI is more suitable for the identification of proteins, activation peptides, lipids and small biomolecules in tissue samples. These articles continue to improve MSI technology in the areas of sample pretreatment, data processing and functional analysis. MSI technology was used to analyze the spatial distribution of biological samples and reveal the molecular distribution mechanism of biological molecules. By combining MSI technology with multi-omics technology, spatial information and accurate quantification can be effectively correlated, which is of great significance for early diagnosis and prognosis of diseases, biomarker discovery, *etc.*

Although MSI has been widely used in recent years, there are still some limitations. For example, the imaging analysis of compounds with low abundance, low ionization efficiency, and easy interference by matrix peaks is poor, and the method of dimensionality reduction and clustering analysis of high-dimensional MSI data is not immaculate. Future work should focus on developing powerful statistical and deep learning methods to rapidly extract

comprehensive molecular information with diagnostic capabilities, and developing new strategies for various qualitative and quantitative MSI based on simulated tissue models or standard deposition. The development of MSI technology has broad application prospects in the fields of omics analysis, precision medicine, toxicology and drug metabolism.

## Author contributions

Conception and design: QY, AZ; Analysis and interpretation of data: QY, YC, SG, ZW, SQ, and AZ; Writing, review, and/or revision of the manuscript: QY, SQ, and AZ; Study supervision: QY, SQ, and AZ.

## Acknowledgments

The authors are grateful for the generous support from the Program of Natural Science Foundation of State (Grant Nos 82104733, 81973745, 81302905), Talent Lift Engineering Project of China Association of TCM (QNRC2-B06), Natural Science Foundation of Heilongjiang Province (YQ 2019H030). We also thank BioRender and MetaboAnalyst for the figure preparation.

## Conflict of interest

The authors declare that the research was conducted in the absence of any commercial or financial relationships that could be construed as a potential conflict of interest.

## Publisher's note

All claims expressed in this article are solely those of the authors and do not necessarily represent those of their affiliated organizations, or those of the publisher, the editors and the reviewers. Any product that may be evaluated in this article, or claim that may be made by its manufacturer, is not guaranteed or endorsed by the publisher.

## References

Abdelmoula, W. M., Lopez, B. G., Randall, E. C., Kapur, T., Sarkaria, J. N., White, F. M., et al. (2021). Peak learning of mass spectrometry imaging data using artificial neural networks. *Nat. Commun.* 12 (1), 5544. doi:10.1038/s41467-021-25744-8

Jin, B., Pang, X., Zang, Q., Ga, M., Xu, J., Luo, Z., et al. (2022). Spatiotemporally resolved metabolomics and isotope tracing reveal CNS drug targets. *Acta Pharm. Sin. B* 2022, 011. doi:10.1016/j.apsb.2022.11.011

Liu, D., Huang, J., Gao, S., Jin, H., and He, J. (2022). A temporo-spatial pharmacometabolomics method to characterize pharmacokinetics and pharmacodynamics in the brain microregions by using ambient mass spectrometry imaging. *Acta Pharm. Sin. B* 12 (8), 3341–3353. doi:10.1016/j.apsb.2022.03.018

Luo, L., Ma, W., Liang, K., Wang, Y., Su, J., Liu, R., et al. (2023). Spatial metabolomics reveals skeletal myofiber subtypes. *Sci. Adv.* 9 (5), eadd0455. doi:10.1126/sciadv.add0455

Qiu, S., Cai, Y., Yao, H., Lin, C., Xie, Y., Tang, S., et al. (2023). Small molecule metabolites: Discovery of biomarkers and therapeutic targets. *Signal Transduct. Target Ther.* 8 (1), 132. doi:10.1038/s41392-023-01399-3

frontiers | Frontiers in Molecular Biosciences

TYPE Review
PUBLISHED 11 August 2023
DOI 10.3389/fmolb.2023.1242059



OPEN ACCESS

EDITED BY
Hector Gallart-Ayala,
Université de Lausanne, Switzerland

REVIEWED BY
Surendra Kumar Shukla,
University of Oklahoma, United States
Lifang Ma,
Shanghai Jiao Tong University, China

*CORRESPONDENCE
Fengming Yi,
ndefy13212@ncu.edu.cn

†These authors have contributed equally to this work and share first authorship

RECEIVED 18 June 2023
ACCEPTED 03 August 2023
PUBLISHED 11 August 2023

CITATION
Ye Y, Yu B, Wang H and Yi F (2023), Glutamine metabolic reprogramming in hepatocellular carcinoma.
*Front. Mol. Biosci.* 10:1242059.
doi: 10.3389/fmolb.2023.1242059



# Glutamine metabolic reprogramming in hepatocellular carcinoma

Yanyan Ye[1†], Bodong Yu[2,3†], Hua Wang[4,5†] and Fengming Yi[4,5*]

[1]Department of Ultrasound, The Second Affiliated Hospital of Nanchang University, Nanchang, China, [2]The Second Clinical Medical College of Nanchang University, The Second Affiliated Hospital of Nanchang University, Nanchang, China, [3]Jiangxi Medical College, Nanchang University, Nanchang, China, [4]Department of Oncology, The Second Affiliated Hospital of Nanchang University, Nanchang, China, [5]Jiangxi Key Laboratory of Clinical and Translational Cancer Research, Nanchang, China

Hepatocellular carcinoma (HCC) is a lethal disease with limited management strategies and poor prognosis. Metabolism alternations have been frequently unveiled in HCC, including glutamine metabolic reprogramming. The components of glutamine metabolism, such as glutamine synthetase, glutamate dehydrogenase, glutaminase, metabolites, and metabolite transporters, are validated to be potential biomarkers of HCC. Increased glutamine consumption is confirmed in HCC, which fuels proliferation by elevated glutamate dehydrogenase or upstream signals. Glutamine metabolism also serves as a nitrogen source for amino acid or nucleotide anabolism. In addition, more glutamine converts to glutathione as an antioxidant in HCC to protect HCC cells from oxidative stress. Moreover, glutamine metabolic reprogramming activates the mTORC signaling pathway to support tumor cell proliferation. Glutamine metabolism targeting therapy includes glutamine deprivation, related enzyme inhibitors, and transporters inhibitors. Together, glutamine metabolic reprogramming plays a pivotal role in HCC identification, proliferation, and progression.

KEYWORDS

**hepatocellular carcinoma, glutamine metabolic reprogramming, metabolic targeting therapy, mTORC, glutamine-related metabolites**

## 1 Introduction

Hepatocellular carcinoma is a heterogeneous and lethal disease with increasing incidence and mortality globally (Wang et al., 2021; Llovet et al., 2022a). More than 80% of HCC occurs in Eastern Asia and sub-Saharan Africa with limited medical resources (Yang et al., 2019). Genetic predisposition, risk factors, tumor microenvironment (TME), and underlying disease promote the malignant hepatocyte transformation, development, and progression (Yang et al., 2019; Llovet et al., 2021). The management of HCC is according to the tumor stages with mostly applicated Barcelona Clinic Liver Cancer (BCLC) staging system. Briefly, curative therapeutics, including liver resection, transplantation, and tumor ablation, are selected for early-stage patients; Transarterial chemoembolization (TACE) is suitable for intermediate stages; systemic therapies are candidates for advanced settings, whereas best supportive care is most appropriate for end-stage of HCC (Llovet et al., 2021). Extended morphometric and biological criteria applied for surgery and liver transplantation for HCC are confirmed to promote the overall survival of some selected patients. However, 22%–25% of patients are recurrent after resection in 10 years, and 50%–70% are recurrent after

transplantation (Vibert et al., 2020). For patients in advanced stages, systemic treatment is recommended as the standard of care. Molecular targeted monotherapy, including sorafenib or lenvatinib in the first line, and regorafenib, cabozantinib, or ramucirumab in the second line, has been confirmed to improve clinical outcomes with limited median overall survival (Llovet et al., 2018; Faivre et al., 2020). Immune-checkpoint inhibitor (ICI)-anti-programmed cell-death protein (ligand)-1 (PD-[L]1), is proven to be effective in the treatment of HCC. However, the ORR is limited to 10%–20% of HCC patients for monotherapy. The combination of the anti-angiogenic drug bevacizumab and immune-checkpoint inhibitor atezolizumab has already reshaped to be the standard first-line treatment regimen (Llovet et al., 2022a), and the expected survival of HCC with advanced stage could reach up to more than 2 years (Finn et al., 2020; Reig et al., 2022). Other dual therapies combing ICIs with multi-kinase inhibitors are proven to be promising in clinical trials. Oncolytic virus immunotherapy, adoptive T-cell transfer, and anti-immunosuppressive environment strategies are under exploration with promising futures (Foerster et al., 2022).

Molecular classifications with molecular signatures, pathological features, genetic features, typical signaling pathways, epigenetic features, and immunological features will be helpful in precise treatment (Rebouissou and Nault, 2020; Llovet et al., 2022b). Mutation of Wnt/β-catenin is revealed in 35% of HCC patients; mounting strategies targeting the Wnt/β-catenin cascade have provided evidence in preclinical trials in recent decades (Xu et al., 2022). Tumor-associated exosomes are proven to shape the local and distant microenvironments of HCC initiation and development. The preclinical application of biomarkers, drug resistance, and treatment are under exploration (Wang et al., 2022). Preclinical studies depict that selective inhibiting tumor-promoting neutrophils, related signaling pathways, and chemotaxis are effective (Geh et al., 2022). Non-cellular components, including hypoxia, cytokines secreted by tumor stroma, and extracellular matrix, also play a pivotal role in forming the cancer stem cell niche in HCC, which might be potential clinical applications in the future (Lam and Ma, 2022).

Metabolic reprogramming has been frequently unveiled in HCC, such as tumor favors Warburg effect rather than oxidative phosphorylation, unbalanced lipid intake, and fatty acid mobilization causing high levels of circulating glucose and fatty acids, which induces alternative source of energy of cancer cells (Satriano et al., 2019). The elucidation of metabolic characteristics is promising in understanding or treating HCC.

## 2 HCC and metabolism

The liver plays a pivotal role in metabolic homeostasis. The oxygen gradient from periportal hepatocytes towards pericentral hepatocytes corresponds to a different function in the hepatic zonation. Periportal hepatocytes (zone 1) have a substantial oxygen supply from arterioles responsible for gluconeogenesis, albumin synthesis, amino acid (AA) catabolism, cholesterol synthesis, and β-oxidation, which need more ATP for energy supply. Pericentral hepatocytes (zone 3) serve glycolysis, glutamine synthesis, lipogenesis, and detoxification. The hepatocytes located between periportal and pericentral hepatocytes (zone 2) serve for iron metabolism and insulin-like growth factor (IGF) homeostasis (Li et al., 2021).

Otto Warburg first demonstrated that HCC tissue consumed glucose and converted it into lactate rather than untaken by mitochondria for the TCA cycle, even in the existence of sufficient oxygen, also termed aerobic glycolysis or the Warburg effect. Aerobic glycolysis in HCC results in more glucose uptake, faster ATP generation, and lactate production (Liberti and Locasale, 2016; Satriano et al., 2019). In addition, the Warburg effect also supports anabolic metabolism by providing the pentose phosphate, hexosamine, and glycerol pathways without preventing mitochondrial respiration. The decreasing of oxidative phosphorylation (OXPHOS) renders the reduction of reactive oxygen species (ROS). Aerobic glycolysis mediates proliferation, growth, immune evasion, invasion, migration, angiogenesis, and drug resistance in HCC (Alannan et al., 2020; Feng et al., 2020).

A higher rate of lipogenesis is a hallmark of cancer cells. HCC has demonstrated that the enhancement of the Warburg effect attributes to an increase in the level of β-oxidation by metabolomics studies. Lipid catabolism also provides energy to promote cancer cell proliferation and produces metabolites for biosynthesis to meet fast-growing tumors. Lipid metabolism reprogramming promotes abnormal gene expression and rewires many oncogeneses and metastasis-related pathways. Targeting lipid metabolism has the potential anti-tumor activity in preclinical studies (Alannan et al., 2020). Dysfunction of lipid metabolism, like nonalcoholic fatty liver disease (NAFLD), is one of the main risk factors for HCC. Treatment of NAFLD might have anti-tumor potential (Orabi et al., 2021). HCV protein has been validated to hijack the patients' lipid and glucose metabolism by stimulating *de novo* lipogenesis, promoting synthesis of phospholipids and sphingomyelins, inhibiting mitochondria fatty acid oxidation, and hijacking the very low-density lipoprotein (VLDL) secretion pathway. HCV promotes hepatocellular carcinogenesis via crosstalk with metabolic dysfunction; it will boost oxidative stress, DNA damage, lipo-toxicity, cell death, and senescence in patients with adipose tissue dysfunction and insulin resistance (Leslie et al., 2022). Metabolic impairment might be the potential reason for HCV-related HCC early recurrence even after direct-acting antivirals (Reig et al., 2016). Cholesterol metabolisms play a double-edged sword in hepatocellular carcinoma. Cholesterol can not only induce ectopic fatty acids accumulation, reshape an immunosuppressive microenvironment, activate hepatic stellate cells, and influence membrane fluidity or protein function, to further promote tumorigenesis in HCC but also activate NK cell proliferation or recruitment, and promote CD44 translocation into lipid rafts, so that prohibit HCC (Zhou and Sun, 2021).

Other metabolism alternations such as proline metabolism, cysteine metabolism, nucleotide metabolism, urea cycle, hexosamine biosynthetic pathway, pentose-phosphate pathway, et al. are also validated in HCC(17, 26–28). Proline metabolism has been confirmed to enhance the tumorigenesis in liver cancer as two enzymes corresponding to proline biosynthesis are upregulated (pyrroline-5-carboxylate reductase (PYCR1), aldehyde dehydrogenase 18 family member A1 (ALDH18A1)), and one proline catabolic enzyme is downregulated (proline dehydrogenase (PRODH)) (Ding et al., 2021). Cysteine

metabolism plays a pivotal role in sorafenib responses during HCC therapy (Byun et al., 2022), maintaining glutathione synthesis to protect HCC cells from ferroptosis (Hu et al., 2022).

Moreover, the interplays between metabolism and tumor microenvironment play crucial roles in the cancerous liver. It could be subclassified into antitumor immunometabolism and protumor immunometabolism. For instance, increased fatty acid synthesis and glycolysis in Th17 cells could enhance the production of IFN-γ, which will function as an antitumor effect; elevation of β-oxidation in tumor-associated macrophages promotes M2 macrophage polarization, which exerts as protumor function (Li et al., 2021). Hypoxia in the HCC also induces the activation of lactate metabolism, serine synthesis pathway and folate cycle, and adenosinergic metabolism to support the growth of tumors (Bao and Wong, 2021).

Glutamine is an indispensable energy fuel and nitrogen source for tumor initiation, survival, and progression; It functions not only as an energy resource but also biosynthesis, signaling pathway regulator, regulating ROS, and maintaining tumor microenvironment; and increased glutamine consumption is conserved in different cancers (Yang et al., 2021; Gyamfi et al., 2022; Ma et al., 2022). Herein, we will conclude the role of glutamine metabolic reprogramming in HCC.

## 3 Glutamine and cancer

Glutamine is a nonessential amino acid (NEAA) that can be synthesized *de novo* by glutamine synthetase. In contrast, the increased demand in tumors results in glutamine, a conditionally essential amino acid. Glutamine also functions as an intracellular exchange factor or deamidated to glutamate, an elemental carbon and nitrogen source, especially for glutamine-addicted cancer cells. Moreover, glutamine metabolism involves substantial biosynthesis, including anti-ROS glutathione/NADPH and lipids synthesis. In addition, glutamine is a nitrogen donor for hexosamine, asparagine, and nucleotide biosynthesis through aminotransferases (Altman et al., 2016; Yang et al., 2021).

Glutamine is a major substrate of the TCA cycle's component; it participates in the biosynthesis of biomolecules, maintaining redox homeostasis, ATP generation, oxidative metabolism, and signaling pathway as one of the major nutrients. Moreover, it also provides the energy for activated or proliferative cells such as cancer cells and activated lymphocytes (Gyamfi et al., 2022). Glutamine metabolism also participates in essential biological processes, including nucleotide/amino acids/extracellular matrix synthesis, protein glycosylation/epigenetic modification, cellular redox balance, and autophagy (Fan et al., 2020). The primary process of glutamine metabolism includes the following steps: cells uptake glutamine by specific transporters (SLC1A5/ASCT2) and then convert glutamine to glutamate in mitochondria by glutaminase (GLS); subsequently, glutamate will convert to α-ketoglutarate (α-KG) as the main component of Tricarboxylic Acid cycle (TCA) by mitochondrial glutamate dehydrogenases (GLUD), α-KG mainly incorporates into TCA cycles to assist the production of NADPH and nucleotide synthesis. Furthermore, α-KG will be exported to the cytoplasm as a source of acetyl-CoA, which is the main substrate of fatty acid synthesis; Or convert to glutathione (GSH) to further stabilize the redox homeostasis (DeBerardinis et al., 2007; Zhang et al., 2017), and it also can transfer the amine group to another nonessential amino acid by transaminases. Besides, it can be subtracted of proline and glutathione biosynthesis (Yang et al., 2021); the details are shown in Figure 1.

Glutamine metabolism also plays a crucial role in the interplay between TME and tumor cells. The competition of glutamine consumption by immune cells and tumor cells results in the immune response from tumor-infiltrating T cells as glutamine deficiency. Moreover, the shortage of glutamine for tumor cells will induce the proliferation and activation of Treg cells, which function as an immunosuppressive effect (Cluntun et al., 2017; Fu et al., 2019; Edwards et al., 2021). However, cancer-associated fibroblasts (CAFs) rescue the glutamine-deficiency microenvironment by complementary secreting glutamine (Yang et al., 2016). Glutamine reprogramming also impacts other immune cells' polarization or function (Ma et al., 2022).

Inhibition of glutamine metabolism has been confirmed to be promising in glutamine-addicted cancer cells, including glutamine analogs like DON, acivicin, and azaserine, glutamine transporter inhibitor GPNA and V-9302, GLS1/2 inhibitors (Shen et al., 2021). GLS1 plays a crucial role in cancer progression by converting glutamine to glutamate in mitochondria. It enhances tumor development, invasion, and migration by maintaining redox homeostasis, cellular energetics, and proliferative signaling pathway. GLS1 demonstrates higher expression in solid tumors such as stomach adenocarcinoma, head and neck squamous cell carcinoma, thymoma, testicular germ cell tumors, hepatocellular carcinoma, and colon adenocarcinoma, according to the TCGA database analysis. It is regulated by Myc, Retinoblastoma, and nuclear transcription factor-κB in cancer cells. GLS1 inhibitors, including DON, BPTES, 968, CB-839, UPGL00004, and ebselen, show promising anti-tumor effects for glutamine-dependent cancers (Yu et al., 2021). bis-2-(5-phenylacetamido-1,3,4-thiadiazol-2-yl) ethyl sulfide (BPTES) and CB-839, GLS inhibitors are confirmed to have anti-tumor effective; especially CD839 has been proved to possess the ability of antiproliferative activity in both solid tumors like pancreatic cancer and breast cancer (Gross et al., 2014; Biancur et al., 2017). However, drug resistance has been validated in targeting glutaminolysis. Numerous studies are trying to explore the treatments to conquer the drug-resistance, including the combination of GLS1 and GLS2 inhibitors; GLS1 inhibitors synergize with glutamate release blockage, targeting glutaminolysis accompanied with other clinical drugs like chemotherapy/molecular targeted therapy/immune therapy, and GLS inhibitors combined with other metabolic inhibitors (Shen et al., 2021; Lemberg et al., 2022). JHU-083 is a pro-drug proven to inhibit tumor growth and reshape the tumor immune microenvironment, promoting CD8+T activation and proliferation and decreasing immunosuppressive myeloid cells (Oh et al., 2020). Moreover, inhibition of glutaminolysis will induce the expression of PD-L1 in tumor cells, which indicates that the combination of anti-glutaminolysis and immune checkpoint blockade would have a synergistic antitumor effect (Byun et al., 2020). Glutamine uptake inhibitors(V-9302), glutamine antimetabolites(L-DON/JHU-083), and glutaminase inhibitors (CB-839) are confirmed to be effective in reshaping glutamine metabolism in immune cells and function as anti-

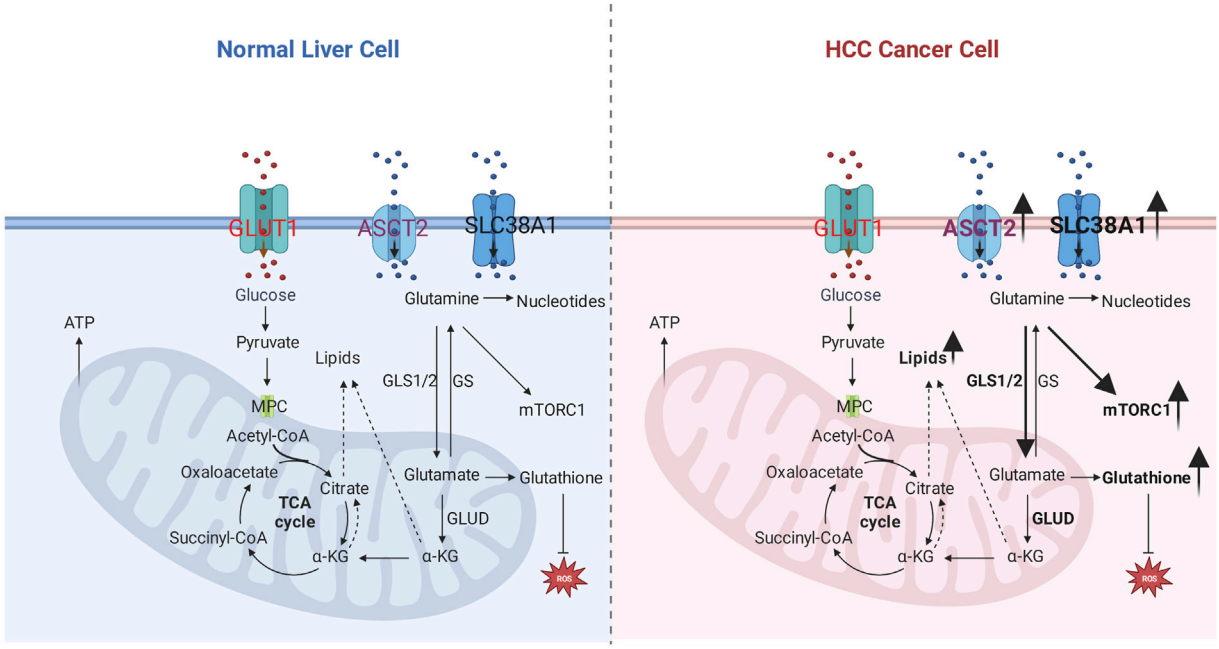


FIGURE 1
Glutamine metabolic reprogramming in hepatocellular carcinoma. Left: glutamine metabolism in the normal liver cell. Right: glutamine metabolism in hepatocellular carcinoma; the number of glutamine transporters increases, which results in more glutamine uptake by the cancer cell, related enzymes such as GLS1/2, GLUD are elevated to enhance sources for carbon and nitrogen, lipids, and nucleotides; improved glutamine uptake activates mTOR1 pathway and antioxidative effect.

tumor immune microenvironment (Ma et al., 2022). Glutamine transporter is upregulated in various tumors, such as SLC7A5, which is regulated by oncogene c-Myc. C-Myc or KRAS mutation also upregulated the expression of GLS(33, 50). MYC, SLC1A5, mTORC1, and glutaminase could be further utilized as a biomarker to recognize glutamine-addicted cancers (Yuneva et al., 2007; Wise and Thompson, 2010; Bhutia and Ganapathy, 2016). SLC1A5 is widely upregulated in tumors among 14 glutamine transporters (Bhutia and Ganapathy, 2016). V-9302, a glutamine transporter inhibitor targeting SLC1A5/ASCT2, has validated the effect of attenuating tumor cell proliferation and increasing the infiltration of CD8+T cells (Schulte et al., 2018; Pallett et al., 2021).

# 4 The components of glutamine metabolism as biomarkers of HCC

Forty-one glutamine metabolism (GM) associated genes are termed as GMScore from The Cancer Genome Atlas (TCGA) and the International Cancer Genome Consortium (ICGC) database. High GMScore indicates tumor growth and poor overall survival. In addition, High GMscore predicts a low response to immune checkpoint inhibitors (Ying et al., 2021). A study tries to depict the different gene expressions between poorly differentiated HCC cell lines and well-differentiated HCC cell lines from public databases. Metabolic-related gene analysis demonstrates that poorly differentiated cell lines profoundly rely on glutamine to fuel the TCA cycle (GLS, SLC1A5, SDHA). However, well-differentiated cell lines depend on glycolysis and glutaminolysis (Nwosu et al., 2018). The components of glutamine metabolism, including metabolic enzymes, metabolites, and metabolite transporters, demonstrate high sensitivity and specificity in diagnosis, relapse monitoring, and stage prediction.

## 4.1 Glutamine synthetase

Glutamine synthetase (GS) is the feature of Wnt/β-catenin pathway activation, expressed in the pericentral hepatocytes, and elevated GS indicates cell proliferation in tissues (Cadoret et al., 2002; Austinat et al., 2008; Bioulac-Sage et al., 2009; Sohn et al., 2018; Ruiz de Galarreta et al., 2019; Tao et al., 2021; Hamaguchi et al., 2022). Liver tumors with different β-catenin activation levels demonstrate distinct tumor phenotypes. Highly activating β-catenin with CTNNB1 mutation types is associated with malignant transformation and intense pattern of GS staining; However, weak mutations display more frequently for hepatocellular adenoma (HCA) (Rebouissou et al., 2016). Activated β-catenin in HCC patients predicts better survival and less sorafenib resistance than inactive ones. The potential mechanism of the β-catenin effect might be mediated by autophagy via increasing GS (Sohn et al., 2018).

Glutamine synthetase could distinguish atypical nodules, early diagnosis, and invasion of HCC. For instance, GS is considered to have high specificity and sensitivity to the differential diagnosis of HCC and dysplastic nodules (Coral et al., 2021). Glypican-3, heat shock protein 70, and GS are utilized to distinguish a <2 cm hepatocellular lesion without classic radiological characters of HCC with cirrhosis by

immunochemistry (IHC) or designed RNA probes (Tremosini et al., 2012; Di Tommaso and Roncalli, 2017; Bakheet et al., 2020). GS and glypican3 staining are sensitive and specific to HCC compared to metastatic cancer, benign hepatocellular lesions, and cirrhosis. They are associated with large tumor sizes and poorly differentiated specimens (Wasfy and Shams Eldeen, 2015). GS positive staining has 43.9%–100% sensitivity for HCC compared with cirrhotic nodules (Dal Bello et al., 2010; Long et al., 2011; Shin et al., 2011; Witjes et al., 2013; Uthamalingam et al., 2018). The sensitivity and specificity of IHC GS staining for the early stage of HCC are 50% and 90%, respectively (Dal Bello et al., 2010); the sensitivity and specificity of GS in distinguishing low-grade HCC from hepatocellular adenoma (HCA) are 80% and 50%, respectively (Lagana et al., 2013). GS has upregulated in steatohepatitis hepatocellular carcinoma, which is validated by RNAseq or immunochemistry (Van Treeck et al., 2021). However, another study shows that GS is expressed in relatively few tumors induced by DEN or metabolic dysfunction associated with fatty liver disease (MAFLD) in mice (Kurosaki et al., 2021). HCC with steatohepatitis has a low incidence of glutamine synthetase overexpression and nuclear accumulation of β-catenin (Ando et al., 2015). GS is highly expressed in serum and tumor tissues of HCC patients and is associated with poor prognosis. Moreover, GS promotes HCC migration and invasion by EMT (Liu et al., 2020). Peri-tumoral hyperintensity in the hepatobiliary phase of gadoxetic acid-enhanced MRI (EOB-MRI) positively associated with high GS and organic anion transporter polypeptides (OATP)1B3 expression in the peri-tumoral zone. Peri-tumoral hyperintensity indicates a high potential for microscopic hepatic venous invasion (Yoneda et al., 2018).

Nevertheless, some studies also show that GS staining in HCC indicates a better prognosis. Wnt/β-catenin related makers (β-catenin, GS) positive HCC mark better differentiation, less portal vein invasion, and intrahepatic metastasis (Tsujikawa et al., 2016). β-catenin activation by fluorescence *in situ* hybridization and glutamine synthetase highly staining by immunohistochemistry demonstrates the character of well-differentiated HCC (Evason et al., 2013). GS-positive patients have reduced tumor-specific mortality and overall mortality (Dal Bello et al., 2010). The positive of glutamine synthetase indicates better survival for HCC patients treated with liver transplantation (Ataide et al., 2017). In mice transgenic the full length of hepatitis B virus X protein, EMT increases, but glutamine synthetase level decreases (Ahodantin et al., 2020).

Glutamine synthetase also correlates with the PD-1 expression and treatment response or is influenced by treatment. For instance, GS overexpression is significantly associated with low expression of PD-1 in HCC patients (Montasser et al., 2021). Lower GS staining predicts better OS and RFS for patients treated with adjuvant TACE after curative resection in HCC patients (Zhang et al., 2015). Glucocorticoid promotes GS expression by transcriptional and posttranscriptional levels in hepatoma cell lines (Gaunitz et al., 2002).

## 4.2 Other glutamine metabolism-related enzymes

Glutamate dehydrogenase (GLUD) serves as a catalyticase that drive L-glutamate towards α-KG and ammonia, and α-KG is a pivotal component of the tricarboxylic acid cycle (TCA cycle). hGLUD1 is highly expressed in HCC human samples and HepG2 cells; The proliferation of HepG2 cells is reduced by silencing hGLUD1, which is mediated by decreasing mitochondria-mediated apoptosis (Marsico et al., 2021). Moreover, Preoperative serum GLUD predicts high microvascular invasion (MVI) and poor overall survival for HCC patients after liver transplantation (Gong et al., 2021).

Glutamine metabolism-related genes are upregulated in the HCC cohort from the TCGA database. Among them, glutaminase (GLS) 1 is increasing in HCC and associated with the stemness of HCC cells, which is also associated with poor prognosis (Jin et al., 2020). Higher expression of GLS1 is positively correlated with poor differentiation, more lymphatic metastasis, advanced stage, more elevated serum AFP, and lower overall survival. GLS1 promotes HCC cell proliferation and could be inhibited by GLS1 inhibitors. The mechanism might relate to GLS1 inducing the activation of the AKT/GSK3β/CyclinD1 pathway (Xi et al., 2019). Conversely, both protein and mRNA levels of glutaminase (GLS) 2 display negatively associated with late stage, vascular invasion, tumor relapse, overall survival, and disease-free survival. Mechanically, GLS2 stabilizes Dicer by ubiquitination system; Induced Dicer promotes miR-34a maturation; mature miR-34a will repress snail expression, which is reported to facilitate HCC cells invasiveness and epithelial-mesenchymal transition (Kuo et al., 2016).

## 4.3 Metabolites

A "serum biomarker model" containing tryptophan, glutamine, and 2-hydroxybutyric acid based on capillary electrophoresis–time-of-flight mass spectrometry is established to diagnose HCC from non-HCC, which is confirmed to be an effective biomarker that compensatory for AFP (Zeng et al., 2014). $^{1}$H- nuclear magnetic resonance (NMR) metabolomics profiling is used to distinguish the early or late stage of HCC and find that glutamine decreases in the late stage of HCC with respect to the early stage of HCC (Casadei-Gardini et al., 2020). A study elucidates the metabolomics of HCC with different etiology by $^{1}$H-NMR and finds that HCC from NAFLD has high levels of glutamine/glutamate, which is also validated by increased expression of GS in immunochemistry and NMR-spectroscopy glutamine quantification. Nevertheless, HCC with cirrhosis acquires high levels of β-hydroxybutyrate, tyrosine, phenylalanine, and histidine (Teilhet et al., 2017). Serum-based metabolomics by $^{1}$H-NMR reveals that pyruvate, glutamine, and α-ketoglutarate are abundant in liver cirrhosis and HCC (Gao et al., 2009). Plasma phenylalanine and glutamine levels in patients with liver cirrhosis are associated with HCC occurrence in the next 3 years. Phenylalanine concentration positively correlates with HCC, and glutamine level is the opposite effectiveness (Liang et al., 2020). Another serum NMR-based metabolomics demonstrates that cirrhosis with large HCC has significant upregulation of glutamate, acetate, and N-acetyl glycoproteins. In contrast, the metabolic fingerprint for cirrhosis without HCC displays a high concentration of lipids and glutamine (Nahon et al., 2012). NAFLD-HCC with no or mild fibrosis predominantly overexpressed choline derivatives and glutamine by 1H-Nuclear Magnetic Resonance spectroscopy (Buchard et al., 2021).

### 4.4 Metabolite transporters

Solute Carrier Family 38 A1 (SLC38A1), a crucial glutamine transporter, is validated to be upregulated in HCC at both mRNA and protein by the Cancer Genome Atlas (TCGA) cohort and a Clinical Proteomic Tumor Analysis Consortium (CPTAC) cohort. Moreover, it is inversely correlated with $CD8^+$ T cell infiltration (Liu et al., 2021). Solute carrier family 1 member 5 (SLC1A5), also terms as alanine–serine-cysteine transporter 2 (ASCT2), is a glutamine transporter. SLC1A5 is highly expressed in HCC and predicts poor prognosis, confirmed by multiple databases according to bioinformatics (Zhao et al., 2021). Glucose transporter GLUT1 and glutamine transporter ASCT2 are upregulated in HCC, and the high expression of GLUT1 and ASCT2 indicates poor OS and recurrence-free survival (RFS) (Sun et al., 2016).

## 5 Glutamine metabolism reprogramming in HCC

### 5.1 Glutamine as fuel for HCC proliferation

Increased glutamine uptake and more glutamine converts to the TCA cycle are confirmed in studies. Glutamate dehydrogenase (GLUD) serves as a catalyticase that drive L-glutamate towards α-KG and ammonia, and α-KG is a pivotal component of the TCA cycle. hGLUD1 is highly expressed in HCC human samples and HepG2 cells; The proliferation of HepG2 cells is reduced by silencing hGLUD1, which is mediated by decreasing mitochondria-mediated apoptosis (Marsico et al., 2021). Discoidin domain receptor 1 (DDR1) is highly expressed in HCC, which promotes glutamine metabolism as fuel by increasing GLUD1, GLS1, and SLC1A (glutamate transporter) in HCC (Lin et al., 2020). circGSK3B is confirmed to promote HCC cell proliferation and metastasis ability by increasing GLS (Li et al., 2020). SIRT4 localizes in mitochondria and regulates glutamine or lipid metabolism. SIRT4 is downregulation in mRNA and protein levels confirmed by human HCC samples; knockout or silence of SIRT4 will promote hepatocarcinogenesis *in vivo* and *in vitro*. Mechanically, SIRT4 inhibits the conversion from glutamine fuel to the TCA cycle. Decreasing glutamine catabolism results in a deficiency of ATP/ADP, leading to the activation of the LKB1/AMPKα/mTOR axis (Wang et al., 2019). High-mobility group box 1 gene (HMGB1) acts as competing endogenous RNAs (ceRNAs) for the mTORC2 component RICTOR, subsequently promoting the expression of RICTOR mRNA. The high expression of RICTOR will induce mTORC2-AKT-C-MYC activation that upregulates GS expression; on the other hand, GLUD will be enhanced as the release of inhibition signal from SIRT4 (Wei et al., 2021).

The HGF-MET axis is confirmed to stimulate glycolysis and glutaminolysis to function as a biogenetic source for HCC cell lines via inhibiting pyruvate dehydrogenase complex (PDHC) activating GLS. However, dephosphorylated MET-mediated autophagy compensates for sustaining biogenesis, leading to the treatment resistance of HGF-MET axis inhibitors or antibodies. Other autophagy blockers to HGF-MET axis inhibitors improve the therapeutic efficiency of HCC *in vitro* and *in vivo* (Huang et al., 2019). High expression of TGF-β in the HCC cell line demonstrates a mesenchymal-like morphology. Glutamine anaplerosis for the fuel compensation to the biosynthetic utility of TCA metabolites is confirmed in TGF-β highly expressed cell line. The mechanism related to TGF-β in the HCC cell line might be elevated glutamine transporter solute Carrier Family 7 Member 5 (SLC7A5) and GLS1 (Soukupova et al., 2017). However, in a doxycycline-regulated Myc transgenic model of HCC, glutamine transporter SLC1A5 is highly expressed, and GLS1/GLS2 is downregulated in both transcripts and protein, which indicates increased extracellular glutamine uptake to anabolic pathway other than fuel source for the TCA cycle (Dolezal et al., 2017). Chemo-resistance HCC cell lines display cancer stem cell-like phenotype with rising CSC markers, poorly developed mitochondrial network, and increasing telomerase activity. The chemo-resistance character is mediated by drug efflux caused by high expression of P-gp protein, which is an ATP-consuming process. However, glucose-dependent OXPHOS and glycolysis are decreasing, indicating a metabolic quiescent in chemo-resistance cell lines. An alternative source from the glutamine-OXPHOS pathway fuels the ATP. Co-treatment of mitochondria-specific antagonist metformin and glutamine-starving condition attenuates the drug efflux in chemo-resistance HCC cell lines (Lee et al., 2021). The details are shown in Figure 1.

### 5.2 The source of nitrogen

Glutamine metabolism supplies carbon and nitrogen sources for amino acid or nucleotide anabolism, as shown in Figure 1. Yap overexpression induces hepatomegaly and promotes carcinogen dimethylbenzanthracene (DMBA)-induced liver tumor formation by activating GLUL as a transcriptional factor. Elevated GLUL enhances glutamine accumulation, which provides sufficient nitrogen into nucleotide biosynthesis that accelerates liver and liver tumor proliferation (Cox et al., 2016). However, a study finds that the serine biosynthesis pathway (SSP) is activated, and cMyc expression is elevated during glucose or glutamine deprivation. Potential mechanisms might be related to cMyc-regulated enzymes like glutathione (GSH) and phosphoserine phosphatase (PSPH), which promote redox hemostasis for cancer cells and activate the serine biosynthesis pathway (Sun et al., 2015).

### 5.3 More glutamine converts to glutathione as an antioxidant in HCC

Glutathione-glutamine-glutamate metabolism aberration is involved in the process of hepatic tumorigenesis (Chen et al., 2019). Glutamine uptake in HCC is not predominantly as carbon or fuel for the TCA cycle but for increasing the conversion of glutamine into glutamate, thereby converting more glutamate into glutathione. Glutathione functions as an antioxidant that prevents oxidative damage to cancer cells. In an HCC mice model induced by co-transfection of c-Myc/h-Ras, glutamine synthetase (GS), expressed in pericentral hepatocytes in a healthy liver, is absent within the tumor in the c-Myc/h-Ras mice model. Glutamate-cysteine ligase catalytic subunit (Gclc) increases, and GLUD1 decreases in the c-Myc/h-Ras mice model, which indicates that more glutamate converts to glutathione other than α-ketoglutarate (Serra et al., 2022). Metabolic competition for glutamine is validated to impair hepatocellular

tumorigenesis. Mitochondrial Pyruvate Carrier (MPC) is located in the inner membrane of mitochondria and serves as a pyruvate transporter from the cytoplasm into mitochondria. This crucial metabolic crossroad links glycolysis and the tricarboxylic acid (TCA) cycle. MPC is elevated in human HCC samples validated by The Cancer Genome Database (TCGA). Liver-specific MPC depletion in N-nitrosodiethylamine (DEN) plus carbon tetrachloride (CCl4) induced HCC mouse model attenuates HCC tumorigenesis. The underlying mechanism is correlated with the glutamine competition; briefly, disrupting MPC causes decreasing pyruvate flux from the cytosol and, subsequently, glutamine metabolic into α-ketoglutarate to compensate for reduced pyruvate uptake caused by MPC depletion in the TCA cycle. Conversely, glutathione synthesis confirmed to protect cancer cells from reactive oxygen species (ROS) damage, will be competitive as glutamine consumption for the TCA cycle (Tompkins et al., 2019), as shown in Figure 1.

GLS1 is highly expressed in HCC patients and cell lines. Upregulated GLS1 promotes the production of glutamate, the precursor of GSH, which serves as the main cellular antioxidant. The reduction of ROS will enhance the translocation of β-catenin, upregulating the stemness-related genes (KFL4, NANOG, OCT4, SOX2, CD13, and CD44) in HCC (Li et al., 2019). Oxoglutarate dehydrogenase-like (OGDHL) is one of the rate-limiting enzymes of oxoglutarate dehydrogenase complex (OGDHC) in the canonical TCA cycle. OGDHL is verified to be low expressed in the TCGA database, Gene Expression Omnibus (GEO) database, and FUDAN database. The downregulation of OGHDL is associated with HCC progression, poor prognosis, and recurrence. Mechanically, low OGDHL reduces the forward TCA cycle for glucose oxidation. Conversely, reductive carboxylation of α-ketoglutarate (αKG) is facilitated to promote lipogenesis. Moreover, increasing glutamine consumption enhances antioxidative function to protect against oxidative stress in HCC, inhibiting glutamine metabolism could improve sorafenib resistance (Dai et al., 2020). Glutamine deprivation promotes a shift of glycolysis towards oxidative phosphorylation (OXPHOS) in HCC cell lines. The mechanism underlying this phenomenon is glutamine deprivation inducing increased NADP1/NADPH ratio and GSH/GSSG ratio that causes an elevation of cellular reactive oxygen species (ROS); increased ROS enhances the overexpression of retinoic acid-related orphan receptor alpha (RORα), and RORα mediates reprogramming of glucose metabolism towards OXPHOS rather than glycolysis by attenuating pyruvate dehydrogenase kinase 2 (PDK2) and lactate dehydrogenase A (LDHA) (Byun et al., 2015). However, a study finds that the serine biosynthesis pathway (SSP) is activated, and cMyc expression is elevated during glucose or glutamine deprivation. The potential mechanism might be related to cMyc-regulated enzymes like glutathione (GSH) and phosphoserine phosphatase (PSPH), which promote redox hemostasis for cancer cells and activate the serine biosynthesis pathway (Sun et al., 2015). Selected sorafenib-resistant HCC cell lines display higher reductive glutamine metabolism than parental cell lines. Mechanisms, increased expression of PPARδ in sorafenib-resistant HCC induces higher expression of enzymes that catalyze glutamine metabolism and pentose phosphate pathway, incredibly reductive glutamine metabolism in the TCA cycle. The redox homeostasis that protects from oxidative stress will be enhanced by more glutamate synthesis from glutamine, and more reductive glutamine metabolism promotes lipid biosynthesis that promotes HCC proliferation. Moreover, more pentose phosphate pathway products facilitate HCC proliferation (Kim et al., 2017).

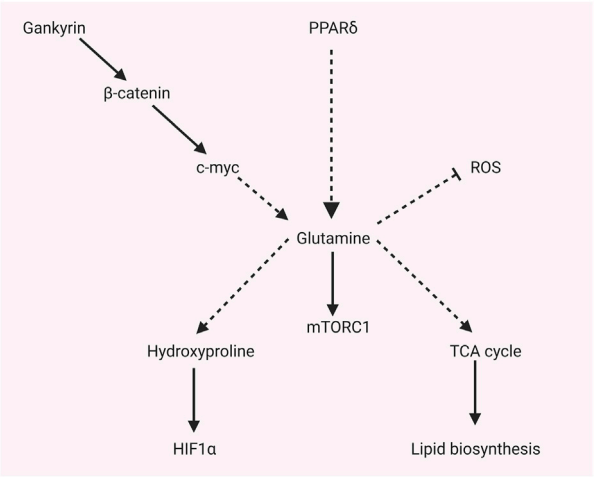


FIGURE 2
Glutamine-related metabolites regulate other metabolisms or signaling pathways.

## 5.4 Glutamine-related metabolites activate the mTORC signaling pathway

GS and mTORC are highly expressed in the β-Catenin gene mutated mouse model with HCC or HCA. In clinical samples, cases with CTNNB1 mutation show intense GS staining, and GS strongly positive cases display high staining for p-mTOR-S2448. In normal mice, GS and p-mTOR-S2448 co-staining in pericentral hepatocytes. The mechanism of β-Catenin mutation-related HCC is induced by β-Catenin -GS-mTORC1 axis. Briefly, CTNNB1-mutation induces GS transcription by β-Catenin translocation and activating transcription factors. The elevated GS will catalyze more glutamate to glutamine; subsequently, glutamine promotes p-mTOR activation, promoting the proliferation of HCC (Adebayo Michael et al., 2019), as shown in Figure 1. Liver receptor homolog 1 (LRH-1) increases in the DEN-induced HCC mouse model. LRH-1 knockout mice display fewer tumors than wild ones. Mechanisms, LRH-1 enhances noncanonical glutamine metabolism by increasing GLS2, which catalyzes Gln to Glu, then Glu converts to α-KG by glutamate pyruvate transaminase 2 (Gpt2). Subsequently, α-KG will modulate mTORC1, facilitating cell proliferation (Xu et al., 2016). c-Myc-dependent hepatocarcinogenesis requires mTORC1 pathway activation to acquire the property of tumorigenesis. Mechanisms, amplification, or activation of c-Myc as a transcriptional factor leads to high expression of amino acid transporters SLC1A5/SLC7A6; increased amino acid transporters are responsible for more amino acid uptake, especially glutamine. After that, increasing amino acids results in mTORC1 activation, a typical pathway that induces cell proliferation (Liu et al., 2017). Nine unique short hairpin RNA (shRNA) vectors and six unique CRISPR-Cas9 vectors are used to

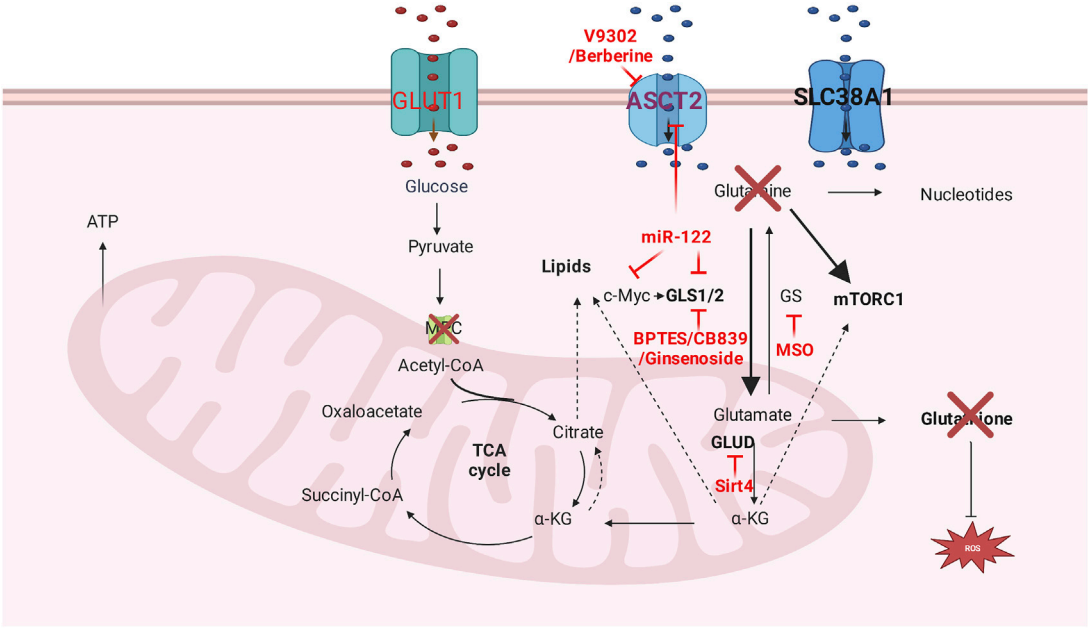


FIGURE 3
Glutamine metabolism targeting therapy. Glutamine transporters inhibitors, glutamine deprivation, and glutamine metabolism related enzyme inhibitors are dominant methods that targeting glutamine metabolism.

repress the expression of glutamine transporter (ASCT2), and L-Type Amino Acid Transporter 1 (LAT1), glutamine or leucine transportation is restrained. However, the mTORC1 pathway and cell proliferation are unchanged (Bothwell et al., 2018).

## 5.5 Glutamine-related metabolites regulate other metabolisms or signaling pathways

As shown in Figure 2, glutamine and related metabolites not only activate the mTORC signaling pathway, but also regulate other metabolisms or signaling pathways. The downstream amino acid of glutamine metabolism, hydroxyproline, is confirmed to play a crucial role in promoting a hypoxic response in HCC. Hydroxyproline is accumulated in HCC according to global metabolic profiling. A high level of hydroxyproline is correlated with elevated AFP and poor prognosis. Mechanically, hydroxyproline blocks hydroxylation of HIF1α and attenuates the binding of HIF1α to tumor suppressor proteins during hypoxia to increase the HIF1α expression. Exogenous hydroxyproline could recover the effect of Myc or ALDH18A1 knockdown, which inhibits the glutamine–hydroxyproline metabolism or proline metabolic pathway. Moreover, hydroxyproline inhibition could attenuate the sorafenib resistance under hypoxia (Tang et al., 2018). Activated mTORC1 induced by knockout of tumor suppressor gene tuberous sclerosis complex (TSC) promotes glutaminolysis, leading to glutamine depletion. Fibroblast growth factor 21 (FGF21) will be activated by glutamine depletion stress by activating peroxisome proliferator–activated receptor γ coactivator-1α (PGC-1α). Elevated FGF21 results in reduced liver triglyceride content, decreased locomotor activity, and body temperature (Cornu et al., 2014). Selected sorafenib-resistant HCC cell lines display higher reductive glutamine metabolism than parental cell lines. Mechanisms, increased expression of PPARδ in sorafenib-resistant HCC induces higher expression of enzymes that catalyze glutamine metabolism and pentose phosphate pathway, incredibly reductive glutamine metabolism in the TCA cycle. The redox homeostasis that protects from oxidative stress will be enhanced by more glutamate synthesis from glutamine, and more reductive glutamine metabolism promotes lipid biosynthesis that promotes HCC proliferation. Moreover, more pentose phosphate pathway products facilitate HCC proliferation (Kim et al., 2017). Uncoupling protein (UCP) 2 is a type of the mitochondrial carrier family involved in metabolic disorders. UCP2 promotes glutaminolysis to decrease glutamine-derived C4 metabolite accumulation in mitochondria. However, it reduces the oxidation of glucose (Vozza et al., 2014). Liver-specific miR-122 is validated to play a critical role in glutamine metabolism. miR-122 is negatively correlated with the expression of GLS, according to the TCGA database. The liver-specific knockout of miR-122 promotes glutaminolysis but inhibits gluconeogenesis in mice by decreasing targets of GLS and SLC1A5 (Sengupta et al., 2020). Gankyrin is a seven ankyrin-repeat domains protein. It promotes HCC tumorigenesis, metastasis, and sorafenib or regrafenib resistance. Mechanisms, it stabilizes RNA-binding protein HuR, which subsequently stabilizes β-catenin mRNA and increases its expression. β-catenin could promote c-myc expression, which regulates glycolysis and glutaminolysis by transcriptionally activating crucial enzymes such as GLUT1, ASCT2, HK2, PKM2, LDHA, and GLS1. Gankyrin displays the characteristics that facilitate glycolysis and glutaminolysis, which c-myc inhibitors could abolish *in vitro* and *in vivo*. High Gankyrin and high β-catenin indicate poor prognosis with low overall survival (Liu et al., 2019).

## 6 Glutamine metabolism targeting therapy

Glutamine metabolism targeting therapy includes glutamine deprivation, related enzyme inhibitors, and transporters inhibitors, as shown in Figure 3. Glutamine deprivation impairs severe metabolism reprogramming in a poorly differentiated cell line, which results in kinase inhibitors resistance as increased phosphorylation of extracellular signal-regulated kinase (Nwosu et al., 2020). Additional glutamine supplement displays dose-dependent anti-tumor effects in HepG2 and Huh7 cell lines and increases the sensitivity of histone deacetylase inhibitor vorinostat in both cell lines (Hassan et al., 2021). 30% of glutamine is metabolized to produce glutamate in the cytoplasm, which functions as the substrate of nucleotide synthesis. Inhibition of glutamate excretion will perturb cell growth *in vitro* (Nilsson et al., 2020).

GLS loss or GLS-specific inhibitor bis-2-(5-phenylacetamido-1,3,4-thiadiazol-2-yl)ethyl sulfide (BPTES) attenuates tumor progression and prolonged survival in Myc-driven HCC mouse model (Xiang et al., 2015). Noncompetitive allosteric GLS1 inhibitor CB-839 monotherapy displays insufficient anti-cancer effectiveness in HCC cell lines. Nevertheless, ASCT-2 inhibitor V-9302 could be synergistic with CB-839 to function as anti-tumor efficacy. Mechanically, the combination of V-9302 and CB-839 disrupts ROS balance by decreasing important antioxidant-glutathione (GSH). Moreover, reducing glutamine intake in TCA results in the reduction of NADPH, which serves as GSH biosynthesis (Jin et al., 2020). Ginsenoside Rk1 demonstrates anti-tumor effectiveness by downregulating GLS1, decreasing GSH, and subsequently accumulating ROS (Lu et al., 2022); and there are two clinical trials that use Ginsenoside in hepatocellular carcinoma(NCT01717066, NCT04523467). Dihydroartemisinin (DHA) induces oxidative stress in cancer cells by increasing intracellular reactive oxygen species (ROS). Glutaminase (GLS) 1 increases the production of antioxidants like GSH by generating the precursor glutamate. The combination of GLS1 inhibitor and DHA has synergistic antitumor efficacy in HCC by increasing ROS and decreasing GSH (Wang et al., 2016).

Berberine inhibits the proliferation of HCC cell lines by suppressing c-myc-induced glutamine transporter SLC1A5, subsequently decreasing glutamine uptake (Zhang et al., 2019). Glutamine depletion by bacterial enzyme Crisantaspase and/or GS inhibitor methionine-L-sulfoximine (MSO) hinders the tumor growth of human HCC xenografts induced by CTNNB1-mutated HCC cell lines (Chiu et al., 2014). β-catenin-mutated HCC cell line is more sensitive to glutaminolysis drug-asparaginase (ASNase) (Tardito et al., 2011). Tigecycline, an electron transport system (ETS) inhibiting antibiotic, is effective in both sorafenib-resistant advanced-stage HCC *in vitro* and in xenograft *in vivo*. The mechanism disrupts the mitochondrial ETS complex biogenesis and impairs glutamine oxidation (Meßner et al., 2020). Oral nutritional supplement (ONS) that contains β-hydroxy-β-methyl butyrate (HMB), L-arginine, and L-glutamine serves as effective prophylactic supplementation for Hand-foot skin reaction (HFSR) caused by sorafenib in advanced HCC patients (Naganuma et al., 2019).

## 7 Conclusion

Metabolism reprogramming plays a pivotal role in HCC; It's not only the outcome of HCC initiation or progression but also the mainstay of factors causing HCC occurrence or promoting HCC metastasis. The components of glutamine metabolism are altered in HCC, indicating biomarkers' potential roles, including related metabolism-related enzymes, metabolites, and metabolites' transporters. The glutamine metabolism reprogramming support HCC cancer cells as carbon and nitrogen sources; It provides antioxidant for HCC survival; It activates the mTORC signaling pathway to support tumor cell proliferation. Targeting glutamine reprogramming, including glutamine deprivation, related enzyme inhibitors, and transporters inhibitors, therefore simultaneously limit energy availability and increase oxidative stress, demonstrate potential therapy in HCC; However, cancers can evade this metabolic trap by reprograming their metabolism (Halama and Suhre, 2022), which is confirmed in ClinicalTrial. Therefore, the effectiveness that rely solely on of glutamine inhibition is limited; cotreatment with other strategies might constitute an attractive and promising option for HCC patients.

## Author contributions

YY, BY, and HW searched the literature; YY and FY designed and drafted the figures; YY, BY, and HW drafted the manuscript; FY revised the manuscript. All authors contributed to the article and approved the submitted version.

## Funding

This work was funded by the National Natural Science Foundation of China (grant No. 82260130), Jiangxi provincial department of science and technology (grant No. 20203BBGL73144, No. 20224BAB206021).

## Acknowledgments

We acknowledged the authors of the paper included in this study.

## Conflict of interest

The authors declare that the research was conducted in the absence of any commercial or financial relationships that could be construed as a potential conflict of interest.

## Publisher's note

# References

Adebayo Michael, A. O., Ko, S., Tao, J., Moghe, A., Yang, H., Xu, M., et al. (2019). Inhibiting glutamine-dependent mTORC1 activation ameliorates liver cancers driven by β-catenin mutations. *Cell Metab.* 29 (5), 1135–1150.e6. doi:10.1016/j.cmet.2019.01.002

Ahodantin, J., Lekbaby, B., Bou Nader, M., Soussan, P., and Kremsdorf, D. (2020). Hepatitis B virus X protein enhances the development of liver fibrosis and the expression of genes associated with epithelial-mesenchymal transitions and tumor progenitor cells. *Carcinogenesis* 41 (3), 358–367. doi:10.1093/carcin/bgz109

Alannan, M., Fayyad-Kazan, H., Trézéguet, V., and Merched, A. (2020). Targeting lipid metabolism in liver cancer. *Biochemistry* 59 (41), 3951–3964. doi:10.1021/acs.biochem.0c00477

Altman, B. J., Stine, Z. E., and Dang, C. V. (2016). From krebs to clinic: glutamine metabolism to cancer therapy. *Nat. Rev. Cancer* 16 (10), 619–634. doi:10.1038/nrc.2016.114

Ando, S., Shibahara, J., Hayashi, A., and Fukayama, M. (2015). β-Catenin alteration is rare in hepatocellular carcinoma with steatohepatitic features: immunohistochemical and mutational study. *Virchows Arch.* 467 (5), 535–542. doi:10.1007/s00428-015-1836-2

Ataide, E. C., Perales, S. R., Silva, M. G., Filho, F. C., Sparapani, A. C., Latuf Filho, P. F., et al. (2017). Immunoexpression of heat shock protein 70, glypican 3, glutamine synthetase, and beta-catenin in hepatocellular carcinoma after liver transplantation: association between positive glypican 3 and beta-catenin with the presence of larger nodules. *Transpl. Proc.* 49 (4), 858–862. doi:10.1016/j.transproceed.2017.01.048

Austinat, M., Dunsch, R., Wittekind, C., Tannapfel, A., Gebhardt, R., and Gaunitz, F. (2008). Correlation between beta-catenin mutations and expression of Wnt-signaling target genes in hepatocellular carcinoma. *Mol. Cancer* 7, 21. doi:10.1186/1476-4598-7-21

Bakheet, A. M. H., Zhao, C., Chen, J. N., Zhang, J. Y., Huang, J. T., Du, Y., et al. (2020). Improving pathological early diagnosis and differential biomarker value for hepatocellular carcinoma via RNAscope technology. *Hepatol. Int.* 14 (1), 96–104. doi:10.1007/s12072-019-10006-z

Bao, M. H., and Wong, C. C. (2021). Hypoxia, metabolic reprogramming, and drug resistance in liver cancer. *Cells* 10 (7), 1715. doi:10.3390/cells10071715

Bhutia, Y. D., and Ganapathy, V. (2016). Glutamine transporters in mammalian cells and their functions in physiology and cancer. *Biochim. Biophys. Acta* 1863 (10), 2531–2539. doi:10.1016/j.bbamcr.2015.12.017

Biancur, D. E., Paulo, J. A., Małachowska, B., Quiles Del Rey, M., Sousa, C. M., Wang, X., et al. (2017). Compensatory metabolic networks in pancreatic cancers upon perturbation of glutamine metabolism. *Nat. Commun.* 8, 15965. doi:10.1038/ncomms15965

Bioulac-Sage, P., Laumonier, H., Rullier, A., Cubel, G., Laurent, C., Zucman-Rossi, J., et al. (2009). Over-expression of glutamine synthetase in focal nodular hyperplasia: A novel easy diagnostic tool in surgical pathology. *Liver Int.* 29 (3), 459–465. doi:10.1111/j.1478-3231.2008.01849.x

Bothwell, P. J., Kron, C. D., Wittke, E. F., Czerniak, B. N., and Bode, B. P. (2018). Targeted suppression and knockout of ASCT2 or LAT1 in epithelial and mesenchymal human liver cancer cells fail to inhibit growth. *Int. J. Mol. Sci.* 19 (7), 2093. doi:10.3390/ijms19072093

Buchard, B., Teilhet, C., Abeywickrama Samarakoon, N., Massoulier, S., Joubert-Zakeyh, J., Blouin, C., et al. (2021). Two metabolomics phenotypes of human hepatocellular carcinoma in non-alcoholic fatty liver disease according to fibrosis severity. *Metabolites* 11 (1), 54. doi:10.3390/metabo11010054

Byun, J. K., Choi, Y. K., Kang, Y. N., Jang, B. K., Kang, K. J., Jeon, Y. H., et al. (2015). Retinoic acid-related orphan receptor alpha reprograms glucose metabolism in glutamine-deficient hepatoma cells. *Hepatology* 61 (3), 953–964. doi:10.1002/hep.27577

Byun, J. K., Lee, S., Kang, G. W., Lee, Y. R., Park, S. Y., Song, I. S., et al. (2022). Macropinocytosis is an alternative pathway of cysteine acquisition and mitigates sorafenib-induced ferroptosis in hepatocellular carcinoma. *J. Exp. Clin. Cancer Res.* 41 (1), 98. doi:10.1186/s13046-022-02296-3

Byun, J. K., Park, M., Lee, S., Yun, J. W., Lee, J., Kim, J. S., et al. (2020). Inhibition of glutamine utilization synergizes with immune checkpoint inhibitor to promote antitumor immunity. *Mol. Cell* 80 (4), 592–606.e8. doi:10.1016/j.molcel.2020.10.015

Cadoret, A., Ovejero, C., Terris, B., Souil, E., Lévy, L., Lamers, W. H., et al. (2002). New targets of beta-catenin signaling in the liver are involved in the glutamine metabolism. *Oncogene* 21 (54), 8293–8301. doi:10.1038/sj.onc.1206118

Casadei-Gardini, A., Del Coco, L., Marisi, G., Conti, F., Rovesti, G., Ulivi, P., et al. (2020). (1)H-NMR based serum metabolomics highlights different specific biomarkers between early and advanced hepatocellular carcinoma stages. *Cancers (Basel)* 12 (1), 241. doi:10.3390/cancers12010241

Chen, M., Lu, S., Zheng, H., Xu, M., Song, J., Yang, W., et al. (2019). Identification of the potential metabolic pathways involved in the hepatic tumorigenesis of rat diethylnitrosamine-induced hepatocellular carcinoma via (1)H NMR-based metabolomic analysis. *Biomed. Res. Int.* 2019, 9367082. doi:10.1155/2019/9367082

Chiu, M., Tardito, S., Pillozzi, S., Arcangeli, A., Armento, A., Uggeri, J., et al. (2014). Glutamine depletion by crisantaspase hinders the growth of human hepatocellular carcinoma xenografts. *Br. J. Cancer* 111 (6), 1159–1167. doi:10.1038/bjc.2014.425

Cluntun, A. A., Lukey, M. J., Cerione, R. A., and Locasale, J. W. (2017). Glutamine metabolism in cancer: understanding the heterogeneity. *Trends Cancer* 3 (3), 169–180. doi:10.1016/j.trecan.2017.01.005

Coral, G. P., Branco, F., Meurer, R., Marcon, P. D. S., Fontes, P. R. O., and Mattos, A. A. (2021). Results of immunohistochemistry in the differential diagnosis of early hepatocellular carcinoma and nodules with high-grade dysplasia in patients with cirrhosis. *Arq. Gastroenterol.* 58 (1), 82–86. doi:10.1590/S0004-2803.202100000-14

Cornu, M., Oppliger, W., Albert, V., Robitaille, A. M., Trapani, F., Quagliata, L., et al. (2014). Hepatic mTORC1 controls locomotor activity, body temperature, and lipid metabolism through FGF21. *Proc. Natl. Acad. Sci. U. S. A.* 111 (32), 11592–11599. doi:10.1073/pnas.1412047111

Cox, A. G., Hwang, K. L., Brown, K. K., Evason, K., Beltz, S., Tsomides, A., et al. (2016). Yap reprograms glutamine metabolism to increase nucleotide biosynthesis and enable liver growth. *Nat. Cell Biol.* 18 (8), 886–896. doi:10.1038/ncb3389

Dai, W., Xu, L., Yu, X., Zhang, G., Guo, H., Liu, H., et al. (2020). OGDHL silencing promotes hepatocellular carcinoma by reprogramming glutamine metabolism. *J. Hepatol.* 72 (5), 909–923. doi:10.1016/j.jhep.2019.12.015

Dal Bello, B., Rosa, L., Campanini, N., Tinelli, C., Torello Viera, F., D'Ambrosio, G., et al. (2010). Glutamine synthetase immunostaining correlates with pathologic features of hepatocellular carcinoma and better survival after radiofrequency thermal ablation. *Clin. Cancer Res.* 16 (7), 2157–2166. doi:10.1158/1078-0432.CCR-09-1978

DeBerardinis, R. J., Mancuso, A., Daikhin, E., Nissim, I., Yudkoff, M., Wehrli, S., et al. (2007). Beyond aerobic glycolysis: transformed cells can engage in glutamine metabolism that exceeds the requirement for protein and nucleotide synthesis. *Proc. Natl. Acad. Sci. U. S. A.* 104 (49), 19345–19350. doi:10.1073/pnas.0709747104

Di Tommaso, L., and Roncalli, M. (2017). Tissue biomarkers in hepatocellular tumors: which, when, and how. *Front. Med. (Lausanne)* 4, 10. doi:10.3389/fmed.2017.00010

Ding, Z., Ericksen, R. E., Lee, Q. Y., and Han, W. (2021). Reprogramming of mitochondrial proline metabolism promotes liver tumorigenesis. *Amino Acids* 53 (12), 1807–1815. doi:10.1007/s00726-021-02961-5

Dolezal, J. M., Wang, H., Kulkarni, S., Jackson, L., Lu, J., Ranganathan, S., et al. (2017). Sequential adaptive changes in a c-Myc-driven model of hepatocellular carcinoma. *J. Biol. Chem.* 292 (24), 10068–10086. doi:10.1074/jbc.M117.782052

Du, D., Liu, C., Qin, M., Zhang, X., Xi, T., Yuan, S., et al. (2022). Metabolic dysregulation and emerging therapeutical targets for hepatocellular carcinoma. *Acta Pharm. Sin. B* 12 (2), 558–580. doi:10.1016/j.apsb.2021.09.019

Edwards, D. N., Ngwa, V. M., Raybuck, A. L., Wang, S., Hwang, Y., Kim, L. C., et al. (2021). Selective glutamine metabolism inhibition in tumor cells improves antitumor T lymphocyte activity in triple-negative breast cancer. *J. Clin. Invest.* 131 (4), e140100. doi:10.1172/JCI140100

Evason, K. J., Grenert, J. P., Ferrell, L. D., and Kakar, S. (2013). Atypical hepatocellular adenoma-like neoplasms with β-catenin activation show cytogenetic alterations similar to well-differentiated hepatocellular carcinomas. *Hum. Pathol.* 44 (5), 750–758. doi:10.1016/j.humpath.2012.07.019

Faivre, S., Rimassa, L., and Finn, R. S. (2020). Molecular therapies for HCC: looking outside the box. *J. Hepatol.* 72 (2), 342–352. doi:10.1016/j.jhep.2019.09.010

Fan, S. J., Kroeger, B., Marie, P. P., Bridges, E. M., Mason, J. D., McCormick, K., et al. (2020). Glutamine deprivation alters the origin and function of cancer cell exosomes. *Embo J.* 39 (16), e103009. doi:10.15252/embj.2019103009

Feng, J., Li, J., Wu, L., Yu, Q., Ji, J., Wu, J., et al. (2020). Emerging roles and the regulation of aerobic glycolysis in hepatocellular carcinoma. *J. Exp. Clin. Cancer Res.* 39 (1), 126. doi:10.1186/s13046-020-01629-4

Finn, R. S., Qin, S., Ikeda, M., Galle, P. R., Ducreux, M., Kim, T. Y., et al. (2020). Atezolizumab plus bevacizumab in unresectable hepatocellular carcinoma. *N. Engl. J. Med.* 382 (20), 1894–1905. doi:10.1056/NEJMoa1915745

Foerster, F., Gairing, S. J., Ilyas, S. I., and Galle, P. R. (2022). Emerging immunotherapy for HCC: A guide for hepatologists. *Hepatology* 75 (6), 1604–1626. doi:10.1002/hep.32447

Fu, Q., Xu, L., Wang, Y., Jiang, Q., Liu, Z., Zhang, J., et al. (2019). Tumor-associated macrophage-derived interleukin-23 interlinks kidney cancer glutamine addiction with immune evasion. *Eur. Urol.* 75 (5), 752–763. doi:10.1016/j.eururo.2018.09.030

Gao, H., Lu, Q., Liu, X., Cong, H., Zhao, L., Wang, H., et al. (2009). Application of 1H NMR-based metabonomics in the study of metabolic profiling of human hepatocellular carcinoma and liver cirrhosis. *Cancer Sci.* 100 (4), 782–785. doi:10.1111/j.1349-7006.2009.01086.x

Gaunitz, F., Heise, K., Schumann, R., and Gebhardt, R. (2002). Glucocorticoid induced expression of glutamine synthetase in hepatoma cells. *Biochem. Biophys. Res. Commun.* 296 (4), 1026–1032. doi:10.1016/s0006-291x(02)02044-2

Geh, D., Leslie, J., Rumney, R., Reeves, H. L., Bird, T. G., and Mann, D. A. (2022). Neutrophils as potential therapeutic targets in hepatocellular carcinoma. *Nat. Rev. Gastroenterol. Hepatol.* 19 (4), 257–273. doi:10.1038/s41575-021-00568-5

Gong, J., Li, Y., Yu, J., Wang, T., Duan, J., Hu, A., et al. (2021). The predictive role of preoperative serum glutamate dehydrogenase levels in microvascular invasion and hepatocellular carcinoma prognosis following liver transplantation-a single center retrospective study. *PeerJ* 9, e12420. doi:10.7717/peerj.12420

Gross, M. I., Demo, S. D., Dennison, J. B., Chen, L., Chernov-Rogan, T., Goyal, B., et al. (2014). Antitumor activity of the glutaminase inhibitor CB-839 in triple-negative breast cancer. *Mol. Cancer Ther.* 13 (4), 890–901. doi:10.1158/1535-7163.MCT-13-0870

Gyamfi, J., Kim, J., and Choi, J. (2022). Cancer as a metabolic disorder. *Int. J. Mol. Sci.* 23 (3), 1155. doi:10.3390/ijms23031155

Halama, A., and Suhre, K. (2022). Advancing cancer treatment by targeting glutamine metabolism-A roadmap. *Cancers (Basel)* 14 (3), 553. doi:10.3390/cancers14030553

Hamaguchi, K., Miyanishi, K., Osuga, T., Tanaka, S., Ito, R., Sakamoto, H., et al. (2022). Association between hepatic oxidative stress related factors and activation of wnt/β-catenin signaling in NAFLD-induced hepatocellular carcinoma. *Cancers (Basel).* 14 (9), 2066. doi:10.3390/cancers14092066

Hassan, Y. A., Helmy, M. W., and Ghoneim, A. I. (2021). Combinatorial antitumor effects of amino acids and epigenetic modulations in hepatocellular carcinoma cell lines. *Naunyn Schmiedeb. Arch. Pharmacol.* 394 (11), 2245–2257. doi:10.1007/s00210-021-02140-z

Hu, X., He, Y., Han, Z., Liu, W., Liu, D., Zhang, X., et al. (2022). PNO1 inhibits autophagy-mediated ferroptosis by GSH metabolic reprogramming in hepatocellular carcinoma. *Cell Death Dis.* 13 (11), 1010. doi:10.1038/s41419-022-05448-7

Huang, X., Gan, G., Wang, X., Xu, T., and Xie, W. (2019). The HGF-MET axis coordinates liver cancer metabolism and autophagy for chemotherapeutic resistance. *Autophagy* 15 (7), 1258–1279. doi:10.1080/15548627.2019.1580105

Jin, H., Wang, S., Zaal, E. A., Wang, C., Wu, H., Bosma, A., et al. (2020). A powerful drug combination strategy targeting glutamine addiction for the treatment of human liver cancer. *Elife* 9, e56749. doi:10.7554/eLife.56749

Kim, M. J., Choi, Y. K., Park, S. Y., Jang, S. Y., Lee, J. Y., Ham, H. J., et al. (2017). PPARδ reprograms glutamine metabolism in sorafenib-resistant HCC. *Mol. Cancer Res.* 15 (9), 1230–1242. doi:10.1158/1541-7786.MCR-17-0061

Kuo, T. C., Chen, C. K., Hua, K. T., Yu, P., Lee, W. J., Chen, M. W., et al. (2016). Glutaminase 2 stabilizes Dicer to repress Snail and metastasis in hepatocellular carcinoma cells. *Cancer Lett.* 383 (2), 282–294. doi:10.1016/j.canlet.2016.10.012

Kurosaki, S., Nakagawa, H., Hayata, Y., Kawamura, S., Matsushita, Y., Yamada, T., et al. (2021). Cell fate analysis of zone 3 hepatocytes in liver injury and tumorigenesis. *JHEP Rep.* 3 (4), 100315. doi:10.1016/j.jhepr.2021.100315

Lagana, S. M., Salomao, M., Bao, F., Moreira, R. K., Lefkowitch, J. H., and Remotti, H. E. (2013). Utility of an immunohistochemical panel consisting of glypican-3, heat-shock protein-70, and glutamine synthetase in the distinction of low-grade hepatocellular carcinoma from hepatocellular adenoma. *Appl. Immunohistochem. Mol. Morphol.* 21 (2), 170–176. doi:10.1097/PAI.0b013e31825d527f

Lam, K. H., and Ma, S. (2022). Noncellular components in the liver cancer stem cell niche: biology and potential clinical implications. *Hepatology*. doi:10.1002/hep.32629

Lee, A. C. K., Lau, P. M., Kwan, Y. W., and Kong, S. K. (2021). Mitochondrial fuel dependence on glutamine drives chemo-resistance in the cancer stem cells of hepatocellular carcinoma. *Int. J. Mol. Sci.* 22 (7), 3315. doi:10.3390/ijms22073315

Lemberg, K. M., Gori, S. S., Tsukamoto, T., Rais, R., and Slusher, B. S. (2022). Clinical development of metabolic inhibitors for oncology. *J. Clin. Invest.* 132 (1), e148550. doi:10.1172/JCI148550

Leslie, J., Geh, D., Elsharkawy, A. M., Mann, D. A., and Vacca, M. (2022). Metabolic dysfunction and cancer in HCV: shared pathways and mutual interactions. *J. Hepatol.* 77 (1), 219–236. doi:10.1016/j.jhep.2022.01.029

Li, B., Cao, Y., Meng, G., Qian, L., Xu, T., Yan, C., et al. (2019). Targeting glutaminase 1 attenuates stemness properties in hepatocellular carcinoma by increasing reactive oxygen species and suppressing Wnt/beta-catenin pathway. *EBioMedicine* 39, 239–254. doi:10.1016/j.ebiom.2018.11.063

Li, K., Cao, J., Zhang, Z., Chen, K., Ma, T., Yang, W., et al. (2020). Circular RNA circGSK3B promotes cell proliferation, migration, and invasion by sponging miR-1265 and regulating CAB39 expression in hepatocellular carcinoma. *Front. Oncol.* 10, 598256. doi:10.3389/fonc.2020.598256

Li, X., Ramadori, P., Pfister, D., Seehawer, M., Zender, L., and Heikenwalder, M. (2021). The immunological and metabolic landscape in primary and metastatic liver cancer. *Nat. Rev. Cancer* 21 (9), 541–557. doi:10.1038/s41568-021-00383-9

Liang, K. H., Cheng, M. L., Lo, C. J., Lin, Y. H., Lai, M. W., Lin, W. R., et al. (2020). Plasma phenylalanine and glutamine concentrations correlate with subsequent hepatocellular carcinoma occurrence in liver cirrhosis patients: an exploratory study. *Sci. Rep.* 10 (1), 10926. doi:10.1038/s41598-020-67971-x

Liberti, M. V., and Locasale, J. W. (2016). The Warburg effect: how does it benefit cancer cells? *Trends Biochem. Sci.* 41 (3), 211–218. doi:10.1016/j.tibs.2015.12.001

Lin, Y., Jin, H., Wu, X., Jian, Z., Zou, X., Huang, J., et al. (2020). The cross-talk between DDR1 and STAT3 promotes the development of hepatocellular carcinoma. *Aging (Albany NY)* 12 (14), 14391–14405. doi:10.18632/aging.103482

Liu, P., Ge, M., Hu, J., Li, X., Che, L., Sun, K., et al. (2017). A functional mammalian target of rapamycin complex 1 signaling is indispensable for c-Myc-driven hepatocarcinogenesis. *Hepatology* 66 (1), 167–181. doi:10.1002/hep.29183

Liu, P., Lu, D., Al-Ameri, A., Wei, X., Ling, S., Li, J., et al. (2020). Glutamine synthetase promotes tumor invasion in hepatocellular carcinoma through mediating epithelial-mesenchymal transition. *Hepatol. Res.* 50 (2), 246–257. doi:10.1111/hepr.13433

Liu, R., Li, Y., Tian, L., Shi, H., Wang, J., Liang, Y., et al. (2019). A miR-18a binding-site polymorphism in CDC42 3'UTR affects CDC42 mRNA expression in placentas and is associated with litter size in pigs. *Cancer Lett.* 443, 34–41. doi:10.1007/s00335-018-9788-x

Liu, Y., Yang, Y., Jiang, L., Xu, H., and Wei, J. (2021). High expression levels of SLC38A1 are correlated with poor prognosis and defective immune infiltration in hepatocellular carcinoma. *J. Oncol.* 2021, 5680968. doi:10.1155/2021/5680968

Llovet, J. M., Castet, F., Heikenwalder, M., Maini, M. K., Mazzaferro, V., Pinato, D. J., et al. (2022a). Immunotherapies for hepatocellular carcinoma. *Nat. Rev. Clin. Oncol.* 19 (3), 151–172. doi:10.1038/s41571-021-00573-2

Llovet, J. M., Kelley, R. K., Villanueva, A., Singal, A. G., Pikarsky, E., Roayaie, S., et al. (2021). Hepatocellular carcinoma. *Nat. Rev. Dis. Prim.* 7 (1), 6. doi:10.1038/s41572-020-00240-3

Llovet, J. M., Montal, R., Sia, D., and Finn, R. S. (2018). Molecular therapies and precision medicine for hepatocellular carcinoma. *Nat. Rev. Clin. Oncol.* 15 (10), 599–616. doi:10.1038/s41571-018-0073-4

Llovet, J. M., Pinyol, R., Kelley, R. K., El-Khoueiry, A., Reeves, H. L., Wang, X. W., et al. (2022b). Molecular pathogenesis and systemic therapies for hepatocellular carcinoma. *Nat. Cancer* 3 (4), 386–401. doi:10.1038/s43018-022-00357-2

Long, J., Wang, H., Lang, Z., Wang, T., Long, M., and Wang, B. (2011). Expression level of glutamine synthetase is increased in hepatocellular carcinoma and liver tissue with cirrhosis and chronic hepatitis B. *Hepatol. Int.* 5 (2), 698–706. doi:10.1007/s12072-010-9230-2

Lu, H., Yin, H., Qu, L., Ma, X., Fu, R., and Fan, D. (2022). Ginsenoside Rk1 regulates glutamine metabolism in hepatocellular carcinoma through inhibition of the ERK/c-Myc pathway. *Food Funct.* 13 (7), 3793–3811. doi:10.1039/d1fo03728e

Ma, G., Zhang, Z., Li, P., Zhang, Z., Zeng, M., Liang, Z., et al. (2022). Reprogramming of glutamine metabolism and its impact on immune response in the tumor microenvironment. *Cell Commun. Signal* 20 (1), 114. doi:10.1186/s12964-022-00909-0

Marsico, M., Santarsiero, A., Pappalardo, I., Convertini, P., Chiummiento, L., Sardone, A., et al. (2021). Mitochondria-mediated apoptosis of HCC cells triggered by knockdown of glutamate dehydrogenase 1: perspective for its inhibition through quercetin and permethylated anigopreissin A. *Biomedicines* 9 (11), 1664. doi:10.3390/biomedicines9111664

Meßner, M., Schmitt, S., Ardelt, M. A., Fröhlich, T., Müller, M., Pein, H., et al. (2020). Metabolic implication of tigecycline as an efficacious second-line treatment for sorafenib-resistant hepatocellular carcinoma. *Faseb J.* 34 (9), 11860–11882. doi:10.1096/fj.202001128R

Montasser, A., Beaufrère, A., Cauchy, F., Bouattour, M., Soubrane, O., Albuquerque, M., et al. (2021). Transarterial chemoembolisation enhances programmed death-1 and programmed death-ligand 1 expression in hepatocellular carcinoma. *Histopathology* 79 (1), 36–46. doi:10.1111/his.14317

Naganuma, A., Hoshino, T., Ohno, N., Ogawa, Y., Murakami, T., Horiguchi, S., et al. (2019). β-Hydroxy-β-methyl butyrate/L-arginine/L-glutamine supplementation for preventing hand-foot skin reaction in sorafenib for advanced hepatocellular carcinoma. *Vivo* 33 (1), 155–161. doi:10.21873/invivo.11452

Nahon, P., Amathieu, R., Triba, M. N., Bouchemal, N., Nault, J. C., Ziol, M., et al. (2012). Identification of serum proton NMR metabolomic fingerprints associated with hepatocellular carcinoma in patients with alcoholic cirrhosis. *Clin. Cancer Res.* 18 (24), 6714–6722. doi:10.1158/1078-0432.CCR-12-1099

Nilsson, A., Haanstra, J. R., Engqvist, M., Gerding, A., Bakker, B. M., Klingmüller, U., et al. (2020). Quantitative analysis of amino acid metabolism in liver cancer links glutamate excretion to nucleotide synthesis. *Proc. Natl. Acad. Sci. U. S. A.* 117 (19), 10294–10304. doi:10.1073/pnas.1919250117

Nwosu, Z. C., Battello, N., Rothley, M., Piorońska, W., Sitek, B., Ebert, M. P., et al. (2018). Liver cancer cell lines distinctly mimic the metabolic gene expression pattern of the corresponding human tumours. *J. Exp. Clin. Cancer Res.* 37 (1), 211. doi:10.1186/s13046-018-0872-6

Nwosu, Z. C., Piorońska, W., Battello, N., Zimmer, A. D., Dewidar, B., Han, M., et al. (2020). Severe metabolic alterations in liver cancer lead to ERK pathway activation and drug resistance. *EBioMedicine* 54, 102699. doi:10.1016/j.ebiom.2020.102699

Oh, M. H., Sun, I. H., Zhao, L., Leone, R. D., Sun, I. M., Xu, W., et al. (2020). Targeting glutamine metabolism enhances tumor-specific immunity by modulating suppressive myeloid cells. *J. Clin. Invest.* 130 (7), 3865–3884. doi:10.1172/JCI131859

Orabi, D., Berger, N. A., and Brown, J. M. (2021). Abnormal metabolism in the progression of nonalcoholic fatty liver disease to hepatocellular carcinoma: mechanistic

insights to chemoprevention. *Cancers (Basel).* 13 (14), 3473. doi:10.3390/cancers13143473

Pallett, L. J., Dimeloe, S., Sinclair, L. V., Byrne, A. J., and Schurich, A. (2021). A glutamine 'tug-of-war': targets to manipulate glutamine metabolism for cancer immunotherapy. *Immunother. Adv.* 1 (1), ltab010. doi:10.1093/immadv/ltab010

Rebouissou, S., Franconi, A., Calderaro, J., Letouzé, E., Imbeaud, S., Pilati, C., et al. (2016). Genotype-phenotype correlation of CTNNB1 mutations reveals different ß-catenin activity associated with liver tumor progression. *Hepatology* 64 (6), 2047–2061. doi:10.1002/hep.28638

Rebouissou, S., and Nault, J. C. (2020). Advances in molecular classification and precision oncology in hepatocellular carcinoma. *J. Hepatol.* 72 (2), 215–229. doi:10.1016/j.jhep.2019.08.017

Reig, M., Forner, A., Rimola, J., Ferrer-Fàbrega, J., Burrel, M., Garcia-Criado, Á., et al. (2022). BCLC strategy for prognosis prediction and treatment recommendation: the 2022 update. *J. Hepatol.* 76 (3), 681–693. doi:10.1016/j.jhep.2021.11.018

Reig, M., Mariño, Z., Perelló, C., Iñarrairaegui, M., Ribeiro, A., Lens, S., et al. (2016). Unexpected high rate of early tumor recurrence in patients with HCV-related HCC undergoing interferon-free therapy. *J. Hepatol.* 65 (4), 719–726. doi:10.1016/j.jhep.2016.04.008

Ruiz de Galarreta, M., Bresnahan, E., Molina-Sánchez, P., Lindblad, K. E., Maier, B., Sia, D., et al. (2019). β-Catenin activation promotes immune escape and resistance to anti-PD-1 therapy in hepatocellular carcinoma. *Cancer Discov.* 9 (8), 1124–1141. doi:10.1158/2159-8290.CD-19-0074

Satriano, L., Lewinska, M., Rodrigues, P. M., Banales, J. M., and Andersen, J. B. (2019). Metabolic rearrangements in primary liver cancers: cause and consequences. *Nat. Rev. Gastroenterol. Hepatol.* 16 (12), 748–766. doi:10.1038/s41575-019-0217-8

Schulte, M. L., Fu, A., Zhao, P., Li, J., Geng, L., Smith, S. T., et al. (2018). Pharmacological blockade of ASCT2-dependent glutamine transport leads to antitumor efficacy in preclinical models. *Nat. Med.* 24 (2), 194–202. doi:10.1038/nm.4464

Sengupta, D., Cassel, T., Teng, K. Y., Aljuhani, M., Chowdhary, V. K., Hu, P., et al. (2020). Regulation of hepatic glutamine metabolism by miR-122. *Mol. Metab.* 34, 174–186. doi:10.1016/j.molmet.2020.01.003

Serra, M., Di Matteo, M., Serneels, J., Pal, R., Cafarello, S. T., Lanza, M., et al. (2022). Deletion of lactate dehydrogenase-A impairs oncogene-induced mouse hepatocellular carcinoma development. *Cell Mol. Gastroenterol. Hepatol.* 14, 609–624. doi:10.1016/j.jcmgh.2022.06.003

Shen, Y. A., Chen, C. L., Huang, Y. H., Evans, E. E., Cheng, C. C., Chuang, Y. J., et al. (2021). Inhibition of glutaminolysis in combination with other therapies to improve cancer treatment. *Curr. Opin. Chem. Biol.* 62, 64–81. doi:10.1016/j.cbpa.2021.01.006

Shin, E., Ryu, H. S., Kim, S. H., Jung, H., Jang, J. J., and Lee, K. (2011). The clinicopathological significance of heat shock protein 70 and glutamine synthetase expression in hepatocellular carcinoma. *J. Hepatobiliary Pancreat. Sci.* 18 (4), 544–550. doi:10.1007/s00534-010-0367-0

Sohn, B. H., Park, I. Y., Shin, J. H., Yim, S. Y., and Lee, J. S. (2018). Glutamine synthetase mediates sorafenib sensitivity in β-catenin-active hepatocellular carcinoma cells. *Exp. Mol. Med.* 50 (1), e421. doi:10.1038/emm.2017.174

Soukupova, J., Malfettone, A., Hyroššová, P., Hernández-Alvarez, M. I., Peñuelas-Haro, I., Bertran, E., et al. (2017). Role of the Transforming Growth Factor-β in regulating hepatocellular carcinoma oxidative metabolism. *Sci. Rep.* 7 (1), 12486. doi:10.1038/s41598-017-12837-y

Sun, H. W., Yu, X. J., Wu, W. C., Chen, J., Shi, M., Zheng, L., et al. (2016). GLUT1 and ASCT2 as predictors for prognosis of hepatocellular carcinoma. *PLoS One* 11 (12), e0168907. doi:10.1371/journal.pone.0168907

Sun, L., Song, L., Wan, Q., Wu, G., Li, X., Wang, Y., et al. (2015). cMyc-mediated activation of serine biosynthesis pathway is critical for cancer progression under nutrient deprivation conditions. *Cell Res.* 25 (4), 429–444. doi:10.1038/cr.2015.33

Tang, L., Zeng, J., Geng, P., Fang, C., Wang, Y., Sun, M., et al. (2018). Global metabolic profiling identifies a pivotal role of proline and hydroxyproline metabolism in supporting hypoxic response in hepatocellular carcinoma. *Clin. Cancer Res.* 24 (2), 474–485. doi:10.1158/1078-0432.CCR-17-1707

Tao, J., Krutsenko, Y., Moghe, A., Singh, S., Poddar, M., Bell, A., et al. (2021). Nuclear factor erythroid 2-related factor 2 and β-catenin coactivation in hepatocellular cancer: biological and therapeutic implications. *Hepatology* 74 (2), 741–759. doi:10.1002/hep.31730

Tardito, S., Chiu, M., Uggeri, J., Zerbini, A., Da Ros, F., Dall'Asta, V., et al. (2011). L-Asparaginase and inhibitors of glutamine synthetase disclose glutamine addiction of β-catenin-mutated human hepatocellular carcinoma cells. *Curr. Cancer Drug Targets* 11 (8), 929–943. doi:10.2174/156800911797264725

Teilhet, C., Morvan, D., Joubert-Zakeyh, J., Biesse, A. S., Pereira, B., Massoulier, S., et al. (2017). Specificities of human hepatocellular carcinoma developed on non-alcoholic fatty liver disease in absence of cirrhosis revealed by tissue extracts $^{1}$H-NMR spectroscopy. *Metabolites* 7 (4), 49. doi:10.3390/metabo7040049

Tenen, D. G., Chai, L., and Tan, J. L. (2021). Metabolic alterations and vulnerabilities in hepatocellular carcinoma. *Gastroenterol. Rep. (Oxf).* 9 (1), 1–13. doi:10.1093/gastro/goaa066

Tompkins, S. C., Sheldon, R. D., Rauckhorst, A. J., Noterman, M. F., Solst, S. R., Buchanan, J. L., et al. (2019). Disrupting mitochondrial pyruvate uptake directs glutamine into the TCA cycle away from glutathione synthesis and impairs hepatocellular tumorigenesis. *Cell Rep.* 28 (10), 2608–2619.e6. doi:10.1016/j.celrep.2019.07.098

Tremosini, S., Forner, A., Boix, L., Vilana, R., Bianchi, L., Reig, M., et al. (2012). Prospective validation of an immunohistochemical panel (glypican 3, heat shock protein 70 and glutamine synthetase) in liver biopsies for diagnosis of very early hepatocellular carcinoma. *Gut* 61 (10), 1481–1487. doi:10.1136/gutjnl-2011-301862

Tsujikawa, H., Masugi, Y., Yamazaki, K., Itano, O., Kitagawa, Y., and Sakamoto, M. (2016). Immunohistochemical molecular analysis indicates hepatocellular carcinoma subgroups that reflect tumor aggressiveness. *Hum. Pathol.* 50, 24–33. doi:10.1016/j.humpath.2015.10.014

Uthamalingam, P., Das, A., Behra, A., Kalra, N., and Chawla, Y. (2018). Diagnostic value of Glypican3, heat shock protein 70 and glutamine synthetase in hepatocellular carcinoma arising in cirrhotic and non-cirrhotic livers. *J. Clin. Exp. Hepatol.* 8 (2), 173–180. doi:10.1016/j.jceh.2017.09.005

Van Treeck, B. J., Mounajjed, T., Moreira, R. K., Orujov, M., Allende, D. S., Bellizzi, A. M., et al. (2021). Transcriptomic and proteomic analysis of steatohepatitic hepatocellular carcinoma reveals novel distinct biologic features. *Am. J. Clin. Pathol.* 155 (1), 87–96. doi:10.1093/ajcp/aqaa114

Vibert, E., Schwartz, M., and Olthoff, K. M. (2020). Advances in resection and transplantation for hepatocellular carcinoma. *J. Hepatol.* 72 (2), 262–276. doi:10.1016/j.jhep.2019.11.017

Vozza, A., Parisi, G., De Leonardis, F., Lasorsa, F. M., Castegna, A., Amorese, D., et al. (2014). UCP2 transports C4 metabolites out of mitochondria, regulating glucose and glutamine oxidation. *Proc. Natl. Acad. Sci. U. S. A.* 111 (3), 960–965. doi:10.1073/pnas.1317400111

Wang, C., Cao, Y., Yang, C., Bernards, R., and Qin, W. (2021). Exploring liver cancer biology through functional genetic screens. *Nat. Rev. Gastroenterol. Hepatol.* 18 (10), 690–704. doi:10.1038/s41575-021-00465-x

Wang, D., Meng, G., Zheng, M., Zhang, Y., Chen, A., Wu, J., et al. (2016). The glutaminase-1 inhibitor 968 enhances dihydroartemisinin-mediated antitumor efficacy in hepatocellular carcinoma cells. *PLoS One* 11 (11), e0166423. doi:10.1371/journal.pone.0166423

Wang, H., Yu, L., Huang, P., Zhou, Y., Zheng, W., Meng, N., et al. (2022). Tumor-associated exosomes are involved in hepatocellular carcinoma tumorigenesis, diagnosis, and treatment. *J. Clin. Transl. Hepatol.* 10 (3), 496–508. doi:10.14218/JCTH.2021.00425

Wang, Y. S., Du, L., Liang, X., Meng, P., Bi, L., Wang, Y. L., et al. (2019). Sirtuin 4 depletion promotes hepatocellular carcinoma tumorigenesis through regulating adenosine-monophosphate-activated protein kinase alpha/mammalian target of rapamycin Axis in mice. *Hepatology* 69 (4), 1614–1631. doi:10.1002/hep.30421

Wasfy, R. E., and Shams Eldeen, A. A. (2015). Roles of combined glypican-3 and glutamine synthetase in differential diagnosis of hepatocellular lesions. *Asian Pac J. Cancer Prev.* 16 (11), 4769–4775. doi:10.7314/apjcp.2015.16.11.4769

Wei, Y., Tang, X., Ren, Y., Yang, Y., Song, F., Fu, J., et al. (2021). An RNA-RNA crosstalk network involving HMGB1 and RICTOR facilitates hepatocellular carcinoma tumorigenesis by promoting glutamine metabolism and impedes immunotherapy by PD-L1+ exosomes activity. *Signal Transduct. Target Ther.* 6 (1), 421. doi:10.1038/s41392-021-00801-2

Wise, D. R., and Thompson, C. B. (2010). Glutamine addiction: A new therapeutic target in cancer. *Trends Biochem. Sci.* 35 (8), 427–433. doi:10.1016/j.tibs.2010.05.003

Witjes, C. D., ten Kate, F. J., Verhoef, C., and de Man, R. A. (2013). Immunohistochemical characteristics of hepatocellular carcinoma in non-cirrhotic livers. *J. Clin. Pathol.* 66 (8), 687–691. doi:10.1136/jclinpath-2012-201156

Xi, J., Sun, Y., Zhang, M., Fa, Z., Wan, Y., Min, Z., et al. (2019). GLS1 promotes proliferation in hepatocellular carcinoma cells via AKT/GSK3β/CyclinD1 pathway. *Exp. Cell Res.* 381 (1), 1–9. doi:10.1016/j.yexcr.2019.04.005

Xiang, Y., Stine, Z. E., Xia, J., Lu, Y., O'Connor, R. S., Altman, B. J., et al. (2015). Targeted inhibition of tumor-specific glutaminase diminishes cell-autonomous tumorigenesis. *J. Clin. Invest.* 125 (6), 2293–2306. doi:10.1172/JCI75836

Xu, C., Xu, Z., Zhang, Y., Evert, M., Calvisi, D. F., Chen, X., et al. (2022). SIRPγ-expressing cancer stem-like cells promote immune escape of lung cancer via Hippo signaling. *J. Clin. Invest.* 132 (4), e141797. doi:10.1172/JCI141797

Xu, P., Oosterveer, M. H., Stein, S., Demagny, H., Ryu, D., Moullan, N., et al. (2016). LRH-1-dependent programming of mitochondrial glutamine processing drives liver cancer. *Genes Dev.* 30 (11), 1255–1260. doi:10.1101/gad.277483.116

Yang, J. D., Hainaut, P., Gores, G. J., Amadou, A., Plymoth, A., and Roberts, L. R. (2019). A global view of hepatocellular carcinoma: trends, risk, prevention and management. *Nat. Rev. Gastroenterol. Hepatol.* 16 (10), 589–604. doi:10.1038/s41575-019-0186-y

Yang, L., Achreja, A., Yeung, T. L., Mangala, L. S., Jiang, D., Han, C., et al. (2016). Targeting stromal glutamine synthetase in tumors disrupts tumor microenvironment-regulated cancer cell growth. *Cell Metab.* 24 (5), 685–700. doi:10.1016/j.cmet.2016.10.011

Yang, W. H., Qiu, Y., Stamatatos, O., Janowitz, T., and Lukey, M. J. (2021). Enhancing the efficacy of glutamine metabolism inhibitors in cancer therapy. *Trends Cancer* 7 (8), 790–804. doi:10.1016/j.trecan.2021.04.003

Ying, L., Cheng, M., Lu, Y., Tao, Q., Chen, X., Shen, B., et al. (2021). Glutamine metabolism scoring predicts prognosis and therapeutic resistance in hepatocellular carcinoma. *Pathol. Oncol. Res.* 27, 1610075. doi:10.3389/pore.2021.1610075

Yoneda, N., Matsui, O., Kitao, A., Komori, T., Kozaka, K., Ikeda, H., et al. (2018). Peri-tumoral hyperintensity on hepatobiliary phase of gadoxetic acid-enhanced MRI in hepatocellular carcinomas: correlation with peri-tumoral hyperplasia and its pathological features. *Abdom. Radiol. (NY)* 43 (8), 2103–2112. doi:10.1007/s00261-017-1437-4

Yu, W., Yang, X., Zhang, Q., Sun, L., Yuan, S., and Xin, Y. (2021). Targeting GLS1 to cancer therapy through glutamine metabolism. *Clin. Transl. Oncol.* 23 (11), 2253–2268. doi:10.1007/s12094-021-02645-2

Yuneva, M., Zamboni, N., Oefner, P., Sachidanandam, R., and Lazebnik, Y. (2007). Deficiency in glutamine but not glucose induces MYC-dependent apoptosis in human cells. *J. Cell Biol.* 178 (1), 93–105. doi:10.1083/jcb.200703099

Zeng, J., Yin, P., Tan, Y., Dong, L., Hu, C., Huang, Q., et al. (2014). Metabolomics study of hepatocellular carcinoma: discovery and validation of serum potential biomarkers by using capillary electrophoresis-mass spectrometry. *J. Proteome Res.* 13 (7), 3420–3431. doi:10.1021/pr500390y

Zhang, B., Liu, K., Zhang, J., Dong, L., Jin, Z., Zhang, X., et al. (2015). Glutamine synthetase predicts adjuvant TACE response in hepatocellular carcinoma. *Int. J. Clin. Exp. Med.* 8 (11), 20722–20731.

Zhang, J., Pavlova, N. N., and Thompson, C. B. (2017). Cancer cell metabolism: the essential role of the nonessential amino acid, glutamine. *Embo J.* 36 (10), 1302–1315. doi:10.15252/embj.201696151

Zhang, P., Wang, Q., Lin, Z., Yang, P., Dou, K., and Zhang, R. (2019). Berberine inhibits growth of liver cancer cells by suppressing glutamine uptake. *Onco Targets Ther.* 12, 11751–11763. doi:10.2147/OTT.S235667

Zhao, J., Yang, Z., Tu, M., Meng, W., Gao, H., Li, M. D., et al. (2021). Correlation between prognostic biomarker SLC1A5 and immune infiltrates in various types of cancers including hepatocellular carcinoma. *Front. Oncol.* 11, 608641. doi:10.3389/fonc.2021.608641

Zhou, F., and Sun, X. (2021). Cholesterol metabolism: A double-edged sword in hepatocellular carcinoma. *Front. Cell Dev. Biol.* 9, 762828. doi:10.3389/fcell.2021.762828

frontiers | Frontiers in Molecular Biosciences

TYPE Original Research
PUBLISHED 20 December 2023
DOI 10.3389/fmolb.2023.1301996



OPEN ACCESS

EDITED BY
Julia Kuligowski,
La Fe Health Research Institute, Spain

REVIEWED BY
Annalaura Mastrangelo,
Spanish National Centre for Cardiovascular Research, Spain
Raúl González-Domínguez,
University of Cádiz, Spain
Guillermo Quintas,
Leitat Technological Center, Spain

*CORRESPONDENCE
Gabriel A. Martos-Moreno,
gabrielangelmartos@yahoo.es
Francisco J. Rupérez,
ruperez@ceu.es

RECEIVED 25 September 2023
ACCEPTED 30 November 2023
PUBLISHED 20 December 2023

CITATION
Chamoso-Sanchez D, Rabadán Pérez F, Argente J, Barbas C, Martos-Moreno GA and Rupérez FJ (2023), Identifying subgroups of childhood obesity by using multiplatform metabotyping.
*Front. Mol. Biosci.* 10:1301996.
doi: 10.3389/fmolb.2023.1301996



# Identifying subgroups of childhood obesity by using multiplatform metabotyping

David Chamoso-Sanchez[1], Francisco Rabadán Pérez[2], Jesús Argente[3,4,5], Coral Barbas[1], Gabriel A. Martos-Moreno[3,4]* and Francisco J. Rupérez[1]*

[1]Centro de Metabolómica y Bioanálisis (CEMBIO), Facultad de Farmacia, Universidad San Pablo-CEU, CEU Universities, Boadilla del Monte, Spain, [2]Departamento Economía Aplicada I, Universidad Rey Juan Carlos, Madrid, Spain, [3]Department of Pediatrics and Pediatric Endocrinology, Hospital Infantil Universitario Niño Jesús, Instituto de Investigación Sanitaria La Princesa, Universidad Autónoma de Madrid, Madrid, Spain, [4]CIBER Fisiopatología de la Obesidad y Nutrición (CIBEROBN), Instituto de Salud Carlos III, Madrid, Spain, [5]IMDEA Food Institute, Madrid, Spain

**Introduction:** Obesity results from an interplay between genetic predisposition and environmental factors such as diet, physical activity, culture, and socioeconomic status. Personalized treatments for obesity would be optimal, thus necessitating the identification of individual characteristics to improve the effectiveness of therapies. For example, genetic impairment of the leptin-melanocortin pathway can result in rare cases of severe early-onset obesity. Metabolomics has the potential to distinguish between a healthy and obese status; however, differentiating subsets of individuals within the obesity spectrum remains challenging. Factor analysis can integrate patient features from diverse sources, allowing an accurate subclassification of individuals.

**Methods:** This study presents a workflow to identify metabotypes, particularly when routine clinical studies fail in patient categorization. 110 children with obesity (BMI > +2 SDS) genotyped for nine genes involved in the leptin-melanocortin pathway (CPE, MC3R, MC4R, MRAP2, NCOA1, PCSK1, POMC, SH2B1, and SIM1) and two glutamate receptor genes (GRM7 and GRIK1) were studied; 55 harboring heterozygous rare sequence variants and 55 with no variants. Anthropometric and routine clinical laboratory data were collected, and serum samples processed for untargeted metabolomic analysis using GC-q-MS and CE-TOF-MS and reversed-phase U(H)PLC-QTOF-MS/MS in positive and negative ionization modes. Following signal processing and multialignment, multivariate and univariate statistical analyses were applied to evaluate the genetic trait association with metabolomics data and clinical and routine laboratory features.

**Results and Discussion:** Neither the presence of a heterozygous rare sequence variant nor clinical/routine laboratory features determined subgroups in the metabolomics data. To identify metabolomic subtypes, we applied Factor Analysis, by constructing a composite matrix from the five analytical platforms. Six factors were discovered and three different metabotypes. Subtle but neat differences in the circulating lipids, as well as in insulin sensitivity could be established, which opens the possibility to personalize the treatment according to the patients categorization into such obesity subtypes. Metabotyping in clinical contexts poses challenges due to the influence of various uncontrolled variables on metabolic phenotypes. However, this strategy reveals the potential to identify

subsets of patients with similar clinical diagnoses but different metabolic conditions. This approach underscores the broader applicability of Factor Analysis in metabotyping across diverse clinical scenarios.

KEYWORDS

multiplatform metabolomics, factor analysis, data integration, obesity, childhood, leptin-melanocortin pathway

## Introduction

Childhood obesity prevalence has increased worldwide in the last decades, including a higher incidence of severe and early onset cases, particularly after the COVID-19 outbreak lockdown (Choi et al., 2023), enhancing the known risk for long-term consequences in these patients (Rupérez et al., 2020; Handakas et al., 2022). Children with obesity are more susceptible to maintain their adiposity in adult life, increasing the risk of multiple comorbidities at an early age, including type 2 diabetes mellitus (T2DM), dyslipidemia, cardiovascular disease (CVD), hypertension, obstructive sleep apnea, cancer and steatohepatitis (da Fonseca et al., 2017; Cote et al., 2013; Butte et al., 2015; Carde et al., 2020; Berger, 2018; Wahl et al., 2012). Obesity has a multifactorial etiology, with lifestyle, including nutritional and physical activity habits, as well as other environmental factors, interacting with an individual's unique genetic background to determine a person's risk to develop obesity (Trang and Grant, 2023). Among the large set of genes influencing obesity, those in the leptin-melanocortin satiety signaling pathway are the most determinant known to date, with homozygous mutations in some causing early onset severe obesity with hyperphagia (Jackson et al., 1997; Chiurazzi et al., 2020; Trang and Grant, 2023). The role of heterozygous variants is under investigation (Trang and Grant, 2023), particularly those with confirmed pathogenicity or high Combined Annotation Dependent Depletion (CADD) scores of "deleteriousness" with low population prevalence [heterozygous rare sequence variants (HetRSVs)]. Additionally, variants in glutamate receptors, pivotal in neuron signaling have also been described in patients with severe obesity (Bell et al., 2005; Fuente-Martín et al., 2016; Serra-Juhé et al., 2017; Fairbrother et al., 2018; Chiurazzi et al., 2020).

Whereas some obesity-associated comorbidities commonly identified in adults can also be observed in children with obesity, others such as T2DM are far less common, with insulin resistance (IR) usually found as the first step in carbohydrate metabolism impairment in childhood obesity (Martos-Moreno et al., 2019). Additionally, not every patient with obesity shows the same risk to develop comorbidities, with the "metabolically healthy obesity" designation proposed for those patients with obesity, even severe obesity, but with no metabolic comorbidities (Wan Mohd Zin et al., 2022). However, this term is under discussion and this condition is known to evolve throughout life in relationship to weight control (Martos-Moreno et al., 2021). The term "metabotype" was defined by Gavaghan et al. (Gavaghan et al., 2000) as "a probabilistic multiparametric description of an organism in a given physiological state based on analysis of its cell types, biofluids, or tissues." Subsequently, this definition has been repeatedly used (Waldram et al., 2009; Sullivan et al., 2011; Palmnäs et al., 2020), establishing itself as the characterization of the metabolic phenotype of an individual. Recent advances in high-throughput sequencing technologies and computational methods have enabled the generation of large and complex *-omics* datasets, providing an unprecedented opportunity to integrate simultaneous information from multiple molecular levels to investigate the complexity of biological systems (T et al., 2019; Park et al., 2022; Argelaguet et al., 2020; Tanabe et al., 2021; Clark et al., 2021). The integration of various *-omics* data, including genomics, transcriptomics, proteomics, metabolomics, and epigenomics, can help to understand the intricate interplay between different biological molecules and pathways, enabling the identification of key regulators and mechanisms of disease (Hoadley et al., 2014; Meng et al., 2016; Marabita et al., 2022). In metabolomics, a multiplatform strategy combines many analytical tools to study the entire metabolic phenotype. Combining data from multiple sources could result in a better comprehension of the underlying biological mechanisms driving complex diseases including cancer, obesity, and cardiovascular disease (Hoadley et al., 2014; Meng et al., 2016; Marabita et al., 2022; Park et al., 2022). Although much effort has been made in recent years to integrate information from different *-omics* technologies into a single analysis, it is still usual to use a multiplatform strategy individually (T et al., 2019; Argelaguet et al., 2020; Tanabe et al., 2021; Zhang et al., 2022).

Factor Analysis is a multivariate statistical technique that can identify underlying patterns in a large dataset by reducing the number of variables into a smaller number of factors (Lee et al., 2019; Acal et al., 2020). In the context of metabolomics, Factor Analysis can identify metabolite modules, which are groups of metabolites that are highly correlated and potentially involved in a common biological process. This approach provides a more comprehensive understanding of the underlying molecular mechanisms of disease and can identify potential biomarkers and therapeutic targets that may not be identifiable using individual metabolites. Recent studies have demonstrated the potential of Factor Analysis in metabolomics for identifying metabolite modules in various fields of research including cancer biology, metabolic disorders, and neurodegenerative diseases (Shen et al., 2009; Zhao et al., 2013; Argelaguet et al., 2018; Kamleh et al., 2018; Clark et al., 2021). However, there are several challenges associated with the application of Factor Analysis in metabolomics. One of the key challenges is the selection of an appropriate Factor Analysis method (principal component analysis, common Factor Analysis, maximum likelihood method, etc.) which depends on the specific research questions and the characteristics of the metabolomics dataset. Also, multicollinearity is a serious problem that must be solved before performing a Factor Analysis (Chan et al., 2022). Another challenge is the interpretation of the identified metabolite modules, as it may be difficult to determine the biological relevance of the modules. This challenge can be addressed by integrating the

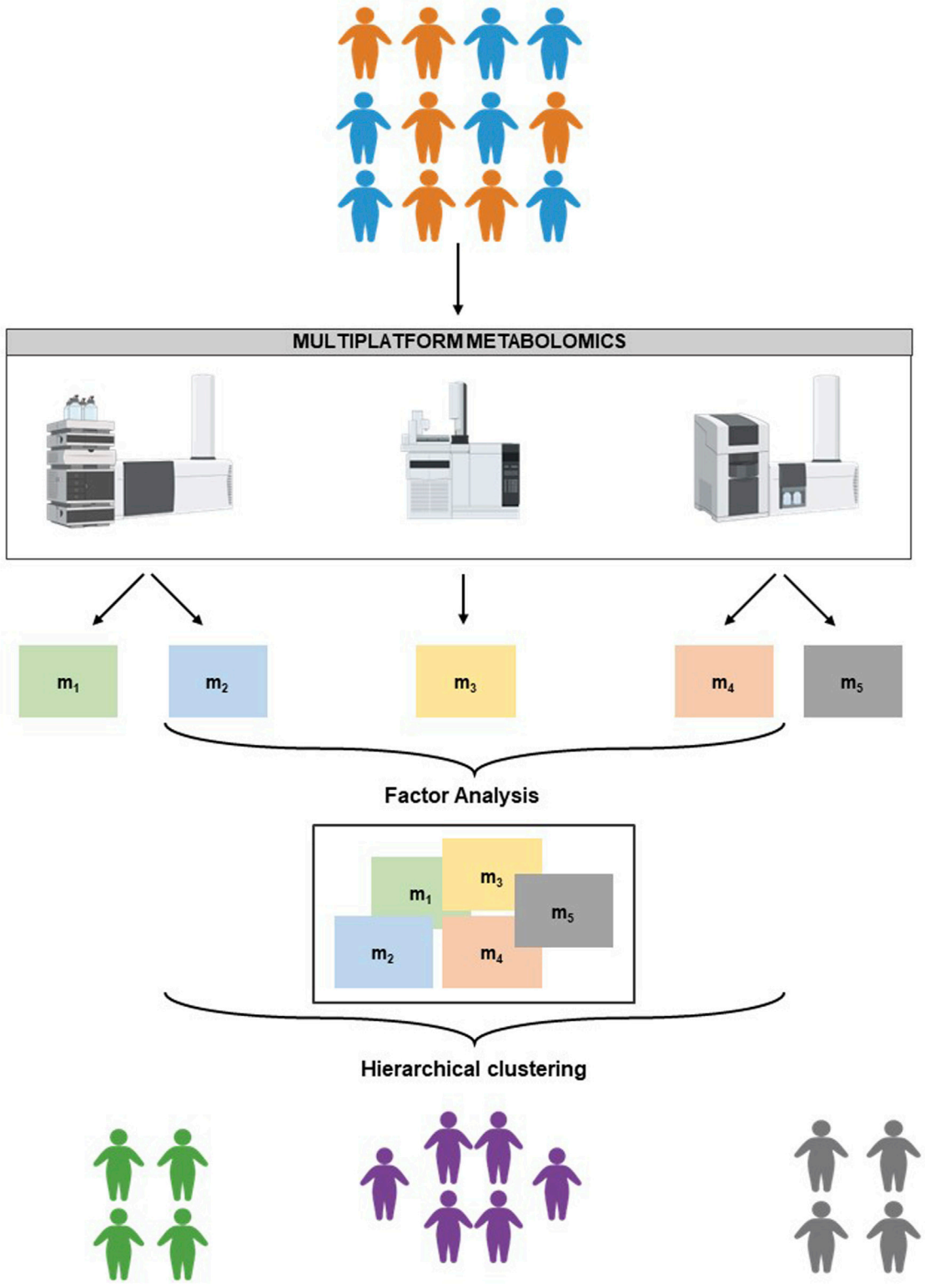


FIGURE 1
Schematic representation of the experimental design.

results of Factor Analysis with other omics data types, such as genomics, transcriptomics, and proteomics, to provide a more comprehensive understanding of the underlying biological processes. Combining Factor Analysis with a hierarchical clustering analysis enables one to classify patients considering all metabolic features detected by a multi-platform approach; to identify patient subgroups based on their metabotype and to provide the optimal treatment for each patient rather than based

**TABLE 1 Gene list.**

| |
|---|
| *CPE* (MIM* 114855. Carboxypeptidase E) |
| *GRIK1* (MIM* 138245. GLUTAMATE RECEPTOR, IONOTROPIC, KAINATE 1) |
| *GRM7* (MIM* 604101. GLUTAMATE RECEPTOR, METABOTROPIC, 7) |
| *MC3R* (MIM* 155540. MELANOCORTIN 3 RECEPTOR) |
| *MC4R* (MIM* 155541. MELANOCORTIN 4 RECEPTOR) |
| *MRAP2* (MIM* 615410. MELANOCORTIN 2 RECEPTOR ACCESSORY PROTEIN 2) |
| *NCOA1* (MIM* 602691. NUCLEAR RECEPTOR COACTIVATOR 1) (Alternative nomenclature: SRC1) |
| *PCSK1* (MIM* 162150. PROPROTEIN CONVERTASE, SUBTILISIN/KEXIN-TYPE, 1) |
| *POMC* (MIM* 176830. PROOPIOMELANOCORTIN) |
| *SH2B1* (MIM* 608937. SH2B ADAPTOR PROTEIN 1) |
| *SIM1* (MIM* 603128. SIM bHLH TRANSCRIPTION FACTOR 1) |

upon the usual anthropometric and routine laboratory parameters used in the clinical setting and even over the presence or absence of HetRSVs in relevant genes in the studied pathology. Such strategy becomes even more powerful when there is no classification available, or the main goal of the research is to unveil the minimum set of parameters which allow for classification/stratification.

# Patients, materials and methods

We tested a multi-platform strategy in combination with Factor Analysis and hierarchical clustering for personalized approaches in the treatment of obesity (Figure 1).

## Patients

One hundred and ten children and adolescents (57 females/53 males) affected with severe obesity referred to a specialized clinic in a third level monographic pediatric hospital and genotyped for nine genes in the leptin-melanocortin pathway downstream of the leptin receptor, and two glutamate receptor genes (Table 1) were studied: 55 of them harboring one heterozygous rare sequence variant [HetRSV, defined as populational frequency <0.01 and with a Combined Annotation Dependent Depletion (CADD) score of "deleteriousness" > 20] and/or confirmed pathogenicity according to ACMG criteria in the studied genes [*CPE* ($n$ = 5), *MC3R* ($n$ = 5), *MC4R* ($n$ = 5), *MRAP2* ($n$ = 5), *NCOA1* ($n$ = 7), *PCSK1* ($n$ = 5), *POMC* ($n$ = 5), *SH2B1* ($n$ = 5), *SIM1* ($n$ = 5), *GRM7* ($n$ = 4) or *GRIK1* ($n$ = 4)] and 55 with no detected variants.

The whole cohort mean age and standardized body mass index (BMI) were 11.01 ± 3.36 years and 4.20 ± 2.20 SDS, respectively with no differences between groups (with vs. without variants) in age, BMI-SDS, routine laboratory metabolic and hormonal features nor in sex, ethnicity, or pubertal status distribution. Their main anthropometric and metabolic features are summarized and compared in Table 2.

All patients and their parents or guardians gave informed written consent as required by the ethics committee at the University Hospital Niño Jesús, which had previously approved the study in accordance with the "Ethical Principles for Medical Research Involving Human Subjects" adopted in the Declaration of Helsinki by the World Medical Association (64th WMA General Assembly, Fortaleza, Brazil, October 2013).

## Methods

Weight, height, BMI, waist circumference, and systolic and diastolic blood pressure (BP, mean of three measurements) were recorded and standardized (Cole et al., 2000; Ferná et al., 2004) in all patients. A 12-hour fasting serum sample (drawn, immediately processed, aliquoted and stored at −80°C until assayed) was used to determine glucose, insulin, HbA1c, lipid profile, uric acid, GOT, GPT, GGT, free thyroxin, thyroid stimulating hormone, IGF-I, IGFBP-3, 25-OH-vitamin D and intact parathyroid hormone (iPTH) levels by standardized assays as previously reported (Martos-Moreno et al., 2019). An oral glucose tolerance test (OGTT, 1.75 g/kg, maximum 75 g) for glucose and insulin determination at 30, 60 and 120 min was performed, HOMA (homeostatic model for insulin resistance) and WBISI (whole body insulin sensitivity) indexes were calculated as previously reported (Martos-Moreno et al., 2019).

## Multiplatform untargeted metabolomics analysis

### Sample treatment

Serum metabolite extraction was carried out according to previously reported standard protocols (Garcia and Barbas, 2011; Pellegrino et al., 2014; Naz et al., 2015). Briefly, for LC-MS analysis, 40 µL of serum was mixed with 800 µL of a cold mixture (−20°C) of methanol:MTBE:Chloroform (1.33:1:1, v/v/v) with Sphinganine (D17:0) and palmitic acid-d31 as internal standards. Samples were vortexed for 30 s and shaken for 20 min at maximum speed at room temperature. Next, samples were centrifuged (13,200 rpm, room temperature, 5 min). After centrifugation, supernatant was directly injected into the system. For GC-MS analysis, protein precipitation was achieved by mixing one volume of serum with three volumes of cold (−20°C) acetonitrile with 25 ppm of palmitic acid-d31 as internal standard, followed by methoximation with O-methoxyamine hydrochloride (15 mg/mL) in pyridine, and sylation with BSTFA: TMCS (99:1). Finally, 20 ppm of tricosane in heptane was added as second internal standard. For CE-MS analysis, 100 µL of serum was mixed with 100 µL of 0.2 M formic acid containing 5% acetonitrile and 0.4 mM methionine sulfone, 2 mM paracetamol and 0.5 mM 4-Morpholineethanesulfonic acid, 2-(N-Morpholino) ethanesulfonic acid (MES) as internal standards. The sample was transferred to an ultracentrifugation device (Millipore Ireland Ltd., Carrigtohill, Ireland) with a 30 kDa protein cutoff for deproteinization through centrifugation (2000 × $g$, 4°C, 90 min). Detailed version of the sample treatment protocols, the reagents, solvents, standards used for the sample treatment and subsequent analyses, and the analytical setup for the LC–MS, GC–MS, and CE–MS analysis are described in

**TABLE 2 Anthropometric and metabolic features.**

| Clinical parameters | Whole cohort | Variant carriers | NO variant | Variant carriers vs. NO |
|---|---|---|---|---|
| Age (years) | 11.01 ± 3.36 | 11.12 ± 3.47 | 10.91 ± 3.28 | N.S. |
| Height (SDS) | 0.84 ± 1.12 | 0.70 ± 1.05 | 0.99 ± 1.19 | N.S. |
| BMI-SDS | 4.20 ± 2.20 | 4.29 ± 2.42 | 4.11 ± 1.99 | N.S. |
| Fasting glucose (mg/dL) | 91.10 ± 6.81 | 90.99 ± 5.98 | 91.91 ± 7.51 | N.S. |
| Glucose at 120′in OGTT (mg/dL) | 120.82 ± 18.87 | 118.11 ± 13.31 | 123.31 ± 18.29 | N.S. |
| Fasting insulin (μU/mL) | 15.13 ± 7.28 | 14.83 ± 7.56 | 15.42 ± 7.05 | N.S. |
| HOMA index | 3.45 ± 1.75 | 3.34 ± 1.78 | 3.56 ± 1.72 | N.S. |
| WBISI index | 3.23 ± 1.67 | 3.35 ± 1.63 | 3.13 ± 1.71 | N.S. |
| HbA1c (%) | 5.43 ± 0.30 | 5.44 ± 0.24 | 5.41 ± 0.35 | N.S. |
| Uric acid (mg/dL) | 5.18 ± 1.16 | 5.04 ± 1.21 | 5.32 ± 1.11 | N.S. |
| GOT (U/L) | 27.72 ± 7.35 | 26.80 ± 6.73 | 28.68 ± 7.89 | N.S. |
| GPT (U/L) | 22.22 ± 9.27 | 21.38 ± 8.48 | 23.19 ± 10.03 | N.S. |
| GGT (U/L) | 14.16 ± 4.72 | 13.91 ± 4.31 | 14.42 ± 5.13 | N.S. |
| HDL-c (mg/dL) | 46.72 ± 14.02 | 46.63 ± 15.93 | 46.82 ± 11.90 | N.S. |
| LDL-c (mg/dL) | 96.21 ± 27.23 | 96.82 ± 30.57 | 97.62 ± 23.55 | N.S. |
| Triglycerides (mg/dL) | 78.69 ± 48.61 | 75.58 ± 42.40 | 81.85 ± 54.43 | N.S. |
| Free thyroxine (T4) (ng/dL) | 0.94 ± 0.13 | 0.95 ± 1.09 | 0.92 ± 01.54 | N.S. |
| TSH (μU/mL) | 2.78 ± 1.57 | 2.91 ± 1.64 | 2.65 ± 1.51 | N.S. |
| IGF-I (ng/mL) | 310.8 ± 171.7 | 324.67 ± 191.76 | 297.77 ± 151.24 | N.S. |
| IGFBP-3 (μg/mL) | 4.90 ± 0.99 | 4.93 ± 0.97 | 4.86 ± 1.02 | N.S. |
| 25-OH-Vitamin D (ng/mL) | 23.36 ± 9.22 | 23.55 ± 8.69 | 23.21 ± 9.74 | N.S. |
| Intact PTH (pg/mL) | 57.13 ± 21.92 | 57.03 ± 22.04 | 57.21 ± 22.13 | N.S. |

Abbreviations: BMI-SDS, Standardized body mass index (Z-score); OGTT, oral glucose tolerance test; HOMA, homeostatic model assessment; WBISI, Whole-body insulin sensitivity index; HDL-c, High density lipoprotein cholesterol; LDL-c, Low density lipoprotein cholesterol; GGT, Gamma-glutamyltransferase; GOT, Glutamic-oxalacetic transaminase; GPT, glutamic-pyruvic transaminase Alanine aminotransferase; IGF-1, Insulin-like growth factor 1; IGFBP3, Insulin-like Growth Factor-binding Protein 3; HbA1c, hemoglobin A1c; TSH, thyroid-stimulating hormone; PTH, parathyroid hormone.

Supplementary Material. Quality control samples (QC) were prepared by pooling and mixing equal volumes of each serum sample and treated as independent samples to check the performance of the systems and the reproducibility of the sample treatment. Then, samples were randomized, and QCs were injected at the beginning, along the sequence, and at the end of the batch. Finally, two blank solutions were prepared along with the rest of the samples and analyzed at the beginning and at the end of the analytical sequence (Dudzik et al., 2018).

## LC-MS and CE-MS data pre-processing

The raw data obtained after the LC-MS and CE-MS analysis were processed using Agilent Technologies MassHunter Profinder B.10.0.2.162 (Santa Clara, United States) to clean the background noise and unrelated ions. This algorithm aligns all ions across the samples using mass and retention time (RT) to create a single spectrum for each group of compounds, and finally obtaining a structured data matrix and appropriate format. Missing values were imputed using the k-nearest neighbors (kNN) algorithm (Armitage et al., 2015) in Matlab R2022a software (Mathwoks, Inc., Natick, United States). Then, the data matrix was filtered by coefficient of variation (CV), maintaining those signals that, in the QCs, presented a CV below 30%. The filtered data matrix was imported into SIMCA 17 Sartorius (Goettingen, Germany) to generate a PCA and thus observe the trend of the QCs, detect possible outliers, and look for natural and analytical trends of the samples. To reduce the impact of instrumental and experimental variations that can interfere with the ability to detect biological variations, a correction method called "quality control samples and support vector regression (QC-SVRC)" was used to adjust the data (Kuligowski et al., 2015) implemented in MATLAB R2022a and then normalized by internal standard (IS).

## Data pre-processing and compound identification GC–MS analysis

The chromatograms obtained from each of the serum samples, the QCs, and the IS signal were visually examined to ensure the

quality of the obtained profiles and the reproducibility of the IS signal using Agilent MassHunter Qualitative B.10.0.010305.0 software (Santa Clara, United States). Deconvolution and metabolite identification was achieved using the Agilent MassHunter Unknowns Analysis Tool 10.0 (Santa Clara, United States). The software assigned a chemical identity to each of the signals obtained after the search in two commercial libraries: the Fiehn library version 2013, and the NIST library version 2017 and "in-house" libraries. The identities were assigned according to the retention time (RT) and spectra extracted during deconvolution when the software compared them with each compound included in the libraries. Next, the obtained data were aligned using the MassProfiler Professional B.15.1 software (Agilent Technologies) (Santa Clara, United States) and exported to Agilent MassHunter Quantitative Analysis version B10.0.707.0 (Santa Clara, United States) to assign the main ions and the integration of each of the signals. As in the LC-MS and CE-MS analysis, the missing values were estimated using the kNN (k-nearest neighbors) algorithm (Armitage et al., 2015). Experimental and analytical variations were excluded by performing normalization. As in the LC-MS and CE-MS analysis the data matrix was normalized by applying the QC-SRVC correction, normalized by internal standard, and filtered by CV in the QCs (Kuligowski et al., 2015).

## Compound identification LC-MS and CE-MS analysis

For the metabolite tentative annotation initially the m/z was searched against multiple databases available online, including METLIN (http://metlin.scripps.edu), LipidsMAPS (http://lipidMAPS.org) and KEGG (http://www.genome.jp/kegg/), all of which have been joined into an "in-house" developed search engine, CEU MassMediator (http://ceumass.eps.uspceu.es/) (Gil-de-la-Fuente et al., 2019). Aiming to obtain additional information for some identities, HMDB (http://hmdb.ca) was also consulted. In parallel, three complementary software, MS-DIAL (http://prime.psc.riken.jp/), LipidAnnotator (Agilent Technologies) and LipidHunter (Ni et al., 2017; Koelmel et al., 2020; Tsugawa et al., 2020) by fragmentation mass/mass spectra were used for LC-MS identification. Features that were tentatively assigned to metabolites from the databases were based on (1): mass accuracy (maximum error mass 20 ppm) (2), isotopic pattern distribution (3), possibility of cation and anion formation (4), adduct formation (5), elution order of the compounds based on the chromatographic conditions, and (6) MS/MS spectra. Additionally, an "in-house" CE-MS library built with authentic standards was used to compare the relative migration time (RMT) to increase the confidence of the annotations. The confidence levels established by the Compound Identification group of the Metabolomics Society at the 2017 annual meeting of the Metabolomics Society (Brisbane, Australia) have been used. The new identification levels (Blaženović et al., 2018) range from level 0 with full identification based on knowledge of its 3D structure, level 1 2D confidence using comparison with reference standards, level 2 probable structure when compared with database, level 3 possible structure or class and level 4 as unidentified compound.

## Statistical analysis

Statistical analysis was carried out by univariate (UVA, Matlab R2022a) and multivariate analysis [MVA, SIMCA 17, R v4.1.2 and IBM SPSS v27 (Armonk, NY, United States)]. For the UVA, parametric (unpaired *t*-test) with a Benjamini–Hochberg False Discovery Rate *post hoc* correction ($q < 0.05$) was applied. For MVA, the PCA plot, PLS-DA plot and OPLS-DA plot was built. The data matrix was analyzed using unsupervised machine learning using R environment (https://www.r-project.org/), applying clustering technique to obtain pattern in our data independently of the initial groups.

The raw data from the various analytical platforms were merged using Factor Analysis and hierarchical clustering to generate a broad perspective of the results and to assign metabotypes based on the metabolic phenotypes of each patient with obesity. The whole process of Factor Analysis and hierarchical clustering was carried out by using IBM SPSS software and Microsoft Excel. First, the Pearson correlations between the variables in each of the matrices were analyzed to eliminate multicollinearity. Correlations between the various matrices (inter-matrix correlations) were examined after filtering by the specific correlations of each matrix (intra-matrix correlations). The individual matrices with the resulting variables were subjected to principal component analysis with varimax rotation (Acal et al., 2020) to reduce dimensionality. Three rules were applied to select the number of principal components in each of the individual matrices, the "Scree plot elbow," the Kaiser-Guttman test (Eigenvalue greater than unity) and a total explained variance greater than 60% (Cattell, 1966). The principal component scores have been analyzed. The variables that present a principal component score higher than 0.5 in any of the selected components and that do not present double saturation are kept for the subsequent Factor Analysis. We consider double saturation to be when the smallest difference in the principal component score of a variable between two components is less than 0.1. The resulting variables have been subjected to a Factor Analysis by maximum likelihood (Babakus et al., 1987) with varimax rotation of each of the matrices separately to further reduce dimensionality. The same three rules were applied as in the PCA. For the final Factor Analysis, variables that displayed double saturation or had factor scores lower than 0.5 in any of the chosen factors were excluded. Finally, all the resulting variables were pooled into a single matrix after applying all these filters and a Factor Analysis was performed using a maximum likelihood extraction method and a varimax rotation method. All variables that entered the combined Factor Analysis of the different platforms were identified using internal databases and mass/mass fragmentation spectra software (LipidAnnotator, MSDial, LipidHunter). Following the criteria applied above, the appropriate number of factors was selected for our data and by regression new variables were created for each of the factors. A hierarchical clustering analysis with squared Euclidean distance and Ward method was applied on the created factors. To select the appropriate number of metabotypes, a discriminant analysis (DA) was performed (Lee et al., 2019).

# Results

1) The presence of heterozygous rare sequence variant in the studied genes, associated to human obesity and energy

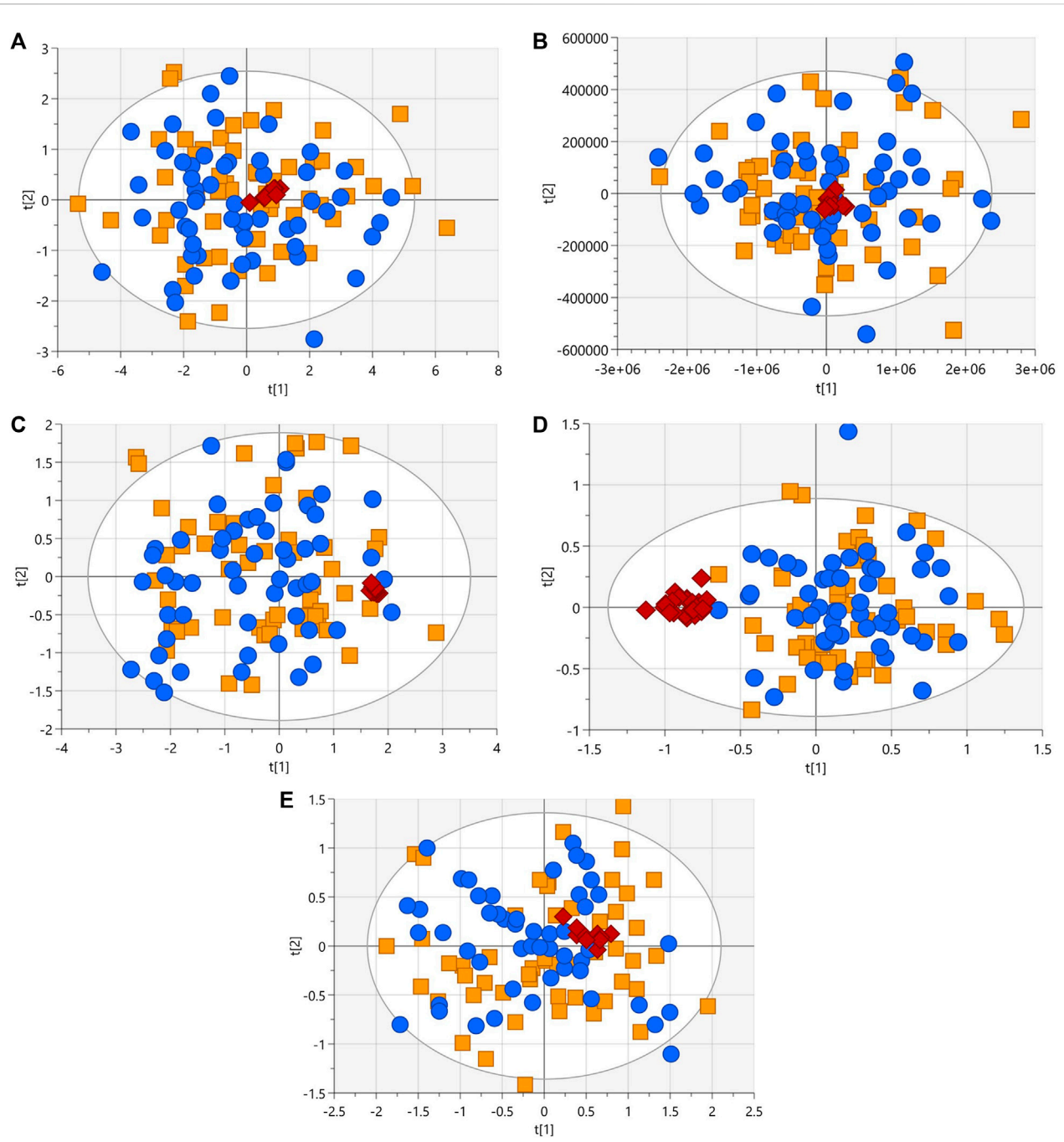


FIGURE 2
PCA-X score plots (blue dots, patients with heterozygous rare sequence variants (HetRSVs); orange square, patients without variants; red diamonds, QC samples) for the five analytical platforms. **(A)** $R^2$ = 0.82, $Q^2$ = 0.78 with log10 transformation and Ctr scale (LC-MS (+)). **(B)** $R^2$ = 0.937, $Q^2$ = 0.594 with Ctr scale (LC-MS (–)). **(C)** $R^2$ = 0.516, $Q^2$ = 0.458 with log10 transformation and Ctr scale. Four samples were eliminated due to the presence of analytical outliers located outside the hoteling's ellipse (CE-MS (+)). **(D)** $R^2$ = 0.536, $Q^2$ = 0.308 with log10 transformation and Ctr scale. Eight samples were eliminated due to the presence of analytical outliers located outside the Hoteling's ellipse (CE-MS (–)). **(E)** $R^2$ = 0.616, $Q^2$ = 0.428 with log10 transformation and Ctr scale. Eight samples were removed due to problems during sample preparation (GC-MS).

homeostasis, does not determine different metabolomic phenotypes.

After following the procedure described in the patients and methods section, we obtained 345 and 170 metabolic features in LC-MS performed in positive and negative ionization modes, 63 signals in GC-MS, and finally in CE-MS we obtained 242 signals in positive ionization and 91 in negative ionization mode. The visual inspection of the PCA plots built for all techniques revealed a tight cluster of the QCs assessing the analytical stability and reproducibility (Figure 2). A homogeneous distribution of patients with and without heterozygous variant was seen in PCA plots.

The identified HetRSVs did not allow for the construction of multivariate supervised model from the results of only one of the

analytical techniques. Only LC-MS (+), enabled the creation of an OPLS-DA model ($R_2X$ = 0.72, $R_2Y$ = 0.82; $Q_2$ = 0.64; p CV-ANOVA$_{OPLS\text{-}DA}$ = 3.1 · $10^{-19}$; as illustrated in Supplementary Figure S1). Correspondingly, the results of three metabolites derived from LC-MS (+) displayed statistically significant differences in means between the variant carrier/no variant groups, whereas no discernible differences between both groups were observed in the means of all the variables from LC-MS (−), GC-MS, CE-MS (+), or CE-MS (−). Furthermore, despite the limited number of samples for each individual gene, the presence of singular metabolic patterns was not observed for any of the studied genes in any of the employed platforms (data not shown).

2) Factor Analysis groups the variability into six factors

Imprecise information is obtained from the examination of the metabolic phenotype using a single analytical platform, which might result in the description of erroneous metabotypes in patients, generating different classifications depending on the analytical platform used (Supplementary Figure S2). Furthermore, the use of a classification based on anthropometric and routine laboratory metabolic and hormonal parameters available in daily clinical practice does not appear to be sufficient to establish distinct metabotype among patients. We also performed a hierarchical clustering analysis, with anthropological and clinical parameters (data not shown). We observed dissimilar outcomes when compared to the classifications produced by individual analytical platforms. Additionally, no statistically significant differences were observed in any of the analytical platforms with the clusters (possible groups) generated after analyzing these parameters.

The multiplatform strategy provided five matrices with 345, 170, 53, 242 and 91 variables analyzed by LC-MS (+), LC-MS (−), GC-MS, CE-MS (+) and CE-MS (−), respectively, from 100 of the studied samples. Due to the presence of analytical outliers caused by errors during sample preparation in GC-MS and analytical error in CE-MS (+), 10 samples had to be eliminated from the analysis of the total of 110 patients enrolled (three patients without genetic variants, and 7 with genetic variants, with a maximum of two individuals per gene studied). As described in detail above (see materials and methods) a Factor Analysis of each of the matrices was performed to subsequently combine the variables present in each Factor Analysis into a single combined Factor Analysis. To eliminate multicollinearity, Pearson correlations were used to analyze the relationships between variables in each matrix (intra-matrix correlations) and between matrices (inter-matrix correlations). In the final Factor Analysis by maximum likelihood and varimax rotation performed on the LC-MS matrix (+), three factors were chosen that explained 75% of the variability accumulated in the matrix, saturating 57 variables that were kept for the final combined Factor Analysis. The Kaiser-Meyer-Olkin (KMO) test was used to determine whether the Factor Analysis was effective, and a result of 0.85 was obtained. In LC-MS (−), two factors were chosen to explain 74.68% of the variability accumulated in the matrix, obtaining a KMO of 0.85 and saturating 17 variables. In GC-MS, three factors were chosen that explain 73.54% of the accumulated variability, obtaining a KMO of 0.89 with 18 variables independently saturated in these factors. In CE-MS (+) 1 factor was chosen that explained 64.09% of the accumulated variation, obtaining a KMO of 0.77 with five saturated variables. In CE-MS (−) no satisfactory factor extraction was achieved, so no variable was retained for the final Factor Analysis. Using in-house databases and mass/mass fragmentation spectra software (LipidAnnotator, MSDial, LipidHunter) all variables that remained after all of these pre-filtering stages for the combined Factor Analysis of the various platforms were identified. The removal of non-annotated variables from the combined Factor Analysis (23 out of 97 variables were removed due to unsuccessful identification) is performed to determine the biological interpretation of the obtained factors. Therefore, variables 43, 11, 14 and 5 analyzed by LC-MS (+), LC-MS (−), GC-MS and CE-MS (+), respectively, were pooled together and the Factor Analysis was performed. The adequacy of the Factor Analysis was tested using the KMO test, obtaining a value of 0.76. Finally, six factors that explained 75% of the accumulated variability were selected. The results show a clustering of the variables into factors depending on the analytical technique. Table 3 shows the variables corresponding to each of the factors (see identification details in Supplementary Table S2). As the resulting factors can be employed to predict discrete clusters of samples, we used all the inferred factors to cluster the patients in the latent factor space, collectively implementing collectively all information from the different analytical platforms.

3) Hierarchical clustering of factors permits to classify patients into metabotypes

A hierarchical clustering analysis with Ward method and squared Euclidean distance was applied in SPSS statistical software (Figure 3A). To determine the optimal number of metabotypes, a discriminant was applied to 2, 3 and 4 metabotypes. It appears that grouping the samples into three distinct metabotypes provides the most robust explanation for the observed relationships, where 94% accuracy was observed after cross-validation, demonstrating the existence of 3 clearly differentiated metabotypes [metabotype 1 (G1) ($n$ = 74), metabotype 2 (G2) ($n$ = 10), metabotype 3 (G3) ($n$ = 16)] (Figure 3B).

The identified factors enabled metabotypes to be characterized. The components of the first two factors, F1 (10 sphingolipids, 4 ether-linked phosphatidylcholines, 2 phosphatidylcholines and 3 cholesterol esters, named "*Lipids1*") and F2 (1 di- and 12 tryacylglycerols, named "*Lipids2*"), accounted for 44% of the variability and were increased in metabotype 3 and decreased in metabotype 1. F3 components (named "*nutritional amino acids*," including eight amino acids) showed increased levels in metabotype 2. F4 elements (including nine circulating free fatty acids, named "*Lipids3*") showed increased levels in metabotype 1. F5 elements (including 10 phosphatidylcholines, named "*Lipids4*") and the components in F6 (glutamic acid, choline, aspartic acid, glutamine, and arginine, named "*signaling amino acids*") showed an accumulated variation of 75% and were increased in metabotype 3.

Univariate statistics were performed on each of the matrices. Each variable was analyzed by ANOVA or its corresponding non-parametric method (Kruskal–Wallis). The overall results show the greatest differences between metabotype 1 and metabotype 3

10.3389/fmolb.2023.1301996

**TABLE 3 Metabolites included in each of the six final factors obtained with their factor scores associated with the factors. Saturations above 0.5 are indicated in dark red. Confidence level in annotation based on Metabolomics Society (Blaženović et al., 2018).**

| Factor | Identification | Confidence level | Factor score | | | | | |
|---|---|---|---|---|---|---|---|---|
| | | | Factor 1 | Factor 2 | Factor 3 | Factor 4 | Factor 5 | Factor 6 |
| 1 | SM (d41:2) | 2 | 0.83 | −0.08 | −0.06 | 0.03 | 0.19 | −0.09 |
| 1 | SM (d42:3) | 2 | 0.85 | 0 | −0.09 | 0.05 | 0.03 | −0.08 |
| 1 | SM (d40:1) | 2 | 0.83 | 0.09 | −0.07 | 0.11 | 0.1 | 0.07 |
| 1 | SM (d39:1) | 2 | 0.72 | 0 | −0.04 | 0.13 | 0.24 | −0.04 |
| 1 | SM (d32:1) | 2 | 0.77 | 0.07 | −0.07 | 0.02 | 0.3 | 0.04 |
| 1 | SM (d36:2) | 2 | 0.82 | 0.22 | −0.1 | 0.15 | 0 | −0.04 |
| 1 | SM (d34:2) | 2 | 0.86 | 0.1 | −0.06 | −0.03 | 0.17 | 0.03 |
| 1 | SM (d34:0) | 2 | 0.9 | 0.09 | −0.02 | 0.11 | 0.1 | −0.03 |
| 1 | SM (d40:2) | 2 | 0.87 | 0.03 | −0.08 | −0.02 | 0.24 | −0.01 |
| 1 | SM (d38:1) | 3 | 0.88 | 0.16 | −0.12 | 0.1 | 0.16 | −0.01 |
| 1 | PC (16:0/16:0) | 3 | 0.78 | 0.26 | −0.03 | 0.04 | 0.44 | −0.06 |
| 1 | PC (O-34:1) | 3 | 0.82 | −0.08 | 0.01 | 0.03 | 0.2 | −0.06 |
| 1 | PC (O-40:4) | 3 | 0.82 | −0.03 | −0.13 | 0.2 | 0.06 | −0.06 |
| 1 | PC (O-32:0) | 3 | 0.8 | 0.04 | −0.01 | 0.01 | 0.17 | −0.03 |
| 1 | PC (O-38:4) | 3 | 0.81 | −0.02 | −0.04 | 0.04 | 0.17 | 0.01 |
| 1 | PC (O-36:5) | 3 | 0.75 | −0.06 | 0.01 | 0.01 | 0.26 | 0.01 |
| 1 | PC (16:0/18:2) | 3 | 0.7 | 0.28 | 0.11 | −0.14 | 0.28 | 0 |
| 1 | CE (18:2) | 2 | 0.86 | 0.11 | 0.05 | −0.1 | 0.18 | 0.06 |
| 1 | CE (20:4) | 2 | 0.83 | 0.05 | −0.12 | 0.06 | 0.15 | 0.03 |
| 1 | CE (18:1) | 2 | 0.83 | 0.23 | −0.03 | 0.01 | 0.3 | 0.02 |
| 2 | DG (36:4) | 3 | 0.13 | 0.81 | 0.11 | 0.06 | 0.23 | 0.25 |
| 2 | TG (16:0_18:0_18:1) | 3 | 0.11 | 0.77 | 0.05 | −0.1 | 0.44 | 0.09 |
| 2 | TG (56:6) | 3 | 0.36 | 0.85 | −0.07 | 0.02 | 0.14 | −0.08 |
| 2 | TG (18:1_18:2_20:4) | 3 | −0.16 | 0.74 | 0.07 | 0.03 | 0 | −0.07 |
| 2 | TG (56:3) | 3 | −0.08 | 0.83 | 0.05 | −0.04 | 0.28 | 0.06 |
| 2 | TG (58:5) | 3 | 0.05 | 0.83 | 0.02 | −0.11 | 0.29 | −0.06 |
| 2 | TG (56:2) | 3 | 0.11 | 0.76 | 0.02 | −0.12 | 0.3 | 0.06 |
| 2 | TG (54:3) | 3 | 0.21 | 0.87 | 0.01 | −0.07 | 0.08 | 0.05 |
| 2 | TG (18:1_18:2_18:2) | 3 | 0.05 | 0.8 | −0.02 | −0.15 | 0.01 | −0.04 |
| 2 | TG (57:2) | 3 | 0.08 | 0.85 | 0.03 | −0.09 | 0.31 | −0.02 |
| 2 | TG (53:3) | 3 | −0.06 | 0.84 | 0.08 | −0.02 | 0.38 | 0 |
| 2 | TG (54:4) | 3 | 0.09 | 0.89 | 0.01 | −0.11 | −0.03 | 0 |
| 2 | TG (16:0_18:1_18:2) | 3 | 0.19 | 0.94 | −0.02 | −0.07 | 0.13 | 0 |
| 3 | Phenylalanine | 2 | −0.08 | 0.02 | 0.84 | 0.03 | 0.05 | 0.33 |
| 3 | Oxalic acid | 2 | −0.17 | −0.08 | 0.64 | −0.1 | −0.05 | −0.24 |
| 3 | Myo-Inositol | 2 | 0.03 | 0.02 | 0.65 | 0.25 | 0 | 0.19 |
| 3 | Cholesterol | 2 | 0.14 | 0.15 | 0.72 | 0.04 | 0.06 | −0.19 |

(Continued on following page)

**TABLE 3 (*Continued*) Metabolites included in each of the six final factors obtained with their factor scores associated with the factors. Saturations above 0.5 are indicated in dark red. Confidence level in annotation based on Metabolomics Society (Blaženović et al., 2018).**

| Factor | Identification | Confidence level | Factor score | | | | | |
|---|---|---|---|---|---|---|---|---|
| | | | Factor 1 | Factor 2 | Factor 3 | Factor 4 | Factor 5 | Factor 6 |
| 3 | **Proline** | 2 | −0.05 | 0.18 | 0.78 | −0.12 | 0.14 | 0.17 |
| 3 | **Serine** | 2 | −0.02 | −0.09 | 0.93 | −0.03 | −0.13 | 0.16 |
| 3 | **Glycine** | 2 | 0 | −0.14 | 0.77 | 0.05 | −0.02 | 0.15 |
| 3 | **Alanine** | 2 | −0.06 | 0.14 | 0.84 | −0.13 | 0.13 | 0.11 |
| 3 | **Methionine** | 2 | −0.09 | 0.01 | 0.84 | −0.14 | 0.03 | 0.11 |
| 3 | **5-Oxoproline/Pyroglutamic acid** | 2 | −0.12 | −0.03 | 0.81 | −0.06 | −0.02 | −0.08 |
| 3 | **Valine** | 2 | 0 | 0.15 | 0.81 | −0.01 | −0.02 | 0.05 |
| 3 | **Threonine** | 2 | −0.03 | −0.03 | 0.85 | −0.21 | −0.05 | −0.01 |
| 4 | **FA (20:4)** | 2 | 0.09 | −0.1 | −0.03 | 0.73 | −0.08 | 0.45 |
| 4 | **FA (20:3)** | 2 | −0.04 | 0.01 | −0.06 | 0.89 | 0.04 | 0.2 |
| 4 | **FA (17:0)** | 2 | 0.04 | −0.14 | 0.05 | 0.86 | −0.05 | 0.1 |
| 4 | **FA (22:4)** | 2 | 0.07 | 0 | −0.15 | 0.86 | −0.08 | 0.06 |
| 4 | **FA (18:3)** | 2 | 0.04 | 0.02 | 0 | 0.88 | 0.11 | 0.03 |
| 4 | **FA (18:0;O6)** | 4 | 0.04 | −0.03 | −0.04 | 0.92 | −0.21 | 0.03 |
| 4 | **FA (14:0)** | 2 | 0.07 | −0.03 | 0 | 0.87 | 0.07 | 0.02 |
| 4 | **FA (22:5)** | 2 | 0.16 | −0.08 | −0.08 | 0.91 | 0.01 | −0.01 |
| 4 | **FA (22:6)** | 2 | 0.2 | −0.09 | 0.04 | 0.64 | −0.05 | 0 |
| 4 | **FA (14:1)** | 2 | 0.04 | −0.11 | −0.03 | 0.88 | 0.01 | 0 |
| 4 | **FAHFA (2:0_20:4)** | 4 | −0.06 | −0.04 | 0.02 | 0.88 | −0.22 | 0.05 |
| 5 | **LPC (20:3/0:0)** | 2 | 0.21 | 0.18 | 0.04 | −0.02 | 0.67 | 0.16 |
| 5 | **PC (18:0_20:3)** | 3 | 0.37 | 0.33 | 0.03 | −0.06 | 0.73 | 0.1 |
| 5 | **PC (30:0)** | 3 | 0.32 | 0.21 | 0.05 | −0.06 | 0.76 | −0.09 |
| 5 | **PC (16:0_16:1)** | 3 | 0.36 | 0.3 | 0.01 | 0.02 | 0.78 | −0.07 |
| 5 | **PC (34:3)** | 3 | 0.39 | 0.27 | 0.03 | −0.15 | 0.79 | −0.06 |
| 5 | **PC (40:5)** | 3 | 0.51 | 0.28 | 0.1 | −0.02 | 0.69 | −0.06 |
| 5 | **PC (33:1)** | 3 | 0.42 | 0.22 | 0.03 | −0.04 | 0.68 | −0.06 |
| 5 | **PC (18:0_18:1)** | 3 | 0.44 | 0.21 | 0.04 | −0.07 | 0.71 | 0.06 |
| 5 | **PC (18:0_22:4)** | 3 | 0.3 | 0.28 | −0.01 | −0.02 | 0.72 | 0.03 |
| 5 | **PC (38:1)** | 3 | 0.52 | 0.18 | −0.04 | −0.11 | 0.65 | 0.01 |
| 6 | **Glutamic acid** | 2 | −0.04 | 0.12 | 0.14 | 0.18 | −0.09 | 0.85 |
| 6 | **Choline** | 2 | 0.01 | 0.13 | 0.17 | 0.03 | 0.07 | 0.74 |
| 6 | **Aspartic acid** | 2 | 0.02 | −0.03 | −0.01 | 0.19 | 0.04 | 0.72 |
| 6 | **Glutamine** | 2 | −0.16 | −0.1 | 0.18 | 0.07 | −0.12 | 0.67 |
| 6 | **Arginine** | 2 | 0.01 | 0.02 | 0.12 | 0.02 | 0.14 | 0.66 |

Bold values means the factor score of each variable in its factor.

(208 metabolites with p-Bonferroni< 0.05 out of a total of 964 variables) mainly in triglyceride, diglyceride and phosphatidylcholine levels. In addition, there are also differences (125 metabolites) between metabotype 2 and metabotype 3. Only one of these 125 significant metabolites is different from the comparison between metabotype 1 and

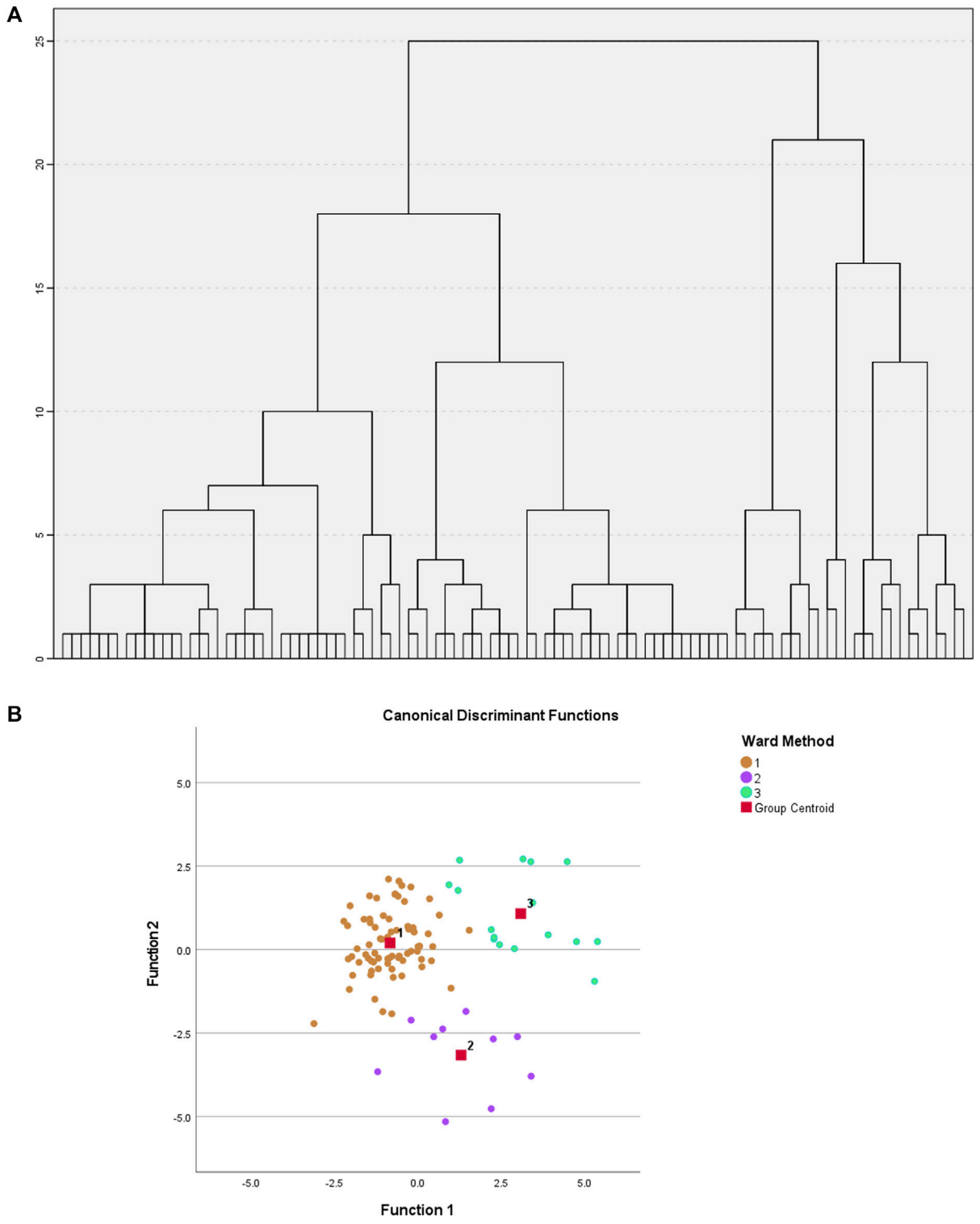


FIGURE 3
**(A)** Hierarchical clustering performed on the factors obtained after Factor Analysis. Ward's method and Euclidean distance squared. **(B)** Graph of individuals on the discriminant dimensions. Shows the relative location of the different groups.

metabotype 3, this was lactic acid. However, differences between metabotype 1 and metabotype 2 are minimal (7 metabolites). It is important to note that the levels of different triglycerides in metabotype 3 are found to be increased over two-fold over those in metabotypes 1 and 2. In addition, we observed a significant reduction of proline in metabotype 1. Intergroup

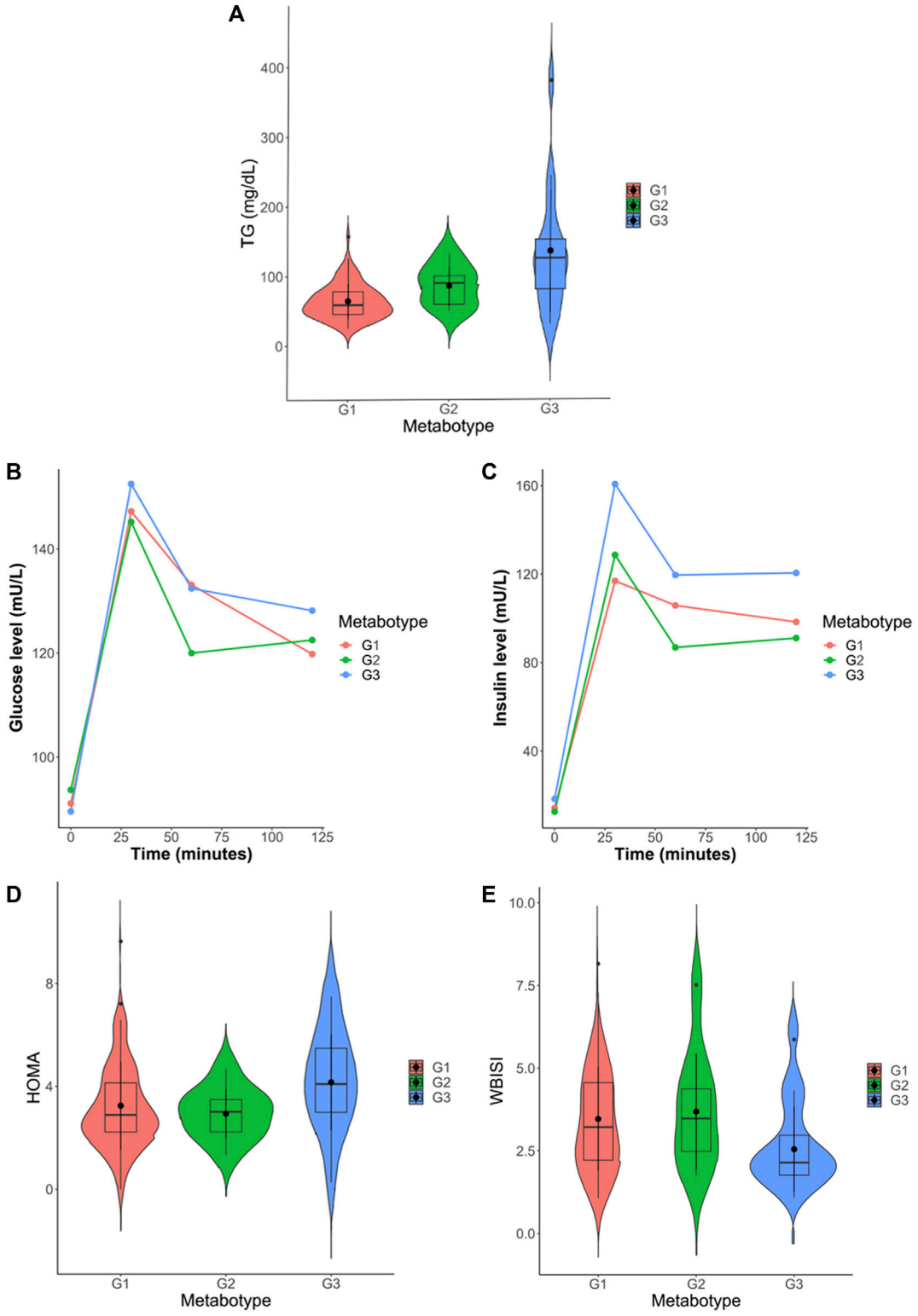


FIGURE 4
**(A)** Violin plot of total triglyceride levels in the three identified metabotypes. **(B)** Progression plot of insulin levels throughout the oral glucose tolerance test (OGTT). **(C)** Progression plot of glucose levels throughout the oral glucose tolerance test (OGTT). **(D)** Violin plot of HOMA-IR (Homeostatic Model Assessment for Insulin Resistance) levels in the three identified metabotypes. **(E)** Violin plot of WBISI (whole-body insulin sensitivity index) levels in the three identified metabotypes.

**TABLE 4 Clinical/biochemical parameters in the studied metabotypes. Values are average ± SEM. *p*-value was computed according to the parametric or non-parametric tests applied (ANOVA/Kruskal–Wallis), selected accordingly. Groups homogeneity (Bonferroni) is indicated with superscript letters. Shared letter involves homogeneous groups.**

| Clinical features | G1 | G2 | G3 | *p*-value |
|---|---|---|---|---|
| Age (years) | 10.8 ± 0.4 | 12 ± 0.9 | 11.8 ± 1 | 0.34 |
| BMI (kg/m$^2$) | 28.4 ± 0.5 | 28 ± 0.9 | 29.8 ± 1.5 | 0.65 |
| BMI-SDS | 4.2 ± 2.4 | 3.6 + 1.0 | 3.9 + 1.6 | 0.87 |
| HOMA | 3.2 ± 0.2 | 2.9 ± 0.3 | 4.2 ± 0.5 | 0.08 |
| Insulin levels 0 min (μU/mL) | 14.2 ± 0.8$^a$ | 12.6 ± 1.2$^{ab}$ | 18.4 ± 1.9$^b$ | **0.03** |
| Insulin levels 30 min (μU/mL) | 116.9 ± 8$^a$ | 128.7 ± 24.5$^{ab}$ | 160.7 ± 17.8$^b$ | **0.03** |
| Insulin levels 60 min (μU/mL) | 105.8 ± 9.3 | 86.9 ± 24.7 | 119.6 ± 14.7 | 0.17 |
| Insulin levels 120 min (μU/mL) | 98.4 ± 8.6 | 91.1 ± 17.9 | 120.6 ± 18.1 | 0.36 |
| WBISI | 3.5 ± 0.2 | 3.7 ± 0.6 | 2.6 ± 0.3 | **0.05** |
| Glucose levels 0 min (mg/dL) | 91.1 ± 0.8 | 93.7 ± 1.9 | 89.6 ± 1.9 | 0.32 |
| Glucose levels 30 min (mg/dL) | 147.2 ± 2.9 | 145.2 ± 7.7 | 152.5 ± 5.9 | 0.68 |
| Glucose levels 60 min (mg/dL) | 133.1 ± 3.3 | 120 ± 5.9 | 132.4 ± 5.7 | 0.35 |
| Glucose levels 120 min (mg/dL) | 119.8 ± 2 | 122.5 ± 5.1 | 128.1 ± 5 | 0.24 |
| Total Cholesterol (mg/dL) | 154.2 ± 3.7$^a$ | 160.9 ± 8.9$^{ab}$ | 178.9 ± 9.9$^b$ | 0.03 |
| TG (mg/dL) | 64.2 ± 2.9$^a$ | 85.5 ± 8.9$^{ab}$ | 135.3 ± 22$^b$ | **0.00** |
| HDL-c (mg/dL) | 48 ± 1.8 | 45.3 ± 3.4 | 41.4 ± 2.2 | 0.19 |
| LDL-c (mg/dL) | 92.7 ± 3.2 | 99.5 ± 7 | 110.5 ± 7.6 | 0.19 |
| GGT (U/L) | 14 ± 0.5 | 15 ± 1.6 | 15.9 ± 1.3 | 0.35 |
| GOT (U/L) | 27.4 ± 0.8 | 26.9 ± 1.4 | 30.1 ± 2.7 | 0.87 |
| GPT (U/L) | 21.2 ± 0.9 | 23 ± 3.7 | 26.9 ± 3.4 | 0.13 |
| IGF-1 (ng/mL) | 320.3 ± 19.9 | 289.4 ± 41.3 | 293 ± 49.5 | 0.64 |
| IGFBP3 (μg/mL) | 4.9 ± 0.1 | 4.6 ± 0.3 | 5.1 ± 0.3 | 0.52 |
| HbA1c (%) | 5.4 ± 0 | 5.5 ± 0.1 | 5.3 ± 0.1 | 0.58 |
| Free T4 (ng/dL) | 0.9 ± 0.1 | 1.0 ± 0.1 | 0.9 ± 0.1 | 0.61 |
| TSH (μU/mL) | 2.7 ± 0.2$^{ab}$ | 1.8 ± 0.3$^a$ | 3.3 ± 0.5$^b$ | **0.03** |
| DBP mmHg | 61.7 ± 0.9 | 62.2 ± 2.1 | 64.7 ± 1.9 | 0.22 |
| SBP mmHg | 116.3 ± 1.5 | 115.6 ± 3.7 | 123.1 ± 3.5 | 0.17 |
| Uric Acid mg/dL | 5.2 ± 0.1 | 5.0 ± 0.4 | 5.3 ± 0.3 | 0.76 |
| Vitamin D (ng/mL) | 24.4 ± 1.3 | 23.1 ± 3.8 | 20.6 ± 2.8 | 0.28 |

Abbreviations: BMI-SDS, Standardized body mass index (Z-score); HOMA, homeostatic model assessment; WBISI, Whole-body insulin sensitivity index; TG, triglycerides; HDL-c, High density lipoprotein cholesterol; LDL-c, Low density lipoprotein cholesterol; GGT, Gamma-glutamyltransferase; GOT, aspartate transaminase; GPT, glutamic-pyruvic transaminase Alanine aminotransferase; IGF-1, Insulin-like growth factor 1; IGFBP3, Insulin-like Growth Factor-binding Protein 3; HbA1c: hemoglobin A1c; TSH, thyroid-stimulating hormone; DBP, diastolic blood pressure; SBP, diastolic blood pressure.

comparison of routine clinical laboratory data revealed significant differences in total triglyceride levels, along with fasting and glucose-stimulated serum insulin but not glucose level among these metabotypes (Figure 4; Table 4), with individuals in metabotype 3 showing lower insulin sensitivity and hypertriglyceridemia, in a higher risk metabolic profile than patients in metabotypes 1 and 2.

## Discussion

In this study, we have highlighted the significance of conducting an in-depth analysis of individuals' metabolic phenotypes, yielding a classification that cannot be attained through anthropometric features or routine clinical laboratory analyses. Furthermore, we have observed an absence of pathognomonic metabolic or

metabolomics signatures due to the presence of specific HetRSVs. In this context, Factor Analysis assumes particular importance in the integration of data from various analytical platforms, bringing us closer to personalized medicine.

The term "personalized medicine" stands for the most suitable specific therapeutic interventions for an individual patient, underscoring the relevance of developing management strategies on specific individuals and not average group response to treatments. This concept has also expanded to nutrition (i.e., personalized nutrition) and current research focuses on the intricate interaction between diet, (epi)genome, and the microbiome, which can determine the effects of bioactive compounds (González-Sarrías et al., 2017).

Using a multiplatform untargeted metabolomics-based approach, we determined the metabolic fingerprint of children with obesity, and by integrating all the data generated by using Factor Analysis to stratify individuals with obesity according to their metabolic phenotype, we defined three different "metabotypes." Bioinformatics tools are currently available to combine information from different omics technologies or from different analytical platforms. Some of these tools allow the performance of supervised multivariate analysis (Westerhuis et al., 1998; Löfstedt and Trygg, 2011; Boccard and Rutledge, 2013) to determine the existing differences between different groups combining the obtained data. Other integrative multi-omics clustering tools are specific unsupervised integrative methods to find coherent groups between samples or features using the information obtained in a multi-omics analysis (Multiblock PCA, iClusterPlus, iClusterBayes, moCluster, LRAcluster, PINSplus, SNF, etc.) (Mo et al., 2013; Wu et al., 2015; Meng et al., 2016; Nguyen et al., 2017; Wang et al., 2017; Mo et al., 2018; Rappoport and Shamir, 2018; Nguyen et al., 2019; Tanabe et al., 2021; Zhang et al., 2022). However, most of these algorithms require knowledge about the parameters to be applied, and some exhibit complex interpretability. The advantage of Factor Analysis is that it allows us to reduce dimensionality (without losing statistically relevant information), which facilitates the discovery of potential biomarkers, as well as simplifies the biological interpretation of differences between individuals' metabolic phenotypes. Data integration based on dimensionality reduction approaches seems to be a powerful tool to combine all metabolomic information obtained from different platforms (Zhang et al., 2022). This study proposes the use of Factor Analysis to combine and summarize the information from the different data matrices. The use of Factor Analysis combined with a hierarchical clustering analysis has made it possible to identify three clearly differentiated metabotypes between children with obesity. It is known that cluster analysis has the potential to yield clusters that are either arbitrary or devoid of biological significance. One strength of the results obtained relies on the fact that the acquisition of a notably elevated score in a supervised analysis (discriminant analysis) employing the metabotypes derived from the cluster analysis, serves to not only validate the efficacy of the Factor Analysis but also to enhance the concrete manifestation of the three identified metabotypes.

In routine clinical laboratories, serum levels of triglycerides, lipoproteins, and transaminases are frequently increased in patients with obesity, revealing underlying dyslipidemia and liver dysfunction (Rauschert et al., 2016). Several studies indicate that some amino acids, such as the branched chain amino acids (BCAA), tyrosine, valine, leucine, or isoleucine, can be used as indicators in early stages of carbohydrate metabolism impairment (Wang et al., 2011; Michaliszyn et al., 2012; Mccormack et al., 2013; Butte et al., 2015; Mastrangelo et al., 2016; Suzuki et al., 2019). Moreover, Suzuki et al. reported a correlation between insulin resistance and free amino acid levels in a cohort of patients with moderate to severe obesity (Suzuki et al., 2019). Our results suggest the existence of large metabolic differences between the identified metabotypes, with a singularly differentiated fingerprint in metabotype 3. Factor Analysis indicates that metabotype 3 is characterized by increased levels of "*Lipids1*," "*Lipids2*," "*Lipids4*," and amino acids related to cell signaling. In addition, univariate analysis showed mainly significant differences in triglycerides, diglycerides, and phosphatidylcholines between metabotype 3 and the rest of the metabotypes, with increased levels of these lipid species in metabotype 3. These results suggest the presence of combined hyperlipidemia (cholesterol + triglyceride) in individuals integrated within metabotype 3. Routine clinical laboratory analyses are partially in agreement with these results as individuals in metabotype 3 had increased total triglyceride levels, as well as impairment of insulin, including increased fasting and glucose stimulated insulin secretion and lower WBISI, along with significantly increased levels of isoleucine and proline (UVA, data not shown), in concordance with Suzuki et al. (Suzuki et al., 2019). However, routine clinical analysis of cholesterol species did not detect the higher cholesterol ester levels in metabotype 3 observed by using metabolomics, even when other studies have associated increased cholesterol and triglyceride levels with a decrease in HDL-c levels (Brown et al., 2000) and higher BMI (Huynh et al., 2019). It is pertinent to emphasize that the more pronounced metabolic perturbation of individuals in metabotype 3 is not correlated with a higher BMI-SDS among these individuals compared to those in other metabotypes. Nevertheless, a higher representation of Hispanic ethnicity was observed in metabotype 3 (25%) compared to metabotypes 1 (12%) or 2 (0%). This is consistent with the lower insulin sensitivity and higher triglyceride levels reported in Hispanic children with obesity compared to Caucasians (Martos-Moreno et al., 2020), thus suggesting an eventual ethnic driven influence in obesity associated metabolomic profiles (Butte et al., 2015), although this does not extend to all difference observed (i.e., higher cholesterol ester levels in metabotype 3, not endorsed in inter-ethnic comparisons) (Martos-Moreno et al., 2019; Martos-Moreno et al., 2020). In contrast, proven the role of pubertal status on the development of obesity associated metabolic comorbidities (particularly insulin resistance), we compared the relative frequence within each defined metabotype of patient Tanner stage and, additionally, of prepubertal vs. pubertal patients (pooling TII to T-V in the latter). No significant differences between metabotypes were observed regarding the distribution of Tanner stages within each metabotype ($\chi 2$ 0.491; $p = 0.782$) nor in the relative proportion of prepubertal vs. pubertal patients ($\chi 2$ 8.596; $p = 0.378$). Despite these results not being supportive, the possibility of pubertal influence on the patient metabotype cannot be completely ruled out and this should be further explored in larger patient cohorts.

Interestingly, Factor Analysis splits the relevant amino acids into two subsets. Phenylalanine, proline, serine, glycine, alanine, methionine, valine, and threonine were part of Factor 3, and were higher in Metabotype 2. Glutamic acid, glutamine, and

arginine, together with choline were higher in Metabotype 3. Even though these amino acids have all been shown to correlate with insulin resistance in childhood obesity (Suzuki et al., 2019), such grouping points towards a non-homogeneous involvement of the different amino acids in the complications of obesity. Besides their role in protein synthesis, each amino acid can be involved in different functions and processes, and it is beyond the possibilities of this observational study to determine the exact relationships between the differences found and the therapeutic approach to treat obesity. Those amino acids grouped in Factor 3 include 4 essential (phenylalanine, threonine, valine, methionine) and 3 of the most abundant amino acids (glycine, serine, alanine), and therefore this factor could be strongly related to the nutritional status of the patients, as it would represent protein intake and turnover in the body. In Factor 6, increased in Metabotype 3, glutamic acid, aspartic acid and glutamine, were grouped with choline and arginine. In addition to also reflecting the nutritional status, this group of factors is of particular relevance as they can be related to neurotransmission (Dalangin et al., 2020), and their circulating levels have been proposed as biomarkers of visceral obesity and metabolic alterations (Maltais-Payette et al., 2018) and have been associated with metabolic stress (Yan et al., 2012).

As stated above, childhood obesity is the result of the action of multiple environmental factors on eating and activity habits and lifestyle, in combination with an individual's unique genetic fingerprint. GWAS studies yielded a large list of genes with SNPs, or variants associated to human obesity, but in the vast majority of cases, a single determinant of childhood obesity cannot be identified, thus classifying these cases as "polygenic" or "idiopathic" obesity. In contrast, the rare cases of monogenic forms of obesity, are mainly caused by biallelic mutations in a single gene, usually in the leptin-melanocortin satiety pathway, and are characterized by vary severe, early-onset obesity, usually with evident hyperphagia, and in some cases associated to other metabolic comorbidities and influencing growth pattern even in the first years of life (Handakas et al., 2022). Several metabolomic studies have been performed in childhood obesity, comprehensively characterizing the metabolic alterations in these conditions, as well as in animal models of leptin resistance thus exploring the effect of the impairment of the leptin-POMC satiety pathway (Pietiläinen et al., 2007; Mastrangelo et al., 2016; Martos-Moreno et al., 2017; Rauschert et al., 2017; Kim et al., 2019; Lawler et al., 2020; Rupérez et al., 2020; Sanz-Fernandez et al., 2020). However, the pathogenic role of heterozygous rare sequence variants in the genes of the leptin-melanocortin pathway (Le Collen et al., 2023), as in other genes relevant for central energy and glucose homeostasis is under discussion (Trang and Grant, 2023). Following previous observations by us and other groups (Serra-Juhé et al., 2017; Gerl et al., 2019; Gonzalez-Riano et al., 2021), the hypothesis that they are eventual pathogenicity was proposed. However, the results of this study, showing no anthropometric, metabolic nor metabolomic differences between patients with or without HetRSVs in the studied genes, and the lack of differences in the prevalence of the different metabotypes between these groups does not verify their pathogenic role (Supplementary Tables), at least from a metabolic and metabolomic point of view. To our knowledge, this study is the first metabolomic study attempting to identify a specific metabolic phenotype associated with the presence of HetRSVs in the leptin-POMC pathway, as well as in glutamate receptors, and demonstrates the absence of a clear differential metabolic phenotype due to the presence of these variants.

**TABLE 5** Mean values of the factor scores of the new factors obtained after Factor Analysis.

| Factor name | | G1 | G2 | G3 |
|---|---|---|---|---|
| | | Mean | Mean | Mean |
| Factor 1 | "*Lipids1*" (SM/CE) | −0.06 | −0.03 | 0.32 |
| Factor 2 | "*Lipids2*" (DAG/TAG) | −0.30 | 0.01 | 1.38 |
| Factor 3 | "*Nutritional amino acids*" | −0.33 | 2.10 | 0.20 |
| Factor 4 | "*Lipids3*" (FFA) | 0.05 | −0.13 | −0.16 |
| Factor 5 | "*Lipids4*" (PC) | −0.15 | −0.29 | 0.88 |
| Factor 6 | "*Signaling amino acids*" | −0.08 | −0.59 | 0.75 |

The association of obesity with lipidomes and the use of technologies to stratify obesity based on lipidomic data has been previously investigated by means of machine learning algorithms (Gerl et al., 2019). However, this is the first study, to combine metabolomic data from different analytical platforms and genetic data to stratify obesity. Moreover, Factor Analysis has not been previously employed for the subclassification of patients with obesity by using the adequate combination of multiplatform MS metabolomics data. We distinguished two antagonic metabotypes (1 and 2 vs. 3) that can be deduced from the examination of the contributing factors. Such subclassification was not possible from the information derived from the routine clinical examination and laboratory analyses. With our approach, subtle but clear differences arose between the three metabotypes: Six groups of metabolites can be combined to evaluate the metabolic phenotype, and promising associations between this metabolic phenotype and insulin sensitivity, circulating triglycerides and TSH levels and ethnicity have been uncovered. Metabotypes 1 and 2 have lower levels of the factors corresponding to "*Lipids1*" (F1), "*Lipids2*" (F2), "*Lipids4*" (F5) and "*Signaling amino acids*" (F6), as compared to Metabotype 3, suggesting a higher metabolic risk phenotype in patients with childhood obesity in Metabotype 3 (Table 5). Among the most promising results, the separation of amino acids into two different factors, and the differential association of these factors with different phenotypes opens the possibility of treating the obese subjects in these two metabotypes with different approaches. Metabotype 2 was associated with higher levels of F2, or *Nutritional amino acids*, than in the other two metabotypes, suggesting a healthier metabolic phenotype of these patients, that could speculatively be associated to higher protein intake in their diet, whereas F6, higher in metabotype 3, could speculatively be associated to a behavioral component of the children in this group. However, the lack of precise control of feeding behavior in these patients, feeding due to the ambulatory modality of management is a limitation to test this hypothesis. Apart from this, the limited number of patients studied, along with the potential confounding factors (such as sex, race or

pubertal status) potentially influencing the described metabotypes raise the need of validating the presented results in larger and independent cohorts, to enhance the reliability and generalizability of the results, i.e., to support the metabotypes here identified and to explore an eventual role of these factors.

The challenge for the near future will be to use new technological advances such as that used here to accurately stratify the state/stage of different diseases, in order to precisely predict disease progression and to provide appropriate treatment for each patient, as well as to monitor their evolution.

## Data availability statement

This study is available at the NIH Common Fund's National Metabolomics Data Repository (NMDR) website, the Metabolomics Workbench, https://www.metabolomicsworkbench.org where it has been assigned Study ID ST002993. The data can be accessed directly via its Project DOI: http://dx.doi.org/10.21228/M8WX4S. This work is supported by NIH grant U2C-DK119886. The study is available for review at http://dev.metabolomicsworkbench.org:22222/data/DRCCMetadata.php?Mode=Study&StudyID=ST002993&Access=ZeeZ9799.

## Ethics statement

The studies involving humans were approved by University Hospital Niño Jesús. The studies were conducted in accordance with the local legislation and institutional requirements. Written informed consent for participation in this study was provided by the participants' legal guardians/next of kin.

## Author contributions

DC-S: Conceptualization, Data curation, Formal Analysis, Investigation, Methodology, Software, Visualization, Writing–original draft, Writing–review and editing. FRP: Data curation, Formal Analysis, Writing–review and editing. JA: Conceptualization, Funding acquisition, Resources, Supervision, Writing–review and editing. CB: Conceptualization, Resources, Supervision, Writing–review and editing. GM-M: Conceptualization, Data curation, Funding acquisition, Project administration, Resources, Supervision, Writing–review and editing. FR: Conceptualization, Funding acquisition, Project administration, Resources, Supervision, Writing–original draft, Writing–review and editing.

## Funding

The authors declare financial support was received for the research, authorship, and/or publication of this article. This study was supported by the Ministry of Science and Innovation of Spain (MICIN), PID2021-122490NB-I00/AEI/10.13039/501100011033 by ERDF-"A way of making Europe"; the Autonomous Community of Madrid P2022/BMD-7232 (TomoXliver2-CM); Instituto de Salud Carlos III (Spain) FIS PI09/91060, FIS PI10/00747, PI13/02195, FIS PI16/00485, FIS PI 19/00166 and FIS PI 22/01820. GM-M and JA are part of the CIBER Fisiopatología de la Obesidad y Nutrición (CB06/03), supported by Instituto de Salud Carlos III. DC-S is supported by a fellowship from CEU International Doctoral School (CEINDO) and Bank Santander.

## Acknowledgments

The authors wish to thank Prof. Luis A. Pérez-Jurado for his collaboration in the classification and CADD scoring of the genetic variants harbored by the patients and Julie Chowen for the critical review and English edition of the manuscript.

## Conflict of interest

The authors declare that the research was conducted in the absence of any commercial or financial relationships that could be construed as a potential conflict of interest.

## Publisher's note



## Supplementary material

The Supplementary Material for this article can be found online at: https://www.frontiersin.org/articles/10.3389/fmolb.2023.1301996/full#supplementary-material

## References

Acal, C., Aguilera, A. M., and Escabias, M. (2020). New modeling approaches based on varimax rotation of functional principal components. *Mathematics* 8 (11), 2085. doi:10.3390/math8112085

Argelaguet, R., Arnol, D., Bredikhin, D., Deloro, Y., Velten, B., Marioni, J. C., et al. (2020). MOFA+: a statistical framework for comprehensive integration of multi-modal single-cell data. *Genome Biol.* 21 (1), 111. doi:10.1186/s13059-020-02015-1

Argelaguet, R., Velten, B., Arnol, D., Dietrich, S., Zenz, T., Marioni, J. C., et al. (2018). Multi-Omics Factor Analysis—a framework for unsupervised integration of multi-omics data sets. *Mol. Syst. Biol.* 14 (6), e8124. doi:10.15252/msb.20178124

Armitage, E. G., Godzien, J., Alonso-Herranz, V., López-Gonzálvez, Á., and Barbas, C. (2015). Missing value imputation strategies for metabolomics data. *Electrophoresis* 36 (24), 3050–3060. doi:10.1002/elps.201500352

Babakus, E., Ferguson, C. E., and Jöreskog, K. G. (1987). The sensitivity of confirmatory maximum likelihood factor analysis to violations of measurement scale and distributional assumptions. *J. Mark. Res.* 24 (2), 222–228. doi:10.2307/3151512

Bell, C. G., Walley, A. J., and Froguel, P. (2005). The genetics of human obesity. *Nat. Rev. Genet.* 6 (3), 221–234. doi:10.1038/nrg1556

Berger, N. A. (2018). Young adult cancer: influence of the obesity pandemic. *Obesity* 26 (4), 641–650. doi:10.1002/oby.22137

Blaženović, I., Kind, T., Ji, J., and Fiehn, O. (2018). Software tools and approaches for compound identification of LC-MS/MS data in metabolomics. *Metabolites*, 8 (2), 31. doi:10.3390/metabo8020031

Boccard, J., and Rutledge, D. N. (2013). A consensus orthogonal partial least squares discriminant analysis (OPLS-DA) strategy for multiblock Omics data fusion. *Anal. Chim. Acta* 769, 30–39. doi:10.1016/j.aca.2013.01.022

Brown, C. D., Higgins, M., Donato, K. A., Rohde, F. C., Garrison, R., Obarzanek, E., et al. (2000). Body mass index and the prevalence of hypertension and dyslipidemia. *Obes. Res.* 8 (9), 605–619. doi:10.1038/oby.2000.79

Butte, N. F., Liu, Y., Zakeri, I. F., Mohney, R. P., Mehta, N., Voruganti, V. S., et al. (2015). Global metabolomic profiling targeting childhood obesity in the Hispanic population. *Am. J. Clin. Nutr.* 102 (2), 256–267. doi:10.3945/ajcn.115.111872

Cardel, M. I., Atkinson, M. A., Taveras, E. M., Holm, J. C., and Kelly, A. S. (2020). Obesity treatment among adolescents: a review of current evidence and future directions. *JAMA Pediatr.* 174 (6), 609–617. doi:10.1001/jamapediatrics.2020.0085

Cattell, R. B. (1966). The scree test for the number of factors. *Multivar. Behav. Res.* 1 (2), 245–276. doi:10.1207/s15327906mbr0102_10

Chan, J. Y. L., Leow, S. M. H., Bea, K. T., Cheng, W. K., Phoong, S. W., Hong, Z. W., et al. (2022). Mitigating the multicollinearity problem and its machine learning approach: a review. *Mathematics* 10 (8), 1283. doi:10.3390/math10081283

Chiurazzi, M., Cozzolino, M., Orsini, R. C., Di Maro, M., Di Minno, M. N. D., and Colantuoni, A. (2020). Impact of genetic variations and epigenetic mechanisms on the risk of obesity. *Int. J. Mol. Sci.* 21 (23), 9035. doi:10.3390/ijms21239035

Choi, J. E., Lee, H. A., Park, S. W., Lee, J. W., Lee, J. H., Park, H., et al. (2023). Increase of prevalence of obesity and metabolic syndrome in children and adolescents in korea during the COVID-19 pandemic: a cross-sectional study using the knhanes. *Children* 10 (7), 1105. doi:10.3390/children10071105

Clark, C., Dayon, L., Masoodi, M., Bowman, G. L., and Popp, J. (2021). An integrative multi-omics approach reveals new central nervous system pathway alterations in Alzheimer's disease. *Alzheimers Res. Ther.* 13 (1), 71. doi:10.1186/s13195-021-00814-7

Cole, T. J., Bellizzi, M. C., Flegal, K. M., and Dietz, W. H. (2000). Establishing a standard definition for child overweight and obesity world-wide: International survey. *BMJ Evid. Based Med.* 320, 1240–1243. doi:10.1136/bmj.320.7244.1240

Cote, A. T., Harris, K. C., Panagiotopoulos, C., Sandor, G. G. S., and Devlin, A. M. (2013). Childhood obesity and cardiovascular dysfunction. *J. Am. Coll. Cardiol.* 62 (15), 1309–1319. doi:10.1016/j.jacc.2013.07.042

da Fonseca, A. C. P., Mastronardi, C., Johar, A., Arcos-Burgos, M., and Paz-Filho, G. (2017). Genetics of non-syndromic childhood obesity and the use of high-throughput DNA sequencing technologies. *J. Diabetes Complicat.* 31 (10), 1549–1561. doi:10.1016/j.jdiacomp.2017.04.026

Dalangin, R., Kim, A., and Campbell, R. E. (2020). The role of amino acids in neurotransmission and fluorescent tools for their detection. *Int. J. Mol. Sci.* 21 (17), 6197. doi:10.3390/ijms21176197

Dudzik, D., Barbas-Bernardos, C., García, A., and Barbas, C. (2018). Quality assurance procedures for mass spectrometry untargeted metabolomics. a review. *J. Pharm. Biomed. Anal.* 147, 149–173. doi:10.1016/j.jpba.2017.07.044

Fairbrother, U., Kidd, E., Malagamuwa, T., and Walley, A. (2018). Genetics of severe obesity. *Curr. Diab Rep.* 18 (10), 85. doi:10.1007/s11892-018-1053-x

Fernández, J. R., Redden, D. T., Pietrobelli, A., and Allison, D. B. (2004). Waist circumference percentiles in nationally representative samples of African-American, European-American, and Mexican-American children and adolescents. *J. Pediatr.* 145, 439–444. doi:10.1016/j.jpeds.2004.06.044

Fuente-Martín, E., Garciá-Cáceres, C., Argente-Arizón, P., Diáz, F., Granado, M., Freire-Regatillo, A., et al. (2016). Ghrelin regulates glucose and glutamate transporters in hypothalamic astrocytes. *Sci. Rep.* 6, 23673. doi:10.1038/srep23673

Garcia, A., and Barbas, C. (2011). Gas chromatography-mass spectrometry (GC-MS)-based metabolomics. *Methods Mol. Biol.* 708, 191–204. doi:10.1007/978-1-61737-985-7_11

Gavaghan, C. L., Holmes, E., Lenz, E., Wilson, I. D., and Nicholson, J. K. (2000). An NMR-based metabonomic approach to investigate the biochemical consequences of genetic strain differences: application to the C57BL10J and Alpk:ApfCD mouse. *FEBS Lett.* 484 (3), 169–174. doi:10.1016/s0014-5793(00)02147-5

Gerl, M. J., Klose, C., Surma, M. A., Fernandez, C., Melander, O., Männistö, S., et al. (2019). Machine learning of human plasma lipidomes for obesity estimation in a large population cohort. *PLoS Biol.* 17 (10), e3000443. doi:10.1371/journal.pbio.3000443

Gil-de-la-Fuente, A., Godzien, J., Saugar, S., Garcia-Carmona, R., Badran, H., Wishart, D. S., et al. (2019). CEU mass mediator 3.0: a metabolite annotation tool. *J. Proteome Res.* 18 (2), 797–802. doi:10.1021/acs.jproteome.8b00720

Gonzalez-Riano, C., Gradillas, A., and Barbas, C. (2021). Exploiting the formation of adducts in mobile phases with ammonium fluoride for the enhancement of annotation in liquid chromatography-high resolution mass spectrometry based lipidomics. *J. Chromatogr. Open* 1, 100018. doi:10.1016/j.jcoa.2021.100018

González-Sarrías, A., García-Villalba, R., Romo-Vaquero, M., Alasalvar, C., Örem, A., Zafrilla, P., et al. (2017). Clustering according to urolithin metabotype explains the interindividual variability in the improvement of cardiovascular risk biomarkers in overweight-obese individuals consuming pomegranate: a randomized clinical trial. *Mol. Nutr. Food Res.* 61 (5), 1600830. doi:10.1002/mnfr.201600830

Handakas, E., Lau, C. H., Alfano, R., Chatzi, V. L., Plusquin, M., Vineis, P., et al. (2022). A systematic review of metabolomic studies of childhood obesity: state of the evidence for metabolic determinants and consequences. *Obes. Rev.* 23 (S1), 23. doi:10.1111/obr.13384

Hoadley, K. A., Yau, C., Wolf, D. M., Cherniack, A. D., Tamborero, D., Ng, S., et al. (2014). Multiplatform analysis of 12 cancer types reveals molecular classification within and across tissues of origin. *Cell* 158 (4), 929–944. doi:10.1016/j.cell.2014.06.049

Huynh, K., Barlow, C. K., Jayawardana, K. S., Weir, J. M., Mellett, N. A., Cinel, M., et al. (2019). High-throughput plasma lipidomics: detailed mapping of the associations with cardiometabolic risk factors. *Cell Chem. Biol.* 26 (1), 71–84. doi:10.1016/j.chembiol.2018.10.008

Jackson, R. S., Creemers, J. W., Ohagi, S., Raffin-Sanson, M. L., Sanders, L., Montague, C. T., et al. (1997). Obesity and impaired prohormone processing associated with mutations in the human prohormone convertase 1 gene. *Nat. Genet.* 16 (3), 303–306. doi:10.1038/ng0797-303

Kamleh, M. A., McLeod, O., Checa, A., Baldassarre, D., Veglia, F., Gertow, K., et al. (2018). Increased levels of circulating fatty acids are associated with protective effects against future cardiovascular events in nondiabetics. *J. Proteome Res.* 17 (2), 870–878. doi:10.1021/acs.jproteome.7b00671

Kim, M. J., Kim, J. H., Kim, M. S., Yang, H. J., Lee, M., and Kwon, D. Y. (2019). Metabolomics associated with genome-wide association study related to the basal metabolic rate in overweight/obese Korean women. *J. Med. Food* 22 (5), 499–507. doi:10.1089/jmf.2018.4310

Koelmel, J. P., Li, X., Stow, S. M., Sartain, M. J., Murali, A., Kemperman, R., et al. (2020). Lipid annotator: towards accurate annotation in non-targeted liquid chromatography high-resolution tandem mass spectrometry (LC-HRMS/MS) lipidomics using a rapid and user-friendly software. *Metabolites* 10 (3), 101. doi:10.3390/metabo10030101

Kuligowski, J., Sánchez-Illana, Á., Sanjuán-Herráez, D., Vento, M., and Quintás, G. (2015). Intra-batch effect correction in liquid chromatography-mass spectrometry using quality control samples and support vector regression (QC-SVRC). *Analyst* 140 (22), 7810–7817. doi:10.1039/c5an01638j

Lawler, K., Huang-Doran, I., Sonoyama, T., Collet, T. H., Keogh, J. M., Henning, E., et al. (2020). Leptin-mediated changes in the human metabolome. *J. Clin. Endocrinol. Metab.* 105 (8), 2541–2552. doi:10.1210/clinem/dgaa251

Le Collen, L., Delemer, B., Poitou, C., Vaxillaire, M., Toussaint, B., Dechaume, A., et al. (2023). Heterozygous pathogenic variants in POMC are not responsible for monogenic obesity: implication for MC4R agonist use. *Genet. Med.* 25 (7), 100857. doi:10.1016/j.gim.2023.100857

Lee, C. F., Chen, H. Y., and Lee, J. (2019). "Multivariate analysis: discriminant analysis and factor analysis," in *Financial econometrics, mathematics and statistics* (New York, NY: Springer), 439–457.

Löfstedt, T., and Trygg, J. (2011). OnPLS-a novel multiblock method for the modelling of predictive and orthogonal variation. *J. Chemom.* 25 (8), 441–455. doi:10.1002/cem.1388

Maltais-Payette, I., Boulet, M. M., Prehn, C., Adamski, J., and Tchernof, A. (2018). Circulating glutamate concentration as a biomarker of visceral obesity and associated metabolic alterations. *Nutr. Metab.* 15 (1), 78. doi:10.1186/s12986-018-0316-5

Marabita, F., James, T., Karhu, A., Virtanen, H., Kettunen, K., Stenlund, H., et al. (2022). Multiomics and digital monitoring during lifestyle changes reveal independent dimensions of human biology and health. *Cell Syst.* 13 (3), 241–255.e7. doi:10.1016/j.cels.2021.11.001

Martos-Moreno, G., Martínez-Villanueva, J., González-Leal, R., Chowen, J. A., and Argente, J. (2019). Sex, puberty, and ethnicity have a strong influence on growth and metabolic comorbidities in children and adolescents with obesity: report on 1300 patients (the Madrid Cohort). *Pediatr. Obes.* 14 (12), e12565. doi:10.1111/ijpo.12565

Martos-Moreno, G. Á., Martínez-Villanueva, J., González-Leal, R., Barrios, V., Sirvent, S., Hawkins, F., et al. (2020). Ethnicity strongly influences body fat distribution determining serum adipokine profile and metabolic derangement in childhood obesity. *Front. Pediatr.* 8, 8. doi:10.3389/fped.2020.551103

Martos-Moreno, G. Á., Martínez-Villanueva Fernández, J., Frías-Herrero, A., Martín-Rivada Á, and Argente, J. (2021). Conservative treatment for childhood and adolescent obesity: real world follow-up profiling and clinical evolution in 1300 patients. *Nutrients* 13 (11), 3847. doi:10.3390/nu13113847

Martos-Moreno, G. Á., Mastrangelo, A., Barrios, V., García, A., Chowen, J. A., Rupérez, F. J., et al. (2017). Metabolomics allows the discrimination of the pathophysiological relevance of hyperinsulinism in obese prepubertal children. *Int. J. Obes.* 41 (10), 1473–1480. doi:10.1038/ijo.2017.137

Mastrangelo, A., Martos-Moreno, G. Á., García, A., Barrios, V., Rupérez, F. J., Chowen, J. A., et al. (2016). Insulin resistance in prepubertal obese children correlates with sex-dependent early onset metabolomic alterations. *Int. J. Obes.* 40 (10), 1494–1502. doi:10.1038/ijo.2016.92

Mccormack, S. E., Shaham, O., Mccarthy, M. A., Deik, A. A., Wang, T. J., Gerszten, R. E., et al. (2013). Circulating branched-chain amino acid concentrations are associated with obesity and future insulin resistance in children and adolescents. *Pediatr. Obes.* 8 (1), 52–61. doi:10.1111/j.2047-6310.2012.00087.x

Meng, C., Helm, D., Frejno, M., and Kuster, B. (2016). moCluster: identifying joint patterns across multiple omics data sets. *J. Proteome Res.* 15 (3), 755–765. doi:10.1021/acs.jproteome.5b00824

Michaliszyn, S. F., Sjaarda, L. A., Mihalik, S. J., Lee, S. J., Bacha, F., Chace, D. H., et al. (2012). Metabolomic profiling of amino acids and β-cell function relative to insulin sensitivity in youth. *J. Clin. Endocrinol. Metabolism* 97 (11), 2119–2124. doi:10.1210/jc.2012-2170

Mo, Q., Shen, R., Guo, C., Vannucci, M., Chan, K. S., and Hilsenbeck, S. G. (2018). A fully Bayesian latent variable model for integrative clustering analysis of multi-type omics data. *Biostatistics* 19 (1), 71–86. doi:10.1093/biostatistics/kxx017

Mo, Q., Wang, S., Seshan, V. E., Olshen, A. B., Schultz, N., Sander, C., et al. (2013). Pattern discovery and cancer gene identification in integrated cancer genomic data. *Proc. Natl. Acad. Sci.* 110 (11), 4245–4250. doi:10.1073/pnas.1208949110

Naz, S., Calderón, Á. A., García, A., Gallafrio, J., Mestre, R. T., González, E. G., et al. (2015). Unveiling differences between patients with acute coronary syndrome with and without ST elevation through fingerprinting with CE-MS and HILIC-MS targeted analysis. *Electrophoresis* 36 (18), 2303–2313. doi:10.1002/elps.201500169

Nguyen, H., Shrestha, S., Draghici, S., and Nguyen, T. (2019). PINSPlus: a tool for tumor subtype discovery in integrated genomic data. *Bioinformatics* 35 (16), 2843–2846. doi:10.1093/bioinformatics/bty1049

Nguyen, T., Tagett, R., Diaz, D., and Draghici, S. (2017). A novel approach for data integration and disease subtyping. *Genome Res.* 27 (12), 2025–2039. doi:10.1101/gr.215129.116

Ni, Z., Angelidou, G., Lange, M., Hoffmann, R., and Fedorova, M. (2017). LipidHunter identifies phospholipids by high-throughput processing of LC-MS and shotgun lipidomics datasets. *Anal. Chem.* 89 (17), 8800–8807. doi:10.1021/acs.analchem.7b01126

Palmnäs, M., Brunius, C., Shi, L., Rostgaard-Hansen, A., Torres, N. E., González-Domínguez, R., et al. (2020). Perspective: metabotyping - A potential personalized nutrition strategy for precision prevention of cardiometabolic disease. *Adv. Nutr.* 11, 524–532. Oxford University Press. doi:10.1093/advances/nmz121

Park, J., Barahona-Torres, N., Jang, S., Mok, K. Y., Kim, H. J., Han, S., et al. (2022). Multi-omics-based autophagy-related untypical subtypes in patients with cerebral amyloid pathology. *Adv. Sci.* 9 (23), e2201212. doi:10.1002/advs.202201212

Pellegrino, R. M., Di Veroli, A., Valeri, A., Goracci, L., and Cruciani, G. (2014). LC/MS lipid profiling from human serum: a new method for global lipid extraction. *Anal. Bioanal. Chem.* 406 (30), 7937–7948. doi:10.1007/s00216-014-8255-0

Pietiläinen, K. H., Sysi-Aho, M., Rissanen, A., Seppänen-Laakso, T., Yki-Järvinen, H., Kaprio, J., et al. (2007). Acquired obesity is associated with changes in the serum lipidomic profile independent of genetic effects-a monozygotic twin study. *PLoS One* 2 (2), e218. doi:10.1371/journal.pone.0000218

Rappoport, N., and Shamir, R. (2018). Multi-omic and multi-view clustering algorithms: review and cancer benchmark. *Nucleic Acids Res.* 46 (20), 10546–10562. doi:10.1093/nar/gky889

Rauschert, S., Kirchberg, F. F., Marchioro, L., Koletzko, B., Hellmuth, C., and Uhl, O. (2017). Early programming of obesity throughout the life course: a metabolomics perspective. *Ann. Nutr. Metab.* 70 (3), 201–209. doi:10.1159/000459635

Rauschert, S., Uhl, O., Koletzko, B., Kirchberg, F., Mori, T. A., Huang, R. C., et al. (2016). Lipidomics reveals associations of phospholipids with obesity and insulin resistance in young adults. *J. Clin. Endocrinol. Metab.* 101 (3), 871–879. doi:10.1210/jc.2015-3525

Rupérez, F. J., Martos-Moreno, G. Á., Chamoso-Sánchez, D., Barbas, C., and Argente, J. (2020). Insulin resistance in obese children: what can metabolomics and adipokine modelling contribute? *Nutrients* 12 (11), 3310. doi:10.3390/nu12113310

Sanz-Fernandez, M. V., Torres-Rovira, L., Pesantez-Pacheco, J. L., Vazquez-Gomez, M., Garcia-Contreras, C., Astiz, S., et al. (2020). A cross-sectional study of obesity effects on the metabolomic profile of a leptin-resistant swine model. *Metabolites* 10 (3), 89. doi:10.3390/metabo10030089

Serra-Juhé, C., Martos-Moreno, G. Á., Bou de Pieri, F., Flores, R., González, J. R., Rodríguez-Santiago, B., et al. (2017). Novel genes involved in severe early-onset obesity revealed by rare copy number and sequence variants. *PLoS Genet.* 13 (5), e1006657. doi:10.1371/journal.pgen.1006657

Shen, R., Olshen, A. B., and Ladanyi, M. (2009). Integrative clustering of multiple genomic data types using a joint latent variable model with application to breast and lung cancer subtype analysis. *Bioinformatics* 25 (22), 2906–2912. doi:10.1093/bioinformatics/btp543

Sullivan, A., Gibney, M. J., Connor, A. O., Mion, B., Kaluskar, S., Cashman, K. D., et al. (2011). Biochemical and metabolomic phenotyping in the identification of a vitamin D responsive metabotype for markers of the metabolic syndrome. *Mol. Nutr. Food Res.* 55 (5), 679–690. doi:10.1002/mnfr.201000458

Suzuki, Y., Kido, J., Matsumoto, S., Shimizu, K., and Nakamura, K. (2019). Associations among amino acid, lipid, and glucose metabolic profiles in childhood obesity. *BMC Pediatr.* 19 (1), 273. doi:10.1186/s12887-019-1647-8

Tanabe, K., Hayashi, C., Katahira, T., Sasaki, K., and Igami, K. (2021). Multiblock metabolomics: an approach to elucidate whole-body metabolism with multiblock principal component analysis. *Comput. Struct. Biotechnol. J.* 19, 1956–1965. doi:10.1016/j.csbj.2021.04.015

Tini, G., Marchetti, L., Priami, C., and Scott-Boyer, M. P. (2019). Multi-omics integration—a comparison of unsupervised clustering methodologies. *Brief. Bioinform* 20 (4), 1269–1279. doi:10.1093/bib/bbx167

Trang, K., and Grant, S. F. A. (2023). "Genetics and epigenetics in the obesity phenotyping scenario," in *Reviews in endocrine and metabolic disorders* (Springer).

Tsugawa, H., Ikeda, K., Takahashi, M., Satoh, A., Mori, Y., Uchino, H., et al. (2020). A lipidome atlas in MS-DIAL 4. *Nat. Biotechnol.* 38 (10), 1159–1163. doi:10.1038/s41587-020-0531-2

Wahl, S., Yu, Z., Kleber, M., Singmann, P., Holzapfel, C., He, Y., et al. (2012). Childhood obesity is associated with changes in the serum metabolite profile. *Obes. Facts* 5 (5), 660–670. doi:10.1159/000343204

Waldram, A., Holmes, E., Wang, Y., Rantalainen, M., Wilson, I. D., Tuohy, K. M., et al. (2009). Top-down systems biology modeling of host metabotype-microbiome associations in obese rodents. *J. Proteome Res.* 8 (5), 2361–2375. doi:10.1021/pr8009885

Wang, B., Zhu, J., Pierson, E., Ramazzotti, D., and Batzoglou, S. (2017). Visualization and analysis of single-cell RNA-seq data by kernel-based similarity learning. *Nat. Methods* 14 (4), 414–416. doi:10.1038/nmeth.4207

Wang, T. J., Larson, M. G., Vasan, R. S., Cheng, S., Rhee, E. P., McCabe, E., et al. (2011). Metabolite profiles and the risk of developing diabetes. *Nat. Med.* 17 (4), 448–453. doi:10.1038/nm.2307

Wan Mohd Zin, R. M., Jalaludin, M. Y., Yahya, A., Nur Zati Iwani, A. K., Md Zain, F., Hong, J. Y. H., et al. (2022). Prevalence and clinical characteristics of metabolically healthy obese versus metabolically unhealthy obese school children. *Front. Endocrinol.* 13, 13. doi:10.3389/fendo.2022.971202

Westerhuis, J. A., Kourti, T., and Macgregor, J. F. (1998). *Analysis of multiblock and hierarchical PCA and pls models*.

Wu, D., Wang, D., Zhang, M. Q., and Gu, J. (2015). Fast dimension reduction and integrative clustering of multi-omics data using low-rank approximation: application to cancer molecular classification. *BMC Genomics* 16 (1), 1022. doi:10.1186/s12864-015-2223-8

Yan, J., Winter, L. B., Burns-Whitmore, B., Vermeylen, F., and Caudill, M. A. (2012). Plasma choline metabolites associate with metabolic stress among young overweight men in a genotype-specific manner. *Nutr. Diabetes* 2 (10), e49. doi:10.1038/nutd.2012.23

Zhang, X., Zhou, Z., Xu, H., and Liu, C. (2022). Integrative clustering methods for multi-omics data. *WIREs Comput. Stat.* 14 (3), e1553. doi:10.1002/wics.1553

Zhao, C., Mao, J., Ai, J., Shenwu, M., Shi, T., Zhang, D., et al. (2013). Integrated lipidomics and transcriptomic analysis of peripheral blood reveals significantly enriched pathways in type 2 diabetes mellitus. *BMC Med. Genomics* 6 (S1), S12. doi:10.1186/1755-8794-6-S1-S12

frontiers | Frontiers in Molecular Biosciences

TYPE Original Research
PUBLISHED 15 January 2024
DOI 10.3389/fmolb.2023.1279645



OPEN ACCESS

EDITED BY
Víctor González-Ruiz,
University of Geneva, Switzerland

REVIEWED BY
Tania C. B. Santos,
Weizmann Institute of Science, Israel
Alessia Ferrarini,
Spanish National Centre for Cardiovascular Research, Spain
Isabel Meister,
University of Geneva, Switzerland

*CORRESPONDENCE
Michal Ciborowski,
michal.ciborowski@umb.edu.pl

RECEIVED 18 August 2023
ACCEPTED 20 December 2023
PUBLISHED 15 January 2024

CITATION
Godzien J, Lopez-Lopez A, Sieminska J, Jablonowski K, Pietrowska K, Kisluk J, Mojsak M, Dzieciol-Anikiej Z, Barbas C, Reszec J, Kozlowski M, Moniuszko M, Kretowski A, Niklinski J and Ciborowski M (2024), Exploration of oxidized phosphocholine profile in non-small-cell lung cancer.
*Front. Mol. Biosci.* 10:1279645.
doi: 10.3389/fmolb.2023.1279645



# Exploration of oxidized phosphocholine profile in non-small-cell lung cancer

Joanna Godzien[1], Angeles Lopez-Lopez[2], Julia Sieminska[1], Kacper Jablonowski[1], Karolina Pietrowska[1], Joanna Kisluk[3], Malgorzata Mojsak[4], Zofia Dzieciol-Anikiej[5], Coral Barbas[2], Joanna Reszec[6], Miroslaw Kozlowski[7], Marcin Moniuszko[8], Adam Kretowski[1], Jacek Niklinski[3] and Michal Ciborowski[1]*

[1]Metabolomics Laboratory, Clinical Research Centre, Medical University of Bialystok, Bialystok, Poland, [2]Centro de Metabolómica y Bioanálisis (CEMBIO), Facultad de Farmacia, Universidad San Pablo-CEU, CEU Universities, Boadilla del Monte, Spain, [3]Department of Clinical Molecular Biology, Medical University of Bialystok, Bialystok, Poland, [4]Independent Laboratory of Molecular Imaging, Medical University of Bialystok, Bialystok, Poland, [5]Department of Rehabilitation, Medical University of Bialystok, Bialystok, Poland, [6]Department of Medical Pathomorphology, Medical University of Bialystok, Bialystok, Poland, [7]Department of Thoracic Surgery, Medical University of Bialystok, Bialystok, Poland, [8]Department of Regenerative Medicine and Immune Regulation, Medical University of Bialystok, Bialystok, Poland

**Introduction:** Lung cancer is one of the most frequently studied types of cancer and represents the most common and lethal neoplasm. Our previous research on non-small cell lung cancer (NSCLC) has revealed deep lipid profile reprogramming and redox status disruption in cancer patients. Lung cell membranes are rich in phospholipids that are susceptible to oxidation, leading to the formation of bioactive oxidized phosphatidylcholines (oxPCs). Persistent and elevated levels of oxPCs have been shown to induce chronic inflammation, leading to detrimental effects. However, recent reports suggest that certain oxPCs possess anti-inflammatory, pro-survival, and endothelial barrier-protective properties. Thus, we aimed to measure the levels of oxPCs in NSCLC patients and investigate their potential role in lung cancer.

**Methods:** To explore the oxPCs profiles in lung cancer, we performed in-depth, multi-level metabolomic analyses of nearly 350 plasma and lung tissue samples from 200 patients with NSCLC, including adenocarcinoma (ADC) and squamous cell carcinoma (SCC), the two most prevalent NSCLC subtypes and COPD patients as a control group. First, we performed oxPC profiling of plasma samples. Second, we analyzed tumor and non-cancerous lung tissues collected during the surgical removal of NSCLC tumors. Because of tumor tissue heterogeneity, subsequent analyses covered the surrounding healthy tissue and peripheral and central tumors. To assess whether the observed phenotypic changes in the patients were associated with measured oxPC levels, metabolomics data were augmented with data from medical records.

**Results:** We observed a predominance of long-chain oxPCs in plasma samples and of short-chain oxPCs in tissue samples from patients with NSCLC. The highest concentration of oxPCs was observed in the central tumor region. ADC patients showed higher levels of oxPCs compared to the control group, than patients with SCC.

**Conclusion:** The detrimental effects associated with the accumulation of short-chain oxPCs suggest that these molecules may have greater therapeutic utility than diagnostic value, especially given that elevated oxPC levels are a hallmark of multiple types of cancer.

KEYWORDS

NSCLC, lung cancer, oxPC, oxidized phospholipids, epilipidomics

## 1 Introduction

Redox balance is one of the most important factors influencing the health status of an organism. It is crucial for proper cellular signaling and communication and is thus essential for the healthy functioning of living organisms. Disruptions in this balance result in an excess of reactive oxygen species (ROS), reducing the antioxidant potential of the cell and causing oxidative stress.

The idea of evaluating the health of an organism based on oxidative stress levels is not new. Among different oxidation products, lipids play an important role, especially since lipid peroxidation is a damaging process that can contribute to the development and progression of various diseases. Lipid oxidation has been deeply investigated not only through stable end-products, such as 4-hydroxynonenal (4-HNE) and malondialdehyde (MDA) (Zabłocka-Słowińska et al., 2019) but currently also through early oxidation products, including oxidized phospholipids (Solati et al., 2021). Oxidized phosphatidylcholines (oxPCs) are among the most thoroughly researched oxidized phospholipids and comprise a broad group of bioactive molecules that differ in structure and function. OxPCs may exist as long-chain solely (LCh-oxPCs) or as short-chain forms (SCh-oxPCs) produced by the oxidative fragmentation of esterified polyunsaturated fatty acids (PUFAs); and cyclized oxPCs (Cyc-oxPCs) form via cyclization of peroxyl radicals (Davies and Guo, 2014). LCh-oxPCs have oxidized fatty acid, usually in the *sn*-2 position of glycerol-phospholipid, containing oxidation-derived functional groups such as hydroxy, hydroperoxy, epoxy or keto. SCh-oxPCs have truncated fatty acid, usually in the *sn*-2 position of glycerol-phospholipid, containing a terminal aldehyde or carboxylic acid (Gil de la Fuente et al., 2018; Villaseñor et al., 2021).

Historically, oxPCs have been considered toxic oxidation by-products; however, current evidence acknowledges them as essential signaling molecules with various, and often pleiotropic, functions (Bochkov et al., 2017). Researchers are investigating these molecules through untargeted approaches (Gil de la Fuente et al., 2018), targeted methods (Solati et al., 2021), or highly sophisticated mechanistic and functional studies (Slatter et al., 2018). Moreover, over the last decade, multiple highly advanced computational solutions were developed for redox lipidomics, with a particular focus on the robust identification of epilipids (Ni et al., 2019).

oxPCs are associated with cardiovascular diseases (Stamenkovic et al., 2017; Paynter et al., 2018), neurodegenerative diseases (Tyurina et al., 2015; Okuzumi et al., 2019), diabetes (Chen et al., 2018; Godzien et al., 2019; Nie et al., 2019), cancer (Reuter et al., 2010; Mantovani et al., 2012; Ingram et al., 2021), and non-alcoholic steatohepatitis (Ikura et al., 2006), all of which can be linked to oxidative stress and chronic inflammation. As reported previously, oxPCs may induce either beneficial or detrimental effects in the lungs (Ke et al., 2019; Karki and Birukov, 2020). Their impact may depend upon their structure and concentration; LCh-oxPCs exhibit a protective effect, and SCh-oxPCs are linked with disruptive effects. Moreover, lower levels of oxPCs protect the endothelial barrier, whereas high concentrations of the same species induce disruptive effects (Karki and Birukov, 2020). The beneficial effects of oxPCs are related to the protective effects on the endothelial barrier (through activation of Rac1, inhibition of Rho, activation of S1P1, or enhanced assembly of EC junctions) and anti-inflammatory effects (through inhibition of TLRs signaling, inhibition of NF-κB activation, increase in cAMP levels, activation of eNOS, Nrf2, HO-1 or LXA4 production) while detrimental effects are linked to the pro-inflammatory effects (through increased levels of MCP1, IL-6, IL-8, MIP-1, CXCL3, STAT3, NLRP3, TLR4, TLR2 CD36, and PRR activation), induction of coagulation (through increased expression of TF and decreased expression of TFPI and thrombomodulin), and increasing the endothelial permeability (via activation of Src kinase, ROS production, phosphorylation of VE-cadherin and EC junctional assembly disruption).

Inflammation and oxidative stress are heavily associated with two major health concerns worldwide: lung cancer and chronic obstructive pulmonary disease (COPD). Lung cancer is the most lethal type of cancer, taking 1.8 million lives annually (Sung et al., 2021). Non-small cell lung cancer (NSCLC) is the most prevalent type of lung cancer, accounting for 85%–90% of all cases (Duma et al., 2019). NSCLC is characterized by high malignancy, strong invasiveness, and easy metastasis, which, together with poor diagnosis and lack of effective treatment, result in high mortality. Therefore, early diagnosis, accurate clinical staging, and subtype determination are important to determine effective treatment plans, prolong survival, and improve the quality of life.

COPD and lung cancer are caused by cigarette smoking, and there is increasing evidence linking the two diseases beyond a common etiology. Smokers displaying airflow obstruction face a considerably elevated risk of lung cancer, with up to a fivefold increase compared to individuals with normal lung function. As pointed out by Durham and Adcock, the high prevalence of lung cancer in COPD suggests that there may be common mechanisms, such as inflammation, oxidative stress, premature aging in the lungs, genetic predispositions to either disease or common pathogenic factors, such as growth factors, activation of intracellular pathways or epigenetics (Durham and Adcock, 2015). Therefore, trying to obtain the oxPCs signature specific to lung cancer, as opposed to inflammation- and oxidative-stress-derived lung diseases, we decided to use COPD patients as our control group instead of healthy volunteers.

For many years, carcinogenesis and cancer proliferation have been mainly linked to disruptions in carbohydrate metabolism (Martinez-Outschoorn et al., 2017). However, over the last decade, researchers have revealed alterations in lipid metabolism and profound lipid reprogramming in malignant cells (Beloribi-Djefaflia et al., 2016; Gong et al., 2022).

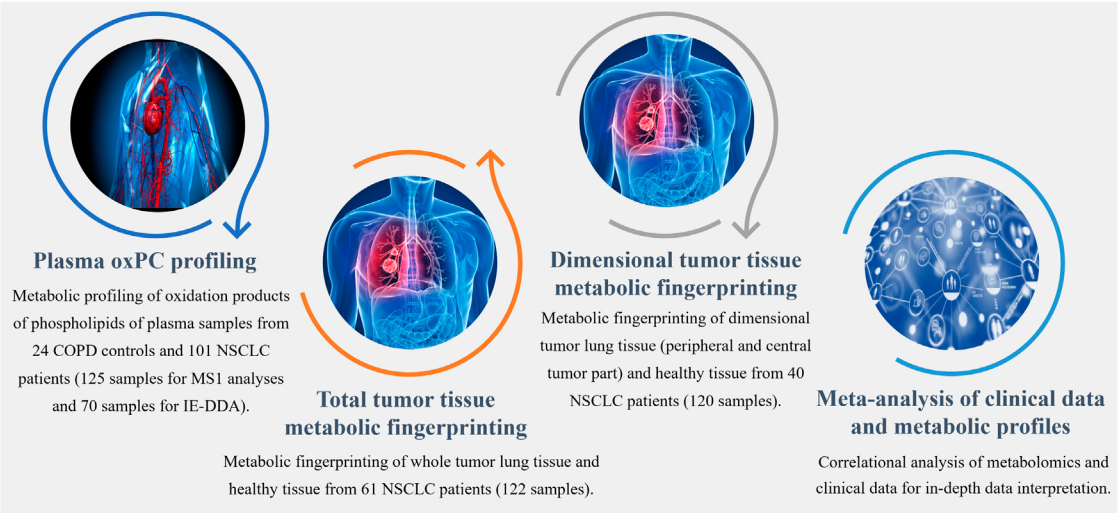


FIGURE 1
Workflow summarizing metabolomics analyses performed to explore the differential profiles of the oxPCs in COPD controls and NSCLC patients.

Elevated oxidative stress has been reported in patients with lung cancer, but the exact mechanisms underlying this association are not fully understood (Mousapasandi et al., 2021). Previous reports have suggested that enhanced oxidative stress in patients with NSCLC occurs through either elevated formation of oxidation products or inactivation of antioxidant mechanisms (Sunnetcioglu et al., 2016). The overall redox status of NSCLC patients has already been investigated by other groups. However, in majority of cases, these studies have focused on end oxidation products, such as reactive aldehydes (Gęgotek et al., 2016; Karki and Birukov, 2020). Given the increased oxidative stress and elevated levels of phospholipids observed in NSCLC patients, it is reasonable to expect elevated levels of oxPCs. Moreover, the structure-related properties of different oxPCs highlight the importance of exploring distinct oxPC species. Therefore, the aim of this study was to determine the levels of oxPCs in NSCLC patients, including those with adenocarcinoma (ADC) and squamous cell carcinoma (SCC), the two most prevalent NSCLC subtypes, and investigate their potential role in the development of lung cancer.

# 2 Materials and methods

## 2.1 Chemicals and reagents

Ultrapure water was used to prepare all aqueous solutions and was obtained using a Milli-Q Integral 3 system (MilliporeSigma, Burlington, MA, United States). Zomepirac sodium salt, formic acid, LC-MS-grade methanol, acetonitrile, and LC-grade ethanol were purchased from Sigma-Aldrich (St. Louis, MO, United States).

## 2.2 Cohort

The study was approved by the Ethics Committee of the Medical University of Bialystok (R-I-003/262/2004, R-I-002/296/2018, and APK 002 5 2021) and was performed in accordance with the Declaration of Helsinki. Before sample collection, written informed consent for specimen collection was obtained from all participants. Samples were obtained from patients undergoing surgical treatment for primary NSCLC at the Department of Thoracic Surgery of the Clinical Hospital of the Medical University of Bialystok in Bialystok in Poland. Three distinct cohorts of patients were included (Figure 1), yielding 125 plasma and 242 tissue samples. Plasma samples were collected from 101 patients with NSCLC (41 ADC and 60 SCC patients) and 24 COPD controls. Control COPD group consisted of patients with an increased risk of NSCLC lung cancer diagnosed with chronic lung disease, chronic cough, wheezing or shortness of breath showing no focal lesions in lungs X-ray.

We collected tumor tissue and adjacent non-malignant control tissue from 61 patients with NSCLC (25 ADC and 36 SCC) for total tumor tissue metabolic fingerprinting, obtaining 122 samples. For dimensional tumor tissue metabolic fingerprinting, three pieces of tissues from central and peripheral tumor regions and adjacent non-malignant control tissues were collected from 40 NSCLC patients (20 ADC and 20 SCC) resulting in 120 samples. Clinicopathological characteristics, such as age, sex, smoking status, body mass index (BMI), tumor grade, lymph node metastases, histological type, clinical stage, and survival data were available. The basic clinical parameters describing each of the three cohorts enrolled in this study are summarized in Table 1.

Whole blood was collected in 9 mL vacuum system tubes with $K_2$EDTA as an anticoagulant. After gentle mixing, the plasma was separated by centrifugation at 1,300 × *g* for 20 min at room temperature. Plasma fractions (0.5 mL each) were collected in Eppendorf tubes and stored at −80°C until analysis.

Tissue samples were histologically reviewed and classified. After lung tumor resection, the whole specimen was examined macroscopically by a pathologist following previously published methods (Ciereszko et al., 2022) to determine the exact tumor localization, identify macroscopic tumor residuals, search for macroscopic infiltration of pulmonary pleura, and evaluate

10.3389/fmolb.2023.1279645

TABLE 1 Basic clinical parameters of patients in three cohorts.

| Plasma samples: oxPC profiling | | | | |
|---|---|---|---|---|
| Patient characteristics | NSCLC (ADC + SCC) *n* = 101 | ADC *n* = 41 | SCC *n* = 60 | COPD controls *n* = 24 |
| Age [years] median (Q1–Q3) | 63.0 (58.0–69.0) | 62.0 (58.0–68.0) | 63.5 (58.8–69.0) | 63.0 (52.8–69.0) |
| BMI median (Q1–Q3) | 25.47 (23.62–27.76) | 25.99 (24.17–28.09) | 25.39 (23.39–27.23) | 24.56 (21.78–27.82) |
| Gender [F/M] | 29/72 | 15/26 | 14/46 | 10/14 |
| pTNM stage | | | | |
| | *n* (%) | *n* (%) | *n* (%) | |
| IA | 16 (16%) | 10 (24%) | 6 (10%) | |
| IB | 10 (10%) | 6 (15%) | 4 (7%) | |
| IIA | 24 (24%) | 8 (20%) | 16 (27%) | |
| IIB | 33 (33%) | 9 (22%) | 24 (40%) | |
| IIIA | 18 (18%) | 8 (20%) | 10 (17%) | |
| Tissue samples: total tumor tissue metabolic fingerprinting | | | | |
| Patient characteristics | NSCLC (ADC + SCC) *n* = 61 | ADC *n* = 25 | SCC *n* = 36 | |
| Age [years] median (Q1–Q3) | 63.0 (56.0–69.0) | 62.0 (55.0–69.0) | 63.5 (57.5–69.0) | |
| BMI Median (Q1–Q3) | 24.93 (23.41–26.09) | 25.00 (23.53–26.37) | 24.53 (23.39–25.39) | |
| Gender [F/M] | 13/48 | 6/19 | 7/29 | |
| pTNM stage | | | | |
| | *n* (%) | *n* (%) | *n* (%) | |
| IA | 0 (0%) | 0 (0%) | 0 (0%) | |
| IB | 0 (0%) | 0 (0%) | 0 (0%) | |
| IIA | 21 (34%) | 9 (36%) | 12 (33%) | |
| IIB | 20 (33%) | 8 (32%) | 12 (33%) | |
| IIIA | 20 (33%) | 8 (32%) | 12 (33%) | |
| Tissue samples: dimensional tumor tissue metabolic fingerprinting | | | | |
| Patient characteristics | NSCLC (ADC + SCC) *n* = 40 | ADC *n* = 20 | SCC *n* = 20 | |
| Age [years] median (Q1–Q3) | 65.5 (59.0–69.0) | 67.5 (59.8–69.5) | 63 (59.0–69.0) | |
| BMI median (Q1–Q3) | 26.565 (22.51–28.23) | 27.04 (23.27–29.38) | 26.255 (22.36–28.02) | |
| Gender [F/M] | 20/20 | 10/10 | 10/10 | |
| pTNM stage | | | | |
| | *n* (%) | *n* (%) | *n* (%) | |
| IA | 1 (3%) | 1 (5%) | 0 (0%) | |
| IB | 10 (27%) | 6 (30%) | 4 (24%) | |
| IIA | 2 (5%) | 0 (0%) | 2 (12%) | |
| IIB | 9 (24%) | 3 (15%) | 6 (35%) | |
| IIIA | 15 (41%) | 10 (50%) | 5 (29%) | |

necrosis in the tumor center. The pathologist cut the tissue samples into tumor center and periphery subsamples. Moreover, the pathologist determined the possibility of collecting adjacent pulmonary tissue (referred to here as normal tissue); if the distance from the tumor border was greater than 2 cm, the pathologist took samples of adjacent tissue. Next, nurses from the biobank placed the tissue samples alternately into cryo-tubes containing the vapor phase of liquid nitrogen (fresh frozen samples) and into tubes with 10% buffered formalin (formalin-fixed samples). In this study we used fresh frozen samples.

Cancer stages were determined according to pathological tumor-node-metastasis (pTNM) staging. All tissue samples were frozen and stored at −80°C until analysis. Sample collection, quenching, and storage were performed according to the approved biobanking standards (Niklinski et al., 2017).

## 2.3 Clinical parameters

Serum C-reactive protein (CRP) and white blood cell (WBC) levels were determined the day before the surgical operation for tumor removal, together with other canonical biochemical parameters, in the diagnostic laboratory at the Clinical Hospital of the Medical University of Bialystok.

Metabolic tumor volume (MTV) and standardized uptake volume (SUV) were determined using simultaneous positron emission tomography-magnetic resonance imaging (PET/MRI) examinations performed using a Biograph mMR scanner (Siemens, Munich, Germany). Whole-body acquisition (from the top of the head to the mid-thigh) was begun 60 ± 10 min after the intravenous administration of 18-F-fluorodeoxyglucose at an activity of 4 MBq/kg body weight. Whole-body MRI was performed with T1- and T2-weighted images taken in the transverse plane; PET/MRI of the chest was performed using T1_vibe, T1_vibe_fatsat, T2_haste sequences, including breath-hold images were taken in the transverse, coronal, and sagittal planes and a magnetic resonance contrast agent was used in the absence of contraindications. The images were assessed by a nuclear medicine specialist and a radiologist with at least 5 years of experience. Radiotracer biodistribution was visually assessed, and semi-quantitative analysis was carried out using the metabolic activity index of lesions (SUVmax/lbm- SUV/lean body mass), and MTV was measured using a threshold-based method with 40% SUVmax.

## 2.4 Plasma and tissue sample preparation

Plasma samples were prepared using a previously described method (Daniluk et al., 2019). On the day of analysis, the samples were thawed on ice. For protein precipitation and metabolite extraction, one volume of plasma sample was mixed with three volumes of ice-cold methanol/ethanol (1:1) containing 1 ppm of zomepirac, used as an internal standard (IS). After extraction, the samples were stored on ice for 10 min and centrifuged at 21,000 × *g* for 20 min at 4°C. The supernatant was filtered through a 0.22 µm nylon filter (Thermo Fisher Scientific, Waltham, MA, United States).

Tissue samples were prepared according to a previously described method (Ciborowski et al., 2017). On the day of analysis, the samples were thawed on ice. Ten milligrams of lung tissue were placed in an Eppendorf tube with two stainless steel beads (5 mm) and 200 µL of ice-cold 50% methanol. Samples were homogenized for 8 min at 30 Hz using a TissueLyser LT instrument (Qiagen, Hilden, Germany). After homogenization, the beads were removed, and 200 µL of ice-cold acetonitrile containing 1 ppm of zomepirac (internal standard) was added to the sample. Metabolites were extracted by vortexing the samples for 1 h. After extraction, the samples were centrifuged at 21,000 × *g* for 20 min at 20°C. The supernatant was filtered through a 0.22 µm nylon filter. The extraction blank was prepared following the same procedure as the biological samples but without tissue, and was analyzed together with biological samples.

Quality control samples (QCs) were prepared by mixing equal volumes of raw plasma and equal volumes of metabolite extract of tissue samples. QCs were treated like the rest of the samples and injected at the beginning of the batch (10 injections) to equilibrate the system and after every ten samples to monitor the stability of the measurement (Godzien et al., 2014).

## 2.5 Analytical setup

Three types of analysis were performed, covering plasma oxPC profiling, total tumor tissue metabolic fingerprinting and dimensional tumor tissue metabolic fingerprinting. However, recoded data was processed in a targeted manner, retrieving from it solely information about oxPCs.

Plasma oxPC profiling was performed using a 6546 iFunnel ESI-QTOF (Agilent Technologies, Santa Clara, CA, United States) coupled with a 1290 Infinity UHPLC system (Agilent Technologies) with a degasser, quaternary pump, and thermostatted autosampler.

Tissue metabolic fingerprinting was performed using a 6545 iFunnel ESI-QTOF instrument (Agilent Technologies, Santa Clara, CA, United States) coupled with the 1290 Infinity UHPLC system (Agilent Technologies) with a degasser, binary pump, and thermostatted autosampler.

Plasma and tissue samples were analyzed in both polarity modes. During all analyses, two reference compounds were used: *m/z* 121.0509 (protonated purine) and *m/z* 922.0098 (protonated hexakis (1H,1H,3H-tetrafluoropropoxy)phosphazine [HP-921]) for the positive ionization mode, and *m/z* 112.9856 (proton abstracted trifluoroacetic acid anion) and *m/z* 966.0007 (formate adduct of HP-921) for the negative ionization mode. These masses were continuously infused into the system to allow internal constant mass correction during data acquisition.

All datasets were acquired in both polarity modes. However, data analysis revealed that more abundant and, therefore, more reproducible signals of oxPCs were obtained in the positive ion mode. The negative-ion mode provided more detailed structural information. Consequently, information from the positive ion mode was used for statistical analyses, whereas information acquired in the negative ion mode was used for lipid annotation.

## 2.6 Plasma oxPC profiling

Four microliters of each sample were injected into a thermostatted Zorbax Extend C18 column (RRHT 2.1 × 50 mm, 1.8 µm; Agilent Technologies) at 60°C. The flow rate was 0.6 mL/min for aqueous phase A (water with 0.1% formic acid) and organic phase B (acetonitrile with 0.1% formic acid). The chromatographic gradient started at 50% phase B, then increased to 80% (1–6 min) and 100% (6–8 min). Finally, the system was re-equilibrated by reverting the phase composition to initial conditions (50% phase B) in 0.5 min, and this was maintained from 8.5 to 10 min. The mass spectrometer was operated in full-scan mode (MS1). Data were acquired at *m/z* values ranging from 50 to 1,000 at a scan rate of 1.0 scan per second. The

drying gas flow rate was 12 L/min, the temperature was 250°C, and the gas nebulizer pressure was set to 52 psig. The nozzle voltage was 1,000 V, and the capillary voltages were 3,000 and 4,000 V in the positive and negative ion modes, respectively.

All samples were analyzed in scan mode (MS1) for both polarities. Then, a subset of 70 samples was analyzed in the negative ion mode using iterative exclusion data-dependent analysis (IE-DDA). The precursor ions were fragmented using ramped collision energy adjusted for each molecule according to its *m/z* value. The first injection was performed as a conventional data-dependent analysis where the top three most abundant precursors were selected for fragmentation considering the active exclusion lists. During the subsequent injection, precursors selected for MS/MS fragmentation in the previous injection were excluded on a rolling basis with a mass error tolerance and 0.5 min retention time tolerance. Five iterative MS/MS runs were performed for each sample, resulting in 350 measurements.

## 2.7 Lung tissue metabolic fingerprinting

One microliter of the extracted sample was injected into a Zorbax Eclipse Plus C8 column (RRHD 2 × 150 mm, 1.8 µm; Agilent Technologies) at 60°C. The flow rate was 0.6 mL/min for aqueous phase A (water with 0.1% formic acid) and organic phase B (acetonitrile with 0.1% formic acid). The gradient started at 25% phase B and increased to 95% phase B over 14 min. This was maintained for 1 min, and then the gradient returned to starting conditions (25% phase B) in 0.1 min and maintained for 4.9 min to re-equilibrate the system before the next injection. The mass spectrometer was operated in the full-scan mode (MS1) from *m/z* 50 to 1,000. The drying gas flow rate was 12 L/min, the temperature was 250°C, and the gas nebulizer pressure was set to 52 psig. The nozzle voltage was 1,000 V, and the capillary voltages were 3,000 and 4,000 V in the positive and negative ion modes, respectively.

## 2.8 Determination of protein content in lung tissue

The precipitated proteins were suspended in radioimmunoprecipitation assay (RIPA) buffer, denatured at 60°C, and sonicated for 30 min in a water bath. The samples were then centrifuged for 15 min at 14,000 × *g*. Protein concentration was measured using the Pierce BCA Protein Assay Kit (Thermo Fisher Scientific) according to the manufacturer's protocol.

## 2.9 Data processing: plasma oxPC profiling

MS1 data were reprocessed using a targeted approach to extract from the acquired data information about oxPCs (Godzien et al., 2019). IE-DDA data were used to confirm the annotation of oxPCs based on the MS/MS spectra. For this purpose, we searched for known fragmentation patterns, inspecting acquired MS/MS spectra in Mass Hunter Qualitative software (Agilent Technologies, B.07.00) (Gil de la Fuente et al., 2018). Moreover, all annotations were confirmed using retention time to compare the elution order between different oxPCs and their non-oxidized precursors. This step was crucial for minimizing false annotations of in-source generated lipids. A list of 45 oxPCs was defined (Supplementary Table S1) and covered 13 LCh-oxPCs and 32 SCh-oxPCs (including isoforms). OxPCs for which we found isomeric forms are denoted with the postfix "iso" followed by the number, signifying the identification of multiple isomers. Conversely, oxPCs lacking this "iso" prefix indicate that isoforms were not detected for those specific compounds.

Retention time and mass data pairs of annotated oxPCs were used as input criteria to search them in MS1 data. This processing was performed using the "Find by Ion" algorithm in Mass Hunter Profinder software (Agilent Technologies, B.10.00). The integration of all extracted peaks was manually curated and corrected if necessary.

## 2.10 Data processing: tissue metabolic fingerprinting

MS1 data were reprocessed using a targeted approach to extract information about oxPCs from the acquired data (Godzien et al., 2019). A list of 45 oxPCs was defined (Supplementary Table S1) and covered 13 LCh-oxPCs and 32 SCh-oxPCs (including isoforms). Annotation of these oxPCs was done in previous projects based on the data-independent analysis (DIA), and incorporated into in-house built library. Retention time and mass data pairs of annotated oxPCs were used as input criteria to search them in MS1 data. This processing was performed using the "Find by Ion" algorithm in Mass Hunter Profinder software (Agilent Technologies, B.10.00). The integration of all extracted peaks was manually curated and corrected if necessary.

## 2.11 Statistical analysis

The acquired data underwent evaluation through a Quality Assurance procedure. oxPCs displaying a Relative Standard Deviation (RSD) of signals in QC samples below 30% were deemed reliably measured and retained for subsequent statistical analyses.

Before statistical analyses, data from the plasma analyses were normalized solely to the IS to minimize analytical drift. Data from the tissue analyses were normalized to the IS and to protein content to minimize differences between different pieces of tissue. Before using IS data for normalization purposes, the quality of measured signals and integrated peaks was evaluated, checking the RSD of IS across all the samples to ensure that its signal was not interfered by co-eluting molecules changing between compared groups.

Plasma samples were analyzed for general comparisons of *i*) control vs. NSCLC; for subtype comparison of *ii*) control vs. ADC subtype and *iii*) control vs. SCC subtype. Tissue samples were analyzed for general comparison between *i*) tumor and non-cancerous lung tissue of NSCLC; for subtype comparison between *ii*) tumor and non-cancerous lung tissue in ADC and *iii*) tumor and non-cancerous lung tissue in SCC.

Differences between compared groups were described with *p*-values and relative differences expressed as percentages, where a positive value indicated higher values in cancer patients than in controls, and a negative value indicated lower signals in cancer

10.3389/fmolb.2023.1279645

TABLE 2 Differences in oxPC profiles of NSCLC patients and COPD controls in plasma samples (Panel A) and non-cancerous lung tissue and tumor tissue from NSCLC patients (Panel B).

| A) Relative plasma oxPC abundance between NSCLC patients and COPD controls | | | | |
|---|---|---|---|---|
| oxPC | Raw *p*-value (Corrected *p*-value) | Change [%] (Fold change) | COPD controls | NSCLC |
| | | | Median abundance (Q1–Q3) [counts] | |
| PC 16:0/20:3; OH | 2.46E-14 | NSCLC[a] | 0 (0–0) | 87,985 (76,390–99,205) |
| | (3.20E-13) | (16.00) | | |
| PC 16:0/18:2; OH | 1.95E-13 | 179 | 62,930 (56,807–72,151) | 145,245 (117,414–190,046) |
| | (1.26E-12) | (2.46) | | |
| PC 16:0/20:4; OH | 2.36E-11 | 88 | 107,090 (89,664–114,582) | 164,852 (139,989–204,070) |
| | (1.02E-10) | (1.74) | | |
| PC 18:0/20:4; OH | 3.23E-08 | 54 | 113,525 (106,043–130,812) | 154,079 (131,649–201,613) |
| | (1.05E-07) | (1.44) | | |
| PC 18:0/18:2; OH | 2.44E-02 | 17 | 216,912 (179,508–247,975) | 232,874 (207,020–285,790) |
| | (5.29E-02) | (1.15) | | |
| PC 18:0/20:4; OOH | 1.75E-02 | 14 | 92,188 (84,837–101,544) | 102,019 (90,049–117,132) |
| | (4.55E-02) | (1.13) | | |
| B) Relative oxPC levels between healthy lung tissue and tumor tissue from NSCLC patients | | | | |
| oxPC | Raw *p*-value (Corrected *p*-value) | Change [%] (Fold change) | Healthy tissue | Tumor tissue |
| | | | Median abundance (Q1–Q3) [counts] | |
| PC 16:0/7:0; COOH iso4 | 6.61E-05 | 87 | 920 (646–1,368) | 1,440 (648–2,761) |
| | (6.61E-05) | (1.70) | | |
| PC 16:0/7:0; COOH iso2 | 8.66E-05 | 10 | 290 (199–568) | 367 (214–644) |
| | (6.06E-04) | (1.09) | | |
| PC 16:0/5:0; COOH | 2.05E-02 | 92 | 567 (433–868) | 458 (0–663) |
| | (4.79E-02) | (1.34) | | |
| PC 16:0/5:0; CHO | 7.79E-03 | 73 | 1,322 (821–1,867) | 1,561 (1,089–2,640) |
| | (2.18E-02) | (1.30) | | |
| PC 16:0/4:0; CHO iso2 | 5.62E-03 | 65 | 539 (285–754) | 636 (356–899) |
| | (1.97E-02) | (1.24) | | |
| PC 16:0/18:2; OH iso2 | 1.59E-03 | 76 | 3,622 (2,954–4,592) | 4,832 (3,829–6,452) |
| | (7.44E-03) | (1.37) | | |

Raw *p*-value computed with the Mann-Whitney unpaired test for plasma comparisons and paired test for tissue comparisons. Corrected *p*-value was calculated employing Benjamini–Hochberg FDR, correction.

The positive value of the change indicates that the average amount of oxPC, is higher in plasma of cancer patients than in controls, and higher in tumor tissue than in healthy lung tissue, while a negative value indicates that the average amount of oxPC, is lower in plasma of cancer patients than in controls, and lower in tumor tissue than in healthy lung tissue.

[a]NSCLC, oxPCs, observed only in NSCLC, samples and not in COPD.

patients than in controls. *p*-values were computed using a non-parametric Mann-Whitney test in Mass Profiler Professional (MPP, Agilent Technologies 15.1). For plasma comparisons between NSCLC and COPD patients unpaired test was applied, while for the tissue comparisons of different tissue sections from the same patients paired test was employed. Obtained *p*-values were corrected employing Benjamini–Hochberg False Discovery Rate correction. However, because of small number of tested variables uncorrected $p < 0.05$ was considered significant.

Variations between groups were inspected by calculating the percentage of change in Excel (Microsoft) and fold change in MPP 15.1 (Agilent Technologies). Furthermore, we calculated using Excel (Microsoft) the median, Q1, and Q3 for each oxPC level in each comparison (Tables 2, 3). To evaluate the prevalence of elevated

TABLE 3 Differential oxPC profiles between ADC, SCC, and COPD patients in plasma (Panel A) and lung tissue (Panel B).

| A) oxPC levels between ADC and SCC patients and COPD controls in plasma | | | | | | | |
|---|---|---|---|---|---|---|---|
| oxPC | ADC | | SCC | | COPD controls | ADC | SCC |
| | Raw *p*-value (Corrected *p*-value) | Change [%] and Fold change | Raw *p*-value (Corrected *p*-value) | Change [%] and Fold change | Median abundance (Q1–Q3) [counts] | | |
| PC 16:0/20:3; OH | 6.77E-12 | ADC | 5.45E-13 | SCC | 0 (0–97,285) | 89,546 (80,989–97,285) | 81,998 (73,048–102,407) |
| | (8.79E-11) | (16.00) | (7.09E-12) | (16.00) | | | |
| PC 16:0/18:2; OH | 5.19E-11 | 220 | 8.37E-12 | 150 | 62,930 (56,807–197,594) | 166,556 (133,276–197,594) | 126,730 (108,060–171,867) |
| | (3.37E-10) | (2.77) | (5.44E-11) | (2.27) | | | |
| PC 16:0/20:4; OH | 7.38E-10 | 99 | 1.28E-09 | 80 | 107,090 (89,664–194,518) | 172,742 (151,500–194,518) | 161,365 (131,994–207,264) |
| | (3.20E-09) | (1.81) | (5.56E-09) | (1.69) | | | |
| PC 18:0/20:4; OH | 7.33E-08 | 72 | 1.49E-06 | 43 | 113,525 (106,043–212,391) | 170,713 (141,629–212,391) | 149,667 (129,091–196,851) |
| | (2.38E-07) | (1.55) | (4.85E-06) | (1.37) | | | |
| PC 18:0/18:2; OH | 2.16E-02 | 23 | ns | 13 | 216,912 (179,508–289,560) | 246,907 (212,977–289,560) | 227,509 (206,884–280,635) |
| | (5.62E-02) | (1.19) | | (1.12) | | | |
| PC 18:0/20:4; OOH | ns | 10 | 8.95E-03 | 17 | 92,188 (84,837–118,456) | 98,488 (87,384–118,456) | 103,146 (92,983–116,214) |
| | | (1.09) | (2.33E-02) | (1.15) | | | |
| PC 16:0/7:0; COOH | ns | 6 | 2.16E-02 | 23 | 8,564 (6,614–12,101) | 9,346 (6,642–12,101) | 10,701 (8,059–14,467) |
| | | (1.04) | (4.68E-02) | (1.22) | | | |

(Continued on following page)





10.3389/fmolb.2023.1279645

TABLE 3 (*Continued*) Differential oxPC profiles between ADC, SCC, and COPD patients in plasma (Panel A) and lung tissue (Panel B).

| B) oxPC levels between healthy lung tissue and tumor tissue from ADC and SCC patients | | | | | | | | |
|---|---|---|---|---|---|---|---|---|
| oxPC | ADC | | SCC | | ADC healthy tissue | ADC tumor tissue | SCC healthy tissue | SCC tumor tissue |
| | Raw *p*-value (Corrected *p*-value) | Change [%] and Fold change | Raw *p*-value (Corrected *p*-value) | Change [%] and Fold change | Median abundance (Q1–Q3) [counts] | | | |
| PC 16:0/7:0; COOH iso4 | 5.76E-05 | 64 | 4.60E-02 | 104 | 888 (665–1,057) | 1,779 (1,259–2,537) | 1,046 (568–1,469) | 1,146 (593–3,007) |
| | (8.06E-04) | (1.79) | (1.60E-01) | (1.65) | | | | |
| PC 16:0/5:0; COOH | ns | 38 | 3.02E-02 | 138 | 293 (224–643) | 377 (214–662) | 278 (183–559) | 352 (219–616) |
| | | (1.01) | (1.60E-01) | (1.65) | | | | |
| PC 16:0/5:0; CHO | ns | 22 | 4.96E-02 | 113 | 1,322 (750–2,259) | 1,691 (1,167–2,640) | 1,321 (843–1,810) | 1,549 (907–2,548) |
| | | (1.19) | (1.60E-01) | (1.38) | | | | |
| PC 16:0/4:0; CHO iso2 | 4.80E-02 | 24 | ns | 96 | 561 (325–754) | 612 (432–914) | 515 (277–757) | 673 (273–852) |
| | (2.02E-01) | (1.16) | | (1.30) | | | | |
| PC 16:0/18:2; OH iso2 | 5.45E-04 | 93 | ns | 66 | 3,658 (3,304–4,237) | 5,399 (4,247–6,436) | 3,413 (2,828–5,150) | 4,349 (2,697–6,645) |
| | (3.82E-03) | (1.62) | | (1.21) | | | | |

Raw *p*-value computed with the Mann-Whitney unpaired test for plasma comparisons and paired test for tissue comparisons. Corrected *p*-value was calculated employing Benjamini–Hochberg FDR, correction.
The positive value of the change indicates that the average amount of oxPC, is higher in plasma of cancer patients than in controls, and higher in tumor tissue than in healthy lung tissue, while a negative value indicates that the average amount of oxPC, is lower in plasma of cancer patients than in controls, and lower in tumor tissue than in healthy lung tissue.
ns–non-significant.





10.3389/fmolb.2023.1279645

oxPC levels, we determined the percentage of patients in whom increased levels of oxPCs were observed in tumor tissue compared to healthy lung tissue.

Metabolomic data were correlated with complex clinical data, including WBC, CRP, PET/MRI, MTV, and SUV values. Spearman correlation analysis was performed using MetaboAnalyst 5.0 (Pang et al., 2021).

# 3 Results

## 3.1 Baseline characteristics and general concerns

The baseline characteristics of the patients with NSCLC and COPD controls are summarized in Table 1. The enrolled subjects were matched without any statistical differences between groups in basic anthropometric measurements. However, more male than female participants were enrolled, reflecting the higher incidence of lung cancer in men compared to women during the sampling period (Mederos et al., 2020). The number of samples per group, splitting the cohort according to the gender, was too small to perform robust correlational analysis, therefore to check if there are gender specific differences in the oxPCs level, we calculated the percentage of change between compared groups separately for female and male. Results of this analysis are summarized in Supplementary Table S2.

## 3.2 Annotation of oxPCs in plasma

Plasma analyses were performed on samples collected from 101 NSCLC patients and 24 COPD controls. Supervised data processing resulted in the annotation of 13 of the 45 oxPCs used for the target search (Supplementary Table S1). These oxPCs were annotated based on DDA-MS/MS structural information and fragmentation rules (Gil de la Fuente et al., 2018; Lange et al., 2021). Among the oxPCs identified, five were SCh-oxPCs and eight were LCh-oxPCs. Among the LCh-oxPCs, six contained hydroxy groups and only two contained hydroperoxy groups. We found three aldehyde- and two carboxylic acid-containing SCh-oxPCs. After the QA procedure, we rejected four oxPCs (one LCh-oxPC and three SCh-oxPC) which RSD was above 30%. For all other oxPCs RSD for QC samples was below 30% with an average of 21.4%.

## 3.3 Annotation of oxPCs in tumor tissue

Total tumor analyses were performed on 122 samples collected from 61 patients with NSCLC: two samples were collected from each patient, covering healthy tissue and tumor tissue. Supervised data processing allowed for the annotation of 16 out of the 45 oxPCs used for the target search (Supplementary Table S1). These oxPCs were annotated based on exact mass and RT matching with the in-house built library. Among these, 15 were SCh-oxPCs and only one was an LCh-oxPC. The LCh-oxPC contained a hydroxy group. Among the SCh-oxPCs, we found nine aldehyde- and six carboxylic acid-containing forms. After the QA procedure, we rejected two oxPCs (one LCh-oxPC and one SCh-oxPC) which RSD was above 30%. For all other oxPCs RSD for QC samples was below 30% with an average of 13.9%.

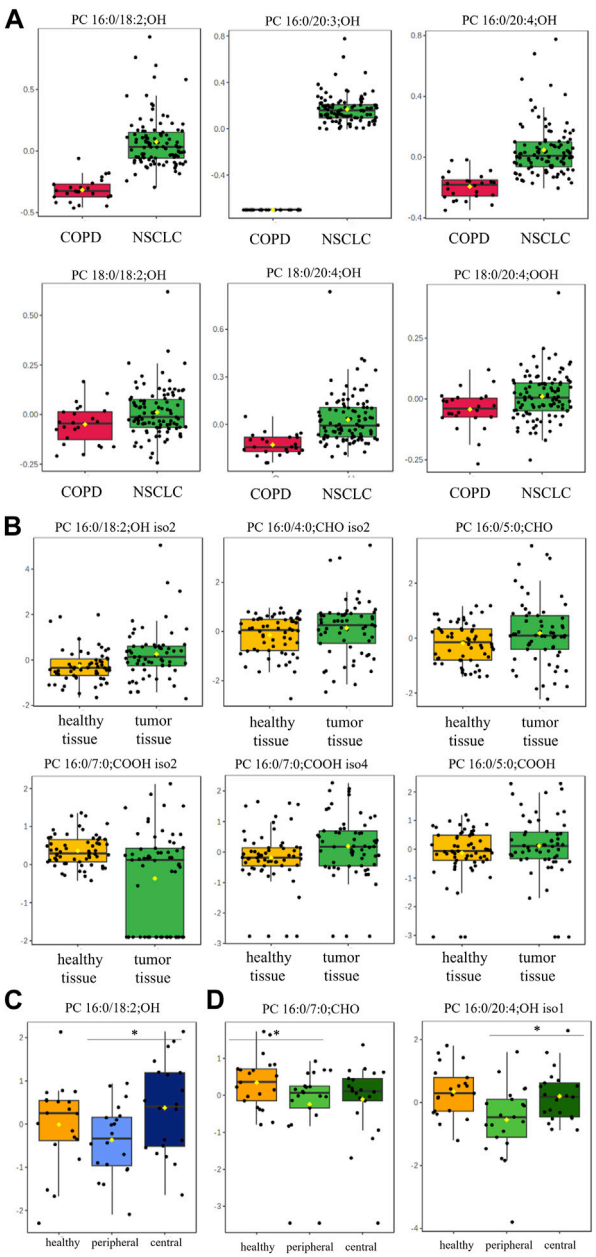


FIGURE 2
Box-and-whisker plots comparing oxPC levels between 101 NSCLC patients and 24 COPD controls in plasma samples (Panel **(A)**) and between healthy lung tissue and tumor tissue from 61 NSCLC patients (Panel **(B)**); non-malignant tissue and in peripheral and central tumor regions in 20 ADC patients (Panel **(C)**) and 20 SCC patients (Panel **(D)**). The levels of oxPCs shown on the figure were found to be significantly different between the compared groups according to the Mann-Whitney unpaired test for plasma comparisons and paired test for tissue comparisons. The y-axis in the graph represents the normalized signal of oxPCs (counts), which have been log-transformed and UV-scaled. The black dots in the graph represent the concentrations of oxPCs from all samples in a given group. The notch represents the 95% confidence interval around the median of each group, which is defined as ±1.58 times the interquartile range divided by the square root of the number of samples. The mean concentration of each group is indicated with a yellow diamond in the graph.

Dimensional tumor tissue analyses were performed on 120 samples collected from 40 NSCLC patients: three samples were collected from each patient, covering healthy tissue, peripheral tumor tissue and central tumor tissue. Supervised data processing resulted in the annotation of 20 out of the 45 oxPCs used for the target search (Supplementary Table S1). These oxPCs were annotated based on exact mass and RT matching with the in-house built library. Among these oxPCs, 14 were SCh-oxPCs and six were LCh-oxPCs. Among the LCh-oxPCs, three contained hydroxy groups and three contained hydroperoxy groups. Among the SCh-oxPCs, we found five aldehyde- and nine carboxylic acid-containing forms. After the QA procedure, we rejected five oxPCs (two LCh-oxPC and three SCh-oxPC) which RSD was above 30%. For all other oxPCs RSD for QC samples was below 30% with an average of 12.3%.

## 3.4 oxPCs in NSCLC vs. COPD: a general comparison

oxPC levels were significantly higher in NSCLC patients than in COPD patients (Table 2). The variation among samples in the NSCLC group was greater than that in the COPD group (Figure 2A). An overall general increase in oxPC levels was also observed in tissue samples; in NSCLC patients, tumor tissues exhibited higher levels of oxPCs than healthy lung tissue (Figure 2B). The magnitude of this difference was smaller than in plasma samples. We also inspected the levels of oxPCs in each patient separately, comparing the levels of oxPCs between healthy and tumor tissues, and we observed elevated oxPC levels in tumor tissue in 63% of NSCLC patients.

Dimensional tissue analyses revealed that oxPC levels were overall lower in the peripheral tumor regions in comparison to both, healthy tissue and central tumor region (Figures 2C, D).

## 3.5 oxPCs in NSCLC vs. COPD: NSCLC subtypes

Next, we assessed oxPC levels by NSCLC subtype (ADC and SCC). We observed a generally higher elevation of oxPC levels in the plasma and tumor tissues of ADC patients than in SCC patients (Figure 3). The observed differences were larger for plasma than for tissue samples. In addition, the magnitude of the difference in oxPC levels between COPD and ADC patients was higher than that between COPD and SCC patients (Table 3). Similar findings were also observed in tissue samples, where a greater difference in oxPC levels was observed between tumor and healthy lung tissue in patients with ADC compared to patients with SCC. Comparisons of tissue oxPC levels, between healthy and tumor tissue, for individual patients revealed elevated levels in 85% of ADC patients and only 56% of SCC patients.

## 3.6 Correlation analysis

Correlation analysis between plasma oxPC levels and clinical parameters revealed a statistically significant ($p$-value<0.05) but weak (correlation coefficient less than 0.5) negative correlation between two oxPCs (PC 16:0/20:3; OH and PC 16:0/18:2; OH) and WBC. No statistically significant correlation was observed between oxPC and CRP levels.

Correlation analysis of tumor oxPC levels with metabolic activity index of lesions, expressed as SUV and MTV, did not reveal any correlations, regardless of whether the correlation was calculated for all NSCLC patients or for only ADC or SCC patients.

# 4 Discussion

The obtained oxPC profiles of the plasma and tumor tissue were different. LCh-oxPCs were the predominant form in the plasma, accounting for 62% of all detected oxPCs. In contrast, SCh-oxPCs were the primary fraction in tissues, representing 94% and 70% of all detected oxPCs in the total tumor and dimensional tissue analyses, respectively. Solati et al. (2021) reported a similar observation of locally predominant SCh-oxPCs in the thrombi of patients with ST-segment elevation myocardial infarction tissue, however it was a different tissue and disease context. It is important to emphasize that the results obtained from plasma samples pertain to the comparison between NSCLC and COPD patients. Conversely, the results obtained from tissue samples involve the comparison between cancerous and healthy lung tissues from NSCLC patients. Therefore, to compare these results directly, ideally, we should include also lung tissue from COPD patients, however we were not able to obtain such biopsy, which is one of the limitations of this study.

We observed an overall elevation of oxPCs in NSCLC patients, including elevated plasma oxPC levels compared to controls and elevated tissue oxPC levels in tumor tissue compared to healthy lung tissue (Figure 2). We observed an overall elevation of oxPC levels in patients with NSCLC compared to those in COPD controls. Considering that oxidative stress is a hallmark of numerous airway diseases (Sunnetcioglu et al., 2016), it can be assumed that the observed elevation would be even more significant if patients with NSCLC were compared with healthy controls.

An interesting observation was made for the results obtained considering gender differences. As can be seen in Supplementary Table S2, a higher magnitude of change is observed for males than for females. This phenomenon is attributed to the protective antioxidant properties of estrogen, frequently combined with lower exposure to exogenous risk factors, including alcohol and tobacco use, leading to diminished levels of ROS generation and mitochondrial impairment in females compared to males (Ethun, 2016; Allegra et al., 2023). However, it is important to mention, that according to the evidence, the number of smoking women during the last decade is increasing, resulting in a higher prevalence of NSCLC in women but also weakening their antioxidant defense capacity (Jafari et al., 2021).

Sunnetcioglu et al. (2016) investigated oxidative damage in three respiratory diseases (COPD, lung cancer, and obstructive sleep apnea syndrome) and revealed oxidative stress and stress responses in plasma samples for all three diagnoses. The highest level of oxidative stress, reflected via levels of coenzyme Q10 and 8-oxo7,8-dihydro-2-deoxyguanosine (8-oxodG), was observed in lung cancer. MDA levels were highest in patients with sleep apnea, but

10.3389/fmolb.2023.1279645

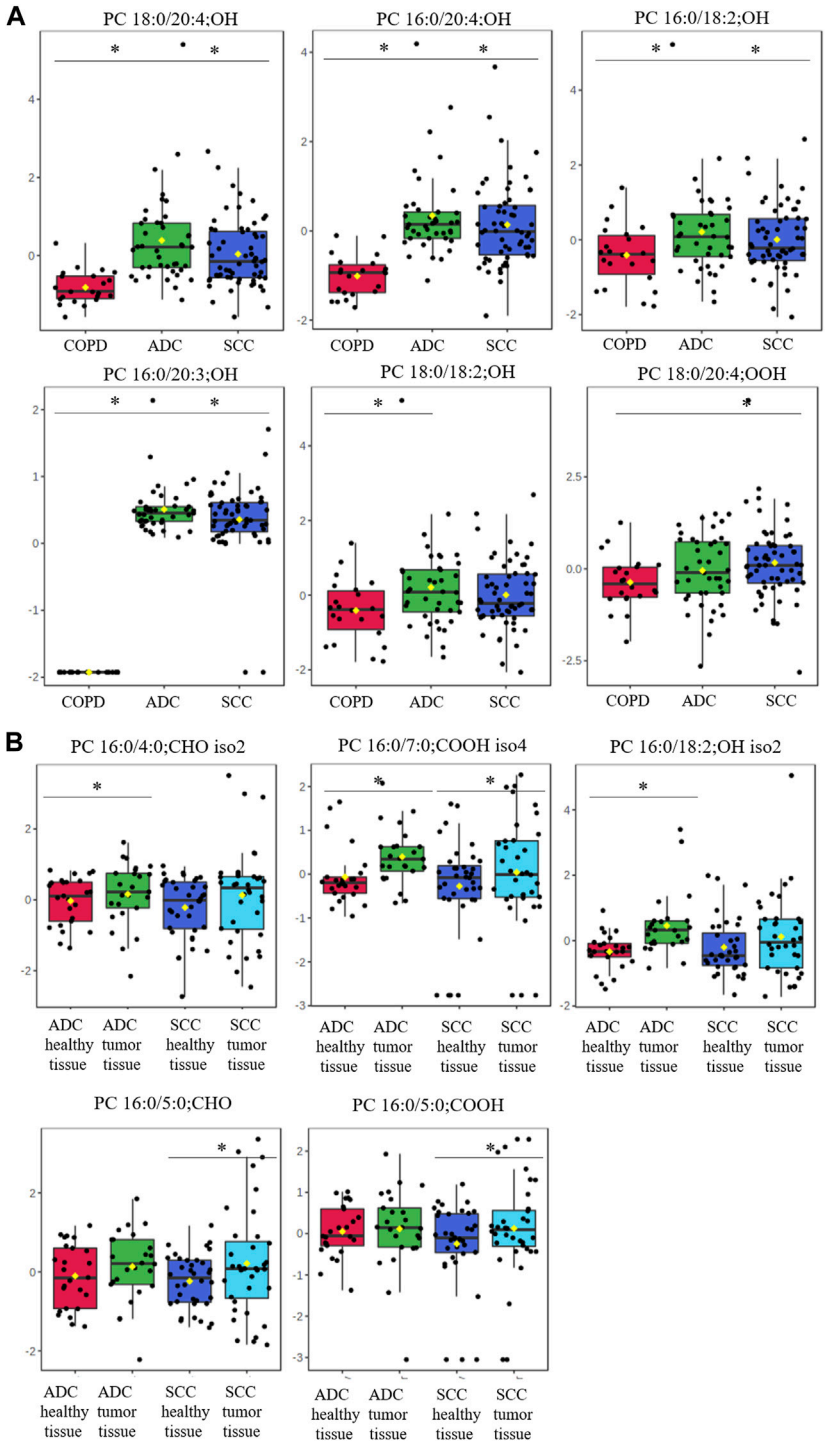


FIGURE 3
Box-and-whisker plots comparing oxPCs levels between plasma samples from 41 ADC and 60 SCC patients and 24 COPD controls (panel **(A)**) and between healthy, non-malignant tissue and tumor tissue in 25 ADC and 36 SCC patients (panel **(B)**). The levels of oxPCs shown on the figure were found to be significantly different between the compared groups according to the Mann-Whitney test. The y-axis in the graph represents the normalized signal of oxPCs (counts), which have been log-transformed and UV-scaled. The black dots in the graph represent the concentrations of oxPCs from all samples in a given group. The notch represents the 95% confidence interval around the median of each group, which is defined as $\pm$1.58 times the interquartile range divided by the square root of the number of samples. The mean concentration of each group is indicated with a yellow diamond in the graph. * indicates statistically significant comparisons.

were also significantly higher in lung cancer and COPD patients than in controls. Primary oxidation products are known to be intermediates in the formation of end products. Therefore, it is crucial to investigate the relationship between them in the context of oxidative stress in NSCLC. For instance, higher levels of primary products may be associated with lower levels of end products. In

comparison, lower levels of primary products could be indicative of a greater accumulation of end products. The reported elevation of end oxidation products and our observation of elevated levels of primary oxidation products suggest that oxidative stress is elevated to such an extent that all oxidation products are increased.

Although both types of oxPCs originate from the same precursors, their formation and biological activity differ. LCh-oxPCs can be formed enzymatically and non-enzymatically, whereas SCh-oxPCs are formed only non-enzymatically (Davies and Guo, 2014). Our data do not provide details about the origin of LCh-oxPCs in the plasma. Furthermore, the measured quantities may correspond to both enzymatically and non-enzymatically formed LCh-oxPCs. Therefore, precise interpretation of the obtained plasma results is challenging.

The origin of tissue SCh-oxPCs is non-enzymatic and most likely induced by ROS (Davies and Guo, 2014). Dimensional tissue analyses revealed that oxPC levels were lower in the peripheral than in the central region of the tumors and healthy lung tissue (Figures 2C, D). It can be concluded that the elevated level of oxPCs observed in tumor tissue resulted from the accumulation of these lipids in the central region. To the best of our knowledge, this is the first study to report the spatial localization of oxPCs in tumor tissue.

The elevated levels of oxPCs in healthy tissue might be linked to the smoking, since it induces oxidative stress. The formation and accumulation of SCh-oxPCs in tumor tissue may occur due to hypoxia of the metabolically hyperactive growing tumor, along with insufficient vascularization (Emami Nejad et al., 2021). Moreover, in agreement with our previous study (Kowalczyk et al., 2021), Marien et al. (2015) demonstrated changes in phospholipid profiles in NSCLC patients, indicating an increase in phosphatidylcholine species in tumor tissue compared to that in healthy lung tissue. Furthermore, previous studies have reported a reduced antioxidant capacity in malignant lung tissues (Gęgotek et al., 2016). Therefore, accumulated phosphatidylcholines can be easily oxidized under hypoxic conditions to form oxPCs. This may explain the accumulation of oxPCs in the tumor.

The magnitude of observed differences between groups in this study was generally smaller in tumor tissues than in the plasma samples (Figures 2, 3). This may be because plasma samples were collected from NSCLC patients and compared with samples from COPD patients, whereas tissue samples (tumor and non-cancerous tissue) were collected from NSCLC patients. Although histologically malignant and non-malignant tissues were separated, non-malignant tissues were collected from the surrounding area, and were likely affected by tumor metabolism. Moreover, tumors are complex and highly heterogeneous structures comprising many different cellular and noncellular elements (Xing et al., 2010). Therefore, different pieces of tumor tissue may not have exactly the same metabolic content, which might contribute to the observed intra-group heterogeneity reflected in the wide range of measured oxPC levels. This phenomenon is common for these molecules and has been observed previously (Solati et al., 2021).

We correlated the levels of tissue oxPCs with MTV values, which reflect tumor size and SUV, which provide evidence of tumor activity. We expected to observe a correlation between the MTV values and the levels of oxPCs since greater tumor size can result in poorer oxygenation leading to increased oxidative stress and consequently higher levels of oxPCs. Similarly, we expected to observe a correlation between SUV values and the levels of oxPCs since metabolic hyperactivity often leads to increased oxidative stress and subsequently higher levels of oxPCs. Surprisingly, no SCh-oxPCs showed a correlation with tumor size or activity. This finding may suggest the non-enzymatic origin of these oxidative products. Indeed, (ROS)-induced formation of oxPCs is uncontrolled and generates wide range oxidation products with wide range of concentrations (O'Donnell et al., 2019).

We observed some differences in oxPC levels between the two cancer subtypes and COPD controls. Our data showed a greater elevation of oxPC levels relative to controls in ADC patients than in SCC patients. This elevation was also more common in the tumor tissue of ADC patients (85%) than in that of SCC patients (56%). Differences between the two NSCLC subtypes concerning redox status have already been reported; however, to our knowledge, this is the first report regarding primary oxidation products. Gęgotek et al. (2016) reported alterations in tissue MDA and 4-HNE levels between ADC and SCC patients. MDA was nearly four times higher in SCC than in healthy tissue and six times higher in ADC than in healthy tissue. Differences in 4-HNE levels were not as substantial (2.7 and 2.3 times higher in SCC and ADC, respectively, than in healthy tissues). Elevated 4-HNE levels relative to those in healthy tissues were seen in 83% of ADC tissues and 46% of SCC tissues. Gęgotek et al. (2016) concluded that lipid peroxidation is more involved in ADC development, whereas endocannabinoids contribute more to SCC growth and development. While we cannot draw conclusions regarding endocannabinoid metabolism, our results do suggest enhanced lipid oxidation in ADC patients compared to those with SCC.

Because oxidative stress is closely related to inflammation, we decided to investigate potential correlations between oxPC levels, CRP, and WBC, which are used as inflammation markers. Moreover, CRP and WBC have been used as markers of the risk of incident lung cancer (Wong et al., 2020), and as predictors of early mortality (Isaksson et al., 2022) or survival (Bacha et al., 2017). We observed a correlation between WBC counts and the plasma levels of two oxPCs, PC 16:0/18:2; OH and PC 16:0/20:3; OH. Elevated neutrophil counts primarily drive the association between WBCs and NSCLC; therefore, further research considering different subtypes of WBCs (e.g., neutrophils or lymphocytes), especially that the neutrophil-to-lymphocyte ratio has been used as a prognostic factor in NSCLC patients (Bacha et al., 2017; Yang et al., 2021).

Both COPD and NSCLC are associated with oxidative stress and inflammation. Our results demonstrate elevated oxidative stress in NSCLC patients compared to that in COPD patients. Interestingly, Berg et al. (2018) observed that markers reflecting inflammation, endothelial activation, and extracellular matrix remodeling were elevated in the serum of patients with COPD compared to levels in lung cancer patients. The observed elevation of oxPC in NSCLC compared to that in COPD patients (our data), together with elevated levels of oxidative stress markers in NSCLC tissues (Gęgotek et al., 2016) and enhanced inflammation mediators in COPD patients (Berg et al., 2018), suggest that the observed alterations in oxPC levels in NSCLC subjects were related to oxidative stress rather than inflammation.

Considering the variety of factors influencing the activity and properties of oxPCs, the very precise interpretation of our results

obtained is challenging. Instead, these results demonstrate a clear need to explore the involvement of oxPCs in NSCLC. Furthermore, because oxPCs are potent stimulators of endothelial barrier disruption, therapies that attenuate their activities can result in novel therapeutic tools for anti-cancer treatment. However, elevated oxidative stress is associated with several tumor types, and increased levels of oxPCs are associated with prostate (Ingram et al., 2021), pancreatic (Stevens et al., 2012) and neuroendocrine cancers (López-López et al., 2020). Therefore, oxPCs themselves cannot be used as potential biomarkers of NSCLC due to their lack of specificity. However, Philippova et al. (2019) pointed out that simultaneous determination of plasma levels of oxPCs and estimation of the detoxifying capacity of plasma to neutralize these lipids can significantly improve the diagnostic importance of oxPCs as a disease biomarker. In the context of our results, oxPCs might be rather considered as potential markers to distinguish between different NSCLC subtypes instead, however this requires more investigation, including the quantification of these lipids in plasma. Although, the implementation of oxPCs into the clinical diagnosis process requires their quantification in plasma samples, this will be very difficult due to the limited availability of standards of these substances, let alone labeled ones.

## 5 Conclusion

Our results revealed that the oxPC profiles of patients with NSCLC were different between plasma and tumor tissues. LCh-oxPCs were the predominant form in plasma (62% of all detected oxPCs), and SCh-oxPCs were the main fraction in tissue (94% and 70% of all detected oxPCs in the total tumor and dimensional tumor tissue analyses, respectively). OxPC levels were significantly elevated in the plasma of patients with NSCLC compared to those in COPD controls. They were also elevated in the tumor tissue of patients with NSCLC compared to levels in the non-cancerous adjacent lung tissue, with the lowest level of oxPCs observed in the peripheral part of the tumor. Moreover, a higher level of oxPCs was observed in ADC patients than in SCC patients compared to that in COPD controls. A higher level of oxPCs was also observed in the tumor tissue of both ADC and SCC patients than in the surrounding non-cancerous lung tissue, but this difference was more prominent in ADC patients. Circulating oxPC levels correlated with WBC count but not with CRP level, whereas tissue oxPC levels did not correlate with tumor size (MTV) or activity (SUV).

Finally, the elevation of oxPC levels in NSCLC relative to that in COPD patients, together with higher levels of oxidative stress markers in NSCLC (Gęgotek et al., 2016) and enhanced inflammation mediators (Berg et al., 2018) in COPD patients, suggest that the observed alterations in oxPC levels in NSCLC are more closely related to oxidative stress than inflammation.

The obtained results confirm the involvement of oxPCs in NSCLC. Given that oxPCs are a common hallmark of oxidative stress accompanying multiple cancer types and the high toxicity of SCh-oxPCs, their accumulation in NSCLC patients highlights their potential as therapeutic targets rather than biomarkers.

## Data availability statement

The raw data supporting the conclusion of this article will be made available by the authors, without undue reservation.

## Ethics statement

The studies involving humans were approved by Ethics Committee of the Medical University of Bialystok, R-I-003/262/2004, R-I-002/296/2018, and APK 002 5 2021. The studies were conducted in accordance with the local legislation and institutional requirements. The participants provided their written informed consent to participate in this study.

## Author contributions

JG: Conceptualization, Formal Analysis, Funding acquisition, Investigation, Methodology, Visualization, Writing–original draft. AL-L: Formal Analysis, Investigation, Methodology, Writing–original draft. JS: Formal Analysis, Investigation, Visualization, Writing–review and editing. KJ: Formal Analysis, Investigation, Visualization, Writing–review and editing. KP: Investigation, Writing–review and editing. JK: Conceptualization, Investigation, Methodology, Resources, Writing–review and editing. MaM: Formal Analysis, Investigation, Writing–review and editing. ZD-A: Investigation, Writing–review and editing. CB: Conceptualization, Supervision, Writing–original draft. JR: Methodology, Resources, Supervision, Writing–review and editing. MK: Conceptualization, Methodology, Resources, Supervision, Writing–review and editing. MiM: Conceptualization, Funding acquisition, Resources, Writing–review and editing. AK: Conceptualization, Funding acquisition, Resources, Supervision, Writing–review and editing. JN: Conceptualization, Funding acquisition, Project administration, Resources, Writing–review and editing. MC: Conceptualization, Funding acquisition, Methodology, Project administration, Resources, Supervision, Writing–original draft.

## Funding

The author(s) declare financial support was received for the research, authorship, and/or publication of this article. This work was supported by grants from the National Science Centre in Poland (2014/13/B/NZ5/01256), the National Centre for Research and Development in Poland: “Prevention practices and treatment of civilization diseases’ program, STRATEGMED” (contract no. STRATEGMED2/266484/2/NCBR/2015), the Medical University of Bialystok, the National Research Centre in Poland (61/KNOW-16 and 66/KNOW/16), the statutory funds of the Medical University of Bialystok (SUB/1/DN/21/005/4406), the Spanish Ministry of Science and Innovation PID 2021-122490NB-I00, and the Polish Ministry of Education and Science within the project “Excellence Initiative–Research University.”

## Conflict of interest

The authors declare that the research was conducted in the absence of any commercial or financial relationships that could be construed as a potential conflict of interest.

## Publisher's note

All claims expressed in this article are solely those of the authors and do not necessarily represent those of their affiliated organizations, or those of the publisher, the editors and the reviewers. Any product that may be evaluated in this article, or claim that may be made by its manufacturer, is not guaranteed or endorsed by the publisher.

## Supplementary material

The Supplementary Material for this article can be found online at: https://www.frontiersin.org/articles/10.3389/fmolb.2023.1279645/full#supplementary-material

## References


Allegra, A., Caserta, S., Genovese, S., Pioggia, G., and Gangemi, S. (2023). Gender differences in oxidative stress in relation to cancer susceptibility and survival. *Antioxidants (Basel)* 12 (6), 1255. doi:10.3390/antiox12061255

Bacha, S., Sghaier, A., Habibech, S., Cheikhrouhou, S., Racil, H., Chaouch, N., et al. (2017). Combined C-reactive protein and Neutrophil to Lymphocyte ratio use predict survival innon-small-cell lung cancer. *Tunis. Med.* 95 (12), 229–235.

Beloribi-Djefaflia, S., Vasseur, S., and Guillaumond, F. (2016). Lipid metabolic reprogramming in cancer cells. *Oncogenesis* 5 (1), e189. doi:10.1038/oncsis.2015.49

Berg, J., Halvorsen, A. R., Bengtson, M. B., Taskén, K. A., Mælandsmo, G. M., Yndestad, A., et al. (2018). Levels and prognostic impact of circulating markers of inflammation, endothelial activation and extracellular matrix remodelling in patients with lung cancer and chronic obstructive pulmonary disease. *BMC Cancer* 18 (1), 739. doi:10.1186/s12885-018-4659-0

Bochkov, V., Gesslbauer, B., Mauerhofer, C., Philippova, M., Erne, P., and Oskolkova, O. V. (2017). Pleiotropic effects of oxidized phospholipids. *Free Radic. Biol. Med.* 111, 6–24. doi:10.1016/j.freeradbiomed.2016.12.034

Chen, Z., Zang, L., Wu, Y., Nakayama, H., Shimada, Y., Shrestha, R., et al. (2018). Lipidomic profiling on oxidized phospholipids in type 2 diabetes mellitus model zebrafish. *Anal. Sci.* 34 (10), 1201–1208. doi:10.2116/analsci.18P281

Ciborowski, M., Kisluk, J., Pietrowska, K., Samczuk, P., Parfieniuk, E., Kowalczyk, T., et al. (2017). Development of LC-QTOF-MS method for human lung tissue fingerprinting. A preliminary application to nonsmall cell lung cancer. *Electrophoresis* 38 (18), 2304–2312. doi:10.1002/elps.201700022

Ciereszko, A., Dietrich, M. A., Słowińska, M., Nynca, J., Ciborowski, M., Kaczmarek, M. M., et al. (2022). Application of two-dimensional difference gel electrophoresis to identify protein changes between center, margin, and adjacent non-tumor tissues obtained from non-small-cell lung cancer with adenocarcinoma or squamous cell carcinoma subtype. *PLoS One* 17 (5), e0268073. doi:10.1371/journal.pone.0268073

Daniluk, U., Daniluk, J., Kucharski, R., Kowalczyk, T., Pietrowska, K., Samczuk, P., et al. (2019). Untargeted metabolomics and inflammatory markers profiling in children with crohn's disease and ulcerative colitis-A preliminary study. *Inflamm. Bowel Dis.* 25 (7), 1120–1128. doi:10.1093/ibd/izy402

Davies, S. S., and Guo, L. (2014). Lipid peroxidation generates biologically active phospholipids including oxidatively N-modified phospholipids. *Chem. Phys. Lipids* 181, 1–33. doi:10.1016/j.chemphyslip.2014.03.002

Duma, N., Santana-Davila, R., and Molina, J. R. (2019). Non–small cell lung cancer: epidemiology, screening, diagnosis, and treatment. *Mayo Clin. Proc.* 94 (8), 1623–1640. doi:10.1016/j.mayocp.2019.01.013

Durham, A. L., and Adcock, I. M. (2015). The relationship between COPD and lung cancer. *Lung Cancer* 90 (2), 121–127. doi:10.1016/j.lungcan.2015.08.017

Emami Nejad, A., Najafgholian, S., Rostami, A., Sistani, A., Shojaeifar, S., Esparvarinha, M., et al. (2021). The role of hypoxia in the tumor microenvironment and development of cancer stem cell: a novel approach to developing treatment. *Cancer Cell Int.* 21 (1), 62. doi:10.1186/s12935-020-01719-5

Ethun, K. (2016). "Chapter 9 - sex and gender differences in body composition, lipid metabolism, and glucose regulation," in *Sex differences in physiology*. Editors GN Neigh and MM Mitzelfelt (Boston: Academic Press), 145–165.

Gęgotek, A., Nikliński, J., Žarković, N., Žarković, K., Waeg, G., Łuczaj, W., et al. (2016). Lipid mediators involved in the oxidative stress and antioxidant defence of human lung cancer cells. *Redox Biol.* 9, 210–219. doi:10.1016/j.redox.2016.08.010

Gil de la Fuente, A., Traldi, F., Siroka, J., Kretowski, A., Ciborowski, M., Otero, A., et al. (2018). Characterization and annotation of oxidized glycerophosphocholines for non-targeted metabolomics with LC-QTOF-MS data. *Anal. Chim. Acta* 1037, 358–368. doi:10.1016/j.aca.2018.08.005

Godzien, J., Alonso-Herranz, V., Barbas, C., and Armitage, E. G. (2014). 'Controlling the quality of metabolomics data: new strategies to get the best out of the QC sample. *Metabolomics* 11, 518–528. doi:10.1007/s11306-014-0712-4

Godzien, J., Kalaska, B., Adamska-Patruno, E., Siroka, J., Ciborowski, M., Kretowski, A., et al. (2019). Oxidized glycerophosphatidylcholines in diabetes through non-targeted metabolomics: their annotation and biological meaning. *J. Chromatogr. B Anal. Technol. Biomed. Life Sci.* 1120, 62–70. doi:10.1016/j.jchromb.2019.04.053

Gong, Z., Li, Q., Shi, J., Liu, E. T., Shultz, L. D., and Ren, G. (2022). Lipid-laden lung mesenchymal cells foster breast cancer metastasis via metabolic reprogramming of tumor cells and natural killer cells. *Cell Metab.* 34 (12), 1960–1976.e9. doi:10.1016/j.cmet.2022.11.003

Ikura, Y., Ohsawa, M., Suekane, T., Fukushima, H., Itabe, H., Jomura, H., et al. (2006). Localization of oxidized phosphatidylcholine in nonalcoholic fatty liver disease: impact on disease progression. *Hepatology* 43 (3), 506–514. doi:10.1002/hep.21070

Ingram, L. M., Finnerty, M. C., Mansoura, M., Chou, C. W., and Cummings, B. S. (2021). Identification of lipidomic profiles associated with drug-resistant prostate cancer cells. *Lipids Health Dis.* 20 (1), 15. doi:10.1186/s12944-021-01437-5

Isaksson, J., Wennström, L., Branden, E., Koyi, H., Berglund, A., Micke, P., et al. (2022). 'Highly elevated systemic inflammation is a strong independent predictor of early mortality in advanced non-small cell lung cancer. *Cancer Treat. Res. Commun.* 31, 100556. doi:10.1016/j.ctarc.2022.100556

Jafari, A., Rajabi, A., Gholian-Aval, M., Peyman, N., Mahdizadeh, M., and Tehrani, H. (2021). National, regional, and global prevalence of cigarette smoking among women/females in the general population: a systematic review and meta-analysis. *Environ. Health Prev. Med.* 26 (1), 5. doi:10.1186/s12199-020-00924-y

Karki, P., and Birukov, K. G. (2020). Oxidized phospholipids in healthy and diseased lung endothelium. *Cells* 9 (4), 981. doi:10.3390/cells9040981

Ke, Y., Karki, P., Kim, J., Son, S., Berdyshev, E., Bochkov, V. N., et al. (2019). Elevated truncated oxidized phospholipids as a factor exacerbating ALI in the aging lungs. *FASEB J.* 33 (3), 3887–3900. doi:10.1096/fj.201800981R

Kowalczyk, T., Kisluk, J., Pietrowska, K., Godzien, J., Kozlowski, M., Reszeć, J., et al. (2021). The ability of metabolomics to discriminate non-small-cell lung cancer subtypes depends on the stage of the disease and the type of material studied. *Cancers (Basel)* 13 (13), 3314. doi:10.3390/cancers13133314

Lange, M., Angelidou, G., Ni, Z., Criscuolo, A., Schiller, J., Blüher, M., et al. (2021). AdipoAtlas: a reference lipidome for human white adipose tissue. *Cell Rep. Med.* 2 (10), 100407. doi:10.1016/j.xcrm.2021.100407

López-López, Á., Godzien, J., Soldevilla, B., Gradillas, A., López-Gonzálvez, Á., Lens-Pardo, A., et al. (2020). Oxidized lipids in the metabolic profiling of neuroendocrine tumors - analytical challenges and biological implications. *J. Chromatogr. A* 1625, 461233. doi:10.1016/j.chroma.2020.461233

Mantovani, G., Madeddu, C., and Macciò, A. (2012). Cachexia and oxidative stress in cancer: an innovative therapeutic management. *Curr. Pharm. Des.* 18 (31), 4813–4818. doi:10.2174/138161212803216889

Marien, E., Meister, M., Muley, T., Fieuws, S., Bordel, S., Derua, R., et al. (2015). Non-small cell lung cancer is characterized by dramatic changes in phospholipid profiles. *Int. J. Cancer* 137 (7), 1539–1548. doi:10.1002/ijc.29517

Martinez-Outschoorn, U. E., Peiris-Pagés, M., Pestell, R. G., Sotgia, F., and Lisanti, M. P. (2017). Cancer metabolism: a therapeutic perspective. *Nat. Rev. Clin. Oncol.* 14 (1), 11–31. doi:10.1038/nrclinonc.2016.60

Mederos, N., Friedlaender, A., Peters, S., and Addeo, A. (2020). Gender-specific aspects of epidemiology, molecular genetics and outcome: lung cancer. *ESMO Open* 5 (Suppl. 4), e000796. doi:10.1136/esmoopen-2020-000796

Mousapasandi, A., Loke, W. S. J., Herbert, C. A., and Thomas, P. S. (2021). "'Chapter 3 - oxidative stress in lung cancer," in *Cancer*. Editors VR Preedy and VB Patel. Second Edition (San Diego: Academic Press), 27–37.

Ni, Z., Goracci, L., Cruciani, G., and Fedorova, M. (2019). Computational solutions in redox lipidomics - current strategies and future perspectives. *Free Radic. Biol. Med.* 144, 110–123. doi:10.1016/j.freeradbiomed.2019.04.027

Nie, Q., Xing, M., Chen, H., Hu, J., and Nie, S. (2019). Metabolomics and lipidomics profiling reveals hypocholesterolemic and hypolipidemic effects of arabinoxylan on type 2 diabetic rats. *J. Agric. Food Chem.* 67 (38), 10614–10623. doi:10.1021/acs.jafc.9b03430

Niklinski, J., Kretowski, A., Moniuszko, M., Reszec, J., Michalska-Falkowska, A., Niemira, M., et al. (2017). Systematic biobanking, novel imaging techniques, and advanced molecular analysis for precise tumor diagnosis and therapy: the Polish MOBIT project. *Adv. Med. Sci.* 62 (2), 405–413. doi:10.1016/j.advms.2017.05.002

O'Donnell, V. B., Aldrovandi, M., Murphy, R. C., and Krönke, G. (2019). Enzymatically oxidized phospholipids assume center stage as essential regulators of innate immunity and cell death. *Sci. Signal* 12 (574), eaau2293. doi:10.1126/scisignal.aau2293

Okuzumi, A., Hatano, T., Ueno, S. I., Ogawa, T., Saiki, S., Mori, A., et al. (2019). Metabolomics-based identification of metabolic alterations in PARK2. *Ann. Clin. Transl. Neurol.* 6 (3), 525–536. doi:10.1002/acn3.724

Pang, Z., Chong, J., Zhou, G., de Lima Morais, D. A., Chang, L., Barrette, M., et al. (2021). MetaboAnalyst 5.0: narrowing the gap between raw spectra and functional insights. *Nucleic Acids Res.* 49 (W1), W388–W396. doi:10.1093/nar/gkab382

Paynter, N. P., Balasubramanian, R., Giulianini, F., Wang, D. D., Tinker, L. F., Gopal, S., et al. (2018). Metabolic predictors of incident coronary heart disease in women. *Circulation* 137 (8), 841–853. doi:10.1161/CIRCULATIONAHA.117.029468

Philippova, M., Oskolkova, O. V., and Bochkov, V. N. (2019). OxPLs-masking/degradation immune assay: an "all-included" analysis of mechanisms detoxifying oxidized phospholipids. *Eur. J. Lipid Sci. Technol.* 121 (9), 1800511. doi:10.1002/ejlt.201800511

Reuter, S., Gupta, S. C., Chaturvedi, M. M., and Aggarwal, B. B. (2010). Oxidative stress, inflammation, and cancer: how are they linked? *Free Radic. Biol. Med.* 49 (11), 1603–1616. doi:10.1016/j.freeradbiomed.2010.09.006

Slatter, D. A., Percy, C. L., Allen-Redpath, K., Gajsiewicz, J. M., Brooks, N. J., Clayton, A., et al. (2018). Enzymatically oxidized phospholipids restore thrombin generation in coagulation factor deficiencies. *JCI Insight* 3 (6), e98459. doi:10.1172/jci.insight.98459

Solati, Z., Surendran, A., Edel, A., Roznik, M., Allen, D., and Ravandi, A. (2021). Increase in plasma oxidized phosphatidylcholines (OxPCs) in patients presenting with ST-elevation myocardial infarction (STEMI). *Front. Med. (Lausanne)* 8, 716944. doi:10.3389/fmed.2021.716944

Stamenkovic, A., O'Hara, K., Nelson, D., Edel, A., Pierce, G., and Ravandi, A. (2017). Oxidized phosphatidylcholines (OXPC) induce cell death in cardiomyocytes through ferroptosis. *Can. J. Cardiol.* 33 (10), S145–S146. doi:10.1016/j.cjca.2017.07.281

Stevens, T., Zhang, R., Parsi, M., and Feldstein, A. (2012). Serum oxidized phospholipids are increased in pancreatic cancer: 243. *Official J. Am. Coll. Gastroenterology | ACG* 107, S104–S105. doi:10.14309/00000434-201210001-00243

Sung, H., Ferlay, J., Siegel, R. L., Laversanne, M., Soerjomataram, I., Jemal, A., et al. (2021). Global cancer statistics 2020: GLOBOCAN estimates of incidence and mortality worldwide for 36 cancers in 185 countries. *CA Cancer J. Clin.* 71 (3), 209–249. doi:10.3322/caac.21660

Sunnetcioglu, A., Alp, H. H., Sertogullarından, B., Balaharoglu, R., and Gunbatar, H. (2016). Evaluation of oxidative damage and antioxidant mechanisms in COPD, lung cancer, and obstructive sleep apnea syndrome. *Respir. Care* 61 (2), 205–211. doi:10.4187/respcare.04209

Tyurina, Y. Y., Polimova, A. M., Maciel, E., Tyurin, V. A., Kapralova, V. I., Winnica, D. E., et al. (2015). LC/MS analysis of cardiolipins in substantia nigra and plasma of rotenone-treated rats: implication for mitochondrial dysfunction in Parkinson's disease. *Free Radic. Res.* 49 (5), 681–691. doi:10.3109/10715762.2015.1005085

Villaseñor, A., Godzien, J., Barker-Tejeda, T. C., Gonzalez-Riano, C., López-López, Á., Dudzik, D., et al. (2021). Analytical approaches for studying oxygenated lipids in the search of potential biomarkers by LC-MS. *TrAC Trends Anal. Chem.* 143, 116367. doi:10.1016/j.trac.2021.116367

Wong, J. Y. Y., Bassig, B. A., Loftfield, E., Hu, W., Freedman, N. D., Ji, B. T., et al. (2020). White blood cell count and risk of incident lung cancer in the UK biobank. *JNCI Cancer Spectr.* 4 (2), pkz102. doi:10.1093/jncics/pkz102

Xing, F., Saidou, J., and Watabe, K. (2010). Cancer associated fibroblasts (CAFs) in tumor microenvironment. *Front. Biosci. (Landmark Ed.* 15 (1), 166–179. doi:10.2741/3613

Yang, T., Hao, L., Yang, X., Luo, C., Wang, G., Lin Cai, C., et al. (2021). Prognostic value of derived neutrophil-to-lymphocyte ratio (dNLR) in patients with non-small cell lung cancer receiving immune checkpoint inhibitors: a meta-analysis. *BMJ Open* 11 (9), e049123. doi:10.1136/bmjopen-2021-049123

Zabłocka-Słowińska, K., Płaczkowska, S., Skórska, K., Prescha, A., Pawełczyk, K., Porębska, I., et al. (2019). Oxidative stress in lung cancer patients is associated with altered serum markers of lipid metabolism. *PLoS One* 14 (4), e0215246. doi:10.1371/journal.pone.0215246

frontiers | Frontiers in Molecular Biosciences

TYPE Original Research
PUBLISHED 25 April 2024
DOI 10.3389/fmolb.2024.1379631



OPEN ACCESS

EDITED BY
Víctor González-Ruiz,
University of Geneva, Switzerland

REVIEWED BY
Michael Girgis,
George Mason University, United States
Hunter N. B. Moseley,
University of Kentucky, United States

*CORRESPONDENCE
Joanna Godzien,
joanna.godzien@umb.edu.pl

RECEIVED 31 January 2024
ACCEPTED 05 April 2024
PUBLISHED 25 April 2024

CITATION
Sieminska J, Miniewska K, Mroz R, Sierko E, Naumnik W, Kisluk J, Michalska-Falkowska A, Reszec J, Kozlowski M, Nowicki L, Moniuszko M, Kretowski A, Niklinski J, Ciborowski M and Godzien J (2024), First insight about the ability of specific glycerophospholipids to discriminate non-small cell lung cancer subtypes. *Front. Mol. Biosci.* 11:1379631. doi: 10.3389/fmolb.2024.1379631



# First insight about the ability of specific glycerophospholipids to discriminate non-small cell lung cancer subtypes

Julia Sieminska[1], Katarzyna Miniewska[1], Robert Mroz[2], Ewa Sierko[3], Wojciech Naumnik[4], Joanna Kisluk[5], Anna Michalska-Falkowska[5], Joanna Reszec[6], Miroslaw Kozlowski[7], Lukasz Nowicki[8], Marcin Moniuszko[9,10], Adam Kretowski[1,11], Jacek Niklinski[5], Michal Ciborowski[1] and Joanna Godzien[1]*

[1]Metabolomics Laboratory, Clinical Research Centre, Medical University of Bialystok, Bialystok, Poland, [2]2nd Department of Lung Diseases and Tuberculosis, Medical University of Bialystok, Bialystok, Poland, [3]Department of Oncology, Medical University of Bialystok, Bialystok, Poland, [4]1st Department of Lung Diseases and Tuberculosis, Medical University of Bialystok, Bialystok, Poland, [5]Department of Clinical Molecular Biology, Medical University of Bialystok, Bialystok, Poland, [6]Department of Medical Patomorphology, Medical University of Bialystok, Bialystok, Poland, [7]Department of Thoracic Surgery, Medical University of Bialystok, Bialystok, Poland, [8]Altium International Sp. z o. o., Warszawa, Poland, [9]Department of Allergology and Internal Medicine, Medical University of Bialystok, Bialystok, Poland, [10]Department of Regenerative Medicine and Immune Regulation, Medical University of Bialystok, Bialystok, Poland, [11]Department of Endocrinology, Diabetology and Internal Medicine, Medical University of Bialystok, Bialystok, Poland

**Introduction:** Discrimination between adenocarcinoma (ADC) and squamous cell carcinoma (SCC) subtypes in non-small cell lung cancer (NSCLC) patients is a significant challenge in oncology. Lipidomics analysis provides a promising approach for this differentiation.

**Methods:** In an accompanying paper, we explored oxPCs levels in a cohort of 200 NSCLC patients. In this research, we utilized liquid chromatography coupled with mass spectrometry (LC-MS) to analyze the lipidomics profile of matching tissue and plasma samples from 25 NSCLC patients, comprising 11 ADC and 14 SCC cases. This study builds upon our previous findings, which highlighted the elevation of oxidised phosphatidylcholines (oxPCs) in NSCLC patients.

**Results:** We identified eight lipid biomarkers that effectively differentiate between ADC and SCC subtypes using an untargeted approach. Notably, we observed a significant increase in plasma LPA 20:4, LPA 18:1, and LPA 18:2 levels in the ADC group compared to the SCC group. Conversely, tumour PC 16:0/18:2, PC 16:0/4:0; CHO, and plasma PC 16:0/18:2; OH, PC 18:0/20:4; OH, PC 16:0/20:4; OOH levels were significantly higher in the ADC group.

**Discussion:** Our study is the first to report that plasma LPA levels can distinguish between ADC and SCC patients in NSCLC, suggesting a potential role for LPAs in NSCLC subtyping. This finding warrants further investigation into the mechanisms underlying these differences and their clinical implications.

KEYWORDS

**non-small cell lung cancer NSCLC, adenocarcioma ADC, squamous call carcinoma SCC, oxidised glycerophosphatidylcholine oxPC, monoacylglycerophosphatidic acid LPA, lipidomics, metabolomics**

# 1 Introduction

Lung cancer is the most lethal cancer worldwide, causing 1.80 million deaths in 2020 (Bray et al., 2018). Two types of lung cancer are distinguished: non-small cell lung cancer (NSCLC) (85% cases) and small cell lung cancer. The most common histological subtypes of NSCLC are adenocarcinoma (ADC), squamous cell carcinoma (SCC), and large cell carcinoma (LCC). Within the NSCLC subtypes, ADC and SCC are predominant (Wang et al., 2020). ADC represents around 40% of NSCLC cases and is the most frequent subtype of lung cancer in non-smokers (Subramanian and Govindan, 2007; Kenfield et al., 2008; Schabath and Cote, 2019). In this subtype, cancer progression starts from lung glandular cells that produce mucin and surfactants. On the other hand, the SCC subtype, representing around 25% of NSCLC cases, is closely related to smoking and usually originates from the central areas of the lung bronchi (Campbell et al., 2016). Despite sharing several characteristics, they differ in clinical parameters and histopathology. The importance of the precise determination of the NSCLC subtype arises from the available treatment and its potential outcomes, which in turn are related to the presence of particular mutations prevalent in the majority of ADC and are rarely detected in SCC patients (Chen et al., 2019). The presence of mutation facilitates the selection of dedicated treatment, however, only around 60% of ADC and 50%–80% of SCC subjects have known oncogenic driver mutation (Yuan et al., 2019). The presence of these abnormalities allowed to propose several molecular targets for therapy, including vascular endothelial growth factor (VEGF), platelet-derived growth factor (PDGF), epidermal growth factor (EGF), insulin-like growth factor I (IGF-I) or anaplastic lymphoma kinase (ALK) (Ray et al., 2010). However, specific mutations were highly associated with ADC subjects. Moreover, for some therapies, even 60% of patients develop drug resistance (Yuan et al., 2019). As a result, despite availability of new treatments and strategies, still for many NSCLC patients' classic histopathology-based therapies are the choice (Niemira et al., 2019), thus proper NSCLC subtyping is crucial (Ettinger et al., 2017).

Even though there are several findings describing differences between ADC and SCC, non-invasive early diagnostic techniques discriminating ADC and SCC are still not available. Recent lipidomics and metabolomics findings revealed a significant variation in lipids in NSCLC samples (Marien et al., 2015; Chen et al., 2018; Zhang et al., 2019; Fan et al., 2020; You et al., 2020; Jianyong et al., 2021; Kowalczyk et al., 2021).

Lipidomics emerged from metabolomics and can be defined as "the large-scale study of lipid species and their related networks and metabolic pathways that exist in cells or any other biologic system" (Sethi and Brietzke, 2017). Thanks to the untargeted approach, a very wide range of lipids can be analysed also in metabolomics studies. The most frequently used separation technique employed for determining lipid profiles is liquid chromatography (LC) coupled with accurate mass spectrometry (MS) (Fan et al., 2020; You et al., 2020).

In the work of our group, LC-MS-based untargeted metabolomics was implemented to discriminate NSCLC subtypes at different stages of the disease. This work covered patients with chronic obstructive pulmonary disease (COPD) as controls as well as ADC, SCC and LCC subjects in early and late stages. All analyses were performed on plasma and tissue samples, covering tumour and adjacent non-malignant lung tissue employing RP- and HILIC-LC/MS. It is important to highlight that this was not a lipidomics but a metabolomics study; however despite amino acids, most of the identified metabolites were lipids, including fatty acids, carnitines, lyso-glycerophospholipids (LPCs), glycerophospholipids, plasmalogens, sphingomyelins (SMs), and glycerophospho (N-acyl)ethanolamines (Kowalczyk et al., 2021). Fan et al. performed RP-LC/MS analyses over the lung cancer tissue and benign lung tissue, both paired with distal noncancerous tissue from the same patient. They reported and described changes in the lipid profile of lung cancer but also provided receiver operating characteristic (ROC) curve analysis of combinational lipid markers to assist in the disease diagnosis (Fan et al., 2020). A similar design was used by You et al., who also analysed the lung cancer tissue and benign lung tissue and paired distal and adjunct noncancerous tissue. They employed RP-LC/MS to explore metabolic reprogramming of lung cancer and to distinguish NSCLC subtypes. They found changes among different metabolite classes associated with the alterations in energy and purine metabolism, biosynthesis of amino acids, membrane lipid metabolism, and glutamine and cysteine and methionine metabolism (You et al., 2020). Zhang et al. used MS imaging to discriminate between post-operative NSCLC tumours and paired normal tissues. This research covered also the recognition of mutations of epidermal growth factor receptor (EGFR), which is crucial from a diagnostic and therapeutic perspective. Glycerophospholipids were found to differentiate between ADC and SCC subtypes, but also between EGFR-mutated-positive and EGFR-wild-type tissue (Zhang et al., 2019). Marien et al. used direct infusion and 2D-imaging MS to profile glycerophospholipids in malignant and non-malignant lung tissue of NSCLC patients. Their results revealed decreased levels of sphingomyelins and glycerophosphoserines (PSs) and elevated levels of glycerophosphoinositols (PIs), glycerophosphoethanolamines (PEs) and glycerophosphocholines (PCs) (Marien et al., 2015).

All these publications pointed to the alterations in the lipid profile, including glycerophospholipids. Glycerophospholipids are

10.3389/fmolb.2024.1379631

susceptible to oxidation, and oxidative stress was reported as one of the underlying processes accompanying NSCLC; therefore, in our previous study, we decided to explore the profile of oxidised glycerophosphocholines (oxPCs) in lung cancer patients (Godzien et al., 2024). We proved, that these early oxidation products are altered in the NSCLC patients in comparison to COPD controls. In this companion paper, we decided to explore oxPCs changes deeper, making direct comparison between NSCLC subtypes but also combining information about oxPCs with lipid profiles of SCC and ADC patients. Considering the high interconnectivity between distinct lipid classes along with the fact that oxidised lipids originate from the native, non-oxidised lipids, we believed that such a strategy can benefit in data interpretation.

OxPCs are currently deeply investigated since their role went beyond oxidation by-products, and nowadays, they are recognised as important molecules with multiple functions. They were associated with cardiovascular diseases (Paynter et al., 2018), diabetes (Godzien et al., 2019), neurogenerative disorders (Okuzumi et al., 2019) and cancer (López-López et al., 2020). Oxidation of PCs can lead to the formation of different types of epi-lipids, a subset of the natural lipidome formed by either enzymatic or non-enzymatic modifications such as, e.g., oxidation, nitration, or sulfation with their own biological functions. oxPCs cover mildly oxidised long-chain oxPCs (LCh-oxPCs), truncated short-chain oxPCs (SCh-oxPCs), and cyclised oxPCs. These molecules have different structures and, therefore, different bio-activities: each group of oxPCs can have a distinct function, or they might have contradictory effects. Moreover, pleiotropic functions of oxPCs were also observed. Because of this, exploration of the involvement of oxPCs in different pathologies is so important.

As pointed above, NSCLC is the most lethal, and, therefore, one of the most frequently studied cancer; however, despite all available knowledge, new diagnostic tools are needed. To propose valid and reliable methods for unequivocal subtypes discrimination, we need to explore and understand metabolic alterations underlying the ADC and SCC. In this study, we have focused on identification of lipids, including oxPCs, in plasma and tissue samples that would allow discrimination between the SCC and ADC subtypes.

TABLE 1 Basic clinical parameters characterising three cohorts of patients enrolled in the study.

| Plasma metabolic fingerprinting whole cohort/subcohort | | | |
|---|---|---|---|
| Patients' characteristic | NSCLC | ADC | SCC |
| Age [years] (median) | 63.0/62.0 | 62.0/62.0 | 63.5/61.0 |
| Q1 | 58.0/56.0 | 58.0/55.5 | 58.8/56.5 |
| Q3 | 69.0/66.0 | 68.0/67.5 | 69.0/65.8 |
| BMI (median) | 25.47/24.69 | 25.99/25.00 | 25.4/24.07 |
| Q1 | 23.62/23.50 | 24.17/23.9 | 23.4/23.3 |
| Q3 | 27.76/26.00 | 28.09/25.7 | 27.23/25.9 |
| Gender [F/M] | [29/72]/[5/20] | [15/26]/[3/8] | [14/46]/[2/12] |
| pTNM | | | |
| IIA | 24/6 | 8/4 | 16/2 |
| IIB | 33/13 | 9/5 | 24/8 |
| IIIA | 18/6 | 8/2 | 10/4 |
| **Tumour tissue metabolic fingerprinting whole cohort/subcohort** | | | |
| Patients' characteristic | NSCLC | ADC | SCC |
| Age [years] (median) | 63.0/63.0 | 62.0/62.0 | 63.5/63.5 |
| Q1 | 56.0/56.0 | 55.0/55.5 | 57.5/59.3 |
| Q3 | 69.0/69.0 | 69.0/67.5 | 69.0/68.3 |
| BMI (median) | 24.93/25.00 | 25.00/25.00 | 24.53/25.06 |
| Q1 | 23.41/23.83 | 23.53/23.90 | 23.39/23.91 |
| Q3 | 26.09/25.69 | 26.37/25.73 | 25.98/25.60 |
| Gender [F/M] | [13/48]/[7/18] | [6/19]/[3/8] | [7/29]/[4/10] |
| pTNM | | | |
| IIA | 21/5 | 9/3 | 12/2 |
| IIB | 20/10 | 8/5 | 12/5 |
| IIIA | 20/10 | 8/3 | 12/7 |

pTNM, pathological tumour-nodemetastasis. For pTNM staging number of patients assigned to given stage is provided for the whole cohort and subcohort.

# 2 Materials and methods

## 2.1 Chemical and reagents

Ultrapure water was used to prepare all the aqueous solutions and was obtained "in-house" from a Milli-Q Integral three system (Millipore, SAS, Molsheim, France). Zomepirac sodium salt, formic acid, LC-MS-grade methanol and acetonitrile, and LC-grade ethanol were purchased from Sigma-Aldrich Chemie GmbH (Steinheim, Germany).

## 2.2 Cohort study

Samples were obtained from patients undergoing surgical treatment for primary NSCLC at the Thoracic Surgery Department of Medical University of Bialystok Clinical Hospital in Poland. The study was approved by the Ethics Committee of the Medical University of Bialystok (R-I-003/262/2004, R-I-002/296/2018 and APK 002 5 2021) and performed in accordance with the Declaration of Helsinki. Before collecting the samples, written informed consent for specimen collection was obtained from all participants.

In this project we included 122 tissue samples collected from 61 NSCLC patients. There were two tissue samples per patient: tumour tissue and adjacent non-malignant control tissue. Among these 61 patients, 25 were classified as ADC and 36 as SCC subjects. Plasma analyses covered samples collected from 101 NSCLC patients, among which 41 were diagnosed with ADC and 60 with

SCC. Analyses of clinical records revealed that 25 patients were common between the plasma and tissue cohorts, covering 11 ADC and 14 SCC subjects. In this study, we focused on these 25 subjects, performing joined analyses of plasma and tissue lipids. Basic clinical parameters describing the available cohort and selected sub-cohort are summarised in Table 1.

Whole blood was collected in 9 mL vacuum system tubes with $K_2$EDTA as an anticoagulant. After gentle mixing, plasma was separated by centrifugation at 1300 *g* for 20 min at room temperature. Plasma fractions (0.5 mL each) were then collected in Eppendorf tubes and stored at −80°C until analysis.

Collected tissue samples were histologically reviewed and classified. After lung tumour resection, whole specimen was examined macroscopically by the pathologist to determine the exact tumour localization, presence or absence of macroscopic residual tumour, presence or absence of macroscopic infiltration of pulmonary pleura, macroscopic evaluation of possible presence of necrosis in the tumour centre. The pathologist cut the exact tissue samples that represent the tumour centre and tumour margin. Moreover, the pathologist determined the possibility to collect adjacent pulmonary tissue (referred as normal tissue): if the distance from the tumour border was greater than 2 cm, the pathologist cut the samples of adjacent tissue. Then, immediately after resection, study nurses from the Biobank put the tissue samples alternately into cryotubes for vapor phase of liquid nitrogen (fresh frozen samples) and into tubes with 10% buffered formalin (formalin-fixed samples). The exact time of resection start, vessel ligation, resection end, and tissue sample preservation were recorded and documented. The details of tissue samples collection in the clinical setting–macroscopic evaluation resected specimens were described previously (Ciereszko et al., 2022), together with the biobanking conditions and Standard Operating Procedures (Niklinski et al., 2017; Michalska-Falkowska et al., 2023). Cancer stages were determined following pathological tumour-node-metastasis (pTNM) staging. All tissue samples were frozen and stored at −80°C until the day of analyses. Sample collection, quenching and storage were performed following approved biobanking standards (Niklinski et al., 2017).

## 2.3 Sample preparation

Plasma samples were prepared using the previously described method (Daniluk et al., 2019). On the day of analysis, samples were thawed on ice. For protein precipitation and metabolite extraction, one plasma sample volume was mixed with three volumes of ice-cold methanol/ethanol (1:1) containing 1 ppm of Zomepirac (internal standard IS). After extraction, samples were stored on ice for 10 min and centrifuged at 21,000 × *g* for 20 min at 4°C. The supernatant was filtered into a glass HPLC-vial through a 0.22 µm nylon filter (ThermoFisher Scientific, Waltham, Massachusetts, United States of America).

Tissue samples were prepared following the previously described method (Ciborowski et al., 2017). On the day of analysis, samples were thawed on ice. Ten milligrams of lung tissue sample were placed in an Eppendorf tube with two stainless steel beads (5 mm) and 200 µL of ice-cold 50% methanol. Samples were homogenised for 8 min at 30 Hz using Tissue Lyser (LT; Qiagen Hilden, Germany). After homogenisation, beads were removed and 200 µL of ice-cold acetonitrile containing 1 ppm of IS was added to the sample. Metabolites were extracted by vortex-mixing the samples for 1 hour. After extraction, samples were centrifuged at 21,000 × *g* for 20 min at 20°C. After centrifugation, the supernatant was filtered through a 0.22 µm nylon filter (ThermoFisher Scientific, Waltham, Massachusetts, United States of America). Extraction blank was prepared following the same procedure as biological samples, but without tissue, and was analysed together with biological samples.

Quality control (QCs) samples were prepared by mixing equal volumes of all raw plasma samples and all extracts for tissue samples. QCs were treated like the rest of the samples and injected at the beginning of the batch (10 injections) to equilibrate the system and every ten samples further to monitor the stability of the measurement (Godzien et al., 2014).

## 2.4 Analytical set-up

Plasma analyses were performed using a 6546 iFunnel ESI-Q-TOF (Agilent Technologies, Germany) coupled with a 1290 Infinity UHPLC system (Agilent Technologies, Germany) with a degasser, quaternary pump and thermostated autosampler.

Tissue analyses were performed using a 6545 iFunnel ESI-Q-TOF (Agilent Technologies, Germany) coupled to a 1290 Infinity UHPLC system (Agilent Technologies, Germany) with a degasser, binary pump and thermostated autosampler.

Plasma and tissue samples were analysed in both polarity modes. During all analyses, two reference compounds were used: *m/z* 121.0509 (protonated purine) and *m/z* 922.0098 (protonated hexakis (1H,1H,3H-tetrafluoropropoxy)phosphazine (HP-921)) for positive ionisation mode and *m/z* 112.9856 (proton abstracted trifluoroacetic acid anion) and *m/z* 966.0007 (formate adduct of HP-921) for negative ionisation mode. These masses were continuously infused into the system to allow internal constant mass correction during data acquisition.

## 2.5 Metabolic profiling

### 2.5.1 Plasma analyses

Four microliters of each sample were injected into a thermostated at 60°C Zorbax Extend C18 column (RRHT 2.1 × 50 mm, 1.8 µm Agilent Technologies, Santa Clara, California, United States of America). The flow rate was 0.6 mL/min with solvent A (water with 0.1% formic acid) and solvent B (acetonitrile with 0.1% formic acid). The chromatographic gradient started at 50% of phase B, then increased the amount of phase B to 80% (from 1 to 6 min) and 100% (from 6 to 8 min). Finally, the system was re-equilibrated by reverting phase composition to initial conditions (50% phase B) in 0.5 min, which was kept from 8.5 to 10 min. The mass spectrometer was operated in full scan mode. Data were acquired at *m/z* ranging from 50 to 1,000 at the scan rate of 1.0 scans per second. Nebulizer pressure was set at 52 psig, nozzle voltage at 1,000 V, and capillary voltages at 3,000 and 4,000 V in the positive and negative ion mode, respectively.

All samples were analysed in scan mode in both polarity modes. Then, a subset of 70 samples was analysed in negative ion mode using iterative exclusion data-dependent analysis (IE-DDA). Precursor ions

were fragmented using ramped collision energy, adjusted for each molecule according to its *m/z*. The first injection was performed as a conventional data-dependent MS/MS analysis, where the top three most abundant precursors were selected for fragmentation, considering active exclusion lists. In subsequent injection, precursors selected for MS/MS fragmentation in the previous injection were excluded on a rolling basis with 20 ppm mass error tolerance and 0.5 min retention time tolerance. Five iterative-MS/MS runs were set for each sample, resulting in 350 measurements.

### 2.5.2 Lung tissue analyses

One µL of the extracted sample was injected into a thermostated at 60°C Zorbax Eclipse Plus C8 column (RRHD 2.1 × 150 mm, 1.8 µm Agilent Technologies, Santa Clara, California, United States of America). The flow rate was 0.6 mL/min with solvent A (water with 0.1% formic acid) and solvent B (acetonitrile with 0.1% formic acid). The gradient started at 25% phase B and increased to reach 95% of phase B in 14 min. This proportion was kept for 1 min, and after that, the gradient returned to starting conditions (25% phase B) in 0.1 min and was maintained for 4.9 min to re-equilibrate the system before the next injection. The mass spectrometer was operated in full scan mode from *m/z* 50 to 1,000. The capillary voltage was set to 3,000 V for ESI+, and 4,000 V for ESI- mode; the drying gas flow rate was 12 L/min, temperature 250°C and gas nebuliser 52 psig. Fragmentor voltage was 250 V for both ESI modes.

## 2.6 Determination of protein content in lung tissue

The precipitated proteins were suspended in radioimmunoprecipitation assay (RIPA) buffer and then denatured at 60°C and sonicated for 30 min in a water bath. The samples were then centrifuged for 15 min at 14,000 × *g*. Protein concentration was measured with the Pierce BCA Protein Assay Kit (Thermo Fisher Scientific) according to the included protocol.

## 2.7 Data processing

### 2.7.1 Plasma metabolic profiling

Plasma data was reprocessed twice: searching for oxPCs and for other lipids. MS1 data were reprocessed using a targeted approach and searching solely for oxPCs (Godzien et al., 2019). Data from iterative exclusion data-dependent analyses were used to confirm the annotation of oxPCs. For this, we searched for known fragmentation patterns (Gil de la Fuente et al., 2018). Moreover, all annotations were confirmed using retention time (RT) to compare the elution order between different oxPCs and their non-oxidised precursors. The list of 45 oxPCs was defined, covering 13 LCh-oxPCs and 32 SCh-oxPCs (including iso-forms). RT and mass data pairs were used as input criteria to find oxPCs. Processing was performed using an algorithm "Find by Ion" in Mass Hunter Profinder software (Agilent, B.10.00). The integration of all extracted peaks was manually curated and corrected if necessary.

Data from IE-DDAs were reprocessed using the untargeted approach in Lipid Annotator software (Agilent, B.01.00). For lipid annotation, a fragmentation-based (MS/MS) library was used. The resulting data comprise the *m/z* of all the precursors identified as lipids, their corresponding RT, and their classification into lipid categories and classes. During the reprocessing, allowed ions covered $[M\text{-}H]^-$, $[M + HCOOH\text{-}H]^-$, and $[M + Cl]^-$. The Q-Score was set at ≥ 50, the mass deviation was established as ≤ 20 ppm, the fragment score threshold was fixed as ≥ 30, and the total score was set at ≥ 60. The list of annotated lipids was then used in Mass Hunter Profinder software (Agilent, B.10.00) for the targeted search, where a sophisticated algorithm searched selected ions across MS1 data. Data were reprocessed considering ions $[M + H]^+$, $[M + Na]^+$, $[M + K]^+$, $[CHNaO_2]^+$ and $[C_2H_2Na_2O_4]^+$ in positive ionisation mode and $[M\text{-}H]^-$, $[M + HCOO]^-$, $[M + Cl]^-$, $[C_2HF_3O_2]$, $[C_3H_2F_3NaO_4]$ in negative ionisation mode. Neutral loss of $[C_2H_4O_2]$ and $[CH_3]$ was used in negative ion mode, while water loss was considered in both polarities. The maximum permitted charge state was double. Alignment was performed based on *m/z* and RT similarities within the samples. Parameters applied were 0.5% and 0.20 min for the RT window and 20 ppm and 2 mDa for mass tolerance. These were selected based on the assessment of raw data.

### 2.7.2 Tissue metabolic profiling

Raw data was reprocessed, searching for oxPCs implementing the targeted approach (Godzien et al., 2019). The list of 45 oxPCs was defined, covering 13 LCh-oxPCs and 32 SCh-oxPCs (including iso-forms). Annotation of these oxPCs was done in previous projects based on the data-independent analysis (DIA), and incorporated into in-house built library. RT and mass data pairs of annotated oxPCs were used as input criteria to search them in MS1 data. Processing was performed using the same algorithm "Find by Ion" in Mass Hunter Profinder software (Agilent, B.10.00) as described above. The integration of all extracted peaks was manually curated and corrected if necessary.

## 2.8 Data analysis

The acquired data underwent evaluation through a Quality Assurance procedure. Lipids displaying a Relative Standard Deviation (RSD) of signals in QC samples below 30% were considered reliably measured and retained for subsequent analyses. An additional filter was applied to keep signals detected in at least 75% of samples in at least one sample group.

Before the statistical analyses, reprocessed data were normalised. Data from plasma analyses were normalised solely to the internal standard to minimise analytical drift. Data from tissue analyses were normalised to the internal standard and the protein content to minimise differences between different pieces of tissue.

Data analyses were done over each matrix, matching the patients, plasma, and tissue samples. Statistics were computed by comparing ADC and SCC subtypes. Differences between compared groups were described with *p*-value and percentage of change, where a positive value indicated an increase in ADC patients compared to the SCC patients, while a negative value illustrated a decrease of the signal in ADC patients compared to the SCC patients. Furthermore, we calculated the median, Q1 and Q3 for the level of each oxPC for each comparison (Table 2). Percentage of change, median, Q1 and Q3 were computed using Excel (Microsoft). *p*-value was computed employing a non-parametric Mann-Whitney test and then corrected by applying Benjamini–Hochberg FDR using in-house-built Matlab

TABLE 2 Lipids discriminate significantly between plasma and tumor tissue samples from ADC and SCC patients.

| Compound | raw *p*-value (corrected *p*-value) | Gini importance score | % of change | ADC | SCC |
|---|---|---|---|---|---|
| | | | | Median (Q1-Q3) | |
| tumour tissue | | | | | |
| PC 16:0/4:0; CHO | 0.0331 (0.1214) | 0.1088 | −59.3 | 0 (0–546) | 497 (399–609) |
| PC 16:0/18:2 | 0.0231 (0.1214) | 0.1245 | +40.5 | 184,585 (172,541–226,863) | 113,284 (91,216–162,270) |
| plasma | | | | | |
| PC 16:0/20:4; OOH | 0.0068 (0.0466) | 0.0944 | +25.1 | 182,738 (159,665–218,149) | 136,157 (118,852–152,437) |
| PC 18:0/20:4; OH | 0.0199 (0.0466) | 0.0904 | +74.7 | 260,157 (212,240–311,125) | 188,303 (133,987–225,592) |
| PC 16:0/18:2; OH | 0.0172 (0.0466) | 0.1039 | +95.4 | 244,459 (213,149–444,861) | 157,436 (118,621–236,128) |
| LPA 18:1 | 0.0172 (0.0862) | 0.0934 | −59.3 | 15,060 (13,913–18,269) | 23,460 (17,022–41,625) |
| LPA 18:2 | 0.0306 (0.0982) | 0.0965 | −37.5 | 15,713 (12,755–16,926) | 23,896 (19,512–33,909) |
| LPA 20:4 | 0.0040 (0.0405) | 0.1476 | −88.7 | 15,689 (13,393–26,941) | 87,239 (36,585–321,949) |

+means an increase in ADC, group in comparison to SCC, group.
- means a decrease in ADC, group in comparison to SCC, group. % of change and median (Q1-Q3) are provided for the signal intensity for a given lipid.

scripts (version 2020a, Mathworks, Natick, MA, United States of America). FDR was performed only for metabolites with the absolute percentage of change equal or greater than 25%. Random Forest analysis was performed using the in-house-written code in RStudio software (version 2023.12 + 369, PBC, Boston, MA, United States of America). Used Matblab scripts and R code are provided in the Supplementary Material (Data Sheet 2). The ROC curve analysis was used to test the discriminating metabolites as potential biomarkers and to evaluate their performance. Areas under the curve (AUCs) were calculated by implementing Random Forest in MetaboAnalyst (version 5.0).

## 2.9 Pathway analysis

Pathway analysis was performed based on the LIPID MAPS® reaction explorer. Different lipid species were linked based on the reactions from various sources, including scientific literature, the lipid research community, and other existing databases such as Rhea, WikiPathways, KEGG, Ecocyc, and MetaCyc. In the analysis, we included all detected and annotated lipids.

# 3 Results and discussion

## 3.1 General concerns

Baseline characteristics of ADC and SCC patients is summarised in Table 1. Enrolled subjects were matched in basic anthropometric measurements, and no between-group statistical differences were observed. The only concern is with the lack of gender balance since more men than women were enrolled. However, this corresponds to a greater number of diagnosed men than women at the time of sample collection.

All samples were analysed in both polarity modes. Metabolite annotation was performed using information acquired in negative ion mode since this polarity provides more details, such as the exact composition of fatty acids. Statistical analysis was performed on the data acquired in positive ion mode because more abundant and, therefore, more reproducible signals for oxPCs were obtained in this polarity mode (Godzien et al., 2024).

Analyses performed for 122 tissue samples collected from 61 NSCLC patients, covering two samples per patient: adjacent non-cancerous lung tissue and lung tumour tissue, allowed measurement and annotation of 16 oxPCs: 15 SCh-oxPCs and only 1 LCh-oxPCs. Analyses performed for 101 plasma samples allowed measurement and annotation of 13 oxPCs: 5 SCh-oxPCs and 8 LCh-oxPCs. Automatic annotation based on IE-DDA provided information about 120 plasma lipids, covering: 17 sphingolipids (2 ceramides (Cer) and 15 SMs), 54 monoacylglycerophospholipids (5 LPAs, 30 LPCs, 14 LPEs, 4 LPIs and 1 LPGs), 31 diacylglycerophospholipids (17 PCs, 9 PEs, 4 PIs and 1 PSs), 11 ether-glycerophospholipids (4 ether PCs and seven ether PEs) and seven fatty acids. Although the maximum allowed error for annotation was set to 20 ppm, the greatest mass error was 1.3 Da, with the average error for all 294 annotated lipids of 0.36 Da. The obtained matrix contained 8% of missing values which were present only in 12 out of 165 features.

## 3.2 Differences in the lipid profile between ADC and SCC subjects

In recent years, lipidomics (especially the untargeted approach) has emerged as a promising tool for medicine, allowing the selection

10.3389/fmolb.2024.1379631

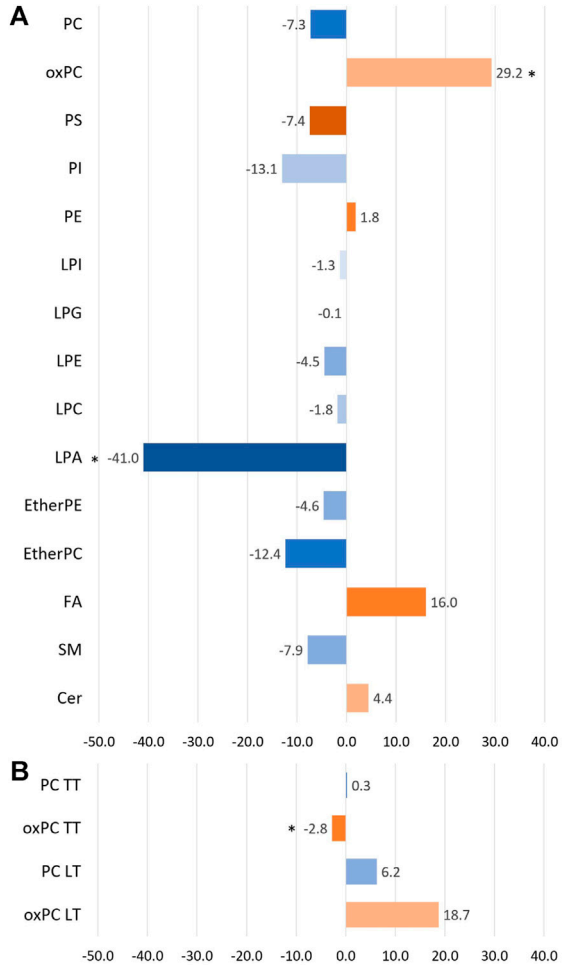


FIGURE 1
The bar plot illustrates the percentage of averaged change between the ADC and SCC patients across the different lipid classes. Panel **(A)** portraits the changes observed in plasma samples, while panel **(B)** shows the changes observed for tumour tissue samples (TT) and healthy lung tissue (LT). A negative value means a decrease in the ADC group compared to the SCC group (marked with bluish colours), and a positive value reflects an increase in the ADC group compared to the SCC group (marked with orangish colours). * indicates the groups of lipids for which observed changes were statistically significant.

of potential biomarkers but also providing insight into the mechanisms underlying different diseases. For this reason, we decided to apply the LC-MS method to search for lipids differentiating main NSCLC subtypes.

We analysed tissue and plasma samples collected from patients diagnosed with ADC or SCC. Univariate Mann-Whitney analysis, followed by Benjamini–Hochberg post-correction, allowed the selection of eight discriminating variables, which are listed in Table 2. We focused on lipids, for which the raw *p*-value was below 0.05. However, considering that the corrected *p*-value was not significant for all of these lipids, we decided to support the statistical evaluation of pre-selected variables by Random Forest and ROC analysis. The given lipid was considered statistically significant if it met three conditions: the *p*-value was below 0.05 and ranked in the top 20 variables according to the Gini score (Table 2), and the AUC for ROC was above 0.75. Random Forest analysis performed for 2000 trees resulted in the model with an out-of-bag (OOB) error rate of 0.32. Among the top 20 most important variables were all eight significant lipids: four of them were in the top 10.

All statistically significant lipids belong to glycerophospholipids. As far as plasma samples are concerned, we found differences in the level of several oxPCs and LPAs. In non-malignant lung samples, there were no discriminating lipids, while in tumour tissue samples, the only lipids discriminating these two subtypes were PC 16:0/18:2 and PC 16:0/4:0; CHO.

Before discussing discriminating lipids, we want to comment on the lipid profile obtained for NSCLC patients. Averaged changes observed for each lipid class are graphically represented in Figure 1. Only three types of lipids, marked with the asterisk, were found to be statistically different between the two lung cancer subtypes. However, as can be noticed, some of the changes, despite their magnitude, are not significant. Not all lipids belonging to a particular class exhibited the same direction of change.

For this reason, we visualised the data and compared the number of individual lipid species in each class that was increasing and decreasing in the ADC compared to the SCC group. Results of this visualisation are presented in Panel A of Figure 2. The first observation leads to the conclusion that most noted changes correspond to the decrease of the signal in ADC patients. It is the case of SMs, plasma PCs, PI, PS, etherPCs and etherPEs, LPA and LPG. An increased signal was observed for oxPCs in healthy lung tissue; however, this change was insignificant for oxPCs in plasma samples. Very different changes, corresponding almost equally to both the increase and the decrease of the signal, were observed mainly for FAs, LPEs, LPIs, PEs, and tumour tissue PCs. Panel B of Figure 2 illustrates the average signal for lipids belonging to a particular class for ADC patients (brown colour) and SCC subjects (green colour). It is essential to highlight that this data can be used to compare ADC and SCC subjects within a given lipid group. A comparison of absolute values for lipids measured in tissue and plasma cannot be performed. This data corresponds to the measured signal and not the total quantitative value. Observed averaged changes are in concordance with the direction of change of lipids: SMs, plasma PCs, PI, PS, etherPCs and etherPEs, LPA and LPG are reduced in ADC patients in comparison to the SCC subjects, while in plasma oxPCs, PCs detected in healthy lung tissue and Cer the signal is higher in ADC patients.

A comparison of NSCLC patients showed that PC 16:0/18:2 was increased in ADC group in comparison to SCC group, and PC 16:0/4:0; CHO was decreased in ADC group compared to SCC group (Figure 3).

Analysis of plasma samples showed a higher number of significant metabolites as compared to tissue results. All differentiating lipids belong to two classes of glycerophospholipids, namely, LPAs and oxPCs. A comparison of NSCLC patients showed that the levels of LPA 20:4, LPA 18:1, and LPA 18:2 in ADC group were significantly decreased compared with SCC, whereas the levels of PC 16:0/18:2; OH, PC 18:0/20:4; OH, PC 16:0/20:4; OOH were significantly increased (Figure 4).

To illustrate the connectivity of measured lipids, we performed pathway analysis. Because lipids, especially complex, are poorly

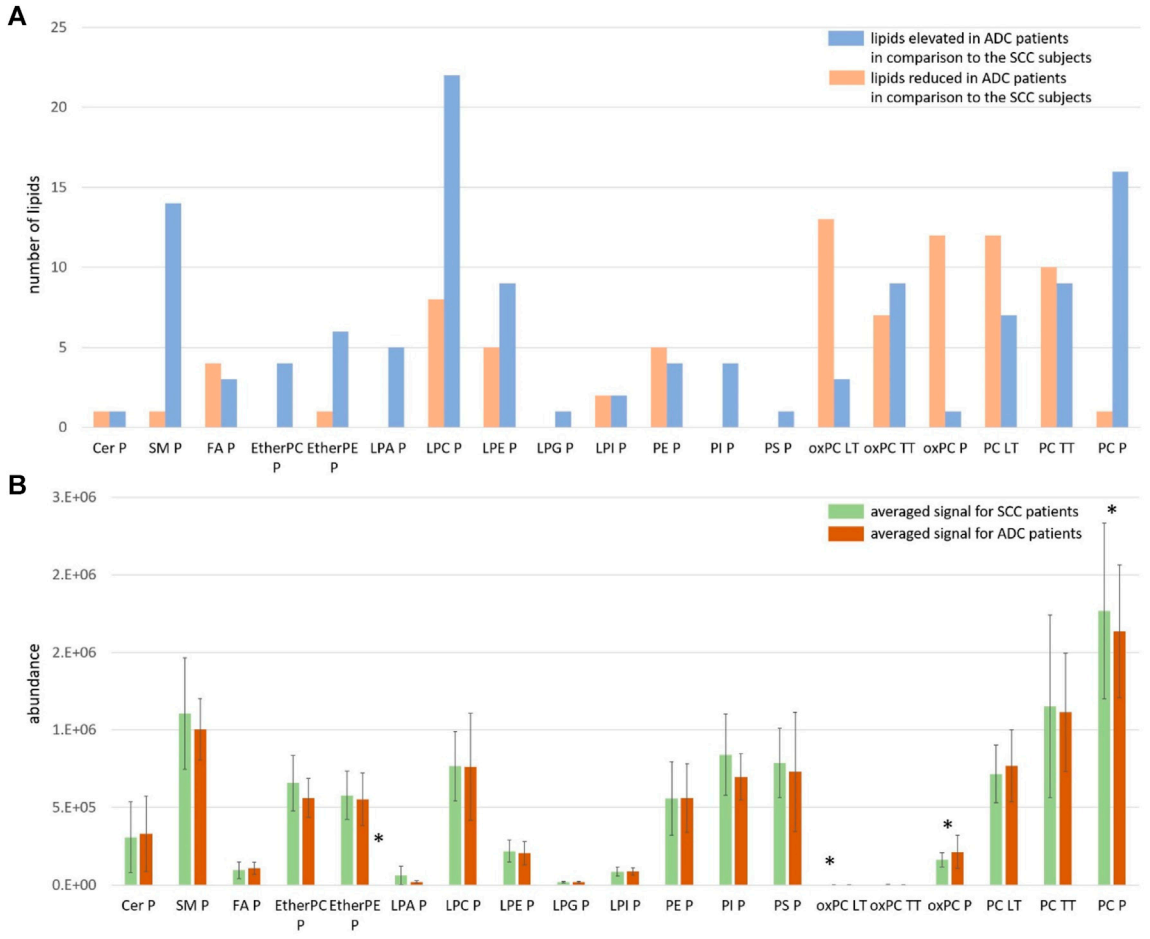


FIGURE 2
Panel **(A)** The number of measured and identified lipids for each class, assigned as elevated (orange colour) and reduced (blue colour) in ADC patients in comparison to the SCC subjects; Panel **(B)** The averaged signal for lipids belonging to each class measured for SCC patients (green colour) and ADC patients (brown colour). The y-axes in the graph represent the abundance of metabolites. The whiskers show the standard deviation of the averaged signal. * indicates the groups of lipids for which observed changes were statistically significant; LT: healthy lung tissue; TT: tumour tissue; P: plasma.

represented in "classic" pathways, we decided to use LIPID MAPS® reaction explorer to connect detected lipids into a network. Lipids were represented as a class instead of individual species. Figure 5 shows the results of this analysis. To build this network, we used all measured lipids marked with grey dotted circles, while the statistically significant lipids were annotated with red dotted circles. All other lipids were kept to maintain the connectivity between other lipid classes.

## 3.3 Implications of found lipid profile differences between ADC and SCC subjects

In order to provide better differential diagnosis and treatment methods, the discovery of molecular patterns of different lung cancer subtypes is needed. Thus, analysis of tissue samples seems to be a key to explore metabolic changes occurring at the site of the action where tumour development and growth occur. On the other hand, plasma samples must be also included since they are minimally invasively collected and routinely used in diagnostics.

In our study, we found the elevated level of PC 16:0/18:2 in tissue samples in ADC compared to SCC patients. It is in line with our previous research where tissue levels of PCs were increased in ADC (compared to SCC) (Kowalczyk et al., 2021). Other researchers also studied differences in lipidome of tumour samples between NSCLC subtypes, and some of the findings are in line with our results. Fan et al. observed elevated levels of PC 18:1_20:4, Cer d18:1/26:0, and several PEs and diradylglycerols (DGs) in ADC compared to SCC (Fan et al., 2020). Direct comparison of these results with our data is impossible, because the method we applied did not allow detection of either Cer or DG. Zhang et al. obtained similar results as they found the increased intensity of PC 34:0 in ADC compared to SCC (Zhang et al., 2019). Although PC 18:1_20:4 and PC 34:0 have different compositions of fatty acids than PC 16:0/18:2 we detected, all these molecules belong to the same lipid class and behave similarly. In contrast, You et al. found a lower level of PC 38:2 in ADC than in SCC samples. They also noted different tendencies in lipidome alterations, depending on the lipid class: PCs (LPC 20:1 and PC 38:2), free fatty acids (FAs) (FA 22:1 and FA 24:1) and carnitines (CARs) (CAR 2:0 and CAR 3:0) exhibited higher levels, while PEs (LPE 16:0 and PE 34:3), SM 35:2, and CAR 18:1 showed

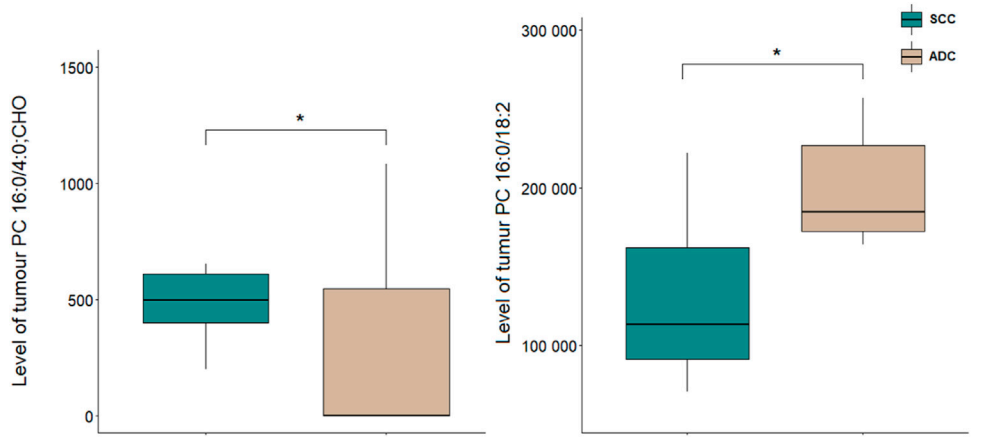


FIGURE 3
Levels of lipid discriminating between tumour tissue samples of ADC and SCC sam-ples. *$p < 0.05$. The $y$-axes in the graph represent the abundance of metabolites. The whiskers show the minimum and maximum values. The bottom and top of the box are the 25$^{th}$ and 75$^{th}$ percentiles, and the line inside the box is the 50$^{th}$ percentile (median).

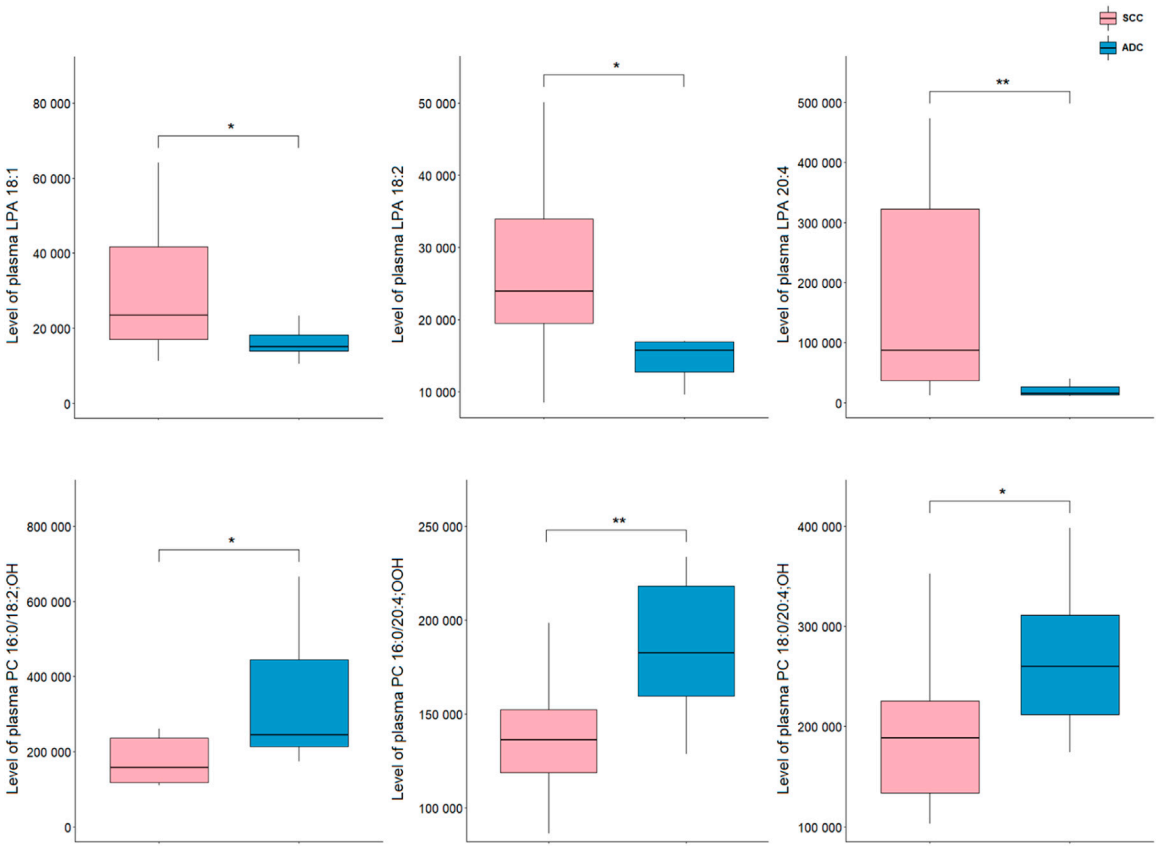


FIGURE 4
Levels of lipid discriminating between plasma samples of ADC and SCC samples. *$p < 0.05$; **$p < 0.01$. The $y$-axes in the graph represent the abundance of metabolites. The whiskers show to the min and max values. The bottom and top of the box are the 25$^{th}$ and 75$^{th}$ percentiles, and the line inside the box is the 50$^{th}$ percentile (median).

lower levels in ADC than in SCC (You et al., 2020). Our dataset contains six FAs, but none of them was found significantly different. However, despite the lack of significance, we observed a decrease in the signals of unsaturated FAs (FA 16:1, FA 18:1, FA 18:2, FA 18:3) and a very slight increase in the signals of saturated FAs (FA 16:0 and FA 18:0). Marien et al. discovered that eight phospholipids,

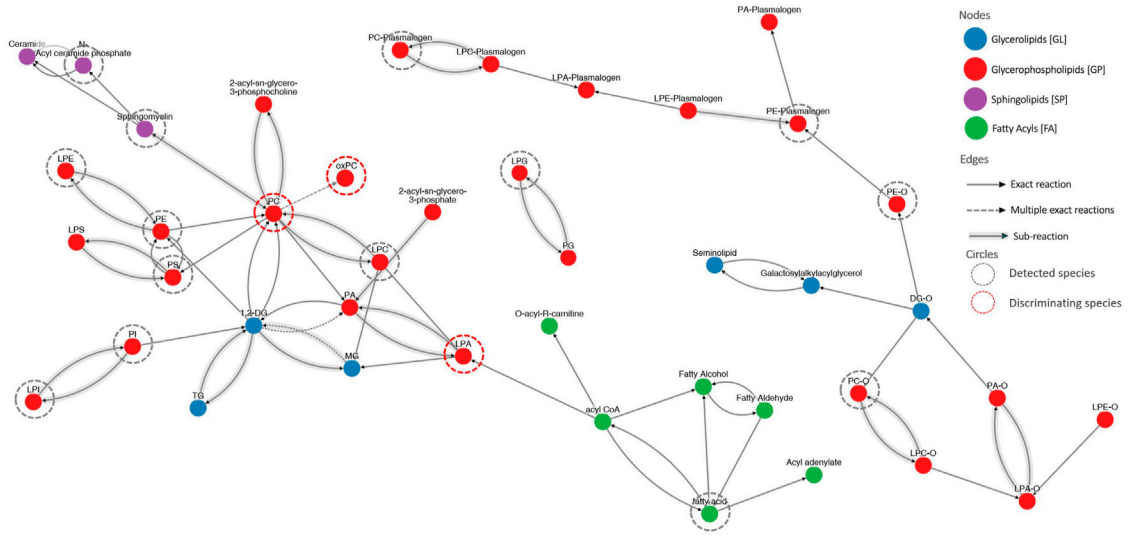


FIGURE 5
The visualization of lipid connectivity is based on the biochemical reactions and metabolic pathways involving lipids. Lipids were linked into a network employing the LIPID MAPS® reaction explorer. To build this network, we used all measured lipids marked with grey dotted circles, while the statistically significant lipids were annotated with red dotted circles. All other lipids were kept to maintain the connectivity between other lipid classes.

including PC, (PC 40:2, PE 42:2, PE 44:5, PI 36:3, PI 36:4, PS 40:8, PS 42:9, SM 36:2) discriminated ADC and SCC, although the direction of change was not mentioned; therefore, a more detailed comparison of this results with our findings is not possible (Marien et al., 2015).

To the best of our knowledge, this study is the first to show significant differences in the level of several plasma LPAs between ADC and SCC patients. Patients suffering from ADC exhibited significantly higher levels of LPA 18:1, LPA 18:2, and LPA 20:4 than those diagnosed with SCC. LPAs originate from LPCs by the action of extracellular autotaxin (ATX) (Xie and Meier, 2004). ATX was found in many body fluids, e.g., plasma or malignant effusions (Tokumura, 2002). So far, there have been seven LPA receptors discovered (Gardell et al., 2006; Lin et al., 2010). LPAs act through activating cell proliferation, differentiation and migration, playing an important role in wound healing (van Corven et al., 1989; Willier et al., 2013; Aiello and Casiraghi, 2021). To date, many findings have shown overexpression of ATX in different pathological conditions, especially in different types of cancer (Yang et al., 2002; Kehlen et al., 2004; Wu et al., 2010). Elevated expression of ATX results in increased LPAs levels which are associated with tumour severity. Among patients with hepatocellular cancer, those with metastasis were characterized with higher serum LPAs level in comparison to those with no metastasis (Mazzocca et al., 2011). What is more, higher serum LPAs level was associated with larger tumour size as well as with poorer survival (Mazzocca et al., 2011). As for studies on lung cancer, LPAs was found to be involved in tumour microenvironment fibrosis. LPA-stimulated fibroblasts produced larger amounts of collagen (type I and VI) and fibronectin (Gudmann et al., 2019). Also, ATX-LPA axis was pointed to play a significant role in inflammation and lung cancer through the increase of proinflammatory cytokines (Valdés-Rives and González-Arenas, 2017). In our study, we noted reduced levels of three different LPAs in the serum of patients with ADC, compared to SCC. Since SCC is considered as more severe and characterized with poorer prognosis (Cooke et al., 2010; Fukui et al., 2015; Wang et al., 2020), our results suggest one of possible explanations for that and indicate the need for further investigation to better understand this phenomenon.

It is worth to note that around 4%–9% of NSCLC tumours contain mixed adenomatous and squamous pathologies within a single lesion, named adenosquamous cell carcinoma (AD-SCC), being the most lethal form of NSCLC with the worst prognosis (Hou et al., 2017). This indicates a potential phenotypic transition between ADC and SCC components in this pathologically mixed lung cancer (Yao et al., 2018). Moreover, there is an evidence that oxidative stress triggers ADC-to-SCC transdifferentiation, thus resistance to therapy. Some studies pointed out the essential role of extracellular matrix remodelling and metabolic reprogramming during this phenotypic transition. As reported, lipoxygenase (LOX) inhibitors and reactive oxygen species (ROS) significantly accelerate this transition. Although more profound research is needed to explain the exact mechanistic principles of this process, already our own evidence suggests that LOX downregulation results in decreased collagen deposition and extracellular matrix remodelling, leading to the transdifferentiation (Li et al., 2015; Yao et al., 2018). These indicate that balanced redox status is critical to control tumour plasticity and therapeutic response in NSCLC (Arfin et al., 2021), pointing to the need to explore changes in the oxPCs either in the transdifferentiation process or in AD-SCC patients.

OxPCs differentiate NSCLC subtypes on the tissue and plasma level. However, stronger differences were observed on plasma level. Three LCh-oxPCs (PC 16:0/20:4; OOH, PC 18:0/20:4; OH and PC 16:0/18:2; OH) were elevated in plasma of ADC patients in comparison to the SCC subjects, while:. in case of tissue samples only one SCh-oxPCs (PC 16:0/4:0; CHO) was significantly reduced in ADC subjects. Smaller differences in case of tumour tissue samples might be related to tumour heterogeneity and presence of different cellular and non-cellular components.

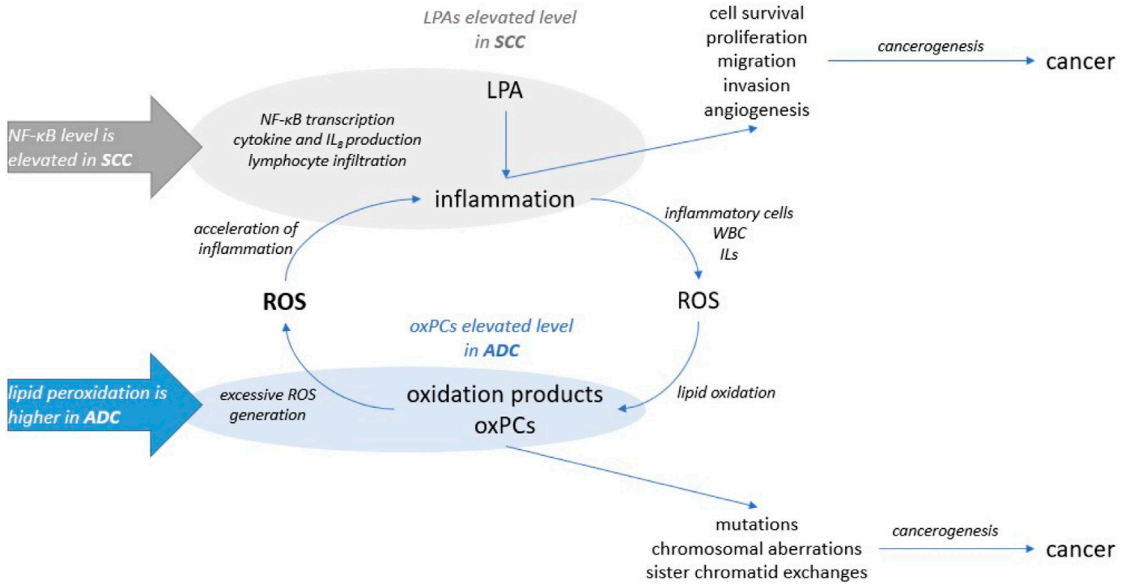


FIGURE 6
The involvement of LPA and oxPCs in the cancerogenesis: LPAs were linked to the inflammation and oxPCs were connected to the oxidative stress.

These results are very important since the relevance of glycerophospholipids, and oxidised phospholipids in lung functioning were already reported. Karki et al. pointed out that circulating and cell membrane oxPCs exhibit protective and deleterious effects on lung endothelium (Karki and Birukov, 2020). LCh-oxPCs were indicated as those with protective functions, while SCh-oxPCs as inducing harmful effects. However, the majority of these reports refer rather to the local activity of tissue oxPCs.

In our other work (Godzien et al., 2024), we found an elevation of oxPCs in NSCLC patients in comparison to the control group. Moreover, it has been reported that oxidative stress is elevated in ADC patients in comparison to SCC subjects (Gęgotek et al., 2016; Zalewska-Ziob et al., 2019), what stays in line with the changes observed in this study. The escalation of oxidative stress and impairment of the antioxidative defence system is greater in ADC patients, which can explain higher plasma levels of oxPCs in these subjects. However, in tumour tissue, we observed a reduced level of PC 16:0/4:0; CHO in ADC subjects. This might be due to already mentioned heterogeneity of tumour tissue or the fact that different oxidation products might exhibit different behaviour under a given condition. This concerns early and end-oxidation products, as well as different oxPCs fractions. Moreover, oxPCs may exhibit different effects depending on the concentration (Karki and Birukov, 2020). This clearly illustrates, that despite already available evidence, there is a need to even further explore the role of oxPCs and other oxidation products in NSCLC patients.

It is essential to mention that oxPCs were found to act as ligands for VEGF receptors (Mohammad and Srivastava, 2012). VEGF promotes tumour angiogenesis through its potent mitogenic effect on vascular endothelial cells (ECs). This links oxPCs with angiogenesis: it was demonstrated that oxPCs, precisely oxPAPC, an LCh-oxPC, stimulate angiogenic reactions in endothelial cells (Bochkov et al., 2017). This is particularly important, because VEGF receptors are known molecular targets for NSCLC therapy (Qu et al., 2018). Moreover, it was reported that hypoxia upregulates the protein levels of VEGF-A in lung cancer cell lines; however, the role of VEGF-A is distinct in ADC and SCC. VEGF-A protein levels were found significantly associated with tumour size and lymph node metastasis, and negatively correlated with the overall survival of ADC subjects, but not SCC patients (Qin et al., 2020). This, together with the differences in the profile of oxPCs between ADC and SCC patients that we observe, suggests that oxPCs should be evaluated as potential prognostic markers to monitor the effectiveness of the treatment and stop or prevent tumour growth. Among all tested lipids, only LPAs and oxPCs were found significantly altered. The linkage between these two groups of phospholipids is inflammation (Figure 5). It was reported that LPAs induce cytokines and interleukin 8 (IL-8) production, promote nuclear factor kappa-light-chain-enhancer of activated B cells (NF-κB) transcription and lymphocyte infiltration. This promotes inflammation and further production of inflammatory cells, white blood cells and interleukins. Inflammatory cells produce a highly oxidative environment, leading to ROS generation. Lipids subjected to the high concentration of ROS undergo oxidation, causing the formation of oxidation products, including also oxPCs. The elevated level of oxPCs (and other peroxidation products) results in excessive ROS generation by ECs. Finally, this increases inflammatory response even more.

Our data show elevated levels of LPAs in SCC patients. For this cohort of patients previous study showed elevated levels of inflammation factor NF-κB (Gęgotek et al., 2016). On the other hand, we observed higher levels of oxPCs for ADC subjects, and higher lipid peroxidation was reported for these patients (Gęgotek et al., 2016). Oxidative stress and inflammation can lead to cancerogenesis; however exact mechanisms underlying this process are distinct. Our results, combined with previously reported evidence, suggest that inflammation might be more involved in SCC development, while oxidative stress underlies

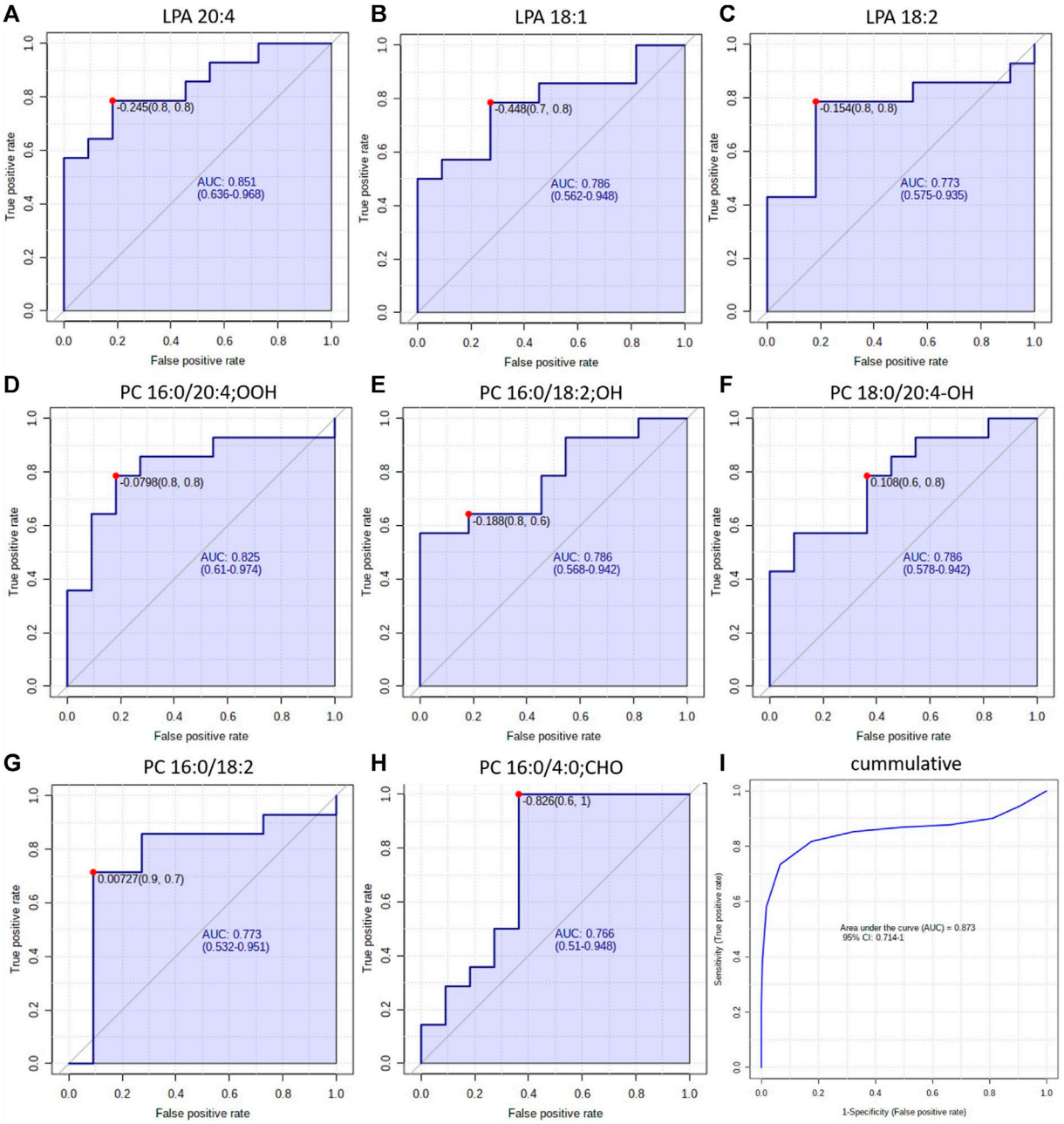


FIGURE 7
ROC curves obtained for each discriminating lipid in plasma (panels **(A–F)**) and tumour tissue panels **(G, H)**. Panel **(I)** shows the ROC obtained for all discriminating lipids simultaneously.

ADC development. However, this statement can be a preliminary hypothesis that requires further examination in a larger group of patients, performing quantitative measurements of discriminating lipids together with determination of inflammatory and oxidative stress markers.

These results provide new insight into the mechanism underlying the development of both NSCLC subtypes. However, the ultimate goal of lipidomics study prognostic, diagnostic, predictive or therapeutic markers can be proposed (Carlomagno et al., 2017). As diagnosis of NSCLC subtypes poses a challenge, we decided to test discriminating LPAs and oxPCs as potential diagnostic markers. For this purpose, we constructed ROC curves for each discriminating lipid (Figure 7). Obtained AUCs were: 0.851, 0.786 and 0.773 for LPA 20:4, LPA 18:1 and LPA 18:2, respectively (Figure 7, panels A–C). For plasma oxPCs computed AUCs were: 0.825, 0.786 and 0.786 for PC 16:0/20:4; OOH, PC 16:0/18:0; OH and PC 18:0/20:4; OH respectively (Figure 6, panels D–F). For tumour PCs calculated AUCs were: 0.773 and 0.766 for PC 16:0/18:2 and PC 16:0/4:0; CHO, correspondingly (Figure 7, panels G and H).

Moreover, we tested different combinations of these lipids to create a biomarker model. The best results, with the highest AUC,

were obtained for the combination of discriminating metabolites, i.e., AUC raised up to 0.873 (Figure 6, panel I). Other researchers used a similar strategy and tested the combined discrimination performance of several metabolites. For five DGs and one Cer, Fan et al. obtained AUC of 0.92 and 0.77 in the discovery and validation set, respectively (Fan et al., 2020). You et al. received even more robust results with AUC of 0.935 and 0.924 for discovery and validation cohorts, respectively. They used a relatively large set of metabolites, which included three carnitines, two free fatty acids, several phospholipids and five polar metabolites such as guanosine, creatinine and oxidised glutathione, among others (You et al., 2020). Zhang et al. performed ROC curve analysis over succinic anhydride, serine phosphorylcholine and PC 34:0, obtaining AUC of 0.827 (Zhang et al., 2019). Analysis of all these reported AUCs suggests that stronger values are obtained either for larger sample sets or for larger sets of discriminating metabolites. Therefore, the performance of our potential markers might be improved by validating them on a larger set of samples or by augmenting them with other metabolites, also polar. All these results show a clear potential of oxPCs and LPAs in the NSCLC subtypes diagnosis; however, they must be validated, covering proper quantification of these molecular lipid species on a larger cohort of patients. This should include a larger number of participants, but also patients with LCC, which were not included in this study due to low availability of the samples. Moreover, diagnostic utility of these glycerophospholipids must be tested in the context of presence of driver mutations such as, e.g., EGFRL858R, KRAS, ALK, among other.

## 4 Conclusion

Our results revealed differences in the profiles of oxPCs and LPAs between ADC and SCC patients. We observed elevated LPAs levels in SCC patients and increased levels of oxPCs in ADC subjects. These results align with publications reporting altered oxidative stress and inflammation markers in NSCLC subtypes. By combining our results with literature reports, we linked the observed increased level of LPAs with inflammation and noticed an increased level of oxPC with oxidative stress. All this suggests that inflammation might be more involved in the SCC development, while oxidative stress seems to underly the development of ADC. However, inflammation and oxidative stress are inherently connected; therefore, their impact on cancer development permeates each other. These results open a new line of research, pointing oxPCs and LPAs as potential markers and/or therapeutic targets in ADC and SCC.

## Data availability statement

The raw data supporting the conclusion of this article will be made available by the authors, without undue reservation.

## Ethics statement

The study was approved by the Ethics Committee of the Medical University of Bialystok (R-I-003/262/2004, R-I-002/296/2018 and APK 002 5 2021) and performed in accordance with the Declaration of Helsinki. The studies were conducted in accordance with the local legislation and institutional requirements. The participants provided their written informed consent to participate in this study.

## Author contributions

JS: Funding acquisition, Writing–original draft, Visualization, Software, Investigation, Formal Analysis, Data curation. KM: Writing–original draft, Visualization, Software, Formal Analysis. RM: Writing–review and editing, Supervision, Resources, Conceptualization. ES: Writing–review and editing, Supervision, Resources, Conceptualization. WN: Writing–review and editing, Supervision, Resources, Conceptualization. JK: Methodology, Investigation, Data curation, Writing–review and editing, Resources, Conceptualization. AM-F: Writing–review and editing, Data curation. JR: Supervision, Software, Resources, Methodology, Writing–review and editing, Data curation. MK: Conceptualization, Writing–review and editing, Supervision, Resources, Methodology. LN: Data curation, Writing–review and editing, Methodology. MM: Validation, Resources, Funding acquisition, Writing–review and editing. AK: Supervision, Writing–review and editing, Resources, Funding acquisition. JN: Validation, Methodology, Writing–review and editing, Supervision, Funding acquisition. MC: Writing–original draft, Resources, Investigation, Conceptualization, Validation, Supervision, Methodology, Funding acquisition. JG: Visualization, Software, Formal Analysis, Data curation, Methodology, Investigation, Writing–original draft, Validation, Supervision.

## Funding

The author(s) declare financial support was received for the research, authorship, and/or publication of this article. This study was funded by the grant from National Science Centre, Poland (2014/13/B/NZ5/01256), the grant from National Centre for Research and Development in the framework of Programme "Prevention practices and treatment of civilization diseases"– STRATEGMED (contract no. STRATEGMED2/266484/2/NCBR/2015), and internal grant from Medical University of Bialystok (B.SUB.23.145).

## Acknowledgments

This study was conducted with the use of equipment purchased by the Medical University of Bialystok as part of the RPOWP 2007–2013 funding, Priority I, Axis 1.1, Contract Nos. UDA-RPPD.01.01.00-20-001/15-00 dated 26 June 2015. The authors want to acknowledge Krzysztof Solowiej's contribution to the statistical data analysis.

## Conflict of interest

Author LN was employed by Altium International Sp. z o. o.

The remaining authors declare that the research was conducted in the absence of any commercial or financial relationships that could be construed as a potential conflict of interest.

## Publisher's note

All claims expressed in this article are solely those of the authors and do not necessarily represent those of their affiliated organizations, or those of the publisher, the editors and the reviewers. Any product that may be evaluated in this article, or claim that may be made by its manufacturer, is not guaranteed or endorsed by the publisher.

## Supplementary material

The Supplementary Material for this article can be found online at: https://www.frontiersin.org/articles/10.3389/fmolb.2024.1379631/full#supplementary-material

## References


Aiello, S., and Casiraghi, F. (2021). Lysophosphatidic acid: promoter of cancer progression and of tumor microenvironment development. A promising target for anticancer therapies? *Cells* 10 (6), 1390. doi:10.3390/cells10061390

Arfin, S., Jha, N. K., Jha, S. K., Kesari, K. K., Ruokolainen, J., Roychoudhury, S., et al. (2021). Oxidative stress in cancer cell metabolism. *Antioxidants (Basel)* 10 (5), 642. doi:10.3390/antiox10050642

Bochkov, V., Gesslbauer, B., Mauerhofer, C., Philippova, M., Erne, P., and Oskolkova, O. V. (2017). Pleiotropic effects of oxidized phospholipids. *Free Radic. Biol. Med.* 111, 6–24. doi:10.1016/j.freeradbiomed.2016.12.034

Bray, F., Ferlay, J., Soerjomataram, I., Siegel, R. L., Torre, L. A., and Jemal, A. (2018). Global cancer statistics 2018: GLOBOCAN estimates of incidence and mortality worldwide for 36 cancers in 185 countries. *CA Cancer J. Clin.* 68 (6), 394–424. doi:10.3322/caac.21492

Campbell, J. D., Alexandrov, A., Kim, J., Wala, J., Berger, A. H., Pedamallu, C. S., et al. (2016). Distinct patterns of somatic genome alterations in lung adenocarcinomas and squamous cell carcinomas. *Nat. Genet.* 48 (6), 607–616. doi:10.1038/ng.3564

Carlomagno, N., Incollingo, P., Tammaro, V., Peluso, G., Rupealta, N., Chiacchio, G., et al. (2017). Diagnostic, predictive, prognostic, and therapeutic molecular biomarkers in third millennium: a breakthrough in gastric cancer. *Biomed. Res. Int.* 2017, 7869802. doi:10.1155/2017/7869802

Chen, Y., Ma, Z., Shen, X., Li, L., Zhong, J., Min, L. S., et al. (2018). Serum lipidomics profiling to identify biomarkers for non-small cell lung cancer. *Biomed. Res. Int.* 2018, 5276240. doi:10.1155/2018/5276240

Chen, Y., Tang, W. Y., Tong, X., and Ji, H. (2019). Pathological transition as the arising mechanism for drug resistance in lung cancer. *Cancer Commun. (Lond)* 39 (1), 53. doi:10.1186/s40880-019-0402-8

Ciborowski, M., Kisluk, J., Pietrowska, K., Samczuk, P., Parfieniuk, E., Kowalczyk, T., et al. (2017). Development of LC-QTOF-MS method for human lung tissue fingerprinting. A preliminary application to nonsmall cell lung cancer. *Electrophoresis* 38 (18), 2304–2312. doi:10.1002/elps.201700022

Ciereszko, A., Dietrich, M. A., Słowińska, M., Nynca, J., Ciborowski, M., Kaczmarek, M. M., et al. (2022). Application of two-dimensional difference gel electrophoresis to identify protein changes between center, margin, and adjacent non-tumor tissues obtained from non-small-cell lung cancer with adenocarcinoma or squamous cell carcinoma subtype. *PLoS One* 17 (5), e0268073. doi:10.1371/journal.pone.0268073

Cooke, D. T., Nguyen, D. V., Yang, Y., Chen, S. L., Yu, C., and Calhoun, R. F. (2010). Survival comparison of adenosquamous, squamous cell, and adenocarcinoma of the lung after lobectomy. *Ann. Thorac. Surg.* 90 (3), 943–948. doi:10.1016/j.athoracsur.2010.05.025

Daniluk, U., Daniluk, J., Kucharski, R., Kowalczyk, T., Pietrowska, K., Samczuk, P., et al. (2019). Untargeted metabolomics and inflammatory markers profiling in children with crohn's disease and ulcerative colitis-A preliminary study. *Inflamm. Bowel Dis.* 25 (7), 1120–1128. doi:10.1093/ibd/izy402

Ettinger, D. S., Wood, D. E., Aisner, D. L., Akerley, W., Bauman, J., Chirieac, L. R., et al. (2017). Non-small cell lung cancer, version 5.2017, NCCN clinical practice guidelines in oncology. *J. Natl. Compr. Canc Netw.* 15 (4), 504–535. doi:10.6004/jnccn.2017.0050

Fan, Y., Noreldeen, H. A. A., You, L., Liu, X., Pan, X., Hou, Z., et al. (2020). Lipid alterations and subtyping maker discovery of lung cancer based on nontargeted tissue lipidomics using liquid chromatography-mass spectrometry. *J. Pharm. Biomed. Anal.* 190, 113520. doi:10.1016/j.jpba.2020.113520

Fukui, T., Taniguchi, T., Kawaguchi, K., Fukumoto, K., Nakamura, S., Sakao, Y., et al. (2015). Comparisons of the clinicopathological features and survival outcomes between lung cancer patients with adenocarcinoma and squamous cell carcinoma. *Gen. Thorac. Cardiovasc Surg.* 63 (9), 507–513. doi:10.1007/s11748-015-0564-5

Gardell, S. E., Dubin, A. E., and Chun, J. (2006). Emerging medicinal roles for lysophospholipid signaling. *Trends Mol. Med.* 12 (2), 65–75. doi:10.1016/j.molmed.2005.12.001

Gęgotek, A., Nikliński, J., Žarković, N., Žarković, K., Waeg, G., Łuczaj, W., et al. (2016). Lipid mediators involved in the oxidative stress and antioxidant defence of human lung cancer cells. *Redox Biol.* 9, 210–219. doi:10.1016/j.redox.2016.08.010

Gil de la Fuente, A., Traldi, F., Siroka, J., Kretowski, A., Ciborowski, M., Otero, A., et al. (2018). Characterization and annotation of oxidized glycerophosphocholines for non-targeted metabolomics with LC-QTOF-MS data. *Anal. Chim. Acta* 1037, 358–368. doi:10.1016/j.aca.2018.08.005

Godzien, J., Kalaska, B., Adamska-Patruno, E., Siroka, J., Ciborowski, M., Kretowski, A., et al. (2019). Oxidized glycerophosphatidylcholines in diabetes through non-targeted metabolomics: their annotation and biological meaning. *J. Chromatogr. B Anal. Technol. Biomed. Life Sci.* 1120, 62–70. doi:10.1016/j.jchromb.2019.04.053

Godzien, J., Lopez-Lopez, A., Sieminska, J., Jablonowski, K., Pietrowska, K., Kisluk, J., et al. (2024). Exploration of oxidized phosphocholine profile in non-small-cell lung cancer. *Front. Mol. Biosci.* 10, 1279645. doi:10.3389/fmolb.2023.1279645

Godzien, J. E., Alonso-Herranz, V., Barbas, C., and Armitage, E. G. (2014). Controlling the quality of metabolomics data: new strategies to get the best out of the QC sample. *Metabolomics* 11, 518–528. doi:10.1007/s11306-014-0712-4

Gudmann, N., Luo, Y., Sand, J. M. B., Trujillo, G., Murphy, B. J., Cheng, P. T., et al. (2019). Fibroblast activation triggered by LPA results in matrix synthesis/fibrogenesis different from that of TGF-ß1. *Eur. Respir. J.* 54, PA2423. doi:10.1183/13993003.congress-2019.PA2423

Hou, S., Zhou, S., Qin, Z., Yang, L., Han, X., Yao, S., et al. (2017). Evidence, mechanism, and clinical relevance of the transdifferentiation from lung adenocarcinoma to squamous cell carcinoma. *Am. J. Pathol.* 187 (5), 954–962. doi:10.1016/j.ajpath.2017.01.009

Jianyong, Z., Yanruo, H., Xiaoju, T., Yiping, W., and Fengming, L. (2021). Roles of lipid profiles in human non-small cell lung cancer. *Technol. Cancer Res. Treat.* 20, 15330338211041472. doi:10.1177/15330338211041472

Karki, P., and Birukov, K. G. (2020). Oxidized phospholipids in healthy and diseased lung endothelium. *Cells* 9 (4), 981. doi:10.3390/cells9040981

Kehlen, A., Englert, N., Seifert, A., Klonisch, T., Dralle, H., Langner, J., et al. (2004). Expression, regulation and function of autotaxin in thyroid carcinomas. *Int. J. Cancer* 109 (6), 833–838. doi:10.1002/ijc.20022

Kenfield, S. A., Wei, E. K., Stampfer, M. J., Rosner, B. A., and Colditz, G. A. (2008). Comparison of aspects of smoking among the four histological types of lung cancer. *Tob. Control* 17 (3), 198–204. doi:10.1136/tc.2007.022582

Kowalczyk, T., Kisluk, J., Pietrowska, K., Godzien, J., Kozlowski, M., Reszeć, J., et al. (2021). The ability of metabolomics to discriminate non-small-cell lung cancer subtypes depends on the stage of the disease and the type of material studied. *Cancers (Basel)* 13 (13), 3314. doi:10.3390/cancers13133314

Li, F., Han, X., Wang, R., Wang, H., Gao, Y., Wang, X., et al. (2015). LKB1 inactivation elicits a redox imbalance to modulate non-small cell lung cancer plasticity and therapeutic response. *Cancer Cell* 27 (5), 698–711. doi:10.1016/j.ccell.2015.04.001

Lin, M. E., Herr, D. R., and Chun, J. (2010). Lysophosphatidic acid (LPA) receptors: signaling properties and disease relevance. *Prostagl. Other Lipid Mediat* 91 (3-4), 130–138. doi:10.1016/j.prostaglandins.2009.02.002

López-López, Á., Godzien, J., Soldevilla, B., Gradillas, A., López-Gonzálvez, Á., Lens-Pardo, A., et al. (2020). Oxidized lipids in the metabolic profiling of neuroendocrine tumors - analytical challenges and biological implications. *J. Chromatogr. A* 1625, 461233. doi:10.1016/j.chroma.2020.461233

Marien, E., Meister, M., Muley, T., Fieuws, S., Bordel, S., Derua, R., et al. (2015). Non-small cell lung cancer is characterized by dramatic changes in phospholipid profiles. *Int. J. Cancer* 137 (7), 1539–1548. doi:10.1002/ijc.29517

Mazzocca, A., Dituri, F., Lupo, L., Quaranta, M., Antonaci, S., and Giannelli, G. (2011). Tumor-secreted lysophostatidic acid accelerates hepatocellular carcinoma progression by promoting differentiation of peritumoral fibroblasts in myofibroblasts. *Hepatology* 54 (3), 920–930. doi:10.1002/hep.24485

Michalska-Falkowska, A., Niklinski, J., Juhl, H., Sulewska, A., Kisluk, J., Charkiewicz, R., et al. (2023). Applied molecular-based quality control of biobanked samples for multi-omics approach. *Cancers (Basel)* 15 (14), 3742. doi:10.3390/cancers15143742

Mohammad, Z. A., and Srivastava, S. (2012). "Oxidized phospholipids: introduction and biological significance," in *Lipoproteins. K. Sasa frank and gerhard* (Rijeka: IntechOpen).

Niemira, M., Collin, F., Szalkowska, A., Bielska, A., Chwialkowska, K., Reszec, J., et al. (2019). Molecular signature of subtypes of non-small-cell lung cancer by large-scale transcriptional profiling: identification of key modules and genes by weighted gene Co-expression network analysis (WGCNA). *Cancers (Basel)* 12 (1), 37. doi:10.3390/cancers12010037

Niklinski, J., Kretowski, A., Moniuszko, M., Reszec, J., Michalska-Falkowska, A., Niemira, M., et al. (2017). Systematic biobanking, novel imaging techniques, and advanced molecular analysis for precise tumor diagnosis and therapy: the Polish MOBIT project. *Adv. Med. Sci.* 62 (2), 405–413. doi:10.1016/j.advms.2017.05.002

Okuzumi, A., Hatano, T., Ueno, S. I., Ogawa, T., Saiki, S., Mori, A., et al. (2019). Metabolomics-based identification of metabolic alterations in PARK2. *Ann. Clin. Transl. Neurol.* 6 (3), 525–536. doi:10.1002/acn3.724

Paynter, N. P., Balasubramanian, R., Giulianini, F., Wang, D. D., Tinker, L. F., Gopal, S., et al. (2018). Metabolic predictors of incident coronary heart disease in women. *Circulation* 137 (8), 841–853. doi:10.1161/CIRCULATIONAHA.117.029468

Qin, S., Yi, M., Jiao, D., Li, A., and Wu, K. (2020). Distinct roles of VEGFA and ANGPT2 in lung adenocarcinoma and squamous cell carcinoma. *J. Cancer* 11 (1), 153–167. doi:10.7150/jca.34693

Qu, J., Zhang, Y., Chen, X., Yang, H., Zhou, C., and Yang, N. (2018). Newly developed anti-angiogenic therapy in non-small cell lung cancer. *Oncotarget* 9 (11), 10147–10163. doi:10.18632/oncotarget.23755

Ray, M. R., Jablons, D., and He, B. (2010). Lung cancer therapeutics that target signaling pathways: an update. *Expert Rev. Respir. Med.* 4 (5), 631–645. doi:10.1586/ers.10.64

Schabath, M. B., and Cote, M. L. (2019). Cancer progress and priorities: lung cancer. *Cancer Epidemiol. Biomarkers Prev.* 28 (10), 1563–1579. doi:10.1158/1055-9965.EPI-19-0221

Sethi, S., and Brietzke, E. (2017). Recent advances in lipidomics: analytical and clinical perspectives. *Prostagl. Other Lipid Mediat* 128-129, 8–16. doi:10.1016/j.prostaglandins.2016.12.002

Subramanian, J., and Govindan, R. (2007). Lung cancer in never smokers: a review. *J. Clin. Oncol.* 25 (5), 561–570. doi:10.1200/JCO.2006.06.8015

Tokumura, A. (2002). Physiological and pathophysiological roles of lysophosphatidic acids produced by secretory lysophospholipase D in body fluids. *Biochim. Biophys. Acta* 1582 (1-3), 18–25. doi:10.1016/s1388-1981(02)00133-6

Valdés-Rives, S. A., and González-Arenas, A. (2017). Autotaxin-Lysophosphatidic acid: from inflammation to cancer development. *Mediat. Inflamm.* 2017, 9173090. doi:10.1155/2017/9173090

van Corven, E. J., Groenink, A., Jalink, K., Eichholtz, T., and Moolenaar, W. H. (1989). Lysophosphatidate-induced cell proliferation: identification and dissection of signaling pathways mediated by G proteins. *Cell* 59 (1), 45–54. doi:10.1016/0092-8674(89)90868-4

Wang, B. Y., Huang, J. Y., Chen, H. C., Lin, C. H., Lin, S. H., Hung, W. H., et al. (2020). The comparison between adenocarcinoma and squamous cell carcinoma in lung cancer patients. *J. Cancer Res. Clin. Oncol.* 146 (1), 43–52. doi:10.1007/s00432-019-03079-8

Willier, S., Butt, E., and Grunewald, T. G. (2013). Lysophosphatidic acid (LPA) signalling in cell migration and cancer invasion: a focussed review and analysis of LPA receptor gene expression on the basis of more than 1700 cancer microarrays. *Biol. Cell* 105 (8), 317–333. doi:10.1111/boc.201300011

Wu, J. M., Xu, Y., Skill, N. J., Sheng, H., Zhao, Z., Yu, M., et al. (2010). Autotaxin expression and its connection with the TNF-alpha-NF-kappaB axis in human hepatocellular carcinoma. *Mol. Cancer* 9, 71. doi:10.1186/1476-4598-9-71

Xie, Y., and Meier, K. E. (2004). Lysophospholipase D and its role in LPA production. *Cell Signal* 16 (9), 975–981. doi:10.1016/j.cellsig.2004.03.005

Yang, S. Y., Lee, J., Park, C. G., Kim, S., Hong, S., Chung, H. C., et al. (2002). Expression of autotaxin (NPP-2) is closely linked to invasiveness of breast cancer cells. *Clin. Exp. Metastasis* 19 (7), 603–608. doi:10.1023/a:1020950420196

Yao, S., Han, X., Tong, X., Li, F., Qin, Z., Huang, H.-Y., et al. (2018). Lysyl oxidase inhibition drives the transdifferentiation from lung adenocarcinoma to squamous cell carcinoma in mice. *bioRxiv*, 314393. doi:10.1101/314393

You, L., Fan, Y., Liu, X., Shao, S., Guo, L., Noreldeen, H. A. A., et al. (2020). Liquid chromatography-mass spectrometry-based tissue metabolic profiling reveals major metabolic pathway alterations and potential biomarkers of lung cancer. *J. Proteome Res.* 19 (9), 3750–3760. doi:10.1021/acs.jproteome.0c00285

Yuan, M., Huang, L. L., Chen, J. H., Wu, J., and Xu, Q. (2019). The emerging treatment landscape of targeted therapy in non-small-cell lung cancer. *Signal Transduct. Target Ther.* 4, 61. doi:10.1038/s41392-019-0099-9

Zalewska-Ziob, M., Adamek, B., Kasperczyk, J., Romuk, E., Hudziec, E., Chwalińska, E., et al. (2019). Activity of antioxidant enzymes in the tumor and adjacent noncancerous tissues of non-small-cell lung cancer. *Oxid. Med. Cell Longev.* 2019, 2901840. doi:10.1155/2019/2901840

Zhang, M., He, J., Li, T., Hu, H., Li, X., Xing, H., et al. (2019). Accurate classification of non-small cell lung cancer (NSCLC) pathology and mapping of EGFR mutation spatial distribution by ambient mass spectrometry imaging. *Front. Oncol.* 9, 804. doi:10.3389/fonc.2019.00804

# Glossary

| | |
|---|---|
| **4-HNE** | 4-hydroxynonenal |
| **ADC** | adenocarcinoma |
| **AD-SCC** | adenosquamous cell carcinoma |
| **ALK** | anaplastic lymphoma kinase |
| **ATX** | autotaxin |
| **BMI** | body mass index |
| **CAR** | carnitine |
| **Cer** | ceramide |
| **COPD** | chronic obstructive pulmonary disease |
| **DG** | diradylglycerol |
| **EC** | endothelial cell |
| **EGF** | epidermal growth factor |
| **EGFR** | epidermal growth factor receptor |
| **FA** | free fatty acid |
| **HILIC** | hydrophilic interactions chromatography |
| **HPLC** | high performance liquid chromatography |
| **IE-DDA** | iterative exclusion data-dependent analysis |
| **IGF-I** | insulin-like growth factor I |
| **IL-8** | interleukin 8 |
| **LC** | liquid chromatography |
| **LCC** | large-cell carcinoma |
| **LCh-oxPC** | long-chain oxidised phosphocholine |
| **LC-MS** | liquid chromatography mass spectrometry |
| **LOX** | lipoxygenase |
| **LPA** | lysophosphatidic acid |
| **LPC** | lysophosphatidylcholine |
| **LPE** | lysophosphatidylethanolamine |
| **LPG** | lysophosphatidylglycerol |
| **LPI** | lysophosphatidylinositol |
| **MDA** | malondialdehyde |
| **MS** | mass spectrometry |
| **NF-κB** | nuclear factor kappa-light-chain-enhancer of activated B cells |
| **NSCLC** | non-small cell lung cancer |
| **oxPC** | oxidised phosphatidylcholine |
| **PC** | phosphatidylcholine |
| **PDFG** | platelet-derived growth factor |
| **PE** | glycerophosphoethanolamine |
| **PI** | glycerophosphoinositol |
| **PS** | glycerophosphoserine |
| **pTNM** | pathological tumour-node-metastasis staging |
| **QC** | quality control |
| **ROS** | reactive oxygen species |
| **RP** | reversed-phase chromatography |
| **RT** | retention time |
| **SCC** | squamous cell carcinoma |
| **SCh-oxPC** | short-chain oxidised phosphocholine |
| **SM** | sphingomyelin |
| **UHPLC** | ultra-high-performance liquid chromatography |
| **VEGF** | vascular endothelial growth factor |

frontiers | Frontiers in Molecular Biosciences

TYPE Original Research
PUBLISHED 09 May 2024
DOI 10.3389/fmolb.2024.1341108



OPEN ACCESS

EDITED BY
Danuta Dudzik,
Medical University of Gdańsk, Poland

REVIEWED BY
Oleg Mayboroda,
Leiden University Medical Center (LUMC), Netherlands
Danuta Siluk,
Medical University of Gdańsk, Poland

*CORRESPONDENCE
Barbara Bojko,
bbojko@cm.umk.pl

RECEIVED 19 November 2023
ACCEPTED 15 April 2024
PUBLISHED 09 May 2024

CITATION
Warmuzińska N, Łuczykowski K, Stryjak I, Rosales-Solano H, Urbanellis P, Pawliszyn J, Selzner M and Bojko B (2024), The impact of normothermic and hypothermic preservation methods on kidney lipidome—comparative study using chemical biopsy with microextraction probes.
*Front. Mol. Biosci.* 11:1341108.
doi: 10.3389/fmolb.2024.1341108



# The impact of normothermic and hypothermic preservation methods on kidney lipidome—comparative study using chemical biopsy with microextraction probes

Natalia Warmuzińska[1], Kamil Łuczykowski[1], Iga Stryjak[1], Hernando Rosales-Solano[2], Peter Urbanellis[3], Janusz Pawliszyn[2], Markus Selzner[3,4] and Barbara Bojko[1]*

[1]Department of Pharmacodynamics and Molecular Pharmacology, Faculty of Pharmacy, Nicolaus Copernicus University in Torun, Collegium Medicum in Bydgoszcz, Bydgoszcz, Poland, [2]Department of Chemistry, University of Waterloo, Waterloo, ON, Canada, [3]Ajmera Transplant Center, Department of Surgery, Toronto General Hospital, University Health Network, Toronto, ON, Canada, [4]Department of Medicine, Toronto General Hospital, Toronto, ON, Canada

**Introduction:** Normothermic *ex vivo* kidney perfusion (NEVKP) is designed to replicate physiological conditions to improve graft outcomes. A comparison of the impact of hypothermic and normothermic preservation techniques on graft quality was performed by lipidomic profiling using solid-phase microextraction (SPME) chemical biopsy as a minimally invasive sampling approach.

**Methods:** Direct kidney sampling was conducted using SPME probes coated with a mixed-mode extraction phase in a porcine autotransplantation model of the renal donor after cardiac death, comparing three preservation methods: static cold storage (SCS), NEVKP, and hypothermic machine perfusion (HMP). The lipidomic analysis was done using ultra-high-performance liquid chromatography coupled with a Q-Exactive Focus Orbitrap mass spectrometer.

**Results:** Chemometric analysis showed that the NEVLP group was separated from SCS and HMP groups. Further in-depth analyses indicated significantly ($p < 0.05$, VIP > 1) higher levels of acylcarnitines, phosphocholines, ether-linked and longer-chain phosphoethanolamines, triacylglycerols and most lysophosphocholines and lysophosphoethanolamines in the hypothermic preservation group. The results showed that the preservation temperature has a more significant impact on the lipidomic profile of the kidney than the preservation method's mechanical characteristics.

**Conclusion:** Higher levels of lipids detected in the hypothermic preservation group may be related to ischemia-reperfusion injury, mitochondrial dysfunction, pro-inflammatory effect, and oxidative stress. Obtained results suggest the NEVKP method's beneficial effect on graft function and confirm that SPME

chemical biopsy enables low-invasive and repeated sampling of the same tissue, allowing tracking alterations in the graft throughout the entire transplantation procedure.

KEYWORDS

**solid-phase microextraction, SPME, LC-MS, kidney transplantation, lipidomics, graft quality assessment, kidney perfusion**

# 1 Introduction

Kidney transplantation is a life-saving method for patients with end-stage renal dysfunction that enables higher survival rates and patient quality of life compared to dialysis treatment. Unfortunately, an ongoing organ shortage has led to the rapid growth in the number of patients on kidney waiting lists (Swanson et al., 2020; Warmuzińska et al., 2022). This growing gap in supply and demand has led clinicians to explore the possibility of using kidneys recovered from extended criteria donors (ECD) or donation after circulatory death (DCD) donors; however, recipients of ECD kidney grafts tend to have worse outcomes than those receiving organs from standard criteria donors, including being at a higher risk of delayed graft function (DGF) and primary nonfunction incidence (Urbanellis et al., 2020; Warmuzińska et al., 2022). Hence, strategies for reducing preservation injury and monitoring graft function are of intense interest. At present, static cold storage (SCS) and hypothermic machine perfusion (HMP) are the most common preservation methods applied in clinical settings. SCS involves submerging the kidney in a cold preservation fluid and then placing it on ice in an icebox; in contrast, HMP entails using a device to pump cold preservation fluid through the renal vasculature, which has been demonstrated to be more effective at preserving marginal and DCD grafts compared to SCS (Lindell et al., 2013; Urbanellis et al., 2020; Warmuzińska et al., 2022). Normothermic *ex vivo* kidney perfusion (NEVKP) is a novel dynamic preservation strategy applying a perfusion solution's circulation through the kidney. NEVKP conditions are developed to replicate physiological conditions as closely as possible to reduce cold ischemia damage and improve graft outcome (Resch et al., 2020; Hosgood et al., 2021). While several studies have attained promising results indicating NEVKP's superiority over SCS, this application is still in the experimental stage (Kaths et al., 2017; Urbanellis et al., 2020). One notable problem is the need for more accurate methods of evaluating graft quality and assessing donor risk, especially concerning marginal grafts. A kidney's suitability for transplantation is determined based on detailed parameters, including the donor's medical history, visual assessment, and examination results (Warmuzińska et al., 2022). The visual evaluation of donor organs is frequently fundamental in decision-making. However, although macroscopic inspection can help diagnose tumors and anatomical changes, this method is subjective and depends on the transplant team's experience level (Dare et al., 2014). Consequently, pretransplant biopsies remain the gold standard for identifying donor kidney injury. Histological examinations are often applied selectively, mainly in marginal grafts, and the frequency of performed biopsies varies between medical facilities and countries (Dare et al., 2014; Moeckli et al., 2019; Warmuzińska et al., 2022). Moreover, the use of biopsies is hampered by two significant limitations: the low reproducibility of results between on-call pathologists and their time-consuming nature (Azancot et al., 2014). Additionally, the number of allowable biopsies during the transplantation procedure is usually restricted to a single sampling due to their invasiveness, which limits their application for capturing dynamic changes and time-series analyses (Bojko, 2022). Therefore, new representative organ-quality assessment methods are needed to increase the number of organs available for transplantation. In this study, we assess the viability of solid-phase microextraction (SPME) chemical biopsy as a method for evaluating the impact of hypothermic and normothermic preservation techniques on the lipidomic profile of the kidney. The small diameter of the SPME probe (~200 μm) enables minimal invasiveness and allows for several samplings of the same organ without damaging the tissue. Furthermore, SPME combines sampling, extraction, and metabolite quenching into a single step, which makes it a valuable tool for on-site analysis. Finally, SPME's low invasiveness enables its application for monitoring of changes in the organ throughout the entire transplantation procedure, beginning with its removal from the donor's body, through its preservation, and ending with its revascularization in the recipient's body (Łuczykowski et al., 2023).

# 2 Materials and methods

## 2.1 Animals

Eight 3-month-old male Yorkshire pigs (≈30 kg) were housed for 1 week prior to the experiments, with water and food being provided *ad libitum*. All animals received humane care in compliance with the "Principles of Laboratory Animal Care" formulated by the National Society for Medical Research and the "Guide for the Care of Laboratory Animals" published by the National Institutes of Health and the ARRIVE guidelines 2.0. The study protocol was approved by the Animal Care Committee at the Toronto General Research Institute, Ontario, Canada.

## 2.2 Study design

SPME fibers coated with a mixed-mode extraction phase (coating length: 7 mm) were applied for direct kidney sampling in three porcine models of renal DCD autotransplantation using different preservation methods: an 8-h SCS group ($n$ = 3), an 8-h NEVKP group ($n$ = 3), and an 8-h HMP group ($n$ = 2). The autotransplantation and anesthetic procedures, warm ischemia induction, and NEVKP, HMP, and SCS conditions are described elsewhere (Kaths et al., 2015; Kaths et al., 2016; Kaths et al., 2018;

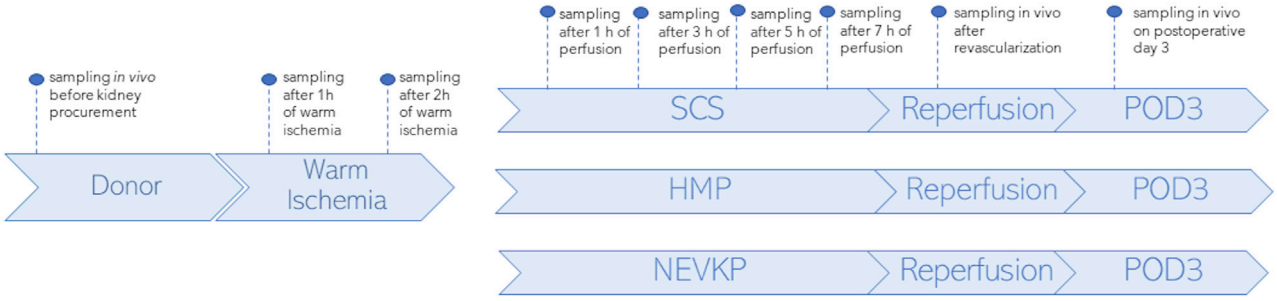


FIGURE 1
Study design. SPME sampling was performed *in vivo* prior to kidney procurement; after 1 h and 2 h of warm ischemia; after 1 h, 3 h, 5 h, and 7 h of perfusion; *in vivo* immediately after revascularization (reperfusion), and *in vivo* under deep anesthesia at the time of sacrifice on postoperative day 3 (POD3). Three types of kidney preservation methods—SCS, HMP, and NEVKP—were compared in the DCD porcine model of renal autotransplantation.

Urbanellis et al., 2020). SPME sampling was performed *in vivo* prior to kidney procurement; after 1 h and 2 h of warm ischemia; after 1 h, 3 h, 5 h, and 7 h of perfusion; *in vivo* immediately after revascularization (reperfusion), and *in vivo* under deep anesthesia at the time of sacrifice on postoperative day 3 (POD3). The study protocol is illustrated in Figure 1. Before sampling, all fibers were preconditioned for 60 min in a methanol/water (50:50 v/v) solution, followed by rinsing with purified water for a few seconds. The extractions were performed by inserting the SPME fiber into the kidney cortex for 30 min at each time point. After sampling, the fibers were removed from the organ, quickly rinsed with water, and then gently dried with kimwipes to remove any tissue or blood residue. Next, the fibers were placed into empty glass vials and stored in a freezer at −80°C until analysis. All fibers were desorbed immediately before instrumental analysis. For desorption, the fibers were inserted into 200 µL of isopropanol:methanol (1:1 v/v) solution with the use of silanized inserts and agitated (1,200 rpm) using a BenchMixer™ MultiTube Vortexer (Benchmark Scientific, Edison, United States) for 120 min. After desorption, extracts were ready for instrumental analysis. The extraction blanks consisted of fibers that were prepared using the same protocol as the rest of the fibers, but with the extraction step being omitted.

## 2.3 Liquid chromatography–high resolution mass spectrometry analysis (LC-HRMS)

Untargeted lipidomics analysis was performed using an LC-HRMS procedure based on the coupling of an ultra-high performance liquid chromatograph and a Q-Exactive Focus Orbitrap mass spectrometer. Data acquisition was performed using dedicated Thermo Scientific software, namely, Xcalibur 4.2 and Free Style 1.4 (Thermo Fisher Scientific, San Jose, California, United States). The instrument was calibrated by injecting calibrants every 72 h, resulting in a mass accuracy of <2 ppm. During analysis, the samples were randomized and pooled quality control (QC) samples containing 10 µL of each sample were run every 8–10 injections to monitor instrument performance and analyte stability. Chromatographic separation was carried out on a hydrophilic interaction liquid chromatography (HILIC) column (SeQuant ZIC-cHILIC, 3 µm, 100 mm × 2.1 mm) and in reversed-phase (RP) using a C18 column (Waters, XSelect CSH C18, 3.5 µm, 2.1 mm × 75 mm) to cover a wide range of lipids. The mobile phases for the HILIC column were 5 mM ammonium acetate in water (A) and acetonitrile (B). The mobile phases for the RP column were: phase A consisted of water: methanol (60:40; v/v) and phase B of isopropanol: methanol (90:10; v/v), both containing 10 mM ammonium acetate and 1 mM acetic acid. The gradients were as described previously (Stryjak et al., 2020). The analyses were performed in positive and negative electrospray ionization mode. For positive ionization mode, the mass spectrometer parameters for the HILIC separations were as follows: a spray voltage of 1,500V; a capillary temperature of 325°C; sheath gas at 60 a.u.; an aux gas flow rate of 30 a.u.; a spare gas flow rate of 2 a.u.; a probe heater temperature of 325°C; an S-Lens radio frequency level of 55%; an S-lens voltage of 25 V; and a skimmer voltage of 15 V. For the RP analysis, the following parameters were employed: a spray voltage of 3500V; a capillary temperature of 275°C; sheath gas at 20 a.u.; an aux gas flow rate of 10 a.u.; a spare gas flow rate of 2 a.u.; a probe heater temperature of 300 °C; an S-Lens radio frequency level of 55%; an S-lens voltage of 25 V; and a skimmer voltage of 15 V. For negative ionization mode, the mass spectrometer parameters for the HILIC separations were as follows: a spray voltage of 1300V; a capillary temperature of 263°C; sheath gas at 60 a.u.; an aux gas flow rate of 30 a.u.; a spare gas flow rate of 2 a.u.; a probe heater temperature of 425°C; an S-Lens radio frequency level of 55%; an S-lens voltage of 25 V; and a skimmer voltage of 15 V. For the RP analysis, the following HESI ion source parameters were employed: a spray voltage of 3,500V; a capillary temperature of 275°C; sheath gas at 30 a.u.; an aux gas flow rate of 10 a.u.; a spare gas flow rate of 2 a.u.; a probe heater temperature of 300°C; an S-Lens radio frequency level of 55%; an S-lens voltage of 25 V; and a skimmer voltage of 15 V. The putative identification of compounds was confirmed in Full MS/dd-MS2 mode using the following fragmentation parameters: mass resolution—35,000 full width at half maximum (FWHM); AGC target—2E4; minimum AGC—8E3; intensity threshold—auto; maximum IT—auto; isolation window—3.0 *m/z*; stepped collision energy—20 V, 30 V, 50 V; loop count—2; dynamic exclusion—auto.

## 2.4 Data processing and statistical analysis

Raw data from each LC-HRMS analysis were processed independently using LipidSearch 4.1.30 (Thermo Fisher Scientific, San Jose, California, United States) software with the following

parameters: peak intensity >10,000; a precursor tolerance of 5 ppm; a product tolerance of 10 ppm; an m-score threshold of 2; a Quan *m/z* tolerance of ±5 ppm; a Quan RT (retention time) range of 0.5 min; and the use of a main isomer filter. $H^+$, $NH4^+$, and $Na^+$ adducts were considered in positive ion mode, while $H^-$ and $^+CH_3COO$ were considered in negative ion mode. After completing the lipid identification step, the alignment process was performed using the LipidSearch software with the following parameters: an m-Score threshold of 10; a retention time tolerance of 0.25 min; a QC-to-extraction-blank ratio of >5; and a max 30% RSD in the QC. The search mode function of the software sought matches of parent peaks (full scan MS) and product peaks (fragments, MS/MS) with the lipid database entries. The software assigns four grades of identification of decreasing quality (A–D) to each feature. Identification grade filtering was applied to filter false positive lipid ID from LipidSearch results. Only lipids species with grades A and B were considered in further analyses. Grade A indicates that both lipid class and all fatty acid chains belonging to a given lipid were completely identified; grade B indicates full identification of lipid class and partial identification of fatty acid chains. The peak areas for the obtained compounds were analyzed using MetaboAnalyst 4.0 and Statistica 13.3 PL software (StatSoft, Inc., Tulsa, Oklahoma, United States). All missing values were replaced with small values that were assumed to be a detection limit. A UpSet plot was made with the lists of compounds annotated in the different LC-HRMS analyses using the UpSet plot generator tool (https://www.chiplot.online/upset_plot.html) to evaluate the number of lipids species identified in each analytical block. Data were normalized by median, log-transformation, and Pareto scaling, and statistical significance was calculated based on the Kruskal-Wallis test and the Mann–Whitney U test with FDR correction. A *post hoc* test with multiple comparisons of mean ranks for all groups with a Bonferroni correction followed the Kruskal-Wallis test. A *p*-value of <0.05 was considered significant. In addition, principal component analysis (PCA) and partial least squares discriminant analysis (PLS-DA) were conducted to visually assess the separation between sample groups, with variable importance in projection (VIP) scores >1 being used as a criterion for detecting the relevant variables in the context of the model's predictive capability. Each model was validated via Leave-one-out cross-validation and refined with a permutation test. The model was considered to have passed permutation when the *p*-value was lower than 0.05. The Friedman test was employed to search for compounds with relative concentrations that changed throughout perfusion (across specific time points). After statistical analysis, the results from each LC-HRMS block were combined in tables to increase the clarity of the results. If a compound was considered statistically significant from more than one analytical condition, it was placed in tables only once with the most significant *p*-value to avoid duplication of information.

# 3 Results

The proposed method was employed to investigate changes in the lipidomic profiles of kidneys during transplantation and preservation. Principal component analysis was employed to confirm the quality of the instrumental analysis for all combinations of chromatographic separation and ionization mode. As shown in Supplementary Figure S1, the pooled QC samples formed a tight cluster, thus confirming the good quality of the analytical performance. Using all four blocks of LC-HRMS analysis, 128 lipid species belonging to 14 lipid classes were annotated with level 2 confidence in metabolomics compound identification. A UpSet plot representing the number of compounds annotated in each analytical block is shown in Figure 2. A list of the identified lipid species is provided in Supplementary Table S1.

The analysis of the results was divided into four parts: 1) analysis of how warm ischemia influenced the lipidomic profiles of the kidneys; 2) comparison of the three organ-preservation methods; 3) monitoring changes across time; and 4) investigation of the influence of transplantation procedure on kidney grafts.

## 3.1 Influence of warm ischemia on kidney lipidomic profiles

The Kruskal-Wallis test, followed by *post hoc* test, was used to identify changes that occurred during warm ischemia. The results indicated that discriminative changes were mostly visible at the first sampling point of warm ischemia time (WIT). Among the identified lipids, an increase in acylcarnitines (CARs), lysophosphocholines (LPCs), and lysophosphoethanolamines (LPEs) was observed after 45 min of warm ischemia, while a corresponding decrease in phosphocholines (PCs) and sphingomyelins (SMs) was also noted. Boxplots of statistically significant lipids are shown in Figure 3.

## 3.2 Comparison of different kidney preservation methods

Chemometric analysis was conducted to visualize the data and investigate the differences in the kidney lipidomic profiles in the SCS, NEVKP, and HMP groups. The two-dimensional scoring plots (PC1 vs. PC2) presented in Supplementary Figure S2 revealed major differences in the lipidomic patterns of samples harvested under different preservation conditions. In all analyses, the lipidomes of the renal tissue from the NEVLP group showed clear separation from those of the SCS and HMP groups. In contrast, the data points in the scoring plots for the SCS and HMP groups had slightly overlapping distributions (Supplementary Figure S2). PLS-DA was applied to more accurately model differences in the lipidomic profiles of the kidneys in each preservation method group (Figure 4). Each model was validated via leave-one-out cross-validation and refined using a permutation test (permutation number = 1,000), which yielded significant ($p < 0.05$) quality parameters. This statistical analysis produced a set of compounds that successfully differentiated the different types of kidney preservation. A VIP score value > 1 was selected as a cut-off value. Furthermore, the Kruskal-Wallis test ($p < 0.05$) was used to compare the NEVKP, HMP, and SCS groups, while the discriminative compounds were selected based on chemometric and univariate analysis. Supplementary Table S2 lists the compounds meeting the above-mentioned criteria.

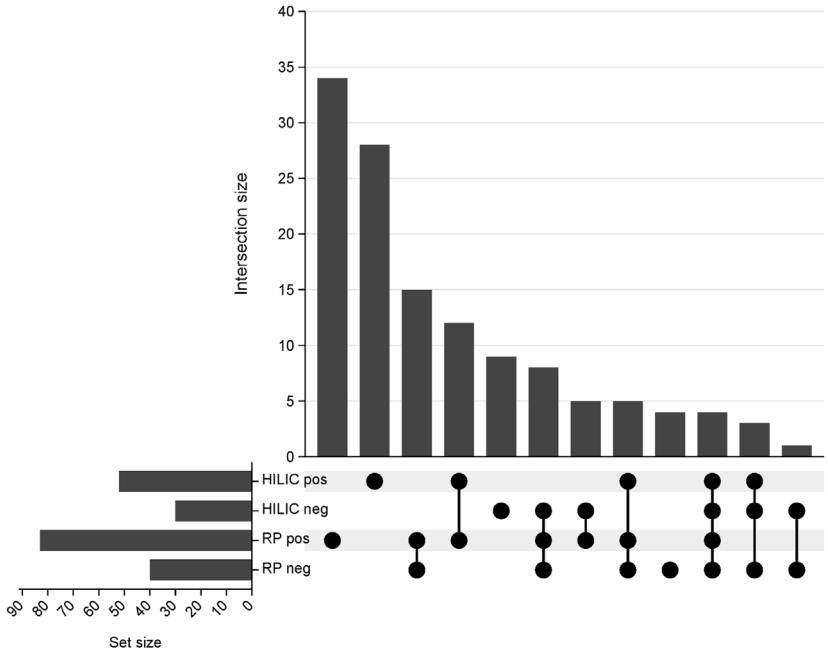


FIGURE 2
UpSet plot representing the number of compounds annotated in each analytical block. RP pos- reversed-phase in positive ionization mode; RP neg- reversed-phase in negative ionization mode; HILIC pos- hydrophilic interaction liquid chromatography in positive ionization; HILIC neg- hydrophilic interaction liquid chromatography in negative ionization mode.

Given that unsupervised analysis indicated that the observed differences were mainly related to the preservation temperature, additional PCA (Supplementary Figure S3) and PLS-DA (Figure 5) analyses were conducted to identify the compounds that statistically differentiated the hypothermic and normothermic preservation methods. These analyses were confirmed via leave-one-out cross-validation and a positive permutation test (permutation number = 1,000; $p < 0.05$). In addition, the Mann–Whitney U test with FDR correction was also applied to select statistically important compounds. Supplementary Table S3 lists the compounds with a $p$-value < 0.05 and/or a VIP value > 1. Moreover, samples collected from all preservation groups after reperfusion were compared to identify differences occurring in kidney tissue *in vivo* after using a given preservation method. Strip plots of statistically significant compounds are shown in Figure 6. After reperfusion, significantly fewer differentiating compounds were identified than during preservation. A similar comparison was performed for samples collected on postoperative day 3. However, this comparison was possible only for the samples from the NEVKP and SCS groups, as the POD3 samples from the HMP group were rendered unrepresentative due to damage, and therefore had to be omitted. Nonetheless, a comparison of samples collected from the NEVKP and SCS groups at POD3 did not reveal any significant differentiating lipids.

## 3.3 Changes across time

The Friedman test was used to evaluate changes throughout perfusion. The majority of statistically significant changes in lipids levels were found in the samples collected during mechanical perfusion (especially HMP). For NEVKP, a decrease was observed for CARs (CAR 12:0, CAR 14:1) and triacylglycerol (TG) 56:7. For HMP samples, changes throughout perfusion were mainly observed for PCs, phosphoethanolamines (PEs), and SMs but no dominant trend was observed. Strip plots of the selected compounds are shown in Figure 7, and a list of statistically significant compounds is provided in Supplementary Table S4.

Next, differences between the reperfusion and POD3 samples were evaluated. As mentioned before, the POD3 samples from the HMP group were removed from the analysis; hence, comparisons were performed only for the samples from the NEVKP and SCS groups. The analysis revealed more differentiating lipids in the SCS group (21 compounds) than in the NEVKP group (3 compounds). In the NEVKP group, all statistically significant lipids were present at higher levels on POD3 than after reperfusion. In the SCS group, elevated levels of ether-linked phospholipids and PCs with 32 carbon chains were observed on POD3, along with a corresponding reduction in SMs, PEs, PC 35:6, and PC 38:5. A list of statistically significant compounds is shown in Supplementary Table S5.

## 3.4 Influence of transplantation procedure on kidney grafts

A Mann-Whitney U test with FDR correction was carried out to determine how the transplantation and preservation procedures affected the lipidomic profiles of the kidneys. For the SCS and NEVKP groups, comparisons of lipidomic profiles at donation and

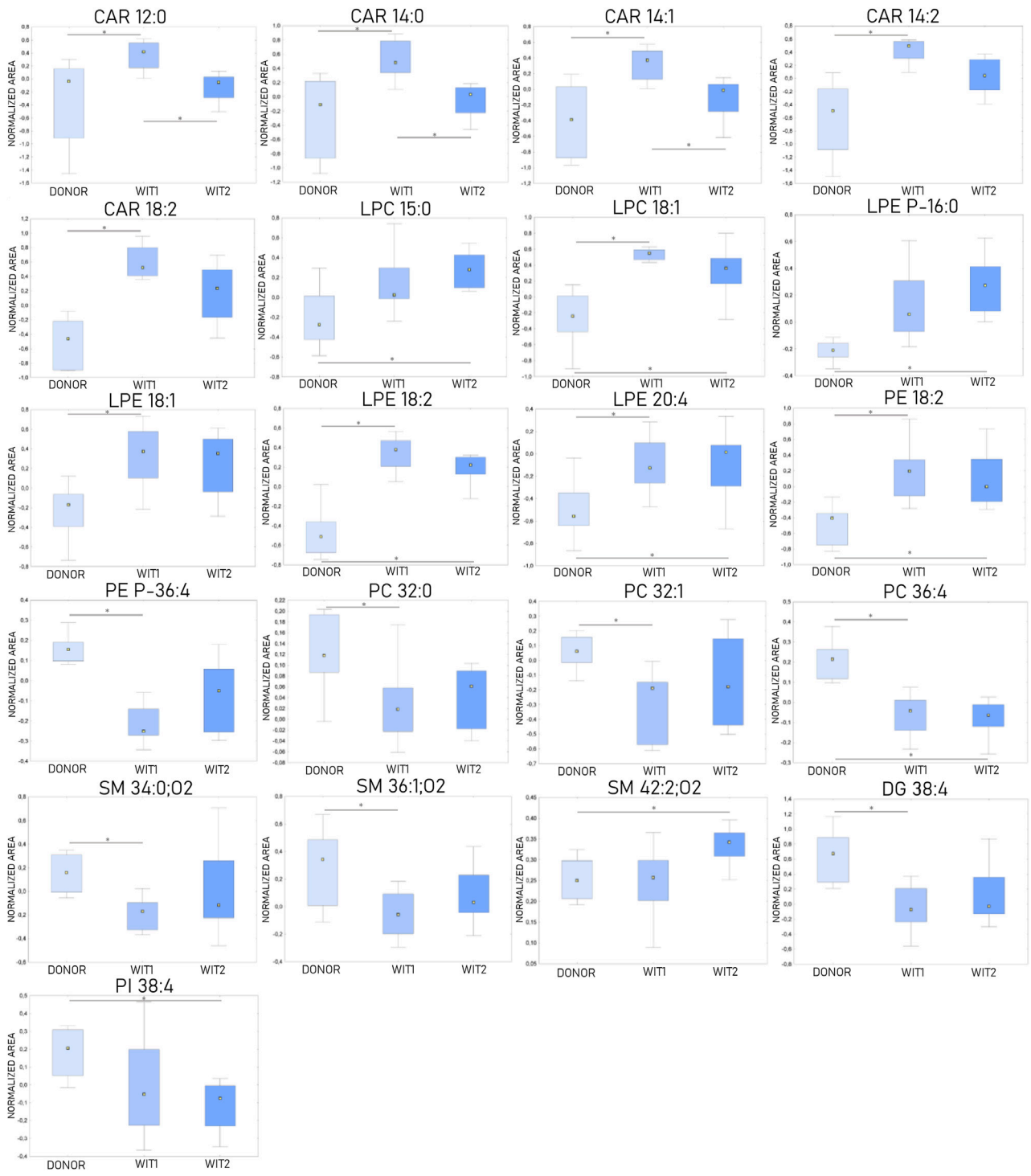


FIGURE 3
Changes in levels of selected lipids during warm ischemia ($n$ = 8). The boxplots display normalized peak areas. The rectangle's height represents the normalized peak areas in the interquartile range (Q1 and Q3). The upper whisker denotes the largest data point (excluding any outliers), while the lower whisker denotes the lowest data point (excluding any outliers). The median normalized peak area of each group is indicated with a yellow square. * is a $p$-value < 0.05. WIT1—1 h of warm ischemia; WIT2—2 h of warm ischemia.

reperfusion and donation and POD3 were performed. For the HMP group, a comparison at donation and reperfusion was conducted. As shown in Supplementary Table S6, most of the statistically significant compounds in the SCS group were found in the donor and POD3 comparison. Conversely, in the comparison of donors and reperfusion, most of the significantly differentiating compounds were found in the NEVKP group; however, most of these compounds were present at lower levels after reperfusion. While the comparison of donors and POD 3 revealed similar change trends for the SCS and NEVKP groups, the alterations were usually

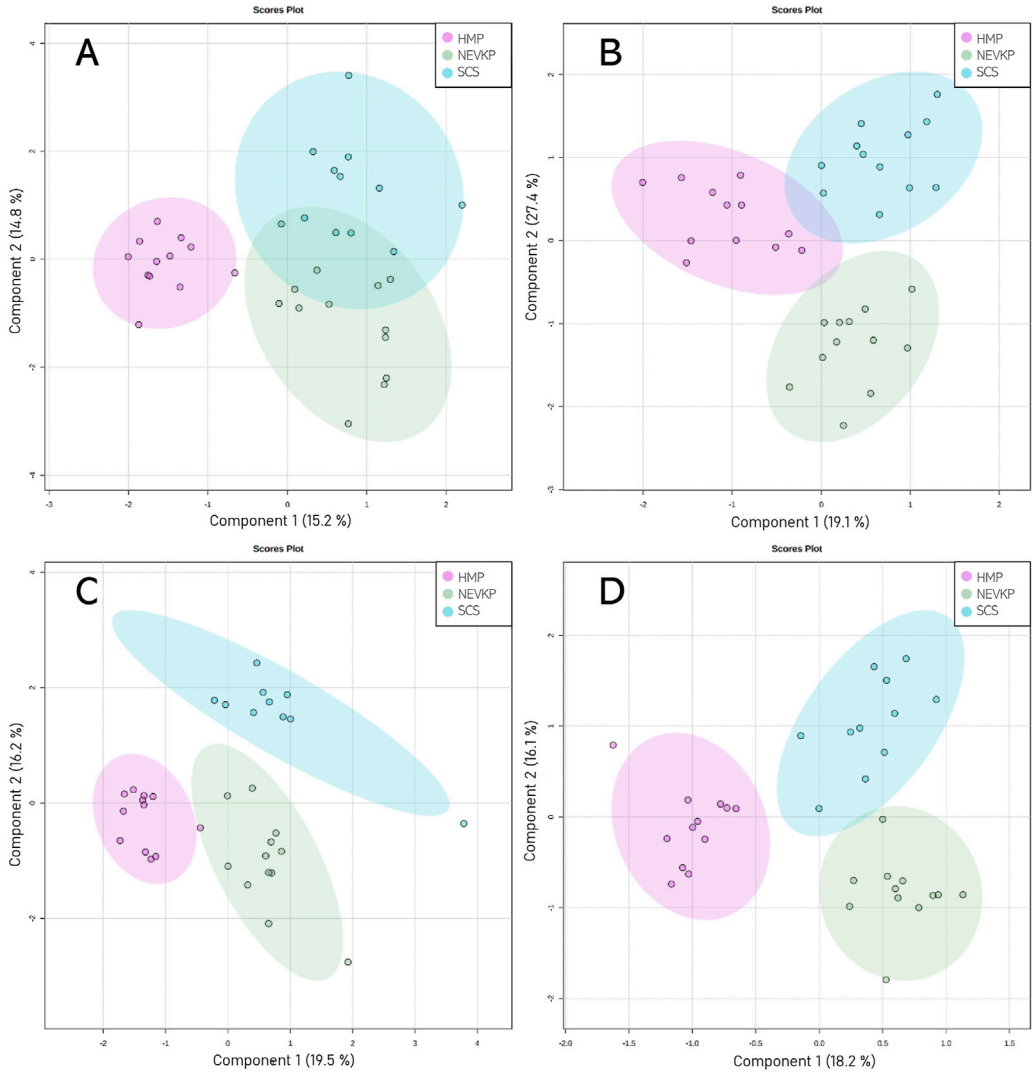


FIGURE 4
Score plots (PLS-DA) showing separation based on different types of kidney preservation. HILIC analyses in **(A)** positive and **(B)** negative ionization modes and RP analyses in **(C)** positive and **(D)** negative ionization modes. For HILIC analyses, the Q2 and R2 values for the PLS-DA model were 71% and 88% for positive ionization mode and 57% and 74% for negative ionization mode, respectively. For the RP analyses, the Q2 and R2 values for the PLS-DA model were 76% and 92% for positive ionization mode and 59% and 87% for negative ionization mode, respectively.

more noticeable in the SCS group, as evidenced by the fold change. On POD3, both groups exhibited elevated levels CARs, LPEs, and PCs and PEs (including ether-linked) with relatively shorter chains, along with a corresponding in PCs with longer chains. Additionally, a reduction in PSs, SMs, and PEs with longer chains was also observed in the SCS group.

## 4 Discussion

Organ-preservation methods have garnered significant interest in graft quality evaluation, advanced organ monitoring, and the treatment of transplanted kidneys during machine perfusion. This study further explores these trends and, to the best of our knowledge, it is the first to apply SPME to compare SCS, NEVKP, and HMP preservation methods in a porcine DCD autotransplantation model. Moreover, this study highlights the alterations in the lipidomic profile during warm ischemia and perfusion, as well as after transplantation. The minimally invasive SPME chemical biopsy allows for the repeated direct sampling of the organ, as it does not require any tissue collection. Thanks to this undisputed advantage, it was possible to validate the PLS-DA models and identify significantly differentiating lipids using a relatively small number of animals. Additionally, this study employed four LC-HRMS analyses to cover a wide range of lipids. The analysis showed that this approach allowed the identification of more lipids than was possible using only one type of chromatographic separation. The largest number of unique compounds were identified with the use of RP and HILIC separation in positive ionization mode. In negative ionization mode, using HILIC and RP separations, 9 and 4 unique compounds were identified, respectively. Therefore, based on the results obtained and taking into account the time-consuming nature

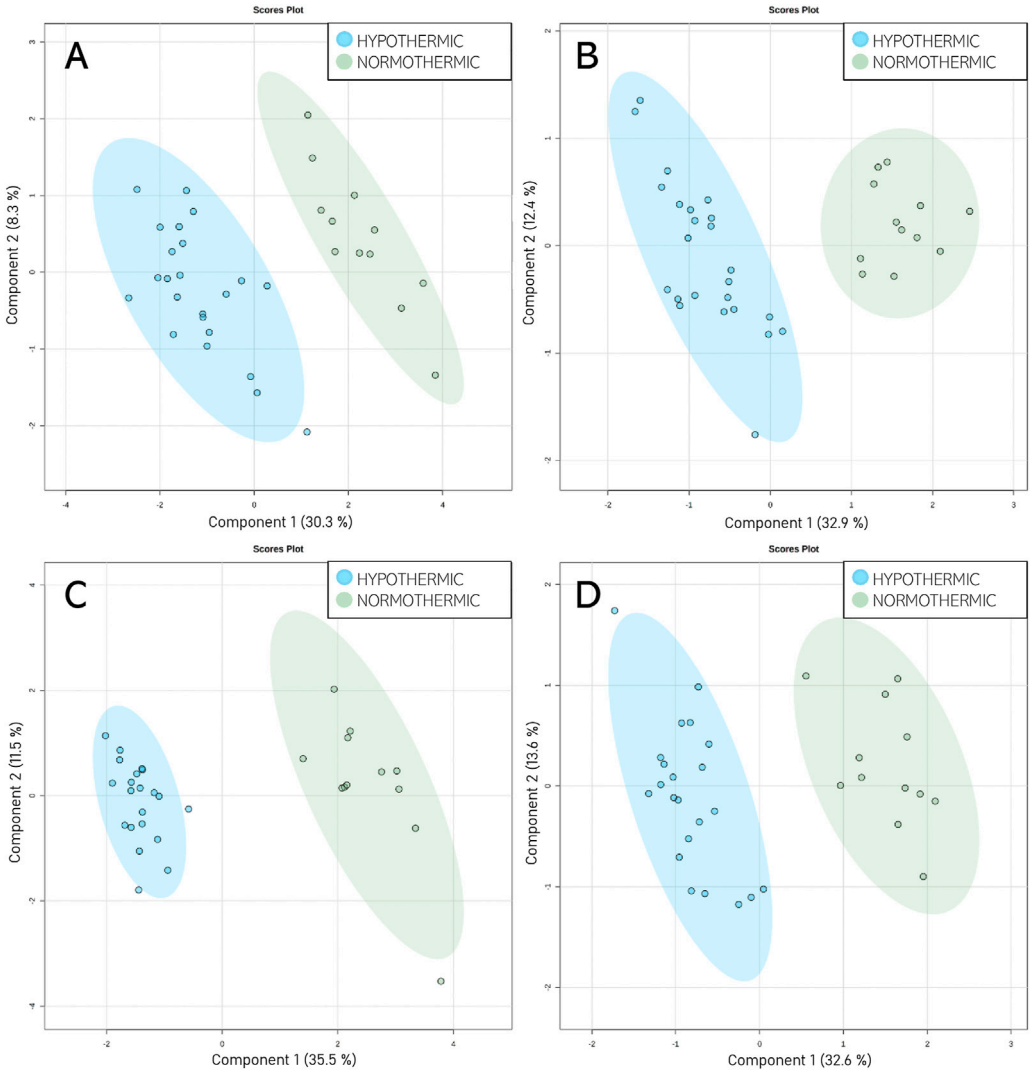


FIGURE 5
Score plots (PLS-DA) showing separation between the normothermic and hypothermic preservation methods. HILIC analyses in **(A)** positive and **(B)** negative ionization modes and RP analyses in **(C)** positive and **(D)** negative ionization modes. For HILIC analyses, the Q2 and R2 values for the PLS-DA model were 84% and 95% for positive ionization mode and 88% and 95% for negative ionization mode, respectively. For the RP analyses, the Q2 and R2 values for the PLS-DA model were 94% and 97% for positive ionization mode and 88% and 95% for negative ionization mode, respectively.

of the analyses, the consumption of organic reagents, the amount of data obtained, and the benefits of using additional LC-HRMS analyses in future studies, it is worth considering limiting the number of analyzes used, thus choosing the best compromise between advantages and disadvantages.

A thorough analysis of kidney graft tissue during warm ischemia indicated increased levels of CARs, LPCs, and LPEs. CARs are established mitochondrial biomarkers in neonatal screening; however, they are not routinely used beyond this screening, despite the growing evidence of their biomarker potential among disorders such as diabetes, sepsis, cancer, and heart failure (Breit and Weinberger, 2016; McCann et al., 2021). Moreover, alterations of CARs related to kidney disease, including acute kidney injury, progression of chronic kidney disease (CKD), and diabetic nephropathy, have been previously reported in several reports (Breit and Weinberger, 2016; Hocher and Adamski, 2017; Afshinnia et al., 2018; Kordalewska et al., 2019; Andrianova et al., 2020). In this study, significantly elevated levels of four long-chain CARs (CAR 14:0, CAR 14:1, CAR 14:2, CAR 18:2) and one medium-chain CAR (CAR 12:0) were mainly observed after 45 min of warm ischemia. CARs are crucial for transporting long-chain fatty acids into the mitochondria to ensure the β-oxidation process (Breit and Weinberger, 2016; Kordalewska et al., 2019). Thus, the increase of CARs observed during warm ischemia may be related to mitochondria dysfunction. Indeed, a similar accumulation of long-chain CARs in ischemic tissue has been reported elsewhere, and it is thought that this accumulation inhibits oxidative phosphorylation, induces mitochondrial membrane hyperpolarization, and stimulates the production of reactive oxygen species (ROS) (Liepinsh et al., 2016; Andrianova et al., 2020). LPCs and LPEs are the products of the phospholipase-induced hydrolysis of PCs and PEs (Xu et al., 2015; Law et al., 2019). These compounds play a role in cellular signal transduction, tumorigenesis, angiogenesis, immunity, atherosclerosis, cancer,

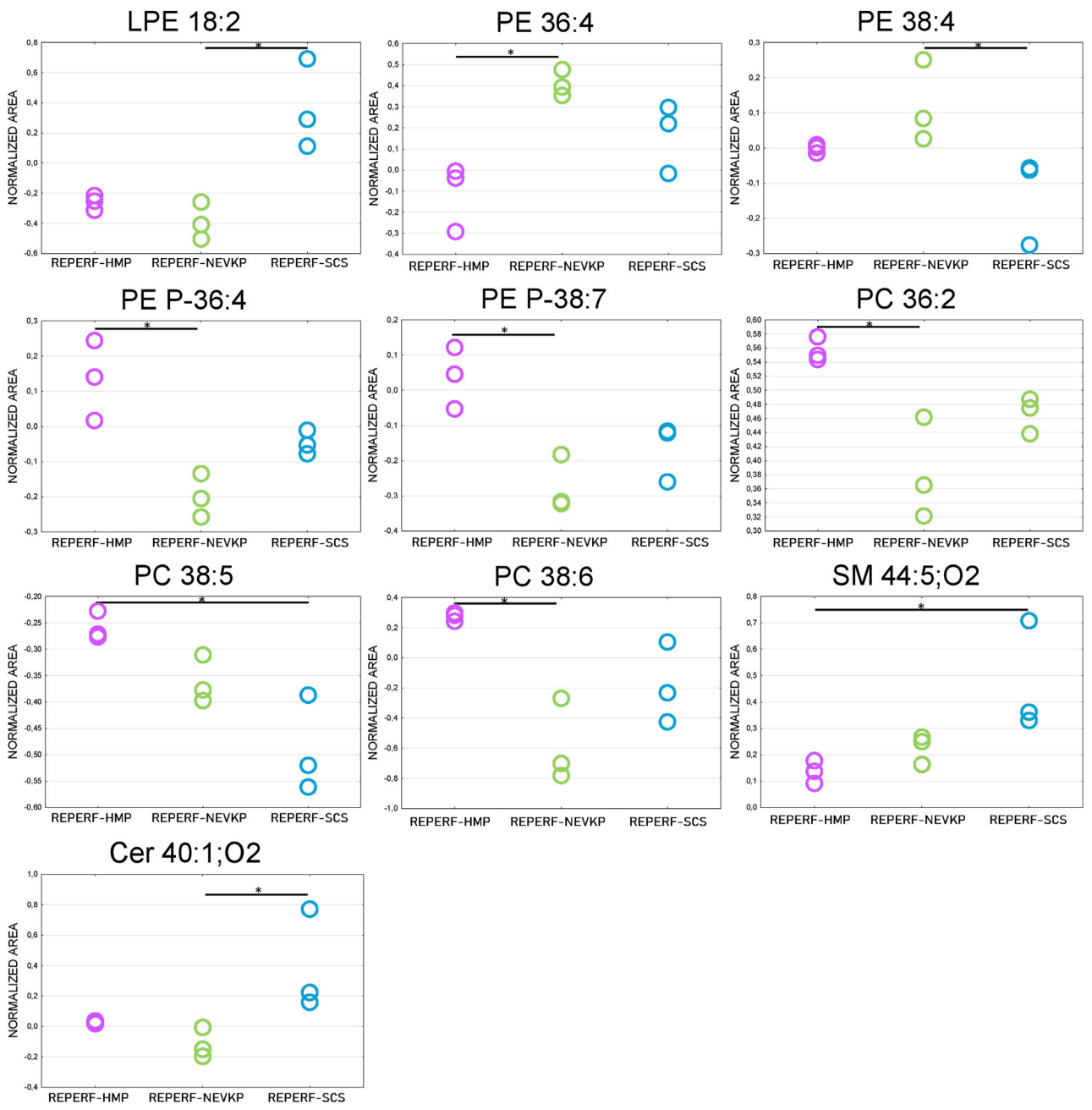


FIGURE 6
Differences in levels of selected compounds detected at reperfusion between the three preservation groups. * is a *p*-value < 0.05. NEVKP = green; HMP = pink; SCS = blue.

and neuronal survival (Kordalewska et al., 2019). Previously, higher levels of LPCs have been associated with oxidative stress and pro-inflammatory effects (Kordalewska et al., 2019). Moreover, similar to the results obtained in this study, Xu et al. (2015) observed higher pretransplant levels of LPCs (LPC 16:0, LPC 18:0) and LPEs (LPE 16:0, LPE 18:0) in donors after circulatory death compared to donors after brain death. Conversely, Rao et al. found higher levels of LPC 18:0, LPC 26:6, LPE 16:0, and LPC 18:0, along with a corresponding reduction in LPC 20:0, LPC 20:4, LPE 22:0, and LPE 24:6, 24 h after IR-induced acute kidney injury (Rao et al., 2016). The inconclusive results obtained in recent studies may be related to the complexity of the enzymatic cascade involved in LPC metabolism (Law et al., 2019).

Chemometric analysis revealed significant differences between the SCS, HMP, and NEVKP preservation methods, with further in-depth analysis demonstrating that the method's preservation temperature has a greater impact on the lipidomic profile than its mechanical character. Higher levels of CARs, PCs, ether-linked PCs, ether-linked PEs, phosphatidylinositols (PIs), TGs, most LPCs and LPEs, and longer-chain PEs were observed in the hypothermic group, while higher levels of ceramides (Cer), PSs, and shorter-chain PEs were observed in the normothermic group. Numerous SMs

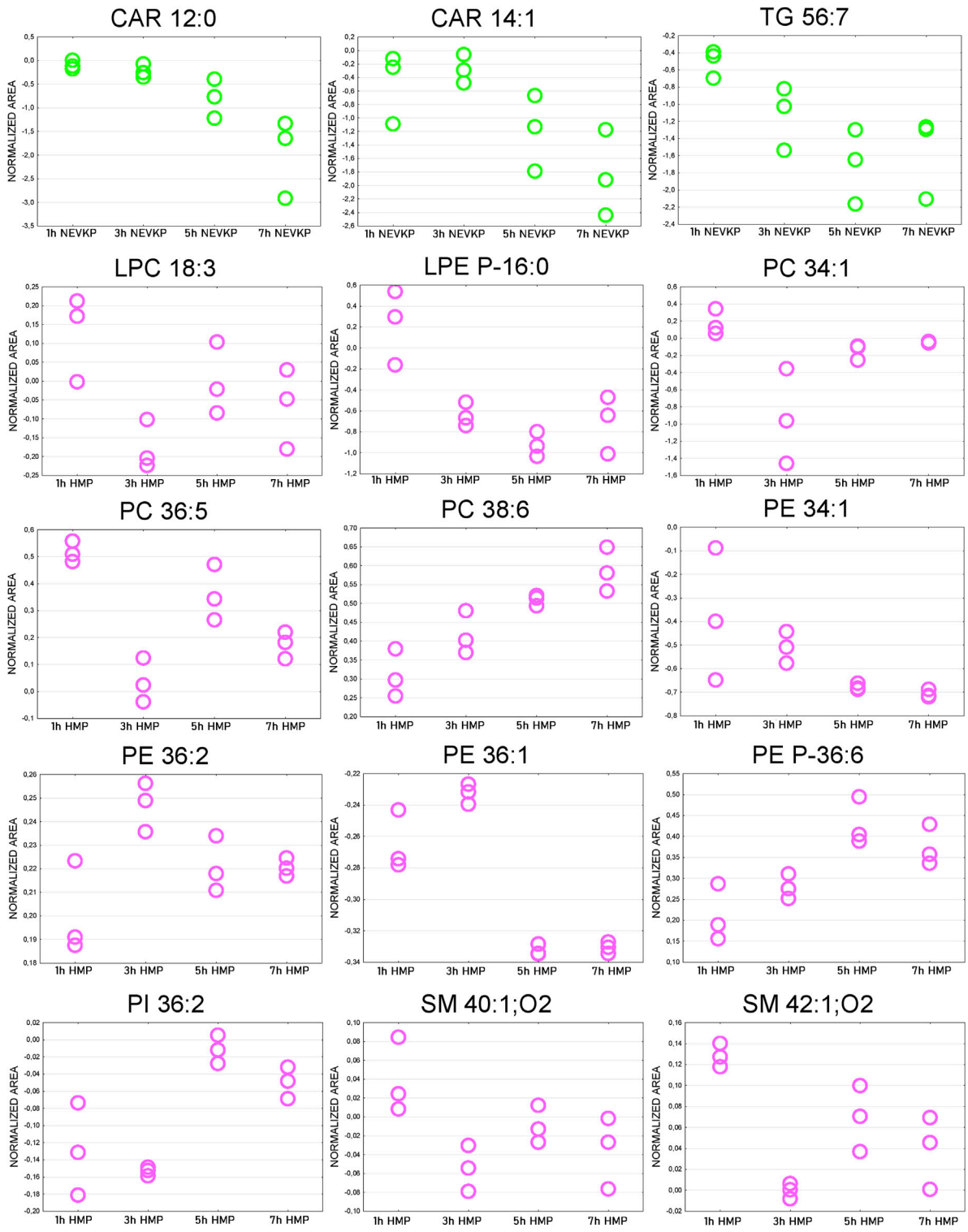


FIGURE 7
Strip plots of selected statistically significant changes between lipids and time points throughout kidney perfusion. NEVKP = green; HMP = pink.

differentiated the preservation methods, but no dominant trend was observed. As mentioned above, increased levels of long-chain CARs may be related to mitochondria dysfunction and increased production of ROS (Liepinsh et al., 2016; Andrianova et al., 2020), and higher levels of LPCs may be associated with oxidative stress and pro-inflammatory effects (Kordalewska et al., 2019). Moreover, higher levels of LPEs were observed in DCD livers compared to livers from donors after brain death (Xu et al., 2015), and increased LPE levels were observed in CKD progression (Kordalewska et al., 2019). Rao et al. (2016) and Solati et al.

(2018) have reported elevated levels of PCs in mice and rat ischemia/reperfusion (I/R) models. Similar to our results, they observed increases in PC 34:1, PC 34:2, PC 36:1, PC 36:2, PC 36:3, PC 36:4, PC 38:3, PC 38:4, PC 38:5, PC 38:6, PC 40:4 and PC 40:5. Additionally, Solati et al. reported increased levels of PIs 6 h and 12 h after I/R, while in this study higher levels of PI 36:2 and PI 38:4 were observed in the hypothermic preservation group (Solati et al., 2018). Ether-linked PCs and ether-linked PE were present at higher levels in the hypothermic group compared to the normothermic group. In Rao et al.'s study, significantly elevated levels of a small number of ether-linked phospholipids were observed 6 h after renal I/R (vs. control animals); notably, levels of these ether phospholipids were correlated with plasma creatinine. However, 24 h after I/R, only PC O-38:1 was still elevated, while ether-linked PEs were reduced at this later time point (Rao et al., 2016). Ether lipids differ from their diacyl counterparts, allowing them to contribute unique structural characteristics to biological membranes. Moreover, previous findings suggest that ether lipids play a role in various biological processes, including cell differentiation, cellular signalling, and oxidative-stress reduction (Dean and Lodhi, 2018). While alterations of ether lipids have been reported in several disorders, including neurodegenerative disease, cancer, and metabolic disorders (Rao et al., 2016; Dean and Lodhi, 2018), the molecular mechanism underlying their role in these pathologies remains unclear. Higher levels of three TGs (TG 44:1, TG 56:6, TG 56:7) and three longer-chain PEs (PE 38:4, PE 38:5, PE 40:4) were also observed in the hypothermic group. Similar elevations were reported by Afshinnia et al. (2018) in their study of lipid profiles in CKD. Their results indicated that higher quantities of long polyunsaturated lipids are related to CKD progression. Elsewhere, Solati et al. (2018) observed an increase in longer-chain PEs and a reduction in shorter-chain PEs 24 h after I/R, which aligns with the trend observed for the hypothermic group in our study. The alterations described above suggest the NEVKP method's beneficial effects with respect to kidney grafts. The lower accumulation of lipids in NEVKP kidneys, especially those with pro-inflammatory properties, results in improved graft function following NEVKP compared to hypothermic preservation methods. Additionally, the reductions of CAR 12:0 and CAR 14:1 across perfusion time points may also be indicative of NEVKP's beneficial effects.

A much smaller number of compounds differentiating the HMP, NEVKP, and SCS methods were identified post-perfusion (vs. during preservation). However, after reperfusion, the trend in changes was similar to that observed during perfusion, with most of the significant changes differentiating NEVKP from other hypothermic methods, rather than from HMP and SCS.

A comparison of the kidneys during reperfusion and on POD3 revealed more significant changes in the SCS group compared to the NEVKP group. In particular, the SCS group exhibited elevated levels of ether-linked PEs and PC P-38:4 on POD3. As noted above, Rao et al. reported higher levels of PC O-38:1, PE O-42:3, and PE O-40:4 6 h after I/R, but only PC O-38:1 remained elevated in I/R at 24 h. However, more research is required to investigate the molecular mechanisms underlying the role of ether lipids in kidney disease. Additionally, in the SCS group, lower levels of SMs were identified on POD3. Previous findings have shown an increase in SMs 24 h after I/R in animal models (Rao et al., 2016; Solati et al., 2018). In contrast, Zhao et al. (2014) observed lower SMs levels in an acute graft rejection group after transplantation, while Tofte et al. (2019) demonstrated that higher levels of specific SMs were associated with a lower risk of end-stage renal disease and all-cause mortality in type 1 diabetes. These findings indicate that lower levels of SMs may be related to impaired graft function. The results of this comparison (donor vs. POD3) provide further evidence that NEKVP enables improved graft function compared to SCS.

The last step of untargeted analysis entailed a comparison of the lipidomic profiles at baseline (donation) and reperfusion and at baseline and POD3. The largest number of statistically significant compounds was identified in the donor-POD3 comparison for the SCS group. While the trends in changes were similar for the SCS and NEVKP groups, the alterations were usually more noticeable in the SCS group. The observed alterations mainly concerned lipids described previously in this study. Higher levels of CARs, a few LPCs and LPEs, several PCs and PEs, and ether-linked PCs on POD3 were observed for both the SCS and NEVKP groups. However, more compounds among these lipid classes were statistically significant for the SCS group. As discussed above, the elevated levels of these lipids may be related to I/R injury, mitochondrial dysfunction, pro-inflammatory effect, and/or oxidative stress. Significant reductions in SM levels on POD3 were observed only for the SCS group. As previously noted, prior findings have shown a connection between reduced SM levels and acute graft rejection (Zhao et al., 2014).

Despite these promising results, this study has several limitations. The first limitation is the small sample sizes. However, since SPME enables multiple analyses over time, it is possible to acquire a large number of samples without requiring more animals. Another limitation was that the obtained results were not compared with routinely assessed clinical parameters; as such, the analysis was not as comprehensive as it might have otherwise been. A final limitation of this study design is the relatively short follow-up period of 3 days post-transplantation. Unfortunately, this interval was necessary, as the porcine experimental setup makes it difficult to investigate over a longer follow-up period of months, or even years.

## 5 Conclusion

SPME chemical biopsy followed by LC-MS/MS analysis enables the minimally invasive and repeated sampling of the same tissue. As such, this method was successfully applied to track alterations in a graft throughout the entire transplantation procedure, and to compare kidney lipidomic profiles during storage with different preservation methods. As a result, we observed that the preservation temperature has a more significant impact on the lipidomic profile of the kidney than the preservation method's mechanical characteristics. Higher levels of CARs, PCs, ether-linked PCs, ether-linked PEs, PIs, TGs, most LPC and LPE, and longer-chain PEs were observed in the hypothermic preservation group, which may be related to I/R injury, mitochondrial dysfunction, pro-inflammatory effect, and oxidative stress. Hence, the obtained results suggest that the use of NEVKP can have a beneficial effect on graft function.

## Data availability statement

The original contributions presented in the study are publicly available. This data can be found here: https://repod.icm.edu.pl/dataset.xhtml?persistentId=doi:10.18150/ATK9DA

## Ethics statement

The animal study was approved by Animal Care Committee at the Toronto General Research Institute, Ontario, Canada. The study was conducted in accordance with the local legislation and institutional requirements.

## Author contributions

NW: Methodology, Formal analysis, Investigation, Data curation, Writing–original draft, Writing–review and editing, Visualization. KŁ: Investigation, Formal analysis, Writing–review and editing. IS: Investigation, Writing–review and editing. HR-S: Methodology, Investigation, Writing–review and editing. PU: Methodology, Investigation, Writing–review and editing. JP: Methodology, Supervision, Resources, Writing–review and editing, MS: Conceptualization, Methodology, Investigation, Resources, Writing–review and editing. BB: Conceptualization, Methodology, Supervision, Resources, Investigation, Writing–review and editing, Funding acquisition.

## Funding

The authors declare that financial support was received for the research, authorship, and/or publication of this article. This study was funded by National Science Centre, grant Opus No. 2017/27/B/NZ5/01013.

## Acknowledgments

The authors would like to acknowledge Supelco/MilliporeSigma for kindly supplying the SPME probes and Thermo Fisher Scientific for granting us access to a Q-Exactive Focus mass spectrometer.

## Conflict of interest

The authors declare that the research was conducted in the absence of any commercial or financial relationships that could be construed as a potential conflict of interest.

## Publisher's note

All claims expressed in this article are solely those of the authors and do not necessarily represent those of their affiliated organizations, or those of the publisher, the editors and the reviewers. Any product that may be evaluated in this article, or claim that may be made by its manufacturer, is not guaranteed or endorsed by the publisher.

## Supplementary material

The Supplementary Material for this article can be found online at: https://www.frontiersin.org/articles/10.3389/fmolb.2024.1341108/full#supplementary-material

## References

Afshinnia, F., Rajendiran, T. M., Soni, T., Byun, J., Wernisch, S., Sas, K. M., et al. (2018). Impaired $\beta$-oxidation and altered complex lipid fatty acid partitioning with advancing CKD. *J. Am. Soc. Nephrol.* 29, 295–306. doi:10.1681/ASN.2017030350

Andrianova, N. V., Popkov, V. A., Klimenko, N. S., Tyakht, A. V., Baydakova, G. V., Frolova, O. Y., et al. (2020). Microbiome-metabolome signature of acute kidney injury. *Metabolites* 10, 142. doi:10.3390/metabo10040142

Azancot, M. A., Moreso, F., Salcedo, M., Cantarell, C., Perello, M., Torres, I. B., et al. (2014). The reproducibility and predictive value on outcome of renal biopsies from expanded criteria donors. *Kidney Int.* 85, 1161–1168. doi:10.1038/ki.2013.461

Bojko, B. (2022). Solid-phase microextraction: a fit-for-purpose technique in biomedical analysis. *Anal. Bioanal. Chem.* 414, 7005–7013. doi:10.1007/s00216-022-04138-9

Breit, M., and Weinberger, K. M. (2016). Metabolic biomarkers for chronic kidney disease. *Arch. Biochem. Biophys.* 589, 62–80. doi:10.1016/j.abb.2015.07.018

Dare, A. J., Pettigrew, G. J., and Saeb-Parsy, K. (2014). Preoperative assessment of the deceased-donor kidney: from macroscopic appearance to molecular biomarkers. *Transplantation* 97, 797–807. doi:10.1097/01.TP.0000441361.34103.53

Dean, J. M., and Lodhi, I. J. (2018). Structural and functional roles of ether lipids. *Protein Cell* 9, 196–206. doi:10.1007/s13238-017-0423-5

Hocher, B., and Adamski, J. (2017). Metabolomics for clinical use and research in chronic kidney disease. *Nat. Rev. Nephrol.* 13, 269–284. doi:10.1038/nrneph.2017.30

Hosgood, S. A., Hoff, M., and Nicholson, M. L. (2021). Treatment of transplant kidneys during machine perfusion. *Transpl. Int.* 34, 224–232. doi:10.1111/tri.13751

Kaths, J. M., Echeverri, J., Chun, Y. M., Cen, J. Y., Goldaracena, N., Linares, I., et al. (2017). Continuous normothermic *ex vivo* kidney perfusion improves graft function in donation after circulatory death pig kidney transplantation. *Transplantation* 101, 754–763. doi:10.1097/TP.0000000000001343

Kaths, J. M., Echeverri, J., Goldaracena, N., Louis, K. S., Yip, P., John, R., et al. (2016). Heterotopic renal autotransplantation in a porcine model: a step-by-step protocol. *J. Vis. Exp.* 2016, 53765–53769. doi:10.3791/53765-v

Kaths, J. M., Hamar, M., Echeverri, J., Linares, I., Urbanellis, P., Cen, J. Y., et al. (2018). Normothermic *ex vivo* kidney perfusion for graft quality assessment prior to transplantation. *Am. J. Transpl.* 18, 580–589. doi:10.1111/ajt.14491

Kaths, J. M., Spetzler, V. N., Goldaracena, N., Echeverri, J., Louis, K. S., Foltys, D. B., et al. (2015). Normothermic *ex vivo* kidney perfusion for the preservation of kidney grafts prior to transplantation. *J. Vis. Exp.* 2015, e52909–e52913. doi:10.3791/52909

Kordalewska, M., Macioszek, S., Wawrzyniak, R., Sikorska-Wiśniewska, M., Śledziński, T., Chmielewski, M., et al. (2019). Multiplatform metabolomics provides insight into the molecular basis of chronic kidney disease. *J. Chromatogr. B Anal. Technol. Biomed. Life Sci.* 1117, 49–57. doi:10.1016/j.jchromb.2019.04.003

Law, S., Chan, M., Marathe, G. K., Parveen, F., Chen, C., and Ke, L. (2019). An updated review of lysophosphatidylcholine metabolism in human diseases. *Int. J. Mol. Sci.* 20, 1149. doi:10.3390/ijms20051149

Liepinsh, E., Makrecka-Kuka, M., Volska, K., Kuka, J., Makarova, E., Antone, U., et al. (2016). Long-chain acylcarnitines determine ischaemia/reperfusion-induced damage in heart mitochondria. *Biochem. J.* 473, 1191–1202. doi:10.1042/BCJ20160164

Lindell, S. L., Muir, H., Brassil, J., and Mangino, M. J. (2013). Hypothermic machine perfusion preservation of the DCD kidney: machine effects. *J. Transpl.* 2013, 802618. doi:10.1155/2013/802618

Łuczykowski, K., Warmuzińska, N., and Bojko, B. (2023). Solid phase microextraction—a promising tool for graft quality monitoring in solid organ transplantation. *Separations* 10, 153. doi:10.3390/separations10030153

McCann, M. R., De la Rosa, M. V. G., Rosania, G. R., and Stringer, K. A. (2021). L-carnitine and acylcarnitines: mitochondrial biomarkers for precision medicine. *Metabolites* 11, 1–21. doi:10.3390/metabo11010051

Moeckli, B., Sun, P., Lazeyras, F., Morel, P., Moll, S., Pascual, M., et al. (2019). Evaluation of donor kidneys prior to transplantation: an update of current and emerging methods. *Transpl. Int.* 32, 459–469. doi:10.1111/tri.13430

Rao, S., Walters, K. B., Wilson, L., Chen, B., Bolisetty, S., Graves, D., et al. (2016). Early lipid changes in acute kidney injury using SWATH lipidomics coupled with MALDI tissue imaging. *Am. J. Physiol. - Ren. Physiol.* 310, F1136–F1147. doi:10.1152/ajprenal.00100.2016

Resch, T., Cardini, B., Oberhuber, R., Weissenbacher, A., Dumfarth, J., Krapf, C., et al. (2020). Transplanting marginal organs in the era of modern machine perfusion and advanced organ monitoring. *Front. Immunol.* 11, 631. doi:10.3389/fimmu.2020.00631

Solati, Z., Edel, A. L., Shang, Y., Karmin, O., and Ravandi, A. (2018). Oxidized phosphatidylcholines are produced in renal ischemia reperfusion injury. *PLoS One* 13, e0195172. doi:10.1371/journal.pone.0195172

Stryjak, I., Warmuzińska, N., Łuczykowski, K., Hamar, M., Urbanellis, P., Wojtal, E., et al. (2020). Using a chemical biopsy for graft quality assessment. *J. Vis. Exp.*, e60946. doi:10.3791/60946-v

Swanson, K. J., Aziz, F., Garg, N., Mohamed, M., Mandelbrot, D., Djamali, A., et al. (2020). Role of novel biomarkers in kidney transplantation. *World J. Transpl.* 10, 230–255. doi:10.5500/wjt.v10.i9.230

Tofte, N., Suvitaival, T., Ahonen, L., Winther, S. A., Theilade, S., Frimodt-Møller, M., et al. (2019). Lipidomic analysis reveals sphingomyelin and phosphatidylcholine species associated with renal impairment and all-cause mortality in type 1 diabetes. *Sci. Rep.* 9, 16398. doi:10.1038/s41598-019-52916-w

Urbanellis, P., Hamar, M., Kaths, J. M., Kollmann, D., Linares, I., Mazilescu, L., et al. (2020). Normothermic *ex vivo* kidney perfusion improves early DCD graft function compared with hypothermic machine perfusion and static cold storage. *Transplantation* 104, 947–955. doi:10.1097/TP.0000000000003066

Warmuzińska, N., Łuczykowski, K., and Bojko, B. (2022). A review of current and emerging trends in donor graft-quality assessment techniques. *J. Clin. Med.* 11, 487. doi:10.3390/jcm11030487

Xu, J., Casas-Ferreira, A. M., Ma, Y., Sen, A., Kim, M., Proitsi, P., et al. (2015). Lipidomics comparing DCD and DBD liver allografts uncovers lysophospholipids elevated in recipients undergoing early allograft dysfunction. *Sci. Rep.* 5, 17737. doi:10.1038/srep17737

Zhao, X., Chen, J., Ye, L., and Xu, G. (2014). Serum metabolomics study of the acute graft rejection in human renal transplantation based on liquid chromatography-mass spectrometry. *J. Proteome Res.* 13, 2659–2667. doi:10.1021/pr5001048

frontiers | Frontiers in Molecular Biosciences

TYPE Original Research
PUBLISHED 14 August 2024
DOI 10.3389/fmolb.2024.1407974



OPEN ACCESS

EDITED BY
Jacopo Troisi,
University of Salerno, Italy

REVIEWED BY
Soumyabrata Banerjee,
Vidyasagar University, India
Lisandro Jorge Falomir Lockhart,
Instituto de Investigaciones Bioquímicas de La Plata (INIBIOLP), Argentina

*CORRESPONDENCE
Petr G. Lokhov,
lokhovpg@rambler.ru

RECEIVED 27 March 2024
ACCEPTED 30 July 2024
PUBLISHED 14 August 2024

CITATION
Lokhov PG, Trifonova OP, Balashova EE, Maslov DL, Ugrumov MV and Archakov AI (2024) Application of clinical blood metabogram for diagnosis of early-stage Parkinson's disease:
a pilot study.
*Front. Mol. Biosci.* 11:1407974.
doi: 10.3389/fmolb.2024.1407974



# Application of clinical blood metabogram for diagnosis of early-stage Parkinson's disease: a pilot study

Petr G. Lokhov[1]*, Oxana P. Trifonova[1], Elena E. Balashova[1], Dmitry L. Maslov[1], Michael V. Ugrumov[2] and Alexander I. Archakov[1]

[1]Laboratory of Mass Spectrometric Metabolomic Diagnostics, Institute of Biomedical Chemistry, Moscow, Russia, [2]Laboratory of Neural and Neuroendocrine Regulations, Koltzov Institute of Developmental Biology of the Russian Academy of Sciences, Moscow, Russia

In terms of time, cost, and reproducibility of clinical laboratory tests, a mass spectrometric clinical blood metabogram (CBM) enables the investigation of the blood metabolome. Metabogram's components provide clinically relevant information by describing related groups of blood metabolites connected to humoral regulation, the metabolism of lipids, carbohydrates and amines, lipid intake into the organism, and liver function. For further development of the CBM approach, the ability of CBM to detect metabolic changes in the blood in the early stages of Parkinson's disease (PD) was studied in this work. In a case-control study (n = 56), CBM enabled the detection of the signature in blood metabolites related to 1–2.5 clinical stages of PD, according to the modified Hoehn and Yahr scale, which is formed by alterations in eicosanoids, phospholipids and, presumably, in the butadione metabolism. The CBM component-based diagnostic accuracy reached 77%, with a specificity of 71% and sensitivity of 82%. The research results extend the range of disorders for which CBM is applicable and offer new opportunities for revealing PD-specific metabolic alterations and diagnosing early-stage PD.

KEYWORDS

**metabolomics, clinical blood metabogram, Parkinson's disease, diagnostics, mass spectrometry, blood plasma, clinical metabolomics, personalized metabolomics**

## 1 Introduction

Parkinson's disease (PD), which usually affects elderly people, is the second most prevalent neurodegenerative condition of the central nervous system. Due to the aging population, the incidence of PD has substantially grown. Since the first description of PD by James Parkinson in 1817 (Parkinson, 2002), the exact mechanism causing this disease is still unknown. Hallmarked dopaminergic neurons that are destroyed in the substantia nigra and the formation of Lewy bodies that are largely made of fibrillar α-synuclein are pathological characteristics of PD (Tansey and Goldberg, 2010). Genetic studies of familial PD have identified mutations in individual genes in monogenic PD. In particular, mutations leading to the development of PD are localized in the genes encoding α-synuclein, dardarin, vacuolar protein sorting-associated protein 35, parkin ligase, DJ1 deglycase, and acid β-glucosidase (Ross, 2013; Deng et al., 2018).

There are evidences that oxidative damage and mitochondrial dysfunction lead to a cascade of events and ultimately contribute to the degeneration of dopaminergic neurons (Rani and Mondal, 2020). Other studies demonstrated that apoptosis plays a substantial role in neurological disorders (Tompkins et al., 1997). Recent studies have linked astrogliosis to the development of PD (Heo et al., 2020).

The neuroinflammatory theory appears to be the most plausible of the potential causes of PD (Tansey and Goldberg, 2010; Gelders et al., 2018). The inflammatory process, which is a protective mechanism against various types of damage, when prolonged, enhances the progression of neurodegeneration (Snyder et al., 2017). A role of neuroinflammation in the pathology of PD was demonstrated in a large number of studies, indicating that neuroinflammatory processes may play a causative role in the development of PD (Salama et al., 2020).

Several other factors causing PD, such as reduced Parkin activity, altered metabolism, aberrant epigenetics, exposure to toxins, telomere shortening, or protein misfolding, were reported in a number of studies (Le et al., 2013; Scheffold et al., 2016; Wen et al., 2016; Rokad et al., 2017; Meng et al., 2020). According to some studies, PD can be classified as a prion-like disease (Olanow and Brundin, 2013).

Due to the still unclear etiology and pathogenesis of PD, the identification of biomarkers for its diagnosis is challenging and has not been successful yet (Chen-Plotkin et al., 2018). In this situation, the omics technologies, which enable measuring the diversity of a biologic system's molecules in a single-run analysis (e.g., DNA sequencing in genomics, protein identification technologies in proteomics, and profiling of low-molecular-weight substances in metabolomics), may be helpful (Omenn et al., 2012). Among the omics sciences, metabolomics is the most promising for supplying useful information for disease diagnostics because metabolites form molecular phenotypes directly reflecting physiological and pathological situations in organisms. Thus, in metabolomics studies of blood, the diagnostic accuracy of diseases often reaches 90%–95% (Trifonova et al., 2013). Such results stimulate the introduction of metabolomics technologies in medicine for the diagnosis of difficult-to-diagnose diseases, including PD, the etiology and pathogenesis of which is often associated with low-molecular substances.

A clinical blood metabogram (CBM), a new personalized metabolomics approach that is a simplified single-subject (N-of-1) metabolomics analysis, was recently introduced (Lokhov et al., 2023b). Direct-infusion mass spectrometry (DIMS), principal component analysis (PCA), and metabolite set enrichment analysis (MSEA) were used to develop the CBM. The metabogram avoids the complexity of each N-of-1 metabolomics study and is characterized by rapid execution, simple data processing, high reproducibility, and uncomplicated result interpretation, which should make it easier to apply CBM in the clinic in the laboratory-developed test (LDT) format (Figure 1). An LDT is a specific kind of diagnostic test that is created, produced, and utilized in a single laboratory (Sharfstein, 2015; FDA., 2018; Genzen, 2019; Schreier et al., 2019) that is commonly used to implement omics tests.

The blood metabolome groups that deal with humoral control, lipid-carbohydrate and lipid-amine metabolism, eicosanoids, amino acids, lipid intake into the body, and liver function are presented in the CBM that makes it clinically valuable. The main objective of this study is to examine the metabogram's clinical potential in relation to revealing metabolic features and diagnosing early PD. To do this, the blood metabolome of patients with PD 1–2.5 stages, as measured by the modified Hoehn and Yahr scale, was examined using the CBM.

# 2 Materials and methods

## 2.1 Blood samples

Samples of blood plasma used in this study were taken from a previously published study, where study participants (n = 56) were recruited at the Republican Clinical Diagnostic Centre of Extrapyramidal Pathology and Botulinum Therapy (Kazan, Russia) (Balashova et al., 2018). Briefly, study cohort included untreated PD patients at 1–2.5 stages according to modified Hoehn and Yahr scale (stage 1 – unilateral involvement only; stage 1.5 – unilateral and axial involvement; stage 2 – bilateral involvement without impairment of balance; stage 2.5 – mild bilateral disease with recovery on pull test) (Goetz et al., 2004) and controls without neurodegenerative diseases. The following exclusion criteria were used for PD patients and control subjects: severe systemic disease, stroke, brain surgery, Alzheimer's disease or any other medical history central nervous system disease, chronic renal failure, systemic infections, malignancy, cardiac or hepatic dysfunction, and autoimmune disease. Informed consent was obtained from all subjects involved in the study. The study was conducted in accordance with the Declaration of Helsinki, and approved by the Institutional Ethics Committee of Koltzov Institute of Developmental Biology of Russian Academy of Sciences (protocol code 55 and date of approval 9 December 2021).

## 2.2 Mass spectrometry analysis of blood samples

The same equipment and materials were used as in the previously reported study (Balashova et al., 2018), including venous blood sampling, sample preparation, mass spectrometer analysis, mass spectra processing, and mass list processing (alignment, standardization, and normalizing).

Blood samples were taken from the vein before the morning meal. Samples (3 mL) were placed into glass tubes containing $K_2$EDTA (BD Vacutainer; Becton, Dickinson and Company, Franklin Lakes, NJ, United States) and centrifuged within 15 min of blood collection at 1,600 × g and room temperature. The resultant blood plasma was subdivided into aliquots that were pipetted into plastic tubes. These tubes were marked, transported in special thermocontainers, frozen, and then stored at −80°C until analysis. The analyzed samples were subjected to one freeze/thaw cycle.

For plasma deproteinization, aliquots (10 µL) were mixed with 10 µL water (LiChrosolv; Merck KGaA, Darmstadt, Germany) and 80 µL methanol (Fluka, Munich, Germany) and incubated at room temperature. After 15 min, samples were centrifuged at 13,000 × g (MiniSpin plus centrifuge; Eppendorf AG, Hamburg, Germany) for 10 min. Deproteinized supernatants were then

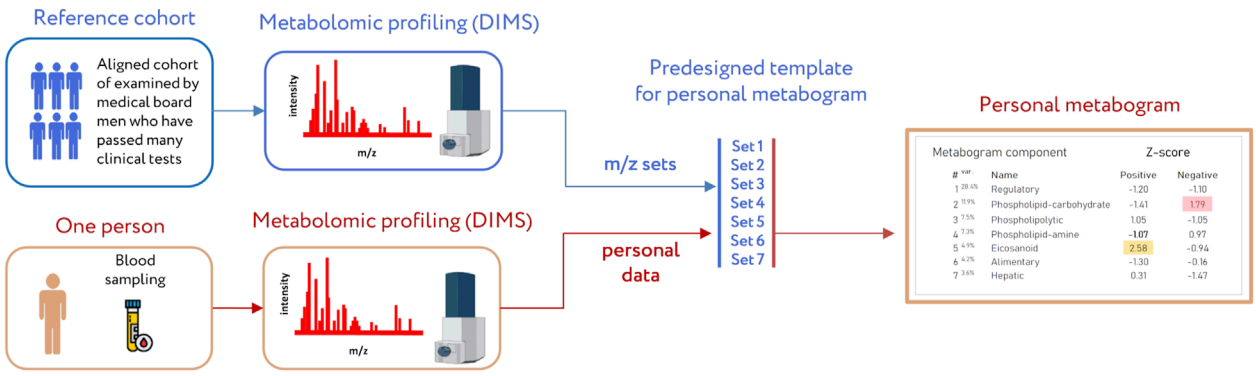


FIGURE 1
Workflow for producing a clinical blood metabogram. Sampled blood, after sample preparation in order to separate the metabolome fraction, is subjected to direct-infusion mass spectrometry (DIMS). The resulting mass peaks are aligned with the predefined sets of mass spectrometric peaks corresponding to the components of the metabogram (predesigned template of personal metabogram). Mass peak intensities are converted into Z-scores and averaged to obtain metabogram component values showing the state (normal, upregulated, or downregulated) of the blood metabolome (i.e., clinically relevant information). Adapted from (Lokhov et al., 2023b).

transferred to clean plastic Eppendorf tubes, and fifty volumes of methanol containing 0.1% formic acid (Fluka) were added to each tube. The resulting solutions were subjected to mass spectrometry analysis.

Samples were analyzed with a maXis hybrid quadrupole time-of-flight mass spectrometer (Bruker Daltonics, Billerica, MA, United States) equipped with an electrospray ionization (ESI) source. The mass spectrometer was set up to prioritize the detection of ions with a mass-to-charge ratio ($m/z$) ranging from 50 to 1,000 and a mass accuracy of 1–2 parts per million (ppm). Spectra were recorded in the positive ion charge detection mode. Samples were injected into the ESI source using a glass syringe (Hamilton Bonaduz AG, Bonaduz, Switzerland) connected to a syringe injection pump (KD Scientific, Holliston, MA, United States). The flow rate of samples to the ionization source was 180 µL/h, and samples were injected in a randomized order (e.g., control samples were run between case samples). Mass spectra were obtained using DataAnalysis version 3.4 (Bruker Daltonics) to summarize 1-min signals. Ion metabolite masses were determined from the mass spectrum peaks obtained using the DataAnalysis program. All peaks above noise level (signal to noise ratio >1) were selected, and the metabolite ion masses were pooled and processed using Matlab program (version R2019a; MathWorks, Natick, MA, United States). For the recalibration of all the peak $m/z$ values, the internal standard losartan (m/z 423.169) was used.

Standardization of mass peak intensities was performed as described previously (Lokhov et al., 2020) by dividing the intensity by the standardization value, which was calculated for each peak separately as follows: the 50 Da range (which started 25 Da before and ended 25 Da after the $m/z$ of the mass peak) was selected; all peaks inside the range were sorted in descending order according to their intensities; the intensity of the 150th peak was selected as the standardization value. Standardized intensities improved further analysis due to the correction of ion suppression of peak intensities (Lokhov et al., 2020). Standardized mass lists were normalized by applying the *normalize* function (which brings the sum of the intensities of the peaks in the spectrum to 1) of the Matlab program.

The alignment of the $m/z$ values of the mass peaks between different mass spectra was performed as described previously (Lokhov et al., 2011). The alignment algorithm used was previously specially developed and tested for the high-resolution mass spectra of blood metabolites obtained by DIMS and implemented as an iterative process based on the detection of correlation of mass spectrometry peak patterns.

## 2.3 Design of metabogram template for personal metabograms

The details of the metabogram construction using a reference cohort of healthy subjects are described in a previous study (Lokhov et al., 2023b). Briefly, DIMS was used to analyze blood plasma samples from 48 healthy people (reference cohort) to develop the metabogram template (Figure 1). The lists of mass peaks that were produced after mass spectra processing (alignment, standardization, and normalization) were analyzed using principal component analysis (PCA). The metabogram components were formed by the mass peaks corresponding to the highest positive or lowest negative coefficients (loadings) of the first seven principal components. The resulting sets of $m/z$ values of mass peaks are presented in Supplementary Table S1. 70% of blood metabolome variance is explained by these sets of mass peaks, which were used in this study as a template to quickly produce personal metabograms. The composition of metabogram components (Figure 2) was determined by identifying the metabolite classes with which they are enriched. For this, MSEA was used (Xia and Wishart, 2010). Clinical blood tests (n = 71) were also used to determine the biological significance of the metabogram components (Lokhov et al., 2023b). Each metabogram component has two Z-score scales reflecting its measure, named the "positive" and "negative" parts, because the principal components involved in the development of the metabogram have both positive and negative coefficients (loadings). In short, the original variables that comprise the principal components are linear combinations of their coefficients. The

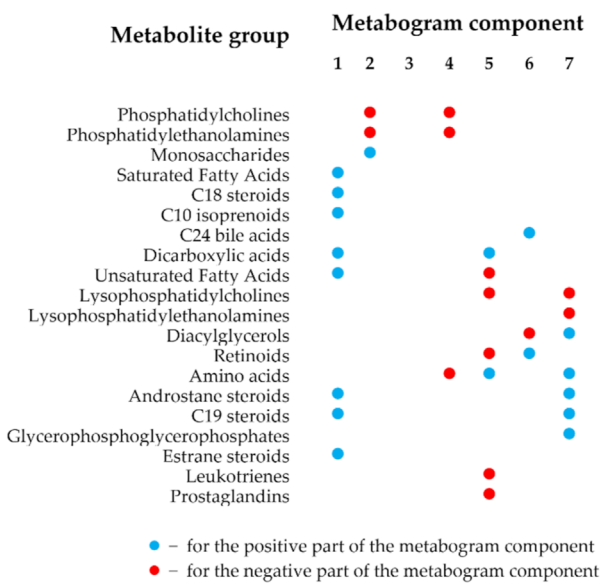


FIGURE 2
Composition of the clinical blood metabogram components. The composition of the metabogram components was measured by determining with which classes of metabolites they are enriched. Enrichment reliability expressed in *p*-values is presented in a previously published paper (Lokhov et al., 2023b).

structure of the data may be seen in the coefficients of each principal component. Larger positive or negative values indicate variables that contribute more to the component. *M/z* values corresponding to the highest and lowest coefficients of the first seven principal components—referred to the "positive" and "negative" parts of the metabogram components—were used to construct CBM reflecting the underlying data of the blood metabolome. In total, it amounted to about 5% each for the "positive" and "negative" parts of the detected peaks. The Z-score is a common way of representing data on a unitless scale and is the raw score minus the population mean, divided by the population standard deviation. With a normal distribution, the Z-score is connected to the *p*-values; for example, 1.64 corresponds to $p = 0.05$ (one-tailed), which is thought to be the cutoff for statistical significance and enables the detection of the sample's deviation from the population. The metabogram's Z-scores from −1.64 to +1.64 are considered to be in the normal range; up- and downregulation are represented by higher and lower Z-score values, respectively.

The components of the metabogram are formed by the functionally related metabolites of the blood involved in humoral regulation (component 1, called "regulatory"), lipid -carbohydrate metabolism (component 2), phospholypolysis (component 3, called "phospholipolytic"), lipid-amine metabolism (component 4), oxidized fatty acids (component 5, called "eicosanoid"), lipid intake into the organism (component 6, called "alimentary"), and liver function (component 7, called "hepatic"), thereby providing clinically relevant information. It should be noted that the identity of obtaining a CBM (sampling, sample processing, mass spectrometry, CBM design, and composition of metabogram components as presented in Supplementary Table S1), established in the first article that introduced the concept of CBM (Lokhov et al., 2023b) and further tested in subsequent studies, allows the obtained data to compare and relate the results obtained to the characteristics of the prototype of the same CBM-based LDT test.

## 2.4 Personal clinical blood metabograms

The study cohort (see Section 2.1), which included control individuals and patients with early-stage PD, was used to obtain personal CBMs. After standardization and normalization, the produced mass lists were aligned with the *m/z* values of the metabogram template (i.e., with 7 *m/z* sets corresponding to seven metabogram components; see Section 2.3). To obtain Z-scores of the metabogram components, the mass peak intensities belonging to the same metabogram component were converted into Z-scores and averaged (Lokhov et al., 2023b).

## 2.5 Cluster analysis

A cluster analysis was performed to give an overview of the metabograms of patients with the early clinical stage of PD. To do this, the *pdist* function (Matlab) was used to determine the Euclidian distances between the Z-scores of the metabograms' components. The *linkage* function created an agglomerative hierarchical cluster tree by calculating the distance between clusters using the "ward" algorithm. The *dendrogram* function was used to plot the dendrogram.

## 2.6 Diagnostic parameters

To assess the diagnostic potential of the metabogram for early clinical stage PD, the following diagnostic parameters were evaluated: sensitivity—the percentage of correctly identified positive results (the deviation is correctly assigned to metabogram component with Z-score out of normal range, i.e., Z-score < −1.64 or >1.64); specificity—the percentage of correctly identified negative results (the deviation from normal range is correctly not assigned to metabogram component with Z-score in normal range); and accuracy—the percentage of correctly identified positive and negative results.

The ROC curve was built by the *perfcurve* function (Matlab). The function also returned sensitivity and specificity values for diagnostics depending on the selected threshold Z-score value separating cases from controls and the optimal Z-score value for the highest diagnostic accuracy.

## 2.7 CBM signature of Parkinson's disease

Considering the cluster analysis data and using the metabogram components that exhibit the greatest diagnostic power, a PD signature was formed. To confirm the inter-disease specificity of the PD signature, the ROC curves were built to separate control and patients with type 2 diabetes mellitus and obesity from control.

TABLE 1 Study cohort characteristics.

| Characteristics | Values | |
|---|---|---|
| | Control subjects | Subjects with PD |
| Number | 28 | 28 |
| Age (years; mean ± s.d. (range)) | 62.8 ± 8.7 (45–77) | 62.6 ± 8.6 (37–77) |
| Gender (males/females) | 14/14 | 14/14 |
| PD stages (1/1.5/2/2.5)[a] | — | 6/6/12/4 |

[a]PD, stages are according to modified Hoehn and Yahr scale (Goetz et al., 2004).

Metabogram data for these subjects was taken from previous studies conducted on CBM research (Lokhov et al., 2023c; Lokhov et al., 2024). In the first case, the PD signature was directly applied to the metabogram data of diabetic patients. In the second case, the difference in the signature of obesity and PD, such as downregulation in the positive part of the first component of CBM at obesity, was additionally taken into consideration. Other differences between signatures were not considered since the absolute unspecificity of the PD signature for obesity was achieved.

# 3 Results

## 3.1 Studied subjects

Equally sized cohorts of patients and control subjects were obtained, aligned by gender and age, allowing for case-control comparison. Table 1 presents the clinical characteristics of the cohorts. The individual characteristics of the subjects are presented in Supplementary Table S2.

## 3.2 Metabogram data

Mass spectrometry analysis, as the first analytical step of the CBM production (Figure 1), generated typical mass spectra of the low-molecular-weight fraction of blood plasma samples. On average, ~9.7 thousand peaks were detected in the spectrum, which corresponds to the number of mass peaks in spectra used to design CBM (Lokhov et al., 2023b) and in other CBM-related studies (Lokhov et al., 2023a; 2023c; Lokhov et al., 2024). Aligned and standardized mass lists are presented in Supplementary Table S3. These mass spectrometry data were used to obtain personal metabograms for all subjects participating in the study (Figure 3).

Figure 3 demonstrates that the components of the metabogram of PD patients deviate more frequently than those of controls, as evidenced by the frequencies of these deviations (Figure 4). Metabolites related to the negative components 3 and 5 and the positive component 4 are downregulated most frequently (Figure 4).

## 3.3 Statistical data and diagnostic parameters

The t-test results demonstrating the significance of the difference in the metabogram components in the case-control comparison are presented in Table 2. The difference for the negative component 5 is statistically significant ($p$-value 0.005), which indicates that PD-specific changes in metabogram can be attributed to the downregulation of the eicosanoids (Figure 2).

To assess the diagnostic capabilities of the CBM, generally used diagnostic parameters were calculated. Table 3 displays sensitivity, specificity, and accuracy calculated based on the divergence of metabogram's components from the normal range. The data in the table show the metabogram's negative component 5 demonstrates the most diagnostic power for detecting the early clinical stage of PD with an accuracy of 62.5% (sensitivity of 32.1%, specificity of 92.9%) when a Z-score of −1.64 (corresponds to $p = 0.05$) is used to separate cases from controls. The lower diagnostic capability was demonstrated by the positive part of component 4 and the negative part of component 3, with diagnostic accuracy of 55.3% and 57.1%, respectively.

The diagnostic potential of these components of the CBM was also assessed by building an ROC curve to determine the optimal threshold for separating cases from controls that provides the best diagnostic parameters. Figure 5A demonstrates that the accuracy of diagnostics was increased for the above-mentioned metabogram components to 76.8%, 67.9%, and 64.3%. This result confirms the diagnostic power of the CBM by a generally accepted method and shows that the Z-scores of the metabogram components can be further processed to improve diagnostic parameters.

In addition to the fact that individual components of the metabogram are associated with PD, and some of them even have diagnostic power, the combinations formed by these components of the metabogram are also an important diagnostic feature—a signature of the disease. To identify such signatures, the patterns formed by deviating metabogram components were identified by cluster analysis (Figure 6). Clusters associated with stages of PD development were not revealed. One cluster, which can be seen as typical for PD, was created by various combinations of the most often deviating metabogram components (see cluster 2 on Figure 6). Therefore, it may be claimed that for a significant part of patients with early-stage PD, the CBM will show a PD-specific signature reflecting disease-associated metabolic alterations.

To confirm the inter-disease specificity of the PD signature, the ROC curves were built and compared with the ROC curves separating control from patients with type 2 diabetes mellitus and obesity (Figure 5B). The PD signature showed high sensitivity to PD at low specificity, while for other diseases the AUC was 0.49 and 0.5, which confirmed the inter-disease specificity of the PD signature. Therefore, if a PD signature is detected, early-stage PD is likely to be suspected. However, the absence of the PD signature does not exclude the underlying pathological condition. Perhaps the signature has not yet been formed at an early stage of disease in many patients, or it reflects only the dominant form of metabolic alterations in PD.

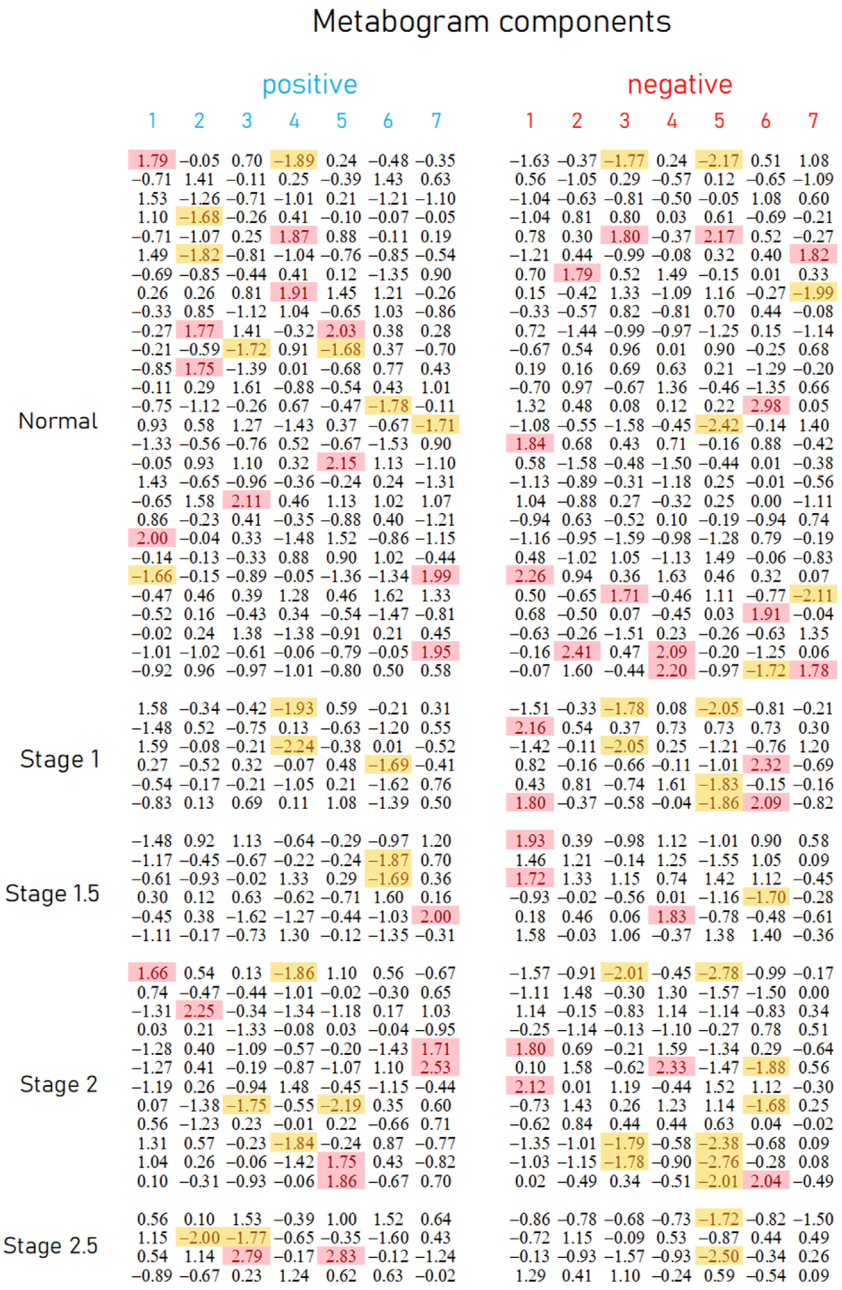


FIGURE 3
Metabogram data for control subjects and subjects with early-stage PD. Each row corresponds to the Z-scores of the metabogram components for an individual (components 1 to 7 for the "positive" and "negative" parts). Z-score is a measure of the metabogram components (from −1.64 to +1.64 is the normal range; up- and downregulation correspond to higher and lower Z-score values, respectively). Background color coding: red indicates upregulation in the corresponding metabogram component; yellow indicates downregulation in the corresponding metabogram component.

## 4 Discussion

The basic methods for diagnosing PD, a progressive degenerative condition of the central nervous system, are a medical history and a neurological examination (Jankovic, 2008). While effective treatment for PD depends on an early diagnosis (Gelb et al., 1999), a clinical diagnosis cannot be made until there is a large loss of dopaminergic neurons (Gibb and Lees, 1988). Moreover, the cost of the imaging of dopamine (Dopa) uptake efficiency diagnostic test based on positron emission tomography (PET) is high. As a result, a novel diagnostic laboratory test is needed. Biomarker discovery for such tests is hampered by PD's ambiguous pathophysiology and complex character, and the use of panoramic techniques, as suggested, is more promising in this situation. Unfortunately, because of the consistency needed for clinical test registration, the clinical use of such 'panoramic' procedures, to which metabolomic analysis is related, is quite difficult. LDT usage gets around this problem. LDTs are defined

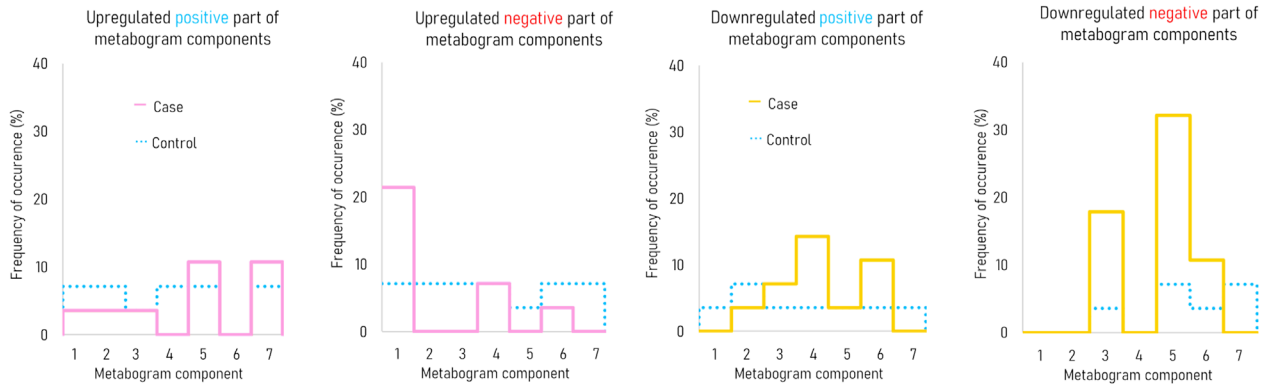


FIGURE 4
The frequency of deviations in the blood metabogram components for early-stage PD. The metabogram component deviates from the norm if the Z-score of the metabogram component is below −1.64 (indicating downregulation of the metabolites related to the metabogram component) or above 1.64 (indicating upregulation of the metabolites related to the metabogram component).

**TABLE 2** Statistical significance of the deviation of the metabogram components in early PD (1–2.5 stages) from the control.

| Metabogram Component | | t-test ($p$-value[a]) |
|---|---|---|
| Positive | 1 | 0.783 |
| | 2 | 0.939 |
| | 3 | 0.424 |
| | 4 | 0.082 |
| | 5 | 0.639 |
| | 6 | 0.129 |
| | 7 | 0.193 |
| Negative | 1 | 0.46 |
| | 2 | 0.499 |
| | 3 | 0.124 |
| | 4 | 0.184 |
| | 5 | 0.005[a] |
| | 6 | 0.913 |
| | 7 | 0.760 |
| All | | 0.180 |

[a]$p$-value of statistically significant deviation from control.

by the Food and Drug Administration (United States) as tests that are created, produced, and used in the same laboratory (FDA, 2018). Therefore, the execution of metabolomics analysis in LDT format is sufficiently streamlined due to putting protocol development and standardization tasks under the purview of a single laboratory.

Although metabolomics, which measures the groups of metabolites that make up the metabolome, has been around for more than 20 years and the technologies it uses are nearly perfect, its application in medicine, even as LDT, is quite limited. Main cause of this is the preciseness of measurements, which allows for the precise measurement of numerous metabolites in a single run. Widely used in metabolomics, mass spectrometry techniques are typically capable of detecting hundreds of metabolites, which is essential for gathering biochemical data (Viant et al., 2017). Despite the use of cutting-edge mass spectrometry-based metabolomics technologies, the vast majority of the sample's metabolites remain unknown (de Jong et al., 2017). Typically, only highly abundant and well-separated metabolites are identified. This is due to the difficulty of producing a clear mass spectrometric image of low-abundance metabolites, which constitute the majority of any metabolome. This means that the complexity of metabolomic measurements restricts the use of metabolomics in LDT format (Nalbantoglu, 2019; Lichtenberg et al., 2021; Lokhov et al., 2021).

The concept of the metabogram—a simplified single-subject metabolomics study—was developed to address this issue. The metabogram technique eliminates metabolite identification step (Lokhov et al., 2023b). Only groups of related metabolites are processed in the metabogram for this reason, and the use of MSEA (Xia and Wishart, 2010) quickly determines the enrichment of these groups with metabolite classes. As a result, group analysis takes the place of the challenging identification of individual metabolites. Additionally, data repeatability is improved by averaging metabolite data (peak intensities) within groups. For metabogram components, the coefficient of variation can be as low as 1.8% (Lokhov et al., 2023b), which is much lower than what is often found for individual metabolites (Crews et al., 2009). In order to validate the clinical utility of CBM for PD diagnosis, people with early PD were evaluated using CBM in this study.

According to the data obtained, it can be argued that, in terms of the frequency of occurrence and the joint appearance, PD-specific changes can be attributed to the downregulation of metabolites related to the eicosanoid component (negative part of component 5), the phospholipolytic component (negative part of component

10.3389/fmolb.2024.1407974

TABLE 3 Diagnostic parameters of the metabogram components for the detection of early-stage PD.

| Metabogram component | Diagnostic parameters (%) | | |
|---|---|---|---|
| | Sensitivity | Specificity | Accuracy |
| Upregulation of the metabolites (Z-score >1.64 for the metabogram components) | | | |
| Positive parts of metabogram components | | | |
| 1 | 3.6 | 92.9 | 48.2 |
| 2 | 3.6 | 92.9 | 48.2 |
| 3 | 3.6 | 96.4 | 50.0 |
| 4 | 0 | 92.9 | 46.4 |
| 5 | 10.7 | 92.9 | 51.8 |
| 6 | 0 | 100.0 | 50.0 |
| 7 | 10.7 | 92.9 | 51.8 |
| All (1–7) | 4.6 | 94.4 | 49.5 |
| Negative parts of metabogram components | | | |
| 1 | 21.4 | 92.9 | 57.1 |
| 2 | 0 | 92.9 | 46.4 |
| 3 | 0 | 92.9 | 46.4 |
| 4 | 7.1 | 92.9 | 50.0 |
| 5 | 0 | 96.4 | 48.2 |
| 6 | 10.7 | 92.9 | 51.8 |
| 7 | 0 | 92.9 | 46.4 |
| All (1–7) | 5.7 | 93.4 | 49.5 |
| Downregulation of the metabolites (Z-score < -1.64 for the metabogram components) | | | |
| Positive parts of metabogram components | | | |
| 1 | 0 | 96.4 | 48.2 |
| 2 | 3.6 | 92.9 | 48.2 |
| 3 | 7.1 | 96.4 | 51.8 |
| 4 | 14.3 | 96.4 | 55.3 |
| 5 | 3.6 | 96.4 | 50.0 |
| 6 | 10.7 | 96.4 | 53.6 |
| 7 | 0 | 96.4 | 48.2 |
| All (1–7) | 5.6 | 95.9 | 50.8 |
| Negative parts of metabogram components | | | |
| 1 | 0 | 100.0 | 50.0 |
| 2 | 0 | 100.0 | 50.0 |

(Continued on the following page)

TABLE 3 (*Continued*) Diagnostic parameters of the metabogram components for the detection of early-stage PD.

| Metabogram component | Diagnostic parameters (%) | | |
|---|---|---|---|
| | Sensitivity | Specificity | Accuracy |
| 3 | 17.9 | 96.4 | 57.1 |
| 4 | 0 | 100.0 | 50.0 |
| 5[a] | 32.1 | 92.9 | 62.5 |
| 6 | 10.7 | 96.4 | 53.6 |
| 7 | 0 | 92.9 | 46.4 |
| All (1–7) | 8.9 | 96.9 | 52.8 |

[a]Metabograms component demonstrating the best diagnostic performance.

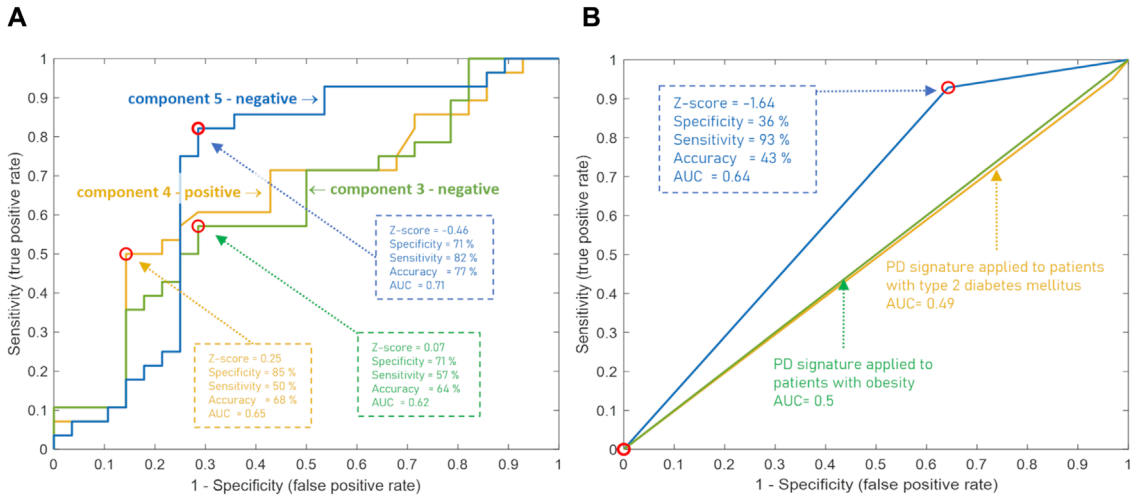


FIGURE 5
ROC curves based on the Z-score of the clinical blood metabogram (CBM) components for the diagnosis of Parkinson's disease (PD). **(A)** ROC curves for the three metabogram components, which consist of the PD-specific signature: the negative parts of components 3 and 5, and the positive part of component 4. **(B)** ROC curve for the PD-specific signature, which consists of three metabogram components. Z-score –1.64 is used to distinguish between PD cases and controls. The PD signature was applied to patients with obesity and type 2 diabetes mellitus to show its inter-disease specificity.

3), and the positive part of component 4 (called the "phospholipid-amine" because of the co-directed changes in phospholipids and amino acids described by its negative part).

The most frequent deviation from the norm was revealed in the eicosanoid component of the metabogram (Figure 4). This deviation in patients with early-stage PD occurred 4.5 times more often than in the control group. A distinctive feature of this component of the metabogram is its enrichment with eicosanoids such as prostaglandins and leukotrienes. The close involvement of various eicosanoids in the development of PD can be read in the review by Chiurchiù V. et al. (2022). A variety of studies using both different biomaterials for research and the diversity of eicosanoids themselves led to the observation of multidirectional changes in their concentrations in PD. However, it can be argued that a group of eicosanoids in the blood decreases with PD (Zhang et al., 2021; Chistyakov et al., 2023) and even some eicosanoids exhibit neuroprotective effects (Rajan et al., 2020). Perhaps this group of eicosanoids is responsible for the decreased Z-score of this component of the metabogram.

The association of blood phospholipids with PD is an established fact and was already proposed for diagnostic purposes (Li et al., 2015). Oxidative stress is a significant factor in the onset and course of PD. Important elements of cellular membranes, phospholipids are essential for preserving the integrity and functionality of cells. Patients with PD have much higher lipid peroxidation products in their brains, which may be a connection between membrane damage and changes in phospholipid levels. However, it is possible that the detected changes in the phospholipolytic component may be due to a change in the concentration of phospholipids or may be associated with the activity of phospholipases. Previously, it was found that there is a link between phospholipases and PD (Mendez-Gomez et al., 2018; Wu et al., 2021). Thus, phosphatidic acid, a

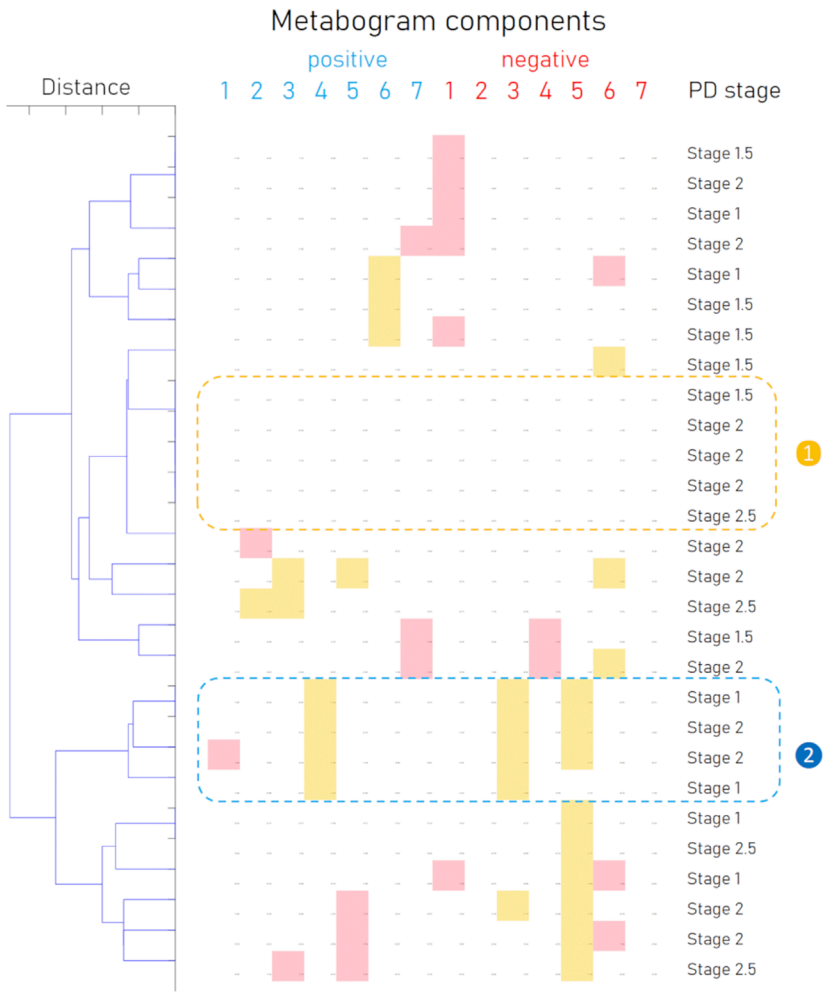


FIGURE 6
Cluster analysis of blood metabograms of PD patients involved in the study. Each row corresponds to the metabogram components for an individual (components 1 to 7 for the "positive" and "negative" parts). Color coding: red indicates upregulation in the corresponding metabogram component; yellow indicates downregulation in the corresponding metabogram component. The metabograms with no deviations (1) in components and metabograms considered PD-specific (2) are selected.

product of phospholipase PLD2 activity, is a second messenger in many cellular pathways and appears to be key to PLD2-induced neurodegeneration. The fact that α-synuclein is a regulator of PLD2 activity suggests that regulation of PLD2 activity may be important in the progression of PD.

Regarding downregulation reflected by the positive component 4, metabolites associated with it were not identified during the CBM design (Lokhov et al., 2023b). The list of molecular weights for which potential candidates exist was sparse and included several quasi-ions to which several elemental compositions corresponded ($C_2H_2O_4$, $C_4H_6O_3$, $C_4H_6O_3$, $C_5H_6O_5$) (Lokhov et al., 2024). The elemental composition of $C_2H_2O_4$ in the metabolite database corresponds only to oxalic acids, a degradation product of vitamin C, a deficiency of which in the body is associated with the development of PD (Brown, 2017). For the elemental formula $C_4H_6O_3$, among the candidates are metabolites related to the butanoate metabolism pathway, such as acetoacetic acid (ketone body) and succinic acid semialdehyde. For $C_5H_6O_5$, there is no alternative to oxoglutaric acid, which also belongs to butanoate metabolism. Interestingly, ketone bodies are associated with the development of PD, attributing neuroprotective properties to them (Maalouf et al., 2009). Moreover, the butadione metabolism pathway includes the formation of gamma-aminobutyric acid (GABA), and the connection between its level decrease and PD is well-known (Błaszczyk, 2016). Since the metabolites of this metabogram component were not reliably identified either according to metabolomics standards or during the design of a metabogram, the connection of this component with the butanoate metabolism pathway is hypothetical.

Based on the results obtained, several types of metabograms can be distinguished in early PD (Figure 6). A metabogram without abnormalities, a metabogram with various non-systematic abnormalities that can be attributed to an individual's disease course, or an individual health condition defined by other diseases, and a metabogram that can be attributed to a PD-specific metabotype. The last one manifests in the blood level of eicosanoids and is often associated with changes in the phospholipolytic and

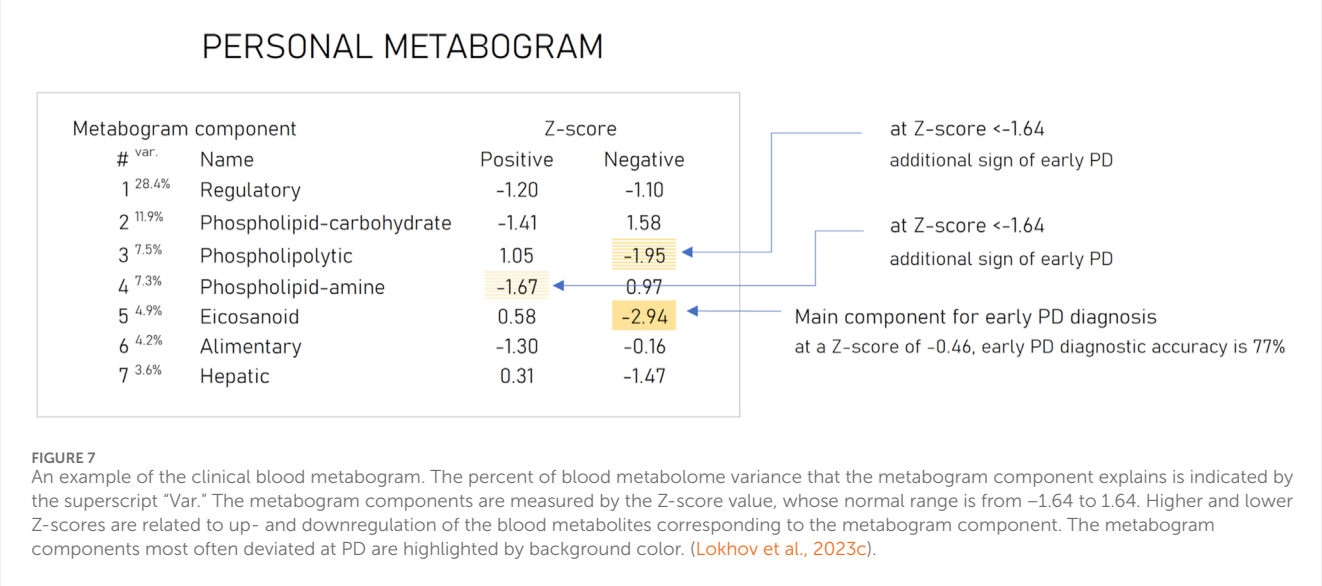


FIGURE 7
An example of the clinical blood metabogram. The percent of blood metabolome variance that the metabogram component explains is indicated by the superscript "Var." The metabogram components are measured by the Z-score value, whose normal range is from −1.64 to 1.64. Higher and lower Z-scores are related to up- and downregulation of the blood metabolites corresponding to the metabogram component. The metabogram components most often deviated at PD are highlighted by background color. (Lokhov et al., 2023c).

phospholipid-amine components. Figure 7 shows a metabogram in a simple format, showing the names of the components, the blood metabolome variance explained by each component, and the Z-scores of the components. The figure also provides a PD-specific signature – the components that contribute to the diagnosis of PD and can be potentially used to monitor the level of metabolic alterations during PD development and treatment. The inability to diagnose PD, as well as to monitor its course and the outcome of treatment in patients who do not have a PD-specific metabotype can be attributed to the limitations of CBM.

As said in the introduction, it's critical to remember that PD has a diverse pathogenesis involving a range of small molecular compounds. The specified metabolite composition of CBM components may cause some PD-specific metabolic alterations in the blood are undetected by CBM. Such alterations either do not have a significant effect on the main groups of blood metabolites reflected in CBM or refer to metabolites assigned to the remaining 30% of the variance of the blood metabolome not covered by CBM. However, modifying the CBM for a specific disease to increase its capabilities is beyond the scope of this work, which consists of testing a previously developed CBM design. The peculiarity of this approach is visible when comparing the results obtained with a previously conducted classical metabolomic study to search for biomarkers or a multimarker diagnostic signature of PD. In contrast to CBM, an AUC of 0.91 was achieved to diagnose PD in this single disease-focused study (Balashova et al., 2018). Contrariwise to such single-disease studies, the same CBM design applied to multiple diseases is more consistent with omics tests that identify changes at a significant portion of the metabolomic level, offering diagnostic capabilities for a variety of diseases.

From the described metabolic alterations, an additional feature of the PD signature can be suggested. The neuroprotective eicosanoids, whose reduction is reflected in the signature, not only inhibit neuroinflammation but also suppress oxidative stress (Tassoni et al., 2008). The change in the phospholipolytic component, as above indicated, can be caused by peroxidase oxidation and activation of phospholipase, which is recognized as an integral component of the oxidant stress response system (Adibhatla and Hatcher, 2008). The change in the metabolism of butadione led to the downregulation of ketone bodies with antioxidative properties (Kolb et al., 2021). Thus, the ketone body β-hydroxybutyrate is a direct antioxidant for hydroxyl radicals, an inhibitor of mitochondrial reactive oxygen species (ROS) production, and promotes the transcriptional activity of antioxidant defenses (Rojas-Morales et al., 2020). It can be assumed that the PD signature not only reflects the role of oxidative stress in PD development but also may indicate the risk of developing PD through the reflection of a reduced level of antioxidant activity in the organism. However, the confirmation of this assumption requires additional research.

The specificity of the identified signature to PD is also confirmed by its difference from previously published signatures of obesity and type 2 diabetes mellitus widespread in the population (Lokhov et al., 2023c; Lokhov et al., 2024). Moreover, when interpreting a PD-specific signature, the influence of the gut microbiota on CBM can be taken into consideration, the link to which was also described (Lokhov et al., 2023a).

The results of this study should also be assessed in the light of atypical parkinsonisms, the differential diagnosis of which from PD remains challenging. Although accurate diagnosis in the early stages of the disease plays an important role in prognosis and treatment strategy, distinguishing PD from, for example, parkinsonian-type multiple system atrophy (MSA-P) due to the similarity of symptoms can be difficult (Wenning et al., 1997; Goetz et al., 2004). The existence of the different clusters formed by metabograms in Figure 6 may be caused by MSA-P or other atypical parkinsonisms (progressive supranuclear palsy, corticobasal degeneration, and dementia with Lewy bodies). However, due to the rarity of their occurrence and the small cohort used, such a connection cannot be identified in this study, and this hypothetical statement rather serves as the basis for further research. Further studies in larger cohorts that include different parkinsonisms in sufficient numbers to obtain statistically significant data will demonstrate the potential of CBM in the differential diagnosis of PD and other parkinsonisms.

As for the clinical implications of the results of this work, an interpretation of the CBM can now be made for PD patients. This makes it possible to accurately analyze the metabolic changes in such patients and the dysfunctions of the body caused by these changes, relating or separating them from those specific to PD. Considering the pilot nature of the study, the feasibility of predicting the course of PD, assessing the effectiveness of treatment, and differentiating PD from atypical parkinsonism will become possible after additional research.

## 5 Conclusion

The measurement of the metabolome for clinical use is eagerly awaited and shows great promise. The metabolome, as its name suggests, is a level of organization of biological systems that is directly related to the global biochemical phenotype. One such attempt is the CBM, which, as demonstrated in previous studies, possesses the performance characteristics of a clinical test, and provides data that is clinically relevant. In this work, CBM was used to diagnose early PD, a condition that is very challenging to diagnose by laboratory testing, and its efficacy was verified. CBM allowed revealing a PD-specific metabotype, the measure of which not only provides diagnostic information but also opens up new opportunities to monitor PD progression and evaluate response to PD treatment.

## Data availability statement

Publicly available datasets were analyzed in this study. This data can be found here: FigShare repository at https://doi.org/10.6084/m9.figshare.25487551.

## Ethics statement

The studies involving humans were approved by Institutional Ethics Committee of Koltzov Institute of Developmental Biology of Russian Academy of Sciences (protocol code 55 and date of approval 9 December 2021). The studies were conducted in accordance with the local legislation and institutional requirements. The participants provided their written informed consent to participate in this study.

## Author contributions

PL: Conceptualization, Methodology, Project administration, Software, Writing–original draft. OT: Data curation, Investigation, Methodology, Writing–review and editing. EB: Investigation, Validation, Writing–review and editing. DM: Formal Analysis, Investigation, Methodology, Writing–review and editing. MU: Data curation, Resources, Supervision, Writing–review and editing. AA: Conceptualization, Funding acquisition, Project administration, Writing–review and editing.

## Funding

The author(s) declare that financial support was received for the research, authorship, and/or publication of this article. The work was performed within the framework of the Program for Basic Research in the Russian Federation for a long-term period (2021–2030) (No. 122030100168-2).

## Conflict of interest

The authors declare that the research was conducted in the absence of any commercial or financial relationships that could be construed as a potential conflict of interest.

## Publisher's note



## Supplementary material

The Supplementary Material for this article can be found online at: https://www.frontiersin.org/articles/10.3389/fmolb.2024.1407974/full#supplementary-material

## References

Adibhatla, R. M., and Hatcher, J. F. (2008). Phospholipase A(2), reactive oxygen species, and lipid peroxidation in CNS pathologies. *BMB Rep.* 41, 560–567. doi:10.5483/bmbrep.2008.41.8.560

Balashova, E. E., Lokhov, P. G., Maslov, D. L., Trifonova, O. P., Khasanova, D. M., Zalyalova, Z. A., et al. (2018). Plasma metabolome signature in patients with early-stage Parkinson disease. *Curr. Metabolomics* 6, 75–82. doi:10.2174/2213235x05666170221161735

Błaszczyk, J. W. (2016). Parkinson's disease and neurodegeneration: GABA-collapse hypothesis. *Front. Neurosci.* 10, 269. doi:10.3389/fnins.2016.00269

Brown, T. M. (2017). Parkinsonism and vitamin C deficiency. *Fed. Pract.* 34, 28–32.

Chen-Plotkin, A. S., Albin, R., Alcalay, R., Babcock, D., Bajaj, V., Bowman, D., et al. (2018). Finding useful biomarkers for Parkinson s disease. *Sci. Transl. Med.* 10, eaam6003. doi:10.1126/scitranslmed.aam6003

Chistyakov, D. V., Azbukina, N. V., Lopachev, A. V., Goriainov, S. V., Astakhova, A. A., Ptitsyna, E. V., et al. (2023). Plasma oxylipin profiles reflect Parkinson's disease stage. *Prostagl. Other Lipid Mediat* 171, 106788. doi:10.1016/j.prostaglandins.2023.106788

Chiurchiù, V., Tiberi, M., Matteocci, A., Fazio, F., Siffeti, H., Saracini, S., et al. (2022). Lipidomics of bioactive lipids in Alzheimer's and Parkinson's diseases: where are we? *Int. J. Mol. Sci.* 23, 6235. doi:10.3390/ijms23116235

Crews, B., Wikoff, W. R., Patti, G. J., Woo, H.-K., Kalisiak, E., Heideker, J., et al. (2009). Variability analysis of human plasma and cerebral spinal fluid reveals statistical significance of changes in mass spectrometry-based metabolomics data. *Anal. Chem.* 81, 8538–8544. doi:10.1021/ac9014947

de Jong, F., Beecher, C., Raskind, A., Chamberlain, C., Guingab, J., and Garrett, T. (2017). MetaboNews. *Do we really know how many unknowns there are a data set?*

*Issure* 72. Available at: http://www.metabonews.ca/Aug2017/MetaboNews_Aug2017.htm (accessed on August 10, 2017).

Deng, H., Wang, P., and Jankovic, J. (2018). The genetics of Parkinson disease. *Ageing Res. Rev.* 42, 72–85. doi:10.1016/j.arr.2017.12.007

FDA (2018). Laboratory developed tests. Available at: https://www.fda.gov/medical-devices/vitro-diagnostics/laboratory-developed-tests (accessed on October 5, 2018).

Gelb, D. J., Oliver, E., and Gilman, S. (1999). Diagnostic criteria for Parkinson disease. *Arch. Neurol.* 56, 33–39. doi:10.1001/archneur.56.1.33

Gelders, G., Baekelandt, V., and Van der Perren, A. (2018). Linking neuroinflammation and neurodegeneration in Parkinson's disease. *J. Immunol. Res.* 2018, 4784268. doi:10.1155/2018/4784268

Genzen, J. R. (2019). Regulation of laboratory-developed tests. *Am. J. Clin. Pathol.* 152, 122–131. doi:10.1093/ajcp/aqz096

Gibb, W. R., and Lees, A. J. (1988). The relevance of the Lewy body to the pathogenesis of idiopathic Parkinson's disease. *J. Neurol. Neurosurg. Psychiatry* 51, 745–752. doi:10.1136/jnnp.51.6.745

Goetz, C. G., Poewe, W., Rascol, O., Sampaio, C., Stebbins, G. T., Counsell, C., et al. (2004). Movement disorder society task force report on the Hoehn and Yahr staging scale: status and recommendations. *Mov. Disord.* 19, 1020–1028. doi:10.1002/mds.20213

Heo, J. Y., Nam, M.-H., Yoon, H. H., Kim, J., Hwang, Y. J., Won, W., et al. (2020). Aberrant tonic inhibition of dopaminergic neuronal activity causes motor symptoms in animal models of Parkinson's disease. *Curr. Biol.* 30, 276–291.e9. doi:10.1016/j.cub.2019.11.079

Jankovic, J. (2008). Parkinson's disease clinical features and diagnosis. *J. Neurol. Neurosurg. Psychiatry* 79, 368–376. doi:10.1136/jnnp.2007.131045

Kolb, H., Kempf, K., Röhling, M., Lenzen-Schulte, M., Schloot, N. C., and Martin, S. (2021). Ketone bodies: from enemy to friend and guardian angel. *BMC Med.* 19, 313. doi:10.1186/s12916-021-02185-0

Le, D. T., Lutz, E., Uram, J. N., Sugar, E. A., Onners, B., Solt, S., et al. (2013). Evaluation of ipilimumab in combination with allogeneic pancreatic tumor cells transfected with a GM-CSF gene in previously treated pancreatic cancer. *J. Immunother.* 36, 382–389. doi:10.1097/CJI.0b013e31829fb7a2

Li, Z., Zhang, J., and Sun, H. (2015). Increased plasma levels of phospholipid in Parkinson's disease with mild cognitive impairment. *J. Clin. Neurosci. Off. J. Neurosurg. Soc. Australas.* 22, 1268–1271. doi:10.1016/j.jocn.2015.02.013

Lichtenberg, S., Trifonova, O. P., Maslov, D. L., Balashova, E. E., and Lokhov, P. G. (2021). Metabolomic laboratory-developed tests: current statusand perspectives. *Metabolites* 11, 423. doi:10.3390/metabo11070423

Lokhov, P. G., Balashova, E. E., Maslov, D. L., Trifonova, O. P., Lisitsa, A. V., Markova, Y. M., et al. (2023a). Linking clinical blood metabogram and gut microbiota. *Metabolites* 13, 1095. doi:10.3390/metabo13101095

Lokhov, P. G., Balashova, E. E., Trifonova, O. P., Maslov, D. L., Grigoriev, A. I., Ponomarenko, E. A., et al. (2023b). Mass spectrometric blood metabogram: acquisition, characterization, and prospects for application. *Int. J. Mol. Sci.* 24, 1736. doi:10.3390/ijms24021736

Lokhov, P. G., Balashova, E. E., Trifonova, O. P., Maslov, D. L., Plotnikova, O. A., Sharafetdinov, K. K., et al. (2023c). Clinical blood metabogram: application to overweight and obese patients. *Metabolites* 13, 798. doi:10.3390/metabo13070798

Lokhov, P. G., Balashova, E. E., Trifonova, O. P., Maslov, D. L., Ponomarenko, E. A., and Archakov, A. I. (2020). Mass spectrometry-based metabolomics analysis of obese patients' blood plasma. *Int. J. Mol. Sci.* 21, 568. doi:10.3390/ijms21020568

Lokhov, P. G., Balashova, E. E., Trifonova, O. P., Maslov, D. L., Shestakova, E. A., Shestakova, M. V., et al. (2024). Application of clinical blood metabogram to type 2 diabetes mellitus. *Metabolites* 14, 168. doi:10.3390/metabo14030168

Lokhov, P. G., Kharybin, O. N., and Archakov, A. I. (2011). Diagnosis of lung cancer based on direct-infusion electrospray mass spectrometry of blood plasma metabolites. *Int. J. Mass Spectrom.* 309, 200–205. doi:10.1016/j.ijms.2011.10.002

Lokhov, P. G., Trifonova, O. P., Maslov, D. L., Lichtenberg, S., and Balashova, E. E. (2021). Personal metabolomics: a global challenge. *Metabolites* 11, 715. doi:10.3390/metabo11110715

Maalouf, M., Rho, J. M., and Mattson, M. P. (2009). The neuroprotective properties of calorie restriction, the ketogenic diet, and ketone bodies. *Brain Res. Rev.* 59, 293–315. doi:10.1016/j.brainresrev.2008.09.002

Mendez-Gomez, H. R., Singh, J., Meyers, C., Chen, W., Gorbatyuk, O. S., and Muzyczka, N. (2018). The lipase activity of phospholipase D2 is responsible for nigral neurodegeneration in a rat model of Parkinson's disease. *Neuroscience* 377, 174–183. doi:10.1016/j.neuroscience.2018.02.047

Meng, Y., Qiao, H., Ding, J., He, Y., Fan, H., Li, C., et al. (2020). Effect of Parkin on methamphetamine-induced α-synuclein degradation dysfunction *in vitro* and *in vivo*. *Brain Behav.* 10, e01574. doi:10.1002/brb3.1574

Nalbantoglu, S. (2019). in *Metabolomics: basic principles and strategies*. Editors S. Nalbantoglu, and H. Amri (London, United Kingdom: Rijeka: IntechOpen). Ch. 8. doi:10.5772/intechopen.88563

Olanow, C. W., and Brundin, P. (2013). Parkinson's disease and alpha synuclein: is Parkinson's disease a prion-like disorder? *Mov. Disord.* 28, 31–40. doi:10.1002/mds.25373

Omenn, G. S., DeAngelis, C. D., DeMets, D. L., Fleming, T. R., Geller, G., Gray, J., et al. (2012). *Evolution of translational omics: lessons learned and the path forward - Institute of medicine*. Washington, DC, USA: National Academies Press.

Parkinson, J. (2002). An essay on the shaking palsy. 1817. *J. Neuropsychiatry Clin. Neurosci.* 14, 223–222. doi:10.1176/jnp.14.2.223

Rajan, S., Jang, Y., Kim, C.-H., Kim, W., Toh, H. T., Jeon, J., et al. (2020). PGE1 and PGA1 bind to Nurr1 and activate its transcriptional function. *Nat. Chem. Biol.* 16, 876–886. doi:10.1038/s41589-020-0553-6

Rani, L., and Mondal, A. C. (2020). Emerging concepts of mitochondrial dysfunction in Parkinson's disease progression: pathogenic and therapeutic implications. *Mitochondrion* 50, 25–34. doi:10.1016/j.mito.2019.09.010

Rojas-Morales, P., Pedraza-Chaverri, J., and Tapia, E. (2020). Ketone bodies, stress response, and redox homeostasis. *Redox Biol.* 29, 101395. doi:10.1016/j.redox.2019.101395

Rokad, D., Ghaisas, S., Harischandra, D. S., Jin, H., Anantharam, V., Kanthasamy, A., et al. (2017). Role of neurotoxicants and traumatic brain injury in α-synuclein protein misfolding and aggregation. *Brain Res. Bull.* 133, 60–70. doi:10.1016/j.brainresbull.2016.12.003

Ross, O. A. (2013). A prognostic view on the application of individualized genomics in Parkinson's disease. *Curr. Genet. Med. Rep.* 1, 52–57. doi:10.1007/s40142-012-0003-1

Salama, R. M., Abdel-Latif, G. A., Abbas, S. S., El Magdoub, H. M., and Schaalan, M. F. (2020). Neuroprotective effect of crocin against rotenone-induced Parkinson's disease in rats: interplay between PI3K/Akt/mTOR signaling pathway and enhanced expression of miRNA-7 and miRNA-221. *Neuropharmacology* 164, 107900. doi:10.1016/j.neuropharm.2019.107900

Scheffold, A., Holtman, I. R., Dieni, S., Brouwer, N., Katz, S.-F., Jebaraj, B. M. C., et al. (2016). Telomere shortening leads to an acceleration of synucleinopathy and impaired microglia response in a genetic mouse model. *Acta Neuropathol. Commun.* 4, 87. doi:10.1186/s40478-016-0364-x

Schreier, J., Feeney, R., and Keeling, P. (2019). Diagnostics reform and harmonization of clinical laboratory testing. *J. Mol. Diagn.* 21, 737–745. doi:10.1016/j.jmoldx.2019.04.002

Sharfstein, J. (2015). FDA regulation of laboratory-developed diagnostic tests: protect the public, advance the science. *JAMA - J. Am. Med. Assoc.* 313, 667–668. doi:10.1001/jama.2014.18135

Snyder, B., Shell, B., Cunningham, J. T., and Cunningham, R. L. (2017). Chronic intermittent hypoxia induces oxidative stress and inflammation in brain regions associated with early-stage neurodegeneration. *Physiol. Rep.* 5, e13258. doi:10.14814/phy2.13258

Tansey, M. G., and Goldberg, M. S. (2010). Neuroinflammation in Parkinson's disease: its role in neuronal death and implications for therapeutic intervention. *Neurobiol. Dis.* 37, 510–518. doi:10.1016/j.nbd.2009.11.004

Tassoni, D., Kaur, G., Weisinger, R. S., and Sinclair, A. J. (2008). The role of eicosanoids in the brain. *Asia Pac. J. Clin. Nutr.* 17 (Suppl 1), 220–228. Available at: http://europepmc.org/abstract/MED/18296342.

Tompkins, M. M., Basgall, E. J., Zamrini, E., and Hill, W. D. (1997). Apoptotic-like changes in Lewy-body-associated disorders and normal aging in substantia nigral neurons. *Am. J. Pathol.* 150, 119–131.

Trifonova, O., Lokhov, P., and Archakov, A. (2013). Postgenomics diagnostics: metabolomics approaches to human blood profiling. *OMICS* 17, 550–559. doi:10.1089/omi.2012.0121

Viant, M. R., Kurland, I. J., Jones, M. R., and Dunn, W. B. (2017). How close are we to complete annotation of metabolomes? *Curr. Opin. Chem. Biol.* 36, 64–69. doi:10.1016/j.cbpa.2017.01.001

Wen, K.-X., Miliç, J., El-Khodor, B., Dhana, K., Nano, J., Pulido, T., et al. (2016). The role of DNA methylation and histone modifications in neurodegenerative diseases: a systematic review. *PLoS One* 11, e0167201. doi:10.1371/journal.pone.0167201

Wenning, G. K., Tison, F., Ben Shlomo, Y., Daniel, S. E., and Quinn, N. P. (1997). Multiple system atrophy: a review of 203 pathologically proven cases. *Mov. Disord.* 12, 133–147. doi:10.1002/mds.870120203

Wu, Z., Wu, S., Liang, T., and Wang, L. (2021). Lipoprotein-associated phospholipase A2 is a risk factor for patients with Parkinson's disease. *Front. Neurosci.* 15, 633022. doi:10.3389/fnins.2021.633022

Xia, J., and Wishart, D. S. (2010). MSEA: a web-based tool to identify biologically meaningful patterns in quantitative metabolomic data. *Nucleic Acids Res.* 38 (Suppl. 2), W71–W77. doi:10.1093/nar/gkq329

Zhang, J., Liu, L., Zhang, L., Chen, S., Chen, Y., and Cai, C. (2021). Targeted fatty acid metabolomics to discover Parkinson's disease associated metabolic alteration. *J. Mass Spectrom.* 56, e4781. doi:10.1002/jms.4781

frontiers | Frontiers in Molecular Biosciences

TYPE Original Research
PUBLISHED 15 January 2025
DOI 10.3389/fmolb.2024.1452312



OPEN ACCESS

EDITED BY
Joana Pinto,
University of Porto, Portugal

REVIEWED BY
Ying Zhang,
BioMarin, United States
Herald Midzi,
Family Health International 360, Zimbabwe

*CORRESPONDENCE
Danuta Dudzik,
danuta.dudzik@gumed.edu.pl
Jose Luis Bartha,
josel.bartha@salud.madrid.org

RECEIVED 20 June 2024
ACCEPTED 30 December 2024
PUBLISHED 15 January 2025

CITATION
Dudzik D, Atanasova V, Barbas C and Bartha JL (2025) First-trimester metabolic profiling of gestational diabetes mellitus: insights into early-onset and late-onset cases compared with healthy controls. *Front. Mol. Biosci.* 11:1452312. doi: 10.3389/fmolb.2024.1452312



# First-trimester metabolic profiling of gestational diabetes mellitus: insights into early-onset and late-onset cases compared with healthy controls

Danuta Dudzik[1]*, Vangeliya Atanasova[2], Coral Barbas[3] and Jose Luis Bartha[2]*

[1]Department of Biopharmaceutics and Pharmacodynamics, Faculty of Pharmacy, Medical University of Gdańsk, Gdańsk, Poland, [2]Division of Maternal and Fetal Medicine, Fundación Para la Investigación Biomédica, La Paz University Hospital, Madrid, Spain, [3]Department of Chemistry and Biochemistry, Centre for Metabolomics and Bioanalysis (CEMBIO), Facultad de Farmacia, Universidad San Pablo-CEU, CEU Universities, Urbanización Montepríncipe, Madrid, Spain

**Introduction:** Gestational diabetes mellitus (GDM) is a global health concern with significant short and long-term complications for both mother and baby. Early prediction of GDM, particularly late-onset, is crucial for implementing timely interventions to mitigate adverse outcomes. In this study, we conducted a comprehensive metabolomic analysis to explore potential biomarkers for early GDM prediction.

**Methods:** Plasma samples were collected during the first trimester from 60 women: 20 with early-onset GDM, 20 with late-onset GDM, and 20 with normal glucose tolerance. Using advanced analytical techniques, including liquid chromatography-tandem mass spectrometry (LC-MS/MS) and gas chromatography-mass spectrometry (GC-MS), we profiled over 150 lipid species and central carbon metabolism intermediates.

**Results:** Significant metabolic alterations were observed in both early- and late-onset GDM groups compared to healthy controls, with a specific focus on glycerolipids, fatty acids, and glucose metabolism. Key findings revealed a 4.0-fold increase in TG(44:0), TG(46:0), TG(46:1) with $p$-values <0.001 and TG(46:2) with 4.7-fold increase and $p$-value <0.0001 as well as changes in several phospholipids as PC(38:3), PC(40:4) with 1.4-fold increase, $p < 0.001$ and PE(34:1), PE(34:2) and PE(36:2) with 1.5-fold change, $p < 0.001$ in late-onset GDM.

**Discussion:** Observed lipid changes highlight disruptions in energy metabolism and inflammatory pathways. It is suggested that lipid profiles with distinct fatty acid chain lengths and degrees of unsaturation can serve as early biomarkers of GDM risk. These findings underline the importance of integrating metabolomic insights with clinical data to develop predictive models for GDM. Such models could enable early risk stratification, allowing for timely dietary, lifestyle, or medical interventions aimed at optimizing glucose regulation and preventing complications such as preeclampsia, macrosomia, and neonatal metabolic disorders. By focusing on metabolic disruptions evident in the first trimester, this approach addresses a critical window for improving maternal and fetal

outcomes. Our study demonstrates the value of metabolomics in understanding the metabolic perturbations associated with GDM. Future research is needed to validate these biomarkers in larger cohorts and assess their integration into clinical workflows for personalized pregnancy care.

KEYWORDS

**gestational diabetes mellitus, pregnancy complications, biomarkers, metabolomics, metabolism, mass spectrometry, metabolic phenotyping, diabetes prediction**

# Introduction

Gestational diabetes mellitus (GDM) defined as hyperglycemia first recognised in pregnancy (World Health Organization, 1999) is a complex condition and a growing health issue worldwide. This definition includes undiagnosed pre-pregnancy hyperglycemia and glucose intolerance with first onset during pregnancy, being one of the most commonly diagnosed pregnancy complications. According to a recent report by the International Diabetes Federation (IDF) Atlas, gestational diabetes mellitus affects 2% to as much as 40% of pregnancies worldwide, depending on the diagnostic and screening criteria, which vary and remain controversial. These discrepancies complicate the comparison and interpretation of research findings (IDF Diabetes Atlas, 2021). Recently, there has been a shift towards adopting the International Association of Diabetes and Pregnancy Study Groups (IADPSG) criteria (IDF Diabetes Atlas, 2021), which has led to an increase in the reported incidence of GDM (IDF Diabetes Atlas, 2021; Saeedi et al., 2021). GDM contributes to several short- and long-term health consequences both for the mother (e.g., cesarean section, preeclampsia, metabolic syndrome, cardiovascular disease) (Damm, 2009; Song et al., 2018; Kramer et al., 2019; Yang and Wu, 2022) and baby (e.g., macrosomia, neonatal hypoglycemia, metabolic syndrome, cardiovascular disease, diabetes) (Bianco and Josefson, 2019; Meek, 2023; Rodolaki et al., 2023; American Diabetes Association Professional Practice Committee, 2024). Therefore, identifying any glucose impairment, especially in early pregnancy, can improve clinical outcomes (Sweeting et al., 2022). It has been demonstrated that patients with gestational diabetes discovered in early pregnancy represent a higher-risk subgroup in terms of associated pregnancy complications (Bartha et al., 2000; Bartha et al., 2003). Bartha et al. were among the first to suggest the hypothesis that this group is mainly represented by type 2 pregestational diabetes and to a lesser extent actual pregnancy-induced glucose intolerance (Bartha et al., 2003). Key epidemiological factors, including rising obesity rates, advanced maternal rage and increased instances of undiagnosed pre-pregnancy diabetes, identified during pregnancy are critical for identifying women at risk for GDM (American Diabetes Association Professional Practice Committee, 2024). With the global GDM concern, it becomes crucial to raise the efforts for early detection of glucose intolerance in pregnancy through studies focusing on the development of new predictive models for improved and accurate GDM diagnosis.

In such a premise, metabolomics offers excellent research solutions for elucidating biochemical changes in human health and disease. The global untargeted metabolomics complements information derived from genomics, transcriptomics and proteomics, supporting a system "omics" approach that might impact our ability to understand pathological conditions including pregnancy complications. Remarkable, disease-specific metabolic signatures can be captured with the potential to drive new developments in clinical biomarkers.

Our study aimed to look for differences at the metabolome level in the first trimester of pregnancy to identify metabolic alterations that could indicate impaired glucose tolerance associated with early and late-onset GDM. Our clinical and research interests focus on giving new insights and directions for the future development of novel prognostic strategies for improved GDM recognition. The graphic representation of the study design is illustrated in Figure 1.

# Materials and methods

## Study population

This is a longitudinal prospective cohort study from the Obstetrics and Gynecology department, La Paz University Hospital in Madrid, carried out between December 2017 and June 2020. The protocol of the study was approved by the local Ethics and Research Committee from La Paz University Hospital in Madrid, Spain. All eligible pregnant women without known diabetes, who were older than 16 years of age and signed the informed consent in their first trimester were invited to participate in the study. Exclusion criteria were maternal age under 16 years, gestational age >14 weeks, multiple pregnancies, known foetal defect at the time of recruitment and pre-gestational diagnosis of Diabetes Mellitus. Women with other medical co-morbidities were excluded from the study. The recruitment took place in the Obstetrical clinics of La Paz University Hospital and the control of the GDM pregnancies was carried out in the Diabetes in Pregnancy unit. The healthy control group had pregnancies followed up in Routine Obstetrical clinics. For each participant enrolled a record of maternal and gestational age at the time of recruitment, maternal characteristics including height, weight, body mass index (BMI), family history of diabetes, obstetrical record including previous history of GDM, past medical history, glycemic test results and type of GDM management including insulin or diet treatment, the course of gestation (presence or absence of further pregnancy complications), way of delivery, gestational age at birth, newborn`s weight, Apgar score and umbilical artery pH at birth was taken. The diagnosis of gestational diabetes mellitus was made based on a two-step approach: screening by 1-h 50 g glucose challenge test (GCT) and

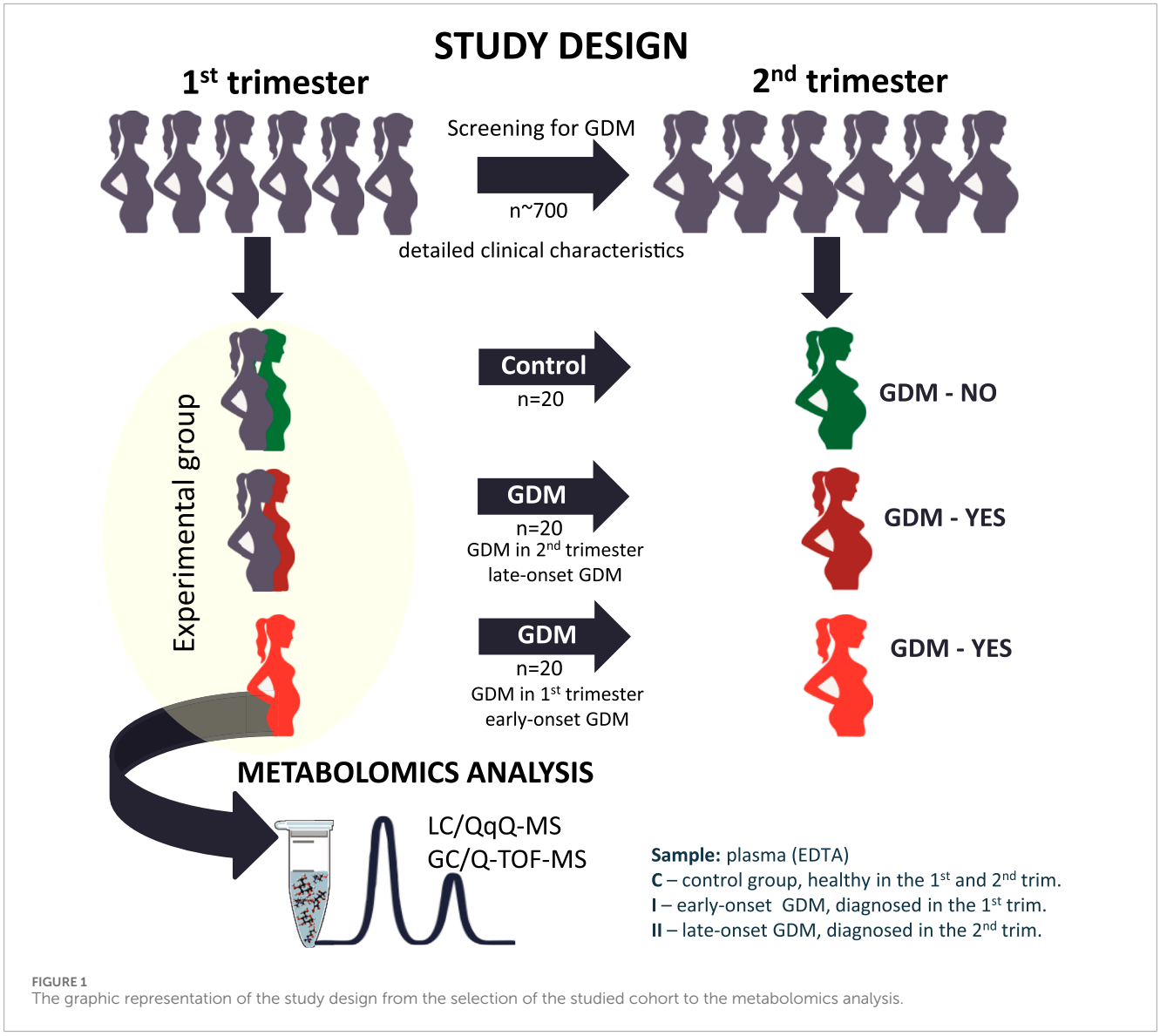


FIGURE 1
The graphic representation of the study design from the selection of the studied cohort to the metabolomics analysis.

diagnostic 3-h oral glucose tolerance test (OGTT) with 100 g glucose load for the GCT positive (glycaemia >140 mg/dL). The diagnostic criteria of Carpenter and Coustan (1982) with two or more glucose plasma levels higher than fasting glucose of 95 mg/dL, 1-h of 180 mg/dL, 2-h of 155 mg/dL, and 3-h glycaemia of 140 mg/dL were applied for this study.

La Paz University Hospital has a strategy of first-trimester screening for gestational diabetes mellitus in high-risk patients. The high-risk group for GDM is determined by the presence of any of the following risk factors: maternal age older than 35 years; maternal pre-pregnancy BMI >30 kg/m2; GDM in previous pregnancy; newborn from previous pregnancy with birth weight >4,500 g; first-grade family history of diabetes mellitus. The high-risk patients in this study were screened with CGT (O`Sullivan test) in their first trimester according to the local protocol. The screen-positive patients had a 3-h OGTT with 100 g glucose. The patients with positive results according to CC criteria were included as early-onset or first-trimester GDM. Patients who screened positive but who had a negative diagnostic test in the early group had a 3-h OGTT at 24–28 weeks instead of GCT. Thus the overall prevalence of GDM in the cohort of patients was 5%.

More than 700 women matched with the inclusion criteria were examined and the control group of healthy pregnant normal glucose tolerance women (C, n = 20), early-onset first-trimester GDM (I, n = 20) and late-onset, first-trimester asymptomatic women that developed GDM in second-trimester (II, n = 20) were selected to perform metabolomics analysis. The groups were initially matched for age, pre-gestational BMI and parity. Venous fasting blood was drawn from each eligible patient in the first trimester (≤14 weeks' gestation) into EDTA-containing tubes. Samples were stored at −80°C until analysis.

## Chemicals and reagents

Methanol (MeOH) MS grade was obtained from Sigma Aldrich (Steinheim, Germany). Acetonitrile (ACN) MS grade

(Fluka Chromassol, Spain), pyridine (Carlo Erba Reagents SAS, France), 2-propanol (PrOH) (Fischer, Austria), ammonia ($NH_3$, 28%) and glacial acetic acid (AcAc) were supplied by VWR Chemicals (Pennsylvania, United States). Ethyl acetate (EtAc) and formic acid (FA, 99.8%) were obtained from Honeywell (New Jersey, United States). Heptane MS grade, C18:0 Methyl stearate, N, O-Bis (trimethylsilyl) trifluoroacetamide (BSTFA) with 1% trimethylchlorosilane (TMCS) obtained from Sigma Aldrich. A mixture of alkanes standards (Supelco, United States), a mixture of methyl acids and fatty acids (FAME C8–C22), O-methoxamine, 4-nitrobenzoic acid and tricosane were obtained from Sigma Aldrich. Ultra-pure water was generated with a Milli-Q Plus 185 water purification system (Millipore S.A., Molsheim, France)). SPLASH® Lipidomix® Mass Spec Standard, an internal standard mixture containing 18:1 (d7) LPE, 15:0–18:1 (d7) PC, 15:0–18:1 (d7) PE, 15:0–18:1 (d7)-15:0 TG, 18:1 (d7) Chol Ester, 18:1 (d7) LPC, 18:1 (d9) SM, 18:1 (d7) DG, 15:0–18:1 (d7)-PA, 15:0–18:1 (d7)-PG, 15:0–18:1 (d7)-PI, 15:0–18:1 (d7)-PS, 18:1 (d7)-MG and cholesterol (d7) was obtained from Avanti® Polar Lipids, Inc. (Alabama, United States), and was 20 times diluted (25 µL/500 µL) in MeOH before analysis. The standard working solution was stored at −20°C.

## Sample preparation

The plasma samples were randomized, thawed on ice and thoroughly vortex-mixed. For lipid extraction 10 µL of the internal standard mixture (SPLASH® Lipidomix® Mass Spec Standard) was added to 10 µL of each plasma sample. Protein precipitation and lipid extraction were performed with 800 µL solvent mixture (EtAc:EtOH, 2:1), followed by centrifugation (13,700 rpm, 10 min, 15°C). 250 µL of the supernatant was transferred to chromatographic vials for LC-MS/MS analysis (Konjevod et al., 2022).

Samples for GC-MS analysis were prepared as previously described (Rey-Stolle et al., 2021). Briefly, proteins were precipitated by mixing 1 volume of plasma with 3 volumes of cold acetonitrile containing 4-nitrobenzoic acid (IS) (1:3), followed by methoximation with O-methoxyamine hydrochloride (15 mg/mL) in pyridine, and silylation with N,O bis(trimethylsilyl)trifluoroacetamide (BSTFA) with 1% trimethylchlorosilane (TMCS). 100 µL of heptane containing 20 ppm of tricosane (IS) was added to each vial and vortex-mixed before GC-MS analysis.

Blank and QC samples were prepared for each analytical platform following specified quality assurance criteria (Dudzik et al., 2018). A pool of plasma (QC) was prepared by mixing an equal volume of all experimental samples, following the same metabolite extraction protocols. All experimental samples were randomized and QCs were injected at the beginning, every 5 samples, and at the end of the batch. The blank samples were analyzed at the beginning and the end of each analytical run.

## LC-MS/MS analysis

The lipidomics analysis was performed on a 1260 Infinity high-pressure liquid chromatography system equipped with a degasser, a binary pump, and an autosampler, interfaced to a 6470 triple-quadrupole mass spectrometer (Agilent Technologies, CA, United States) (Konjevod et al., 2022). 5 µL of the extracted plasma samples were injected into a Gemini® C6-phenyl column (3.5 µm, 2.1 mm × 15 cm, Phenomenex®), maintained at 60°C. The mobile phase consisting of 1 mmol/L ammonium acetate ($NH_4Ac$) in 30:70 MeOH:$H_2O$ (phase A) and MeOH (phase B), both containing 0.1% formic acid (*v/v*), with a flow rate of 0.6 mL/min and the gradient started at 0% B, increasing to 100% B in 1 min, then held until 12 min. Starting conditions were reached at 13 min, and 5 min of re-equilibration was applied. The electrospray ionization (ESI) was operated in positive ion mode and the following parameters: gas temperature: 250°C, gas flow rate: 7 L/min, nebulizer pressure: 30 psi, sheath gas temperature: 350°C, sheath gas flow rate: 12 L/min, capillary voltage: 4000 V, and nozzle voltage: 500 V. MS/MS data were acquired in dynamic multiple reaction monitoring modes (dMRM) by using the most abundant precursor and product ions of each compound. The list of 156 targeted compounds with the acquisition parameters is presented in Supplementary Table S1.

## GC/Q-TOF-MS analysis

The analysis was performed with a GC system (7890B, Agilent Technologies) coupled to an accurate mass Q-TOF mass spectrometer (7250, Agilent Technologies). The derivatized samples (1 µL) were injected (autosampler 7693, Agilent Technologies) in split mode (ratio 1:12) into a deactivated glass-wool split liner (Restek 20782) in a GC column DB5-MS (30 m length, 0.25 mm internal diameter, 0.25 µm film 95% dimethyl/5% diphenylpolysiloxane) coupled to a pre-column (10 mJ & W integrated with Agilent 122-5532G). The injector port was held at 250°C, and the helium carrier gas flow rate was set at 0.917 mL/min. The temperature gradient was programmed as follows: the initial oven temperature was set to 60°C (held for 1 min), with a ramping rate of 10°C/min up to 325°C. The system was allowed to cool down for 10 min before the next injection. The total analysis time was 37.5 min per sample. The detector transfer line, the filament source and the quadrupole temperature were set to 280, 200°C and 150°C, respectively. MS detection was performed in electron impact (EI) mode at −70 eV. The mass spectrometer was operated in scan mode over a mass range of 40–600 *m/z* at a rate of 10 scan/s (Rey-Stolle et al., 2021).

Fatty Acid Methyl Esters (FAME) mix was analyzed at the beginning of the analytical batch. This procedure was performed to establish retention index markers across chromatograms, ensuring accurate alignment and identification of metabolites using Fiehn's library.

## Data processing

The acquired LC-MS data were reprocessed with the MassHunter Qualitative Analysis and MassHunter Quantitative Analysis software (Ver. B10.00, Agilent Technologies). The MRM signal runs as well as pressure curves were visually inspected to confirm homogeneity and reproducibility across

the chromatograms. In the next step peaks of the targeted compounds were integrated to determine the peak area size for each analyzed metabolite. The representative MRM chromatogram is presented in Supplementary Figure S1.

Spectral deconvolution (GC-MS) and annotation of metabolites comparing the mass spectrum obtained with those of a compound library (Fiehn GC-MS Metabolomics Retention Time Locked (RTL) library and the NIST (National Institute of Standards and Technology) mass spectra library (Ver. 2014) was performed with Unknown Analysis tool (Ver. B.08.00. Agilent Technologies). Alignment of drift (by retention time and mass) and data filtering were performed with the Mass Profiler Professional software (Ver. B.12.1, Agilent Technologies). Assignment of the target ion and the qualifiers, entire batch pre-processing and manual inspection of the acquired data including peak area and RT integration was performed with MassHunter Quantitative Analysis (Ver. B.10.00, Agilent Technologies). The dataset was interrogated to remove system contaminants. The data were evaluated for signal drift and corrected by applying a quality control-based support vector regression algorithm (QC-SVRC) (Kuligowski et al., 2015).

The metrics of the analysis quality were performed by the application of the unsupervised Principal Component Analysis (PCA) for QC sample prediction. Shewhart control charts were used to plot acquired signals versus the sample acquisition and the performance of internal standards was evaluated to overview the analytical performance. The precision of the metabolite measurements was calculated for QCs and expressed as relative standard deviation (RSD), with a cut-off value of 20% and 30% for LC-MS and GC-MS data, respectively. The assessment of data quality is presented in Supplementary Figure S2.

## Statistical analysis

Statistical analyses for metabolomics data were performed using Matlab R2015 (Mathworks) and GraphPad Prism 7 (GraphPad Software Inc., San Diego, CA). Statistical significance was assessed by ANOVA or the Kruskal-Wallis tests according to the normality of the variable distribution, with a *post hoc* test for multiple comparisons. Differences were considered statistically significant at a value of $p < 0.05$ ($^{*}p < 0.05$,$^{**}p < 0.01$,$^{***}p < 0.001$). Multivariate calculations and plots were performed in SIMCA-P + 16.0 (Umetrics, Umea, Sweden). A combination of VIP-p (corr) (correlation coefficient combined with VIP, Variable Influence on the Projection) based on the OPLS-DA model was applied for specified interpretations with the threshold value for variable selection set to VIP >1.0 and p (corr) > 0.4. MetaboAnalyst tool for metabolomic data analysis, visualization, and functional interpretation was used to test associations between variables and hierarchical heat map clustering (Chong et al., 2019). For clinical data evaluation, a Student's *t*-test was applied. Stepwise forward logistic binary multivariate regression was used to account for co-correlations among clinical variables. The significance level was previously set at 95% ($p < 0.05$).

# Results

## Clinical data

The basic characteristics of the study population are presented in Table 1. In the first-trimester GDM compared with the control group, the mean maternal age, pre-gestational BMI, pregnancy BMI and parity were higher and there was a high proportion of caesarean delivery. Additionally, the GDM-related groups (I and II) delivered earlier, but their neonates' birth weights did not vary. Glucose levels were significantly different in both GDM-related groups with a *p*-value <0.05. In the logistic binary stepwise forward regression model, the $R^2$ value of 0.12 ($p = 0.02$) refers to the overall explanatory power of the model. When pregestational BMI was included as an independent variable, other parameters such as parity ($p = 0.19$), gestational BMI ($p = 0.45$), and maternal age ($p = 0.06$) lost statistical significance, indicating that their associations with maternal diabetes were mediated by their correlation with BMI. This analysis underscores pregestational BMI as the primary risk factor for maternal diabetes in our cohort.

## Metabolomics analysis

The lipidomics analysis considered 156 lipid species belonging to the class of glycerophospholipids (68 compounds, including 26 lysoglycerophospholipids, 31 glycerophosphocholines, 11 glycerophosphoethanolamines), sphingolipids (29 compounds, including 4 ceramides and 25 sphingomyelins), cholesteryl esters (11 compounds) and glycerolipids (48 compounds, including 8 diacylglycerols and 40 triacylglycerols). GC-MS-based metabolomics analysis identified a total of 49 compounds mostly belonging to the class of organic acids, fatty acids, carbohydrates, amino acids and derivatives. Statistical analysis revealed significant metabolic profile differences associated with glucose intolerance in both in early-onset and late-onset GDM. Following univariate and multivariate statistical analysis 70 metabolites were significantly increased or decreased (*p*-value <0.05 or p (corr) > 0.4 and VIP >1.0), in the specified comparison (C *vs.* I, control group compared to early-onset GDM; C *vs.* II, control group compared to late-onset GDM; I *vs.* II, the differences between early-onset and late-onset GDM). The statistical significance and metabolic changes associated with underlying diabetes are detailed in Tables 2, 3 and Figures 3, 4. Hexose levels were significantly elevated in both early-onset ($p < 0.001$) and late-onset GDM ($p < 0.01$). Several lipid species exhibited marked dysregulation, with the most notable changes observed in diacylglycerols such as DG (32:0), DG (34:0), DG (34:1), DG (36:1), and DG (36:2), as well as triacylglycerols, including TG (52:5), TG (56:5), TG (60:8), and TG (60:10), which showed 1.5- to 2.4-fold increases ($p < 0.001$). In late-onset GDM, our analysis revealed a 4.0-fold increase in TG (44:0), TG (46:0), and TG (46:1) ($p < 0.001$), while TG (46:2) displayed a striking 4.7-fold increase ($p < 0.0001$). Additionally, significant changes were observed in glycerophospholipids, with PC (38:3) and PC (40:4) showing a 1.4-fold increase ($p < 0.001$), and PE (34:1), PE (34:2),

10.3389/fmolb.2024.1452312

TABLE 1 The basal clinical characteristics of the cohort involved in this study.

| Variable | Control C | Early-onset GDM (I) | Late-onset GDM (II) | *p*-value C vs. I | *p*-value C vs. II | *p*-value I vs. II |
|---|---|---|---|---|---|---|
| Maternal age (years) | 33.5 ± 6.16 | 38.8 ± 5.37 | 34.9 ± 4.29 | 0.006 | ns | 0.016 |
| Parity (number) | 0.6 ± 0.88 | 1.35 ± 1.3 | 0.8 ± 0.83 | 0.04 | ns | ns |
| Pre-gestational BMI ($kg/m^2$) | 23.9 ± 4.25 | 29.8 ± 6.12 | 25.2 ± 6.15 | 0.001 | ns | 0.025 |
| Pregnancy BMI ($kg/m^2$) | 28.3 ± 3.46 | 33.9 ± 6.43 | 29 ± 5.60 | 0.002 | ns | 0.015 |
| Weight gain (kg) | 11.7 ± 4.96 | 10.4 ± 5.34 | 10.1 ± 3.85 | ns | ns | ns |
| Fasting glucose 1st trim (mg/dL) | 75.8 ± 5.63 | 93.9 ± 13.74 | 82.7 ± 9.79 | <0.001 | 0.01 | 0.006 |
| Basal glucose 2nd trim (mg/dL) | 76 ± 5.15 | 94.3 ± 14.04 | 85.5 (7.32) | 0.001 | <0.0001 | ns |
| 1 h glucose 1st trim (GCT) (mg/dL) | 110.7 ± 20 | 184.3 (30.6) | 149.5 (16.4) | <0.0001 | <0.0001 | 0.001 |
| Gestational age at delivery (weeks) | 39.5 ± 1.49 | 38.3 ± 1.72 | 37.5 ± 3.04 | 0.032 | 0.013 | ns |
| Cesarean delivery, n (%) | 1 ± 5.26 | 7 ± 35 | 4 ± 20 | 0.017 | ns | ns |
| Birth weight (kg) | 3,161.5 ± 436.07 | 3,106 ± 758.46 | 2,830.2 ± 714.35 | ns | ns | ns |

Presented data are mean ± SD; Results were considered significant when $p < 0.05$.

and PE (36:2) exhibiting 1.5-fold increases ($p < 0.001$), specifically in late-onset GDM.

Figure 2 represents a specific metabolic signature associated with glucose disturbance during pregnancy. The constructed heatmap revealed considerable differences between healthy pregnant women (C) and those with early-onset GDM (I), what is even more important these differences could be noticed between control and late-onset GDM (II). It could be seen the diabetes-affected groups (I and II) are clustered together, and the metabolite levels significantly differ from the control (C). Additionally, the PLS-DA VIP projection algorithm ranked 25 metabolites to retain the most contrasting metabolic patterns (Figure 2). Among these, several glycerolipids species, including diacylglycerols (DG) and triacylglycerols (TG), belong to the group of metabolites particularly associated with observed pregnancy glucose disturbances. As depicted in Figure 3 and detailed in Table 3 all reported DG and TG were highly elevated, in both GDM-associated groups (I and II). Moreover, in most cases, those changes were also statistically significant, indicating their possible predictive proprieties. The glucose levels measured in GC-MS were statistically elevated in both GDM-related groups (Figure 4). Other compounds like organic hydroxy acids and fatty acids, with prominent changes under impaired glucose metabolism, are depicted in Figure 4. Interestingly, the Shared and Unique Structures (SUS) plot presented in Figure 5, based on two OPLS models (C *vs.* I and C *vs.* II), further emphasizes the shared and distinct metabolic alterations, capturing consistent relationships among variables. Metabolites consistently upregulated in both groups (I and II) included diacylglycerols (e.g., DG (32:0), DG (34:0), DG (34:1), DG (36:1), DG (36:2), DG (36:3), DG (36:4), DG (38:5)), triacylglycerols (e.g., TG (48:1), TG (48:2), TG (50:0), TG (50:1), TG (50:2), TG (50:3), TG (50:4), TG (52:1), TG (52:2), TG (52:3), TG (52:4), TG (52:5), TG (52:6), TG (54:1), TG (54:2), TG (56:4), TG (56:5), TG (56:6), TG (56:7), TG (56:8), TG (58:10), TG (60:8), TG (60:10)), as well as phosphatidylcholines (PC(36:4), PC(38:4)), phosphatidylethanolamines (PE (38:4), PE (40:6)), sphingomyelins (SM (d18:0/18:0)), cholesteryl ester (CE (18:3)), and hexose. These metabolites are visually represented as red dots. Conversely, metabolites consistently downregulated in those both groups, represented as navy blue dots, included L-alanine, glycine, 2-methylalanine, urea, 2-butyne-1-4-diol, L-5-oxoproline, asparagine, N-methylguanine, and PC(34:2e). Elevated levels of saturated and unsaturated fatty acids, including palmitic acid, palmitoleic acid, linoleic acid, oleic acid, and stearic acid, along with hydroxy acids such as 2-hydroxybutyric acid, 3-hydroxybutyric acid, and glycerol (yellow), combined with decreased levels of PC (34:1e), PC (36:2), PC (36:2e), PC (40:7), PC (40:8), SM (d18:1/21:0), phenylalanine, and p-cresol (green), are distinctive features of early-onset GDM. Metabolites uniquely upregulated in group II (late-onset GDM), represented by orange dots, include PC (30:0), PC (38:3), PC (40:4), PE (34:1), PE (34:2), PE (36:2), PE (36:3), PE (36:4), PE (38:6), CE (16:1), CE (14:0), CE (16:2), TG (44:0), TG (46:0), TG (46:1), TG (46:2), TG (48:0), TG (48:3), and TG (51:0). In contrast, creatinine,

10.3389/fmolb.2024.1452312

TABLE 2 The list of the metabolites found to be significant in GC-MS analysis.

| Compound name | *p*-value ANOVA | *p*-value | | | p (corr) and VIP | | | | | | Changes [%] | | |
|---|---|---|---|---|---|---|---|---|---|---|---|---|---|
| | | C vs. I | C vs. II | I vs. II | C vs. I | | C vs. II | | I vs. II | | C vs. I | C vs. II | I vs. II |
| 2-Hydroxybutyric acid | ns | ns | ns | ns | 0.6 | 1.2 | ns | ns | 0.5 | 1.5 | +26 | +4 | −17 |
| 3-Hydroxybutyric acid | ns | ns | ns | ns | 0.5 | 1.6 | ns | ns | 0.7 | 2.5 | +51 | −10 | −41 |
| Glycerol | ns | ns | ns | ns | 0.6 | 1.5 | ns | ns | 0.6 | 1.8 | +16 | +3 | −11 |
| Urea | ns | ns | ns | ns | 0.6 | 1.6 | 0.7 | 2 | ns | ns | −21 | −15 | +8 |
| 2-butyne-1,4-diol | ns | ns | ns | ns | 0.6 | 1.5 | 0.7 | 1.9 | ns | ns | −21 | −16 | +6 |
| p-cresol | ns | ns | ns | ns | 0.5 | 1.1 | ns | ns | ns | ns | −26 | −11 | +22 |
| L-Proline | ns | ns | ns | ns | 0.5 | 1.1 | 0.7 | 1.6 | ns | ns | −12 | −11 | +2 |
| L-5-Oxoproline | 2.20E-04 | 8.41E-05 | 2.05E-03 | ns | 0.6 | 1 | ns | ns | ns | ns | −21 | −16 | +6 |
| Creatinine | 4.59E-02 | ns | 1.35E-02 | ns | ns | ns | 0.6 | 2.3 | ns | ns | −29 | −62 | −47 |
| Glycine | 2.42E-02 | 1.08E-02 | 3.29E-02 | ns | 0.6 | 1.4 | 0.6 | 1.3 | ns | ns | −26 | −21 | +6 |
| Asparagine | 1.14E-03 | 4.16E-04 | 6.26E-03 | ns | 0.5 | 1.4 | 0.6 | 2.1 | ns | ns | −43 | −33 | +18 |
| L-Tryptophan | ns | ns | ns | ns | 0.5 | 1 | 0.5 | 1.2 | ns | ns | −12 | −13 | −1 |
| L-serine | 2.32E-02 | 3.50E-02 | 8.00E-03 | ns | ns | ns | ns | ns | ns | ns | −11 | −12 | −1 |
| L-Phenylalanine | ns | 4.01E-02 | ns | ns | 0.7 | 1 | ns | ns | ns | ns | −12 | −9 | +4 |
| 2-Methylalanine | 2.88E-02 | ns | 8.55E-03 | ns | ns | ns | 0.6 | 1.4 | ns | ns | −17 | −28 | −13 |
| N-Methylguanine | 2.46E-02 | 2.46E-02 | ns | ns | 0.5 | 1.8 | ns | ns | ns | ns | −71 | −44 | +97 |
| Palmitoleic acid | ns | ns | ns | ns | 0.7 | 2.1 | ns | ns | 0.7 | 2.8 | +11 | −3 | −12 |
| Palmitic acid | ns | ns | ns | ns | 0.7 | 1.5 | ns | ns | 0.8 | 2.1 | +19 | +2 | −15 |
| Linoleic acid | ns | ns | ns | ns | 0.7 | 1.8 | ns | ns | 0.7 | 2.2 | +26 | −6 | −25 |
| Oleic acid | ns | ns | ns | ns | 0.7 | 2 | ns | ns | 0.8 | 2.9 | +26 | −3 | −23 |
| Stearic acid | ns | ns | ns | ns | 0.6 | 1 | ns | ns | 0.6 | 1.2 | +10 | +6 | −4 |
| Hexose | 2.49E-03 | 8.35E-04 | 1.23E-02 | ns | 0.5 | 1.2 | 0.5 | 1.2 | ns | ns | +43 | +31 | −8 |

Percentage of the changes in the specified comparison. The sign indicates the direction of change in the diabetes-associated groups: group I, early-onset GDM or group II, late-onset GDM.

shown as fuchsia, was downregulated and appears to be associated with late-onset GDM.

## Discussion

There is no doubt that gestational diabetes is a major obstetrical clinical problem carrying a significant health burden for both the mother and the child. Growing evidence suggests that GDM imposes a considerable risk of developing type 2 diabetes mellitus (T2DM) postpartum among other conditions (Khan et al., 2019). Therefore, early recognition of GDM opens a window for better management of affected women and their babies (Adam et al., 2023). In most cases, GDM is the result of impaired glucose tolerance due to pancreatic β-cell dysfunction and shares the pathophysiological mechanisms with metabolic disorders associated with insulin resistance as metabolic syndrome, obesity or T2DM (Plows et al., 2018). Several risk factors contribute to the development of gestational insulin resistance, including placental, hormonal, genetic, and epigenetic variables, alongside an increase in visceral adipose tissue, changes in gut microbiota, and the coexistence of overweight or obesity (Kampmann et al.,

10.3389/fmolb.2024.1452312

TABLE 3 The list of the metabolites found to be significant in LC-MS/MS analysis.

| Compound name | *p*-value ANOVA | *p*-value | | | p (corr) and VIP | | | | | | Changes [%] | | |
|---|---|---|---|---|---|---|---|---|---|---|---|---|---|
| | | C vs. I | C vs. II | I vs. II | C vs. I | | C vs. II | | I vs. II | | C vs. I | C vs. II | I vs. II |
| PC (34:2e) | ns | ns | ns | ns | 0.6 | 1.2 | 0.5 | 1.0 | ns | ns | −22 | −16 | +7 |
| PC (38:3) | 9.90E-03 | ns | 7.80E-03 | ns | ns | ns | 0.5 | 1.2 | ns | ns | +23 | +39 | +13 |
| PC (40:4) | 3.11E-02 | ns | 2.61E-02 | ns | ns | ns | 0.5 | 1.0 | ns | ns | +16 | +32 | +14 |
| PC (40:7) | 3.35E-02 | 2.85E-02 | ns | ns | 0.5 | 1.1 | ns | ns | 0.4 | 1.0 | −19 | −9 | +13 |
| PC(40:8) | 2.60E-02 | 2.34E-02 | ns | ns | 0.5 | 1.0 | ns | ns | ns | ns | −18 | −12 | +8 |
| PE (34:1) | 1.41E-02 | ns | 1.13E-02 | ns | ns | ns | 0.6 | 1.2 | 0.5 | 1.7 | +20 | +46 | +22 |
| PE (34:2) | 3.50E-02 | ns | 2.98E-02 | ns | ns | ns | 0.5 | 1.2 | 0.4 | 1.8 | +24 | +46 | +18 |
| PE (36:2) | 3.68E-02 | ns | 3.19E-02 | ns | ns | ns | 0.5 | 1.2 | 0.4 | 1.5 | +20 | +37 | +14 |
| PE (36:3) | 3.47E-02 | ns | 4.15E-02 | 4.15E-02 | ns | ns | ns | ns | 0.6 | 2.2 | +1 | +29 | +27 |
| PE (36:4) | 8.20E-03 | ns | 9.40E-03 | 3.15E-02 | ns | ns | 0.6 | 1.2 | 0.4 | 2.2 | +10 | +42 | +29 |
| PE (40:6) | 2.49E-02 | ns | 2.05E-02 | ns | ns | ns | 0.5 | 1.2 | ns | ns | +24 | +46 | +18 |
| SM (d18:0/18:0) | 4.00E-03 | 2.98E-02 | 3.70E-03 | ns | 0.4 | 1.1 | 0.7 | 1.2 | ns | ns | +31 | +45 | +10 |
| Cer (d18:1/22:0) | 1.35E-02 | 3.96E-02 | ns | 1.62E-02 | ns | ns | ns | ns | 0.4 | 2.6 | +30 | −8 | −29 |
| CE (16:1) | 1.61E-02 | 3.73E-02 | 2.15E-02 | ns | ns | ns | 0.6 | 1.2 | ns | ns | +40 | +48 | +6 |
| CE (18:3) | 2.42E-02 | ns | 2.09E-02 | ns | 0.4 | 1.1 | 0.6 | 1.2 | ns | ns | +30 | +43 | +10 |
| CE (16:2) | 9.50E-03 | ns | 7.70E-03 | ns | ns | ns | 0.6 | 1.4 | 0.5 | 1.3 | +34 | +56 | +16 |
| DG (36:2) | 1.80E-03 | 3.20E-03 | 3.20E-03 | ns | 0.7 | 1.7 | 0.7 | 1.4 | ns | ns | +59 | +60 | +1 |
| DG (32:0) | 1.80E-03 | 6.70E-03 | 3.20E-03 | ns | 0.6 | 2.0 | 0.7 | 1.8 | ns | ns | +112 | +144 | +15 |
| DG (34:0) | 2.00E-03 | 5.80E-03 | 4.20E-03 | ns | 0.6 | 1.7 | 0.7 | 1.6 | ns | ns | +76 | +91 | +8 |
| DG (34:1) | 9.00E-04 | 2.70E-03 | 1.90E-03 | ns | 0.7 | 2.1 | 0.8 | 1.8 | ns | ns | +97 | +107 | +5 |
| DG (36:1) | 4.00E-04 | 8.00E-04 | 8.00E-04 | ns | 0.7 | 1.9 | 0.7 | 1.6 | ns | ns | +76 | +74 | −1 |
| DG (36:3) | 2.08E-02 | 2.74E-02 | 4.78E-02 | ns | 0.7 | 1.7 | 0.4 | 1.1 | ns | ns | +50 | +45 | −3 |
| DG (38:5) | 2.50E-03 | 5.30E-03 | 5.30E-03 | ns | 0.8 | 2.0 | 0.6 | 1.5 | ns | ns | +73 | +78 | +3 |
| TG (44:0) | 2.03E-02 | ns | 1.59E-02 | ns | ns | ns | 0.6 | 2.3 | 0.5 | 3.0 | +109 | +295 | +89 |
| TG (46:0) | 1.19E-02 | ns | 1.01E-02 | ns | ns | ns | 0.6 | 2.3 | ns | ns | +154 | +298 | +57 |
| TG (46:1) | 2.16E-02 | ns | 1.78E-02 | ns | ns | ns | 0.6 | 2.1 | ns | ns | +189 | +291 | +35 |
| TG (46:2) | 4.80E-03 | ns | 3.40E-03 | ns | ns | ns | 0.7 | 2.4 | ns | ns | +188 | +371 | +64 |
| TG (48:0) | 7.90E-03 | 3.14E-02 | 9.20E-03 | ns | ns | ns | 0.6 | 2.0 | ns | ns | +120 | +168 | +22 |
| TG (48:1) | 3.30E-03 | 3.22E-02 | 2.90E-03 | ns | 0.4 | 1.9 | 0.7 | 2.2 | ns | ns | +134 | +214 | +35 |
| TG (48:2) | 4.70E-03 | 5.35E-02 | 3.80E-03 | ns | 0.4 | 1.6 | 0.7 | 2.1 | ns | ns | +111 | +199 | +42 |

(Continued on the following page)

TABLE 3 (*Continued*) The list of the metabolites found to be significant in LC-MS/MS analysis.

| Compound name | *p*-value ANOVA | *p*-value | | | p (corr) and VIP | | | | | | Changes [%] | | |
|---|---|---|---|---|---|---|---|---|---|---|---|---|---|
| | | C vs. I | C vs. II | I vs. II | C vs. I | | C vs. II | | I vs. II | | C vs. I | C vs. II | I vs. II |
| TG (48:3) | 4.92E-02 | ns | 4.35E-02 | ns | ns | ns | 0.6 | 1.7 | ns | ns | +71 | +140 | +40 |
| TG (50:0) | 2.80E-03 | 1.37E-02 | 3.70E-03 | ns | 0.4 | 1.7 | 0.7 | 1.7 | ns | ns | +82 | +98 | +9 |
| TG (50:1) | 1.12E-02 | 2.86E-02 | 1.50E-02 | ns | 0.5 | 1.7 | 0.7 | 1.7 | ns | ns | +83 | +101 | +10 |
| TG (50:2) | 4.10E-03 | 2.35E-02 | 4.50E-03 | ns | 0.5 | 1.6 | 0.7 | 1.7 | ns | ns | +82 | +98 | +9 |
| TG (50:3) | 6.50E-03 | 3.60E-02 | 6.40E-03 | ns | 0.6 | 1.5 | 0.6 | 1.6 | ns | ns | +64 | +88 | +15 |
| TG (51:0) | 9.50E-03 | 6.25E-02 | 8.40E-03 | ns | ns | ns | 0.7 | 2.1 | 0.4 | 1.8 | +79 | +157 | +43 |
| TG (52:1) | 7.00E-04 | 1.70E-03 | 1.70E-03 | ns | 0.6 | 1.9 | 0.8 | 1.7 | ns | ns | +74 | +78 | +2 |
| TG (52:2) | 6.00E-03 | 8.60E-03 | 8.60E-03 | ns | 0.6 | 1.5 | 0.6 | 1.3 | ns | ns | +54 | +55 | +1 |
| TG (52:3) | 1.30E-02 | 1.80E-02 | 1.80E-02 | ns | 0.6 | 1.3 | 0.5 | 1.0 | ns | ns | +34 | +33 | −1 |
| TG (52:5) | 8.80E-03 | 1.48E-02 | 1.48E-02 | ns | 0.7 | 1.8 | 0.5 | 1.5 | ns | ns | +46 | +96 | +34 |
| TG (52:6) | 8.90E-03 | ns | 6.80E-03 | ns | 0.5 | 1.6 | 0.6 | 2.0 | ns | ns | +93 | +154 | +31 |
| TG (54:1) | 5.00E-03 | 1.40E-02 | 8.20E-03 | ns | 0.5 | 1.6 | 0.6 | 1.5 | ns | ns | +64 | +71 | +4 |
| TG (54:2) | 1.03E-02 | 3.27E-02 | 1.25E-02 | ns | 0.5 | 1.3 | 0.6 | 1.3 | ns | ns | +44 | +55 | +8 |
| TG (56:4) | 1.86E-02 | ns | 2.03E-02 | ns | 0.5 | 1.3 | 0.6 | 1.4 | ns | ns | +38 | +51 | +9 |
| TG (56:5) | 1.10E-03 | 3.80E-03 | 2.00E-03 | ns | 0.7 | 1.8 | 0.7 | 1.5 | ns | ns | +49 | +56 | +5 |
| TG (56:6) | 1.17E-02 | 1.44E-02 | 1.44E-02 | ns | 0.8 | 1.4 | 0.5 | 1.0 | ns | ns | +32 | +32 | 0 |
| TG (60:10) | 1.88E-02 | 2.40E-02 | 4.68E-02 | ns | 0.7 | 1.9 | 0.4 | 1.2 | ns | ns | +79 | +60 | −11 |
| TG (60:8) | 1.80E-03 | 3.30E-03 | 3.30E-03 | ns | 0.8 | 2.5 | 0.6 | 1.9 | ns | ns | +125 | +142 | +7 |

Percentage of the changes in the specified comparison. The sign indicates the direction of change in the diabetes-associated groups: group I, early-onset GDM or group II, late-onset GDM.

2019). Understanding the metabolic disturbances underlying GDM holds promise for advancing our knowledge of its pathophysiology and developing targeted interventions to mitigate its adverse effects on maternal and fetal health. This insight is crucial for identifying women at risk of metabolic complications, enabling tailored prevention and personalized treatment strategies.

In our study, we look into the metabolic profile of pregnant women in the first trimester of pregnancy. The value of our research design was that we were able to select a group of asymptomatic in the first trimester individuals who had GDM diagnosed in later pregnancy (late-onset GDM). Our study offers a glimpse into molecular mechanisms of disease and enables the identification of compounds that could serve as novel players for early GDM prediction.

Advanced maternal age is recognized as a contributing factor to the development of gestational diabetes mellitus. Our study population consists of controls and women who were diagnosed with GDM in the first trimester (early onset) or a group diagnosed with GDM in the second trimester (late onset). Since we initially cross-matched the control group and the 2nd-trimester GDM group for maternal age, a potential association between maternal age and risk for GDM could only be looked for in the comparison between first-trimester GDM group and controls on one hand and 1st-trimester GDM and 2nd-trimester GDM on the other. We found statistical differences in both aforementioned comparisons that confirm the increased risk for GDM with maternal age. This finding is in line with a comprehensive systemic review and meta-analysis presented by Li et al. (2020) which involves the data on 127,275,067 participants and demonstrates a clear linear association between maternal age and the risk for GDM. In our study group, the parity was also a significantly different variable when controls were compared to 1st-trimester GDM. The control group had a lower parity than the 1st-trimester GDM group. There were no statistically significant differences between controls and 2nd-trimester GDM or between 1st- and 2nd-trimester GDM. The literature review shows little or no impact of parity on subsequent non-insulin dependent diabetes mellitus (NIDDM) which would be the case of the women with newly diagnosed or 1st-trimester GDM in our group. It is known that most women with sufficient pancreatic β-cell population tolerate well pregnancy-related insulin resistance.

10.3389/fmolb.2024.1452312

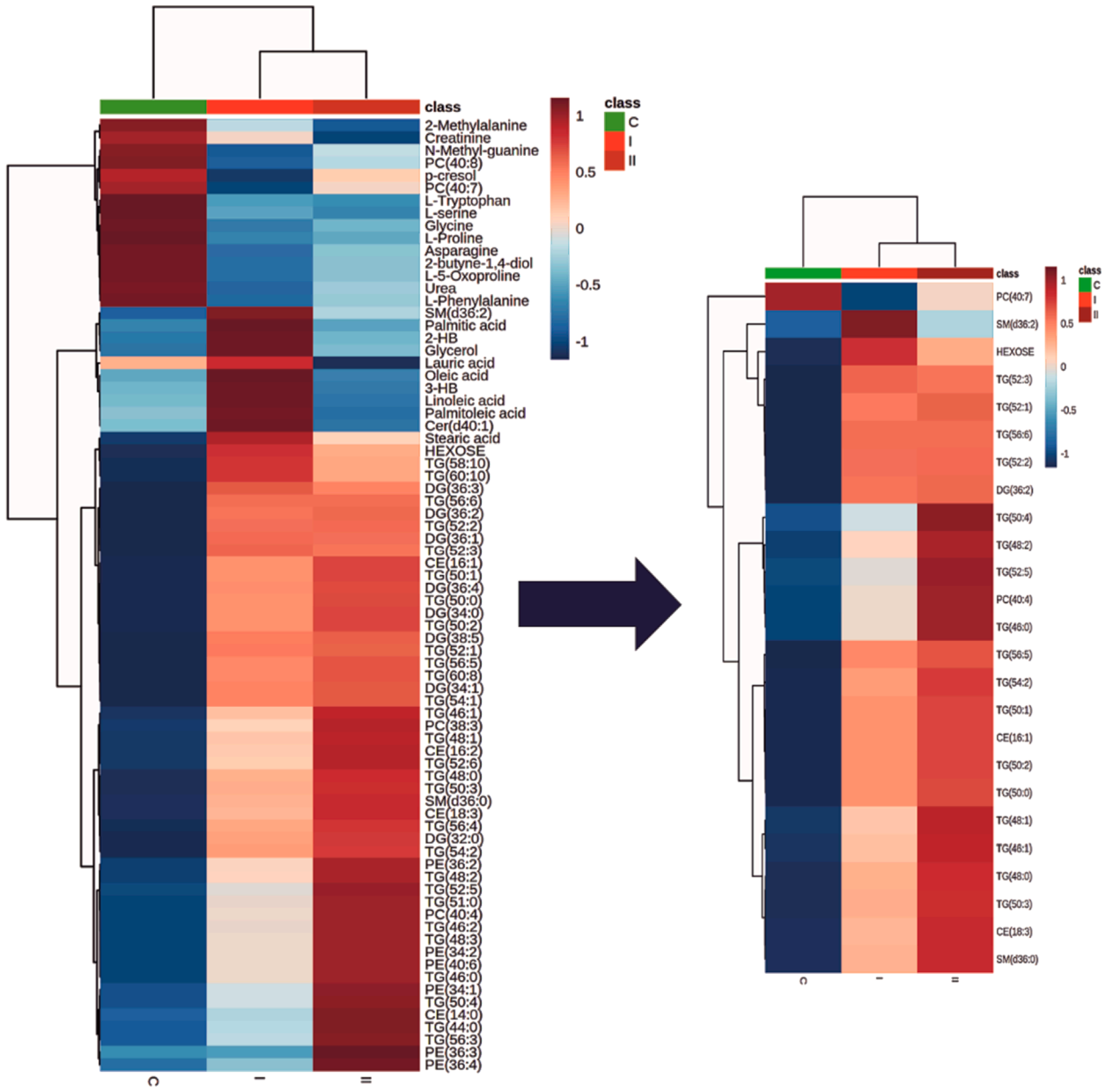


FIGURE 2
The heatmap and dendrogram show the metabolic differences and a clear cluster formation between control (C) and groups associated with diabetes (I and II). Only metabolites which were significantly associated with diabetes are presented. Each coloured cell on the map corresponds to an average of the relative metabolite abundance in the specified group (blue, the lowest; red the highest). The top 25 discriminative metabolites based on the PLS-DA VIP projection are highlighted. Rows: metabolites; Columns: experimental groups (C, green; I, bright red, II dark red). Hierarchical clustering based on Euclidean distances and Ward clustering algorithm.

However, according to Peters et al., previous GDM increases close to threefold the risk of NIDDM (Peters et al., 1996) and our data on the history of previous GDM in parous women is based on self-reported information which could have a certain bias. The differences in parity appear to align, to some extent, with variations in maternal age and pre-gestational BMI, both of which are well-established risk factors for GDM. A high pre-gestational BMI not only elevates the risk of hypertensive disorders during pregnancy but also contributes to GDM by exacerbating physiological pregnancy-induced insulin resistance. As noted earlier, the control and second-trimester GDM groups were matched for pre-gestational BMI. Thus, comparisons between the first-trimester GDM group and the controls, as well as between the first- and second-trimester GDM groups, revealed statistically significant differences. Interestingly the median birth weight in our study was not elevated and differences in the newborn birth weight are neither significant between controls and GDM-related groups (I and II). Therefore we could not associate high triglyceride levels observed in our study, with increased newborn birth weight, macrosomia or large for gestational age as was concluded by other authors (Vrijkotte et al., 2011; Whyte et al.,

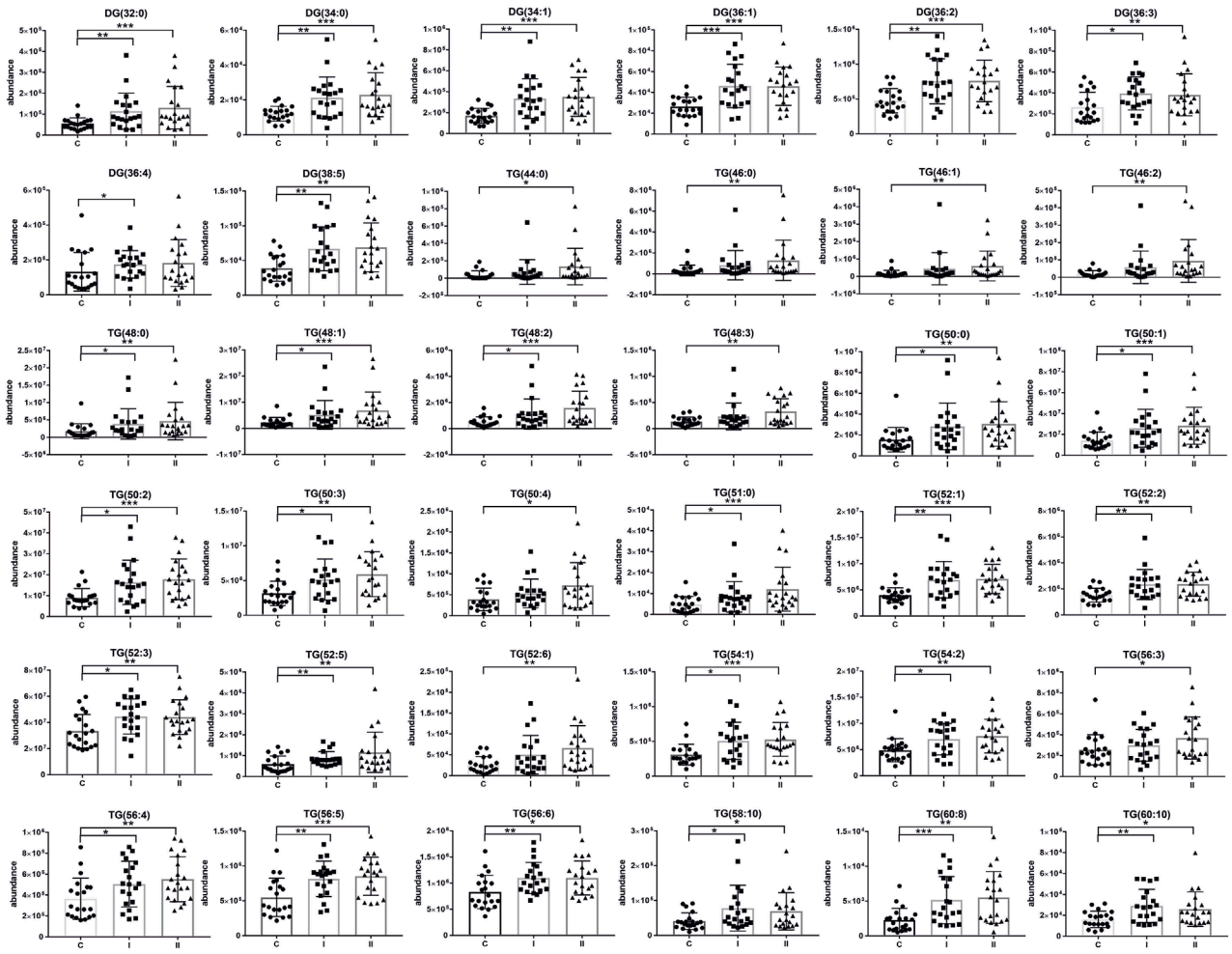


FIGURE 3
Scatter plots of the relative abundances for the group of glycerolipids representing observed changes between control (C) and diabetic groups (I, early-onset GDM and II, late-onset GDM). mean ± SD; *P*-values*$p < 0.05$,**$p < 0.01$,***$p < 0.001$.

2013; Zhu et al., 2022). This could be associated with the sample size and proper pregnancy management. Maternal lipid metabolism undergoes significant adaptations during pregnancy to meet the increased energy demands of the developing fetus and to ensure proper fetal development (Soma-Pillay et al., 2016). There is no doubt that we should still deepen our understanding of the complex interplay between lipid metabolism and other pathophysiological mechanisms, such as insulin resistance or placental dysfunction. The rise in triglyceride levels is a result of increased synthesis by the liver and reduced enzymatic activity of lipoprotein lipase, leading to decreased catabolism of adipose tissue (Soma-Pillay et al., 2016). Increased triglycerides were correlated with impaired glucose metabolism in muscle tissue and inhibited insulin signalling pathways, leading to insulin resistance (Yaribeygi et al., 2019). Insulin promotes TG storage by driving the differentiation of pre-adipocytes into mature adipocytes enhancing lipogenesis through ADD-1/SREBP-1c which regulates genes for fatty acid synthesis and lipogenesis in adipocytes and the liver facilitating glucose transport for conversion into triglycerides and inhibiting lipolysis to prevent triglyceride breakdown (Kahn and Flier, 2000; Yaribeygi et al., 2019).

Our findings in alterations in TG levels in the early stages of GDM-affected pregnancies are in line with a vast literature that reported the association between high TG during pregnancy and increased risk of GDM (Li et al., 2014; Furse et al., 2019; Zhu et al., 2020). Hou et al. in a case-control study of 100 GDM and 100 normal glucose tolerance women defined the lipidomic signature in plasma across pregnancy, and proposed new lipid biomarkers for GDM prediction. The authors conclude that particularly diacylglycerols and triacylglycerols were upregulated across three trimesters of pregnancy, and demonstrated good performance in the prediction of GDM in the first and the second trimesters (Hou et al., 2023). Our data support those findings, making this evidence stronger. Moreover, Hu et al. in a large meta-analysis investigated the outcome of 292 studies, comprising 97,880 pregnant women (28,232 GDM and 69,648 controls) and also concluded that women with GDM had significantly higher TG levels that occurred in the first trimester and persisted afterwards (Hu et al., 2021).

Several studies indicate that high levels of sphingolipids, including ceramides and sphingosine-1-phosphate are correlated with pregnancy complications including gestational diabetes

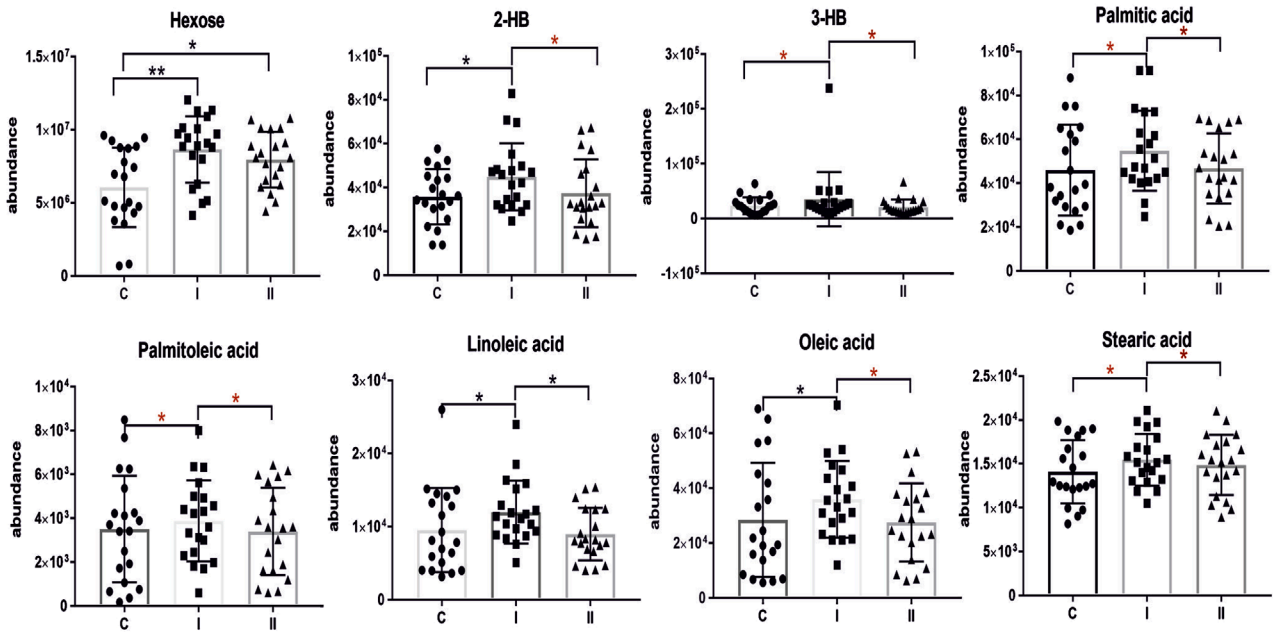


FIGURE 4
Scatter plots of the relative abundances for selected metabolites representing observed changes between control (C) and diabetic groups (I, early-onset GDM and II, late-onset GDM). The red asterisk indicates the significance according to multivariate analysis. mean ± SD; *P*-values*$p < 0.05$,**$p < 0.01$,***$p < 0.001$.

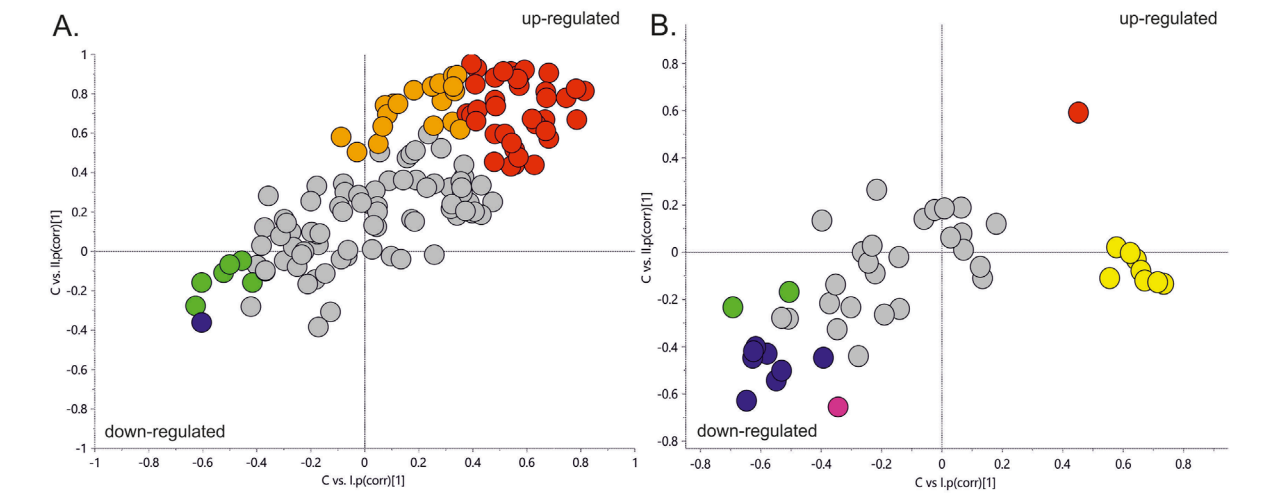


FIGURE 5
The SUS plot is based on two OPLS models (C *vs.* I and C *vs.* II). The coordinates of each variable are their correlation coefficients to the predictive components derived from each model. The position of the variables on the plot reflects their relationships to the responses of specified models. The X-axis is the predictive component of early-onset GDM, and the Y-axis is the predictive component associated with late-onset GDM. Panel **(A)**. SUS plot for LC-MS/MS data. Panel **(B)**. SUS plot for GC-MS data. Red dots–metabolites upregulated in both groups (I and II); Orange dots, represent metabolites upregulated, specific for group II; Yellow dots, metabolites upregulated, specific for group I; Navy blue dots, metabolites downregulated in both groups (I and II); fuchsia colour dot, downregulated in group II; green dots, metabolites downregulated in early-onset GDM women (I).

(Fakhr et al., 2021; Enthoven et al., 2023; Hou et al., 2023). Those bioactive compounds have been implicated in the regulation of insulin signalling pathways. Ceramides represent a major subclass of sphingolipids that interfere with insulin signalling by inhibiting Akt phosphorylation and promoting serine phosphorylation of insulin receptor substrate-1 (IRS-1) (Kanety et al., 1996). Ceramide triggers β-cell apoptosis by enhancing the permeability of the mitochondrial membrane, leading to the activation of the intrinsic apoptosis pathway that, significantly contributes to the pathogenesis of diabetes (Galadari et al., 2013; Hammad and Lopes-Virella,

2023). The results of our study are in line with the literature and indicate elevated levels of Cer(d18:1/22:0) in the group of late-onset GDM, whereas the level of SM(d18:0/18:0) increased in both GDM-related groups.

We also found the relationship between plasma levels of glycerophospholipids such as phosphatidycholines and phosphatidylethanolamines and GDM. Dysregulated glycerophospholipid metabolism has been linked to inflammation which is recognized as a key feature of diabetes. Many of those compounds can serve as precursors for pro-inflammatory lipid mediators that can activate inflammatory signalling pathways and promote the production of inflammatory cytokines, contributing to insulin resistance. According to the literature disrupted glycerophospholipid metabolism is common in GDM (Dudzik et al., 2014; Liu et al., 2016; Zhan et al., 2021), however, due to the diversity of glycerophospholipids structures further research is needed to elucidate the specific role in GDM molecular mechanisms.

Our data confirm the significance of fatty acids in the pathophysiology of GDM which is consistent with our first data from the study performed in GDM plasma from the second trimester of pregnancy (Dudzik et al., 2014; Dudzik et al., 2017) and others (Chen et al., 2010; Scholtens et al., 2014; Enquobahrie et al., 2015). All reported fatty acids including saturated palmitic acid (C16:0), stearic acid (C18:0) and unsaturated linoleic acid (ω-6, C18:2), palmitoleic acid (ω-7, C16:1), oleic acid (ω-9, C18:1) were elevated in the group of early-onset GDM, however, this trend was not observed in late-onset GDM. Several studies confirm that the circulation of maternal free fatty acids (FFAs) plays an important role in the pathophysiology of GDM due to their involvement in various metabolic processes. Elevated levels of FFAs in pregnancy inhibit total body glucose uptake and oxidation. Chronic exposure to high levels of FFAs can impair pancreatic β-cell function leading to reduced insulin secretion and insulin resistance (Sivan et al., 1998; Sun et al., 2022). Meta-analysis and original data presented by Sun et al. indicate that GDM women are characterized by a particular circulating saturated FA profile with altered levels of palmitic acid and lower levels of very-long-chain FA. The results demonstrated that palmitic acid has a strong positive correlation with GDM both in the early and second trimesters of pregnancy (Sun et al., 2022). Other studies conducted by Ogundipe et al. have shown that GDM has a unique fatty acid profile with elevated levels of omega 6 fatty acids compared to omega 3 an abnormal pattern of sequential *n*-6 metabolism (Ogundipe et al., 2020).

Special attention should be also placed on hydroxy acids, namely, 2-hydroxybutyric acid (2-HB) and 3-hydroxybutyric acid (3-HB). Its specific role in the pathological process that leads to GDM has not been extensively studied so far however, there are several potential mechanisms through which those compounds may contribute to this condition. Gall et al. postulated that 2-HB, an organic acid derived from 2-ketobutyric acid, could be an early indicator for both insulin resistance (IR) and impaired glucose regulation (Gall et al., 2010). Elevated 2-HB is strongly linked to impairment of β-cells function and may reflect disruptions in metabolic pathways, such as increased fatty acid oxidation, ketogenesis and oxidative stress which are common features of insulin resistance state and GDM (Gall et al., 2010; Sousa et al., 2021). Moreover, 2-HB has been implicated in chronic low-grade inflammation which is a hallmark feature of obesity and a major risk factor for GDM (Sousa et al., 2021). The role of the ketone body as 3-hydroxybutyric acid in the pathophysiology of GDM remains an area of active investigation. High 3-HB levels observed in GDM may reflect metabolic dysregulation including increased lipolysis and ketogenesis, which contribute to alterations in energy metabolism and glucose homeostasis. 3-HB is produced during fatty acid oxidation and serves as an alternative energy substrate (Qi et al., 2022). This compound was found to be associated with GDM reported in many metabolomics studies (White et al., 2017; Lu et al., 2021; McMichael et al., 2021; Sikorski et al., 2022). What is more interesting, hydroxybutyric acid has been connected with gut microbiota-derived metabolites showing significantly higher levels in women with GDM (Singh et al., 2023; Ye et al., 2023). Growing evidence suggests that ketone bodies may serve as immunomodulators to attenuate pathological inflammation (Qi et al., 2022). A very recent study by Neudorf et al. postulates that it is plausible that 3-HB could mitigate inflammatory signalling pathways implicated in diabetes (Neudorf et al., 2024). Considering the potential of β-HB and the intriguing literature data we believe this compound is worthy of particular attention. In our study, we observed that higher levels of both 2-HB and 3-HB were associated with early-onset GDM, although not significant in late-onset GDM. The results are consistent with our first data where we identified a panel of plasma metabolites implicated in GDM pathophysiology (Dudzik et al., 2014; Dudzik et al., 2017; Burzynska-Pedziwiatr et al., 2023), however, those studies were performed on the plasma samples from the second trimester, different cohort and diagnosis of GDM were based on different criteria. Nevertheless, in both cases, the observed changes were associated with glucose impairment and diagnosed GDM.

It is worth mentioning that our study identified other metabolites like p-cresol, 2-butyne-1,4-diol or tryptophan (Trp) linked to the intestinal microbiota. There is limited evidence linking those compounds to GDM, but their possible association with inflammation suggests that they may play a role in the molecular background of GDM. The essential amino acid L-tryptophan is particularly important in pregnancy due to the high demand for maternal protein synthesis and fetal growth and development (Badawy, 2015). Our findings from present and previous experiments show a reduced level of tryptophan in GDM (Dudzik et al., 2014), which is in line with other studies (Leitner et al., 2017; Özdemir et al., 2023). This decrease may be attributed to increased degradation or altered utilization of Trp in GDM. The recent systematic review by van Zundert et al. indicates that decreased Trp levels in maternal blood in the second and third trimester of pregnancy was associated with several pregnancy complications including gestational diabetes (van Zundert et al., 2022).

We found that changes observed in amino acid profile are not entirely consistent across studies, most likely due to differences in the trimesters of pregnancy at which the study was performed and the criteria for GDM definition. In our study, glycine, serine and proline levels were lower in the GDM group which is consistent with findings reported in previous studies performed in the first and the second trimester of pregnancy (Zhao et al., 2019; Lu et al., 2021). Nevertheless, other studies report that first-trimester, early-onset GDM was associated with higher concentrations of glycine and proline compared to the control group (Razo-Azamar et al., 2023).

Our study point also an association between significant depletion in creatinine levels and late-onset GDM. The results are concordant with the other findings (Chen et al., 2023) and literature describing a positive correlation between lower serum creatinine and abnormal glucose metabolism (Harita et al., 2009; Bao et al., 2018). Finally, our study confirmed high glucose levels observed both in the early- and late-onset GDM group.

## Conclusion

The metabolomics approach provides a powerful tool for understanding the metabolic changes associated with gestational diabetes mellitus (GDM). It offers a snapshot of the phenotypic state at the time of sampling, allowing for hypothesis generation and translational insights that can serve both researchers and clinicians in better understanding disease mechanisms and enabling earlier recognition of impaired glucose tolerance during pregnancy. Our study indicates several molecules providing biomarker candidates, especially for late-onset GDM prediction. Although several studies have been performed so far, no metabolite-based prediction factor for late-onset GDM exists, therefore, more effort is required to elucidate the molecular landscape of GDM. Nevertheless, we recognise some limitations in our study. The relatively small sample size and single-centre design may limit the significance of the findings. Expanding the study to larger, multi-centre cohorts with greater ethnic and geographic diversity would enhance the robustness of the identified metabolic patterns. Future research should address the limitations of inter-individual variability resulting from genetics, diet, and environmental factors.

## Data availability statement

The original contributions presented in the study are included in the article/Supplementary Material, further inquiries can be directed to the corresponding authors.

## Ethics statement

The studies involving humans were approved by the local Ethics and Research Committee from La Paz University Hospital in Madrid, Spain. The studies were conducted in accordance with the local legislation and institutional requirements. The participants provided their written informed consent to participate in this study.

## Author contributions

DD: Data curation, Formal Analysis, Investigation, Methodology, Software, Visualization, Writing–original draft, Writing–review and editing. VA: Investigation, Writing–original draft. CB: Supervision, Validation, Writing–review and editing. JB: Conceptualization, Funding acquisition, Project administration, Supervision, Writing–review and editing.

## Funding

The author(s) declare that financial support was received for the research, authorship, and/or publication of this article. This work was supported by the Ministry of Science, Innovation and Universities of Spain (MICINN) (Ref. RTI2018-095166-B-I00), FEDER funding and grant PI15/01563, PI23/01837 from "Instituto de Salud Carlos III" (ISCIII), Spain.

## Conflict of interest

The authors declare that the research was conducted in the absence of any commercial or financial relationships that could be construed as a potential conflict of interest.

## Publisher's note

All claims expressed in this article are solely those of the authors and do not necessarily represent those of their affiliated organizations, or those of the publisher, the editors and the reviewers. Any product that may be evaluated in this article, or claim that may be made by its manufacturer, is not guaranteed or endorsed by the publisher.

## Supplementary material

The Supplementary Material for this article can be found online at: https://www.frontiersin.org/articles/10.3389/fmolb.2024.1452312/full#supplementary-material

## References

Adam, S., McIntyre, H. D., Tsoi, K. Y., Kapur, A., Ma, R. C., Dias, S., et al. (2023). Pregnancy as an opportunity to prevent type 2 diabetes mellitus: FIGO Best Practice Advice. *Int. J. Gynecol. Obstet.* 160, 56–67. doi:10.1002/IJGO.14537

American Diabetes Association Professional Practice Committee (2024). 15. Management of diabetes in pregnancy: standards of care in diabetes—2024. *Diabetes Care* 47, S282–S294. doi:10.2337/DC24-S015

Badawy, A. A. B. (2015). Tryptophan metabolism, disposition and utilization in pregnancy. *Biosci. Rep.* 35, e00261. doi:10.1042/BSR20150197

Bao, X., Gu, Y., Zhang, Q., Liu, L., Meng, G., Wu, H., et al. (2018). Low serum creatinine predicts risk for type 2 diabetes. *Diabetes. Metab. Res. Rev.* 34, e3011. doi:10.1002/DMRR.3011

Bartha, J. L., Martinez-Del-Fresno, P., and Comino-Delgado, R. (2000). Gestational diabetes mellitus diagnosed during early pregnancy. *Am. J. Obstet. Gynecol.* 182, 346–350. doi:10.1016/S0002-9378(00)70222-5

Bartha, J. L., Martinez-Del-Fresno, P., and Comino-Delgado, R. (2003). Early diagnosis of gestational diabetes mellitus and prevention of diabetes-related complications. *Eur. J. Obstet. Gynecol. Reprod. Biol.* 109, 41–44. doi:10.1016/S0301-2115(02)00480-3

Bianco, M. E., and Josefson, J. L. (2019). Hyperglycemia during pregnancy and long-term offspring outcomes. *Curr. Diab. Rep.* 19, 143–148. doi:10.1007/s11892-019-1267-6

Burzynska-Pedziwiatr, I., Dudzik, D., Sansone, A., Malachowska, B., Zieleniak, A., Zurawska-Klis, M., et al. (2023). Targeted and untargeted metabolomic approach for GDM diagnosis. *Front. Mol. Biosci.* 9, 997436. doi:10.3389/fmolb.2022.997436

Carpenter, M. W., and Coustan, D. R. (1982). Criteria for screening tests for gestational diabetes. *Am. J. Obstet. Gynecol.* 144, 768–773. doi:10.1016/0002-9378(82)90349-0

Chen, N., Zeng, R., Xu, C., Lai, F., Chen, L., Wang, C., et al. (2023). Low serum creatinine levels in early pregnancy are associated with a higher incidence of postpartum abnormal glucose metabolism among women with gestational diabetes mellitus: a retrospective cohort study. *Nutrients* 15, 2193. doi:10.3390/NU15092193

Chen, X., Scholl, T. O., Leskiw, M., Savaille, J., and Stein, T. P. (2010). Differences in maternal circulating fatty acid composition and dietary fat intake in women with gestational diabetes mellitus or mild gestational hyperglycemia. *Diabetes Care* 33, 2049–2054. doi:10.2337/dc10-0693

Chong, J., Wishart, D. S., and Xia, J. (2019). Using MetaboAnalyst 4.0 for comprehensive and integrative metabolomics data analysis. *Curr. Protoc. Bioinforma.* 68, e86. doi:10.1002/cpbi.86

Damm, P. (2009). Future risk of diabetes in mother and child after gestational diabetes mellitus. *Int. J. Gynaecol. Obstet.* 104 (Suppl. l), S25–S26. doi:10.1016/j.ijgo.2008.11.025

Dudzik, D., Barbas-Bernardos, C., García, A., and Barbas, C. (2018). Quality assurance procedures for mass spectrometry untargeted metabolomics. a review. *J. Pharm. Biomed. Anal.* 147, 149–173. doi:10.1016/j.jpba.2017.07.044

Dudzik, D., Zorawski, M., Skotnicki, M., Zarzycki, W., García, A., Angulo, S., et al. (2017). GC–MS based Gestational Diabetes Mellitus longitudinal study: identification of 2-and 3-hydroxybutyrate as potential prognostic biomarkers. *J. Pharm. Biomed. Anal.* 144, 90–98. doi:10.1016/j.jpba.2017.02.056

Dudzik, D., Zorawski, M., Skotnicki, M., Zarzycki, W., Kozlowska, G., Bibik-Malinowska, K., et al. (2014). Metabolic fingerprint of gestational diabetes mellitus. *J. Proteomics* 103, 57–71. doi:10.1016/j.jprot.2014.03.025

Enquobahrie, D. A., Denis, M., Tadesse, M. G., Gelaye, B., Ressom, H. W., and Williams, M. A. (2015). Maternal early pregnancy serum metabolites and risk of gestational diabetes mellitus. *J. Clin. Endocrinol. Metab.* 100, 4348–4356. doi:10.1210/jc.2015-2862

Enthoven, L. F., Shi, Y., Fay, E., Kim, A., Moreni, S., Mao, J., et al. (2023). Effects of pregnancy on plasma sphingolipids using a metabolomic and quantitative analysis approach. *Metabolites* 13, 1026. doi:10.3390/metabo13091026

Fakhr, Y., Brindley, D. N., and Hemmings, D. G. (2021). Physiological and pathological functions of sphingolipids in pregnancy. *Cell. Signal.* 85, 110041. doi:10.1016/J.CELLSIG.2021.110041

Furse, S., White, S. L., Meek, C. L., Jenkins, B., Petry, C. J., Vieira, M. C., et al. (2019). Altered triglyceride and phospholipid metabolism predates the diagnosis of gestational diabetes in obese pregnancy. *Mol. Omi.* 15, 420–430. doi:10.1039/C9MO00117D

Galadari, S., Rahman, A., Pallichankandy, S., Galadari, A., and Thayyullathil, F. (2013). Role of ceramide in diabetes mellitus: evidence and mechanisms. *Lipids Heal. Dis.* 12, 98. doi:10.1186/1476-511X-12-98

Gall, W. E., Beebe, K., Lawton, K. A., Adam, K. P., Mitchell, M. W., Nakhle, P. J., et al. (2010). alpha-hydroxybutyrate is an early biomarker of insulin resistance and glucose intolerance in a nondiabetic population. *PLoS One* 5, e10883. doi:10.1371/JOURNAL.PONE.0010883

Hammad, S. M., and Lopes-Virella, M. F. (2023). Circulating sphingolipids in insulin resistance, diabetes and associated complications. *Int. J. Mol. Sci.* 24, 14015. doi:10.3390/IJMS241814015

Harita, N., Hayashi, T., Sata, K. K., Nakamura, Y., Yoneda, T., Endo, G., et al. (2009). Lower serum creatinine is a new risk factor of type 2 diabetes: the Kansai healthcare study. *Diabetes Care* 32, 424–426. doi:10.2337/DC08-1265

Hou, G., Gao, Y., Poon, L. C., Ren, Y., Zeng, C., Wen, B., et al. (2023). Maternal plasma diacylglycerols and triacylglycerols in the prediction of gestational diabetes mellitus. *BJOG Int. J. Obstet. Gynaecol.* 130, 247–256. doi:10.1111/1471-0528.17297

Hu, J., Gillies, C. L., Lin, S., Stewart, Z. A., Melford, S. E., Abrams, K. R., et al. (2021). Association of maternal lipid profile and gestational diabetes mellitus: a systematic review and meta-analysis of 292 studies and 97,880 women. *EClinicalMedicine* 34, 100830. doi:10.1016/J.ECLINM.2021.100830

IDF Diabetes Atlas (2021). *IDF diabetes Atlas 10th edition*. Brussels, Belgium: International Diabetes Federation. Available at: https://diabetesatlas.org/atlas/tenth-edition/(Accessed March 16, 2024).

Kahn, B. B., and Flier, J. S. (2000). Obesity and insulin resistance. *J. Clin. Invest.* 106, 473–481. doi:10.1172/JCI10842

Kampmann, U., Knorr, S., Fuglsang, J., and Ovesen, P. (2019). Determinants of maternal insulin resistance during pregnancy: an updated overview. *J. Diabetes Res.* 2019, 5320156. doi:10.1155/2019/5320156

Kanety, H., Hemi, R., Papa, M. Z., and Karasik, A. (1996). Sphingomyelinase and ceramide suppress insulin-induced tyrosine phosphorylation of the insulin receptor substrate-1. *J. Biol. Chem.* 271, 9895–9897. doi:10.1074/jbc.271.17.9895

Khan, S. R., Mohan, H., Liu, Y., Batchuluun, B., Gohil, H., Al Rijjal, D., et al. (2019). The discovery of novel predictive biomarkers and early-stage pathophysiology for the transition from gestational diabetes to type 2 diabetes. *Diabetologia* 62, 687–703. doi:10.1007/S00125-018-4800-2

Konjevod, M., Sáiz, J., Nikolac Perkovic, M., Nedic Erjavec, G., Tudor, L., Uzun, S., et al. (2022). Plasma lipidomics in subjects with combat posttraumatic stress disorder. *Free Radic. Biol. Med.* 189, 169–177. doi:10.1016/J.FREERADBIOMED.2022.07.012

Kramer, C. K., Campbell, S., and Retnakaran, R. (2019). Gestational diabetes and the risk of cardiovascular disease in women: a systematic review and meta-analysis. *Diabetologia* 62, 905–914. doi:10.1007/s00125-019-4840-2

Kuligowski, J., Sánchez-Illana, Á., Sanjuán-Herráez, D., Vento, M., and Quintás, G. (2015). Intra-batch effect correction in liquid chromatography-mass spectrometry using quality control samples and support vector regression (QC-SVRC). *Analyst* 140, 7810–7817. doi:10.1039/C5AN01638J

Leitner, M., Fragner, L., Danner, S., Holeschofsky, N., Leitner, K., Tischler, S., et al. (2017). Combined metabolomic analysis of plasma and urine reveals AHBA, tryptophan and serotonin metabolism as potential risk factors in Gestational Diabetes Mellitus (GDM). *Front. Mol. Biosci.* 4, 84. doi:10.3389/fmolb.2017.00084

Li, G., Kong, L., Zhang, L., Fan, L., Su, Y., Rose, J. C., et al. (2014). Early pregnancy maternal lipid profiles and the risk of gestational diabetes mellitus stratified for body mass index. *Reprod. Sci.* 22, 712–717. doi:10.1177/1933719114557896

Li, Y., Ren, X., He, L., Li, J., Zhang, S., and Chen, W. (2020). Maternal age and the risk of gestational diabetes mellitus: a systematic review and meta-analysis of over 120 million participants. *Diabetes Res. Clin. Pract.* 162, 108044. doi:10.1016/j.diabres.2020.108044

Liu, T., Li, J., Xu, F., Wang, M., Ding, S., Xu, H., et al. (2016). Comprehensive analysis of serum metabolites in gestational diabetes mellitus by UPLC/Q-TOF-MS. *Anal. Bioanal. Chem.* 408, 1125–1135. doi:10.1007/s00216-015-9211-3

Lu, W., Luo, M., Fang, X., Zhang, R., Li, S., Tang, M., et al. (2021). Discovery of metabolic biomarkers for gestational diabetes mellitus in a Chinese population. *Nutr. Metab.* 18, 79–16. doi:10.1186/s12986-021-00606-8

McMichael, L. E., Heath, H., Johnson, C. M., Fanter, R., Alarcon, N., Quintana-Diaz, A., et al. (2021). Metabolites involved in purine degradation, insulin resistance, and fatty acid oxidation are associated with prediction of Gestational diabetes in plasma. *Metabolomics* 17, 105. doi:10.1007/S11306-021-01857-5

Meek, C. L. (2023). An unwelcome inheritance: childhood obesity after diabetes in pregnancy. *Diabetologia* 66, 1961–1970. doi:10.1007/s00125-023-05965-w

Neudorf, H., Islam, H., Falkenhain, K., Oliveira, B., Jackson, G. S., Moreno-Cabañas, A., et al. (2024). Effect of the ketone beta-hydroxybutyrate on markers of inflammation and immune function in adults with type 2 diabetes. *Clin. Exp. Immunol.* 216, 89–103. doi:10.1093/CEI/UXAD138

Ogundipe, E., Samuelson, S., and Crawford, M. A. (2020). Gestational diabetes mellitus prediction? A unique fatty acid profile study. *Nutr. Diabetes* 10, 36. doi:10.1038/s41387-020-00138-9

Özdemir, M., Abusoglu, S., Baldane, S., Kıraç, C. O., Unlu, A., Onmaz, D. E., et al. (2023). Analyzing serum tryptophan metabolites in patients with gestational diabetes mellitus. *Rev. Rom. Med. Lab.* 31, 251–262. doi:10.2478/RRLM-2023-0027

Peters, R. K., Kjos, S. L., Xiang, A., and Buchahan, T. A. (1996). Long-term diabetogenic effect of single pregnancy in women with previous gestational diabetes mellitus. *Lancet (London, England)* 347, 227–230. doi:10.1016/S0140-6736(96)90405-5

Plows, J. F., Stanley, J. L., Baker, P. N., Reynolds, C. M., and Vickers, M. H. (2018). The pathophysiology of gestational diabetes mellitus. *Int. J. Mol. Sci.* 19, 3342. doi:10.3390/IJMS19113342

Qi, J., Gan, L., Fang, J., Zhang, J., Yu, X., Guo, H., et al. (2022). Beta-Hydroxybutyrate: a dual function molecular and immunological barrier function regulator. *Front. Immunol.* 13, 805881. doi:10.3389/FIMMU.2022.805881

Razo-Azamar, M., Nambo-Venegas, R., Meraz-Cruz, N., Guevara-Cruz, M., Ibarra-González, I., Vela-Amieva, M., et al. (2023). An early prediction model for gestational diabetes mellitus based on metabolomic biomarkers. *Diabetol. Metab. Syndr.* 15, 116. doi:10.1186/S13098-023-01098-7

Rey-Stolle, F., Dudzik, D., Gonzalez-Riano, C., Fernández-García, M., Alonso-Herranz, V., Rojo, D., et al. (2021). Low and high resolution gas chromatography-mass spectrometry for untargeted metabolomics: a tutorial. *Anal. Chim. Acta* 1210, 339043. doi:10.1016/J.ACA.2021.339043

Rodolaki, K., Pergialiotis, V., Iakovidou, N., Boutsikou, T., Iliodromiti, Z., and Kanaka-Gantenbein, C. (2023). The impact of maternal diabetes on the future health and neurodevelopment of the offspring: a review of the evidence. *Front. Endocrinol. (Lausanne)* 14, 1125628. doi:10.3389/FENDO.2023.1125628

Saeedi, M., Cao, Y., Fadl, H., Gustafson, H., and Simmons, D. (2021). Increasing prevalence of gestational diabetes mellitus when implementing the IADPSG criteria: a systematic review and meta-analysis. *Diabetes Res. Clin. Pract.* 172, 108642. doi:10.1016/J.DIABRES.2020.108642

Scholtens, D. M., Muehlbauer, J., Daya, N. R., Stevens, R. D., Dyer, A. R., Lowe, L. P., et al. (2014). Metabolomics reveals broad-scale metabolic perturbations in hyperglycemic mothers during pregnancy. *Diabetes Care* 37, 158–166. doi:10.2337/dc13-0989

Sikorski, C., Azab, S., De Souza, R. J., Shanmuganathan, M., Desai, D., Teo, K., et al. (2022). Serum metabolomic signatures of gestational diabetes in South Asian and white European women. *BMJ Open Diabetes Res. Care* 10, e002733. doi:10.1136/BMJDRC-2021-002733

Singh, P., Elhaj, D. A. I., Ibrahim, I., Abdullahi, H., and Al Khodor, S. (2023). Maternal microbiota and gestational diabetes: impact on infant health. *J. Transl. Med.* 21, 364. doi:10.1186/S12967-023-04230-3

Sivan, E., Homko, C. J., Whittaker, P. G., Reece, E. A., Chen, X., and Boden, G. (1998). Free fatty acids and insulin resistance during pregnancy. *J. Clin. Endocrinol. Metab.* 83, 2338–2342. doi:10.1210/JCEM.83.7.4927

Soma-Pillay, P., Nelson-Piercy, C., Tolppanen, H., and Mebazaa, A. (2016). Physiological changes in pregnancy. *Cardiovasc. J. Afr.* 27, 89–94. doi:10.5830/CVJA-2016-021

Song, C., Lyu, Y., Li, C., Liu, P., Li, J., Ma, R. C., et al. (2018). Long-term risk of diabetes in women at varying durations after gestational diabetes: a systematic review and meta-analysis with more than 2 million women. *Obes. Rev.* 19, 421–429. doi:10.1111/OBR.12645

Sousa, A. P., Cunha, D. M., Franco, C., Teixeira, C., Gojon, F., Baylina, P., et al. (2021). Which role plays 2-hydroxybutyric acid on insulin resistance? *Metabolites* 11, 835. doi:10.3390/METABO11120835

Sun, Z., Deng, Z., Wei, X., Wang, N., Yang, J., Li, W., et al. (2022). Circulating saturated fatty acids and risk of gestational diabetes mellitus: a cross-sectional study and meta-analysis. *Front. Nutr.* 9, 903689. doi:10.3389/fnut.2022.903689

Sweeting, A., Wong, J., Murphy, H. R., and Ross, G. P. (2022). A clinical update on gestational diabetes mellitus. *Endocr. Rev.* 43, 763–793. doi:10.1210/ENDREV/BNAC003

van Zundert, S. K. M., Broekhuizen, M., Smit, A. J. P., van Rossem, L., Mirzaian, M., Willemsen, S. P., et al. (2022). The role of the kynurenine pathway in the (Patho) physiology ofMaternal pregnancy and fetal outcomes: a systematic review. *Int. J. Tryptophan Res.* 15, 11786469221135545. doi:10.1177/11786469221135545

Vrijkotte, T. G. M., Algera, S. J., Brouwer, I. A., Van Eijsden, M., and Twickler, M. B. (2011). Maternal triglyceride levels during early pregnancy are associated with birth weight and postnatal growth. *J. Pediatr.* 159, 736–742. doi:10.1016/J.JPEDS.2011.05.001

White, S. L., Pasupathy, D., Sattar, N., Nelson, S. M., Lawlor, D. A., Briley, A. L., et al. (2017). Metabolic profiling of gestational diabetes in obese women during pregnancy. *Diabetologia* 60, 1903–1912. doi:10.1007/S00125-017-4380-6

Whyte, K., Kelly, H., O'Dwyer, V., Gibbs, M., O'Higgins, A., and Turner, M. J. (2013). Offspring birth weight and maternal fasting lipids in women screened for gestational diabetes mellitus (GDM). *Eur. J. Obstet. Gynecol. Reprod. Biol.* 170, 67–70. doi:10.1016/J.EJOGRB.2013.04.015

World Health Organization (1999). *Definition, diagnosis and classification of diabetes mellitus and its complications Part 1: diagnosis and classification of diabetes mellitus*. World Health Organization. Available at: https://apps.who.int/iris/bitstream/handle/10665/66040/WHO_NCD_NCS_99.2.pdf?sequence=1 (Accessed March 17, 2021).

Yang, Y., and Wu, N. (2022). Gestational diabetes mellitus and preeclampsia: correlation and influencing factors. *Front. Cardiovasc. Med.* 9, 831297. doi:10.3389/FCVM.2022.831297

Yaribeygi, H., Farrokhi, F. R., Butler, A. E., and Sahebkar, A. (2019). Insulin resistance: review of the underlying molecular mechanisms. *J. Cell. Physiol.* 234, 8152–8161. doi:10.1002/JCP.27603

Ye, D., Huang, J., Wu, J., Xie, K., Gao, X., Yan, K., et al. (2023). Integrative metagenomic and metabolomic analyses reveal gut microbiota-derived multiple hits connected to development of gestational diabetes mellitus in humans. *Gut Microbes* 15, 2154552. doi:10.1080/19490976.2022.2154552

Zhan, Y., Wang, J., He, X., Huang, M., Yang, X., He, L., et al. (2021). Plasma metabolites, especially lipid metabolites, are altered in pregnant women with gestational diabetes mellitus. *Clin. Chim. Acta* 517, 139–148. doi:10.1016/J.CCA.2021.02.023

Zhao, H., Li, H., Chung, A. C. K., Xiang, L., Li, X., Zheng, Y., et al. (2019). Large-scale longitudinal metabolomics study reveals different trimester-specific alterations of metabolites in relation to gestational diabetes mellitus. *J. Proteome Res.* 18, 292–300. doi:10.1021/acs.jproteome.8b00602

Zhu, H., He, D., Liang, N., Lai, A., Zeng, J., and Yu, H. (2020). High serum triglyceride levels in the early first trimester of pregnancy are associated with gestational diabetes mellitus: a prospective cohort study. *J. Diabetes Investig.* 11, 1635–1642. doi:10.1111/JDI.13273

Zhu, S. M., Zhang, H. Q., Li, C., Zhang, C., Yu, J. L., Wu, Y. T., et al. (2022). Maternal lipid profile during early pregnancy and birth weight: a retrospective study. *Front. Endocrinol. Lausanne* 13, 951871. doi:10.3389/fendo.2022.951871

10.3389/fmolb.2024.1452312

## Glossary

| | |
|---|---|
| **AcAc** | Glacial Acetic Acid |
| **ACN** | Acetonitrile |
| **ADD1** | Adipocyte Determination and Differentiation-Dependent Factor 1 |
| **BSTFA** | N,O bis(trimethylsilyl)trifluoroacetamide |
| **dMRM** | dynamic Multiple Reaction Monitoring Mode |
| **EI** | Electron Impact |
| **ESI** | Electrospray Ionization |
| **EtAc** | Ethyl Acetate |
| **FA** | Formic Acid |
| **GC/Q-TOF-MS** | Gas Chromatography-Quadrupole-Time of Flight Mass Spectrometry |
| **IRS-1** | Insulin Receptor Substrate-1 |
| **IR** | Insulin Resistance |
| **IS** | Internal Standard |
| **LC-MS/MS** | Liquid Chromatography-Tandem Mass Spectrometry |
| **MeOH** | Methanol |
| **MS** | Mass Spectrometry |
| **MS/MS** | Tandem Mass Spectrometry |
| **NIDDM** | Non-Insulin Dependent Diabetes Mellitus |
| **NIST** | National Institute of Standards and Technology |
| **OPLS-DA** | Orthogonal Partial Least Squares Discriminant Analysis |
| **PCA** | Principal Component Analysis |
| **PrOH** | 2-propanol |
| **QC-SVRC** | Quality Control based Support Vector Regression |
| **RSD** | Relative Standard Deviation |
| **RT** | Retention Time |
| **RTL** | Retention Time Locked |
| **SREBP** | Sterol Regulatory Element Binding Protein |
| **SUS** | Shared and Unique Structures Plot Analysis |
| **TMCS** | 1% trimethylchlorosilane |
| **VIP** | Variable Influence on the Projection |

# Frontiers in
# Molecular Biosciences

**Explores biological processes in living organisms on a molecular scale**

Focuses on the molecular mechanisms underpinning and regulating biological processes in organisms across all branches of life.

---

## Discover the latest Research Topics

See more →

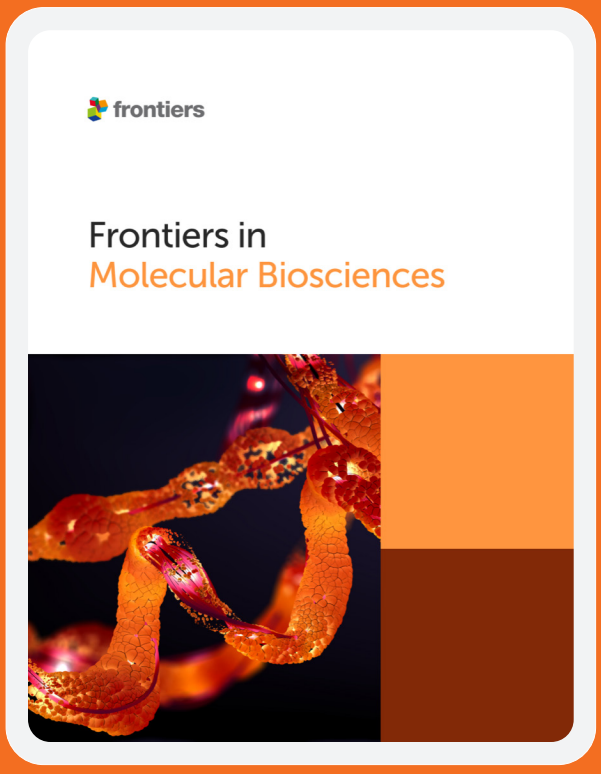


**Frontiers**

Avenue du Tribunal-Fédéral 34
1005 Lausanne, Switzerland
frontiersin.org

**Contact us**

+41 (0)21 510 17 00
frontiersin.org/about/contact